The Effect of Composition and Structure of Crude-Oil Models on Fouling Phenomena using a Stirred Batch Reactor

---

Imperial College London

Department of Chemical Engineering

Jonathan Ball

Thesis Submitted for the degree of Doctor of Philosophy (PhD) to Imperial College London

Supervised by Marcos Millan-Agorio

September 2021

Declaration of Originality

This is to certify that the contents of this work are the original work of the author and that anything else has been appropriately referenced.

Copyright Declaration

The copyright of this thesis rests with the author. Unless otherwise indicated, its contents are licensed under a Creative Commons Attribution-Non Commercial 4.0 International Licence (CC BY-NC).

Under this licence, you may copy and redistribute the material in any medium or format. You may also create and distribute modified versions of the work. This is on the condition that: you credit the author and do not use it, or any derivative works, for a commercial purpose.

When reusing or sharing this work, ensure you make the licence terms clear to others by naming the licence and linking to the licence text. Where a work has been adapted, you should indicate that the work has been changed and describe those changes.

Please seek permission from the copyright holder for uses of this work that are not included in this licence or permitted under UK Copyright Law.

Abstract

Fouling of crude oils in the heat exchangers of the refinery preheat train (PHT) is a common problem. The varying composition and complex phase behaviour of crude oils presents significant challenges when processing at high temperatures. Precipitation of asphaltenes from the oil and corrosion fouling at high temperatures results in the build-up of deposits on heat exchanger wall surfaces, reducing heat and momentum transfer. This results in significant economic and environmental impact. Studying this phenomenon from a physicochemical perspective remains challenging as crude oil compositions vary widely. In particular, asphaltenes, the heaviest oil fraction, exhibits phase behaviour which is highly dependent on temperature and blend composition.

This work augments existing understanding of fouling behaviour of crude oils at high temperature by focusing on their compositions by blending, fractionation (into asphaltenes and maltenes) and recombination with model solvents. Synthetic asphaltene model-compound solutions were developed to study fouling in a repeatable and controlled manner, and their fouling characteristics were validated against those of naturally occurring crude oils. Fouling experiments for crude oils were conducted in a purpose – built laboratory scale system described in this work. This apparatus simulated the hydrodynamic conditions found in latter stage PHT heat exchangers. These studies formed the basis of comparison for later experiments, testing both fractionated oil solutions and synthetic asphaltene solutions utilising high boiling-point solvents (n-dodecane and 1-methylnaphthalene).

Commissioning experiments revealed that fouling behaviour was influenced by several factors. Not only was the production of deposits highly dependent on the process conditions, blend composition and preparation of the test fluids, but also the cleaning procedure of the system. Traces of residual deposits were believed to act as nucleation sites for further deposit production and activity of the heated wall surface was subject to cycling passivation. When fractionated oil solutions were used, solution stability at process conditions was the primary driver of fouling; high concentrations of asphaltenes were relatively stable in 1-methylnaphthalene, but low concentrations were highly unstable in solutions containing large proportions of n-dodecane, an incompatible solvent. Maltene fouling was similarly dependant on its solution stability. Solutions of synthesised model asphaltenes based on alkylpyrene and perylene diimides, exhibited very different behaviour under process conditions. A long alkyl-chain perylene diimide (PDI-C12) alone exhibited strong fouling behaviour at process conditions. It exhibited marginal solubility in 1-methylnaphthalene and high thermal lability, resulting in significant insoluble deposits which also caused corrosion of the steel wall surface.

Acknowledgements

I would like to thank Marcos Millan-Agorio, for his academic and technical knowledge, support, encouragement, and tuition through this PhD journey. I have been lucky to have the opportunity to be a part of his research group and made welcome throughout my years at Imperial.

I would also like to thank the group for their academic knowledge and experience and help, Dr. Pedro Arcelus Arrillaga, Dr. Holda Puron, Dr. Beatriz Fidalgo Fernandez, Dr. Eneritz Fernandez, Dr. Xiangyi Long, Dr. Anastassia Sivena and Dr. Anthony Odongo and Dr. Aderlanio Cardoso. Separately I would also like to thank Dr. Parth Shah for his support, friendship and generous tea provisions! I have been blessed to know and work with some great people and their combined knowledge has helped me grow both academically and mentally.

I also thank my family who have been there for me and supported me from the very beginning. I owe them a great debt of gratitude for all the encouragement and sacrifice they have made to support me up to and through this process.

Last but most importantly, I would like to thank my wife Ana for believing in me and helping me through difficult periods of this journey. My joy has been her joy and my struggle has been her struggle. She has continued to believe in me even in moments when I did not believe in myself.

Table of Contents

ABSTRACT **2**

ACKNOWLEDGEMENTS **3**

TABLE OF CONTENTS **4**

LIST OF TABLES **9**

LIST OF FIGURES **10**

SYMBOLS **16**

LIST OF ABBREVIATIONS **16**

CHAPTER 1 INTRODUCTION **18**

1.1 Energy outlook and Crude oil 18

1.2 Economic and Environmental Impact from Crude Oil Fouling 19

1.3 Crude oil Preheat train Overview 19

1.4 Research Objectives 21

1.5 Structure of the thesis 22

CHAPTER 2 BACKGROUND/LITERATURE REVIEW **24**

2.1 Chemical composition of crude oil 24

2.2 SARA fractionation analysis 24

2.2.1 Saturates *26*

2.2.2 Aromatics *26*

2.2.3 Resins *26*

2.2.4 Asphaltenes *27*

2.3 Asphaltene structure 27

2.3.1 Island and archipelago models *27*

2.3.2 Asphaltene/oil phase behaviour - The modified Yen model *28*

2.4 Effects of asphaltenes on viscosity 29

2.5 Asphaltene solubility and colloidal stability models 30

2.6 Heteroatom effects 31

2.6.1 Heteroatoms present in crude oils *31*

2.6.2 Metals *33*

2.6.3 Salts, sediments and corrosion products *33*

2.6.4 Porphyrins and other biomarkers *33*

2.7 Crude oil compatibility 34

2.8 Thermal cracking mechanism leading to coke formation 34

2.8.1 Role of resins in stabilising asphaltenes *36*
2.9.1 Fouling mechanisms 37
Particulate fouling *37*
Crystallisation fouling *37*
Corrosion fouling *37*
Chemical reaction fouling *38*
2.9.2 Ageing 39
Precipitation onset time *40*
2.9.3 Hydrodynamic effects due to fouling 41
2.9.4 Thermal effects due to fouling 41
2.9.5 Fouling mitigation strategies 42
Surface modifications *42*
Heat exchanger design and overall fluid process *42*
Chemical additives *43*
2.10 Characterisation of asphaltenes 43
2.10.1 Mass analysis *43*
2.10.2 Mass spectrometry *43*
2.10.3 Other mass analysis techniques *44*
2.10.4 Translational diffusion measurements *44*
2.10.5 Molar concentration measurements *45*
2.11 Characterisation of asphaltene structure 45
Polyaromatic ring groups (PAH moieties *45*
are *45*
2.12 Organic compounds as asphaltenes models 46
2.12.1 ..... *47*
Use case for model asphaltene compounds to assist fundamental understanding of the crude oil fouling processes *47*
2.13 Laboratory scale crude oil fouling research 48
2.13.1 Crude oil fouling systems without dynamic flow *48*
2.13.2 Crude oil fouling systems with dynamic flow *51*
2.13.3 Recommended process conditions and the pros and cons of various configurations *54*
CHAPTER 3 DESIGN, DEVELOPMENT AND COMMISSIONING OF A STIRRED BATCH FOULING APPARATUS 56
3.1 Introduction 56
3.2 Reactor design process 56
3.3 Details of the reactor design 57
3.3.1 Radiant heated Taylor-Couette Cell apparatus *57*
3.3.2 Stirring *60*
3.3.3 Heating *60*

3.3.4 Gas purging, loading, measurement and product collection *61*
3.3.5 Pressure measurement and safety considerations *63*
3.3.6 Lifting mechanism *64*
3.3.7 Thermal expansion considerations *66*
3.4. HYDRODYNAMIC PROPERTIES: COMPARISON BETWEEN THE TAYLOR COUETTE REACTOR AND A HEAT EXCHANGER TUBE 67
3.4.1 Fluid velocity *67*
3.4.2 Flow Behaviour in a steel heat exchanger tube *69*
3.4.3 Flow behaviour in the Taylor Couette reactor *69*
3.4.4 Hydrodynamic prediction for Paratherm® NF - heat transfer oil *70*
3.5 Conclusions of reactor dynamic model *75*
CHAPTER 4 EXPERIMENTAL METHODS 76
4.1 INTRODUCTION 76
4.2 CRUDE OIL PREPARATION TECHNIQUES 76
4.2.1 Oil Blending *76*
4.2.2 Desalting Method for crude oil used in fouling experiments *76*
4.2.3 Large Scale Crude oil Fractionation *77*
4.3 TAYLOR COUETTE REACTOR STANDARD OPERATION PROCEDURE 78
4.3.1 Start-up Procedure *78*
4.3.2 Reactor Products Recovery Procedure *80*
4.3.3 Reactor cleaning procedure *82*
4.3.4 Mass analysis of insoluble reaction deposits *84*
4.3.5 Deposit recovery and quantification from bulk fluid *86*
4.3.6 Analytical asphaltene fractionation *86*
4.3.7 Repeatability and error estimation *87*
4.4 CHARACTERISATION TECHNIQUES 88
4.4.1 X-Ray fluorescence spectroscopy *88*
4.4.2 Scanning electron microscopy with energy dispersive x-rays *89*
4.4.3 UV fluorescence spectroscopy *89*
4.4.4 Combustion microanalysis *90*
4.4.5 Inductively coupled plasma with optical emission spectroscopy (ICP-OES) *90*
4.4.6 Fourier transform infra-red spectroscopy (FTIR) *90*
4.4.7 Thermogravimetric analysis (TGA) *91*
4.4.8 Gas chromatography - flame ionisation detection (GC-FID) *92*
CHAPTER 5 CHARACTERIZATION OF CRUDE OILS 95
5.1 INTRODUCTION 95
5.2 CRUDE OIL ANALYSIS 95
5.2.1 Solvent fractionation and mass balances of crude fractions *96*

5.2.2 Density *97*
5.2.3 Elemental analysis (EA) *97*
5.2.4 Characterization by GC-FID *98*
5.2.5 UV-fluorescence spectroscopy of crude oil fractions separated by solubility *102*
5.2.6 FTIR-ATR spectroscopy of crude oil and solubility-fractions *103*
5.2.7 Thermogravimetric analysis (TGA) of crude oil and its solubility fractions *106*
5.2.8 Conclusions for the analysis of crude oils *111*

CHAPTER 6 COMMISSIONING OF THE FOULING APPARATUS 112

6.1 Introduction 112
6.2 Reactor hydrodynamic visualisation using rheoscopic fluids 112
6.2.1 Reactor fluid loading test *113*
6.2.2 Motor speed calibration *115*
6.2.3 Rheology visualisation *116*
6.3 High temperature testing 118
6.3.1 Thermal behaviour with non-fouling fluid tests *119*
6.3.2 Thermal wall/bulk temperature gradient *123*
6.3.3 Pressure and thermal expansion *124*
6.3 Fouling fluid commissioning tests 125
6.3.1 Initial Tests *125*
6.3.3 Commissioning trials with desalted oils *128*
6.3.4. Repeatability study *130*
6.3.4 Modifications following commissioning experiments *132*
6.3.5 Later Modifications to the Taylor-Couette cell body to enable wall surface analysis 133
6.4 Conclusions 134

CHAPTER 7 FOULING EXPERIMENTS USING BLENDED CRUDE OILS 136

7.1 Use of crudes H and L for fouling experiments in the Taylor Couette fouling rig 136
7.1.1 Crude oil blend composition - mass analysis of fouling solids 137
7.2 Time dependence on fouling with desalted 3:2 H:L crude oil 138
7.2.1 Mass analysis of fouling solids *139*
7.3 Conclusions of crude oil fouling experiments 140

CHAPTER 8 FOULING EXPERIMENTS WITH FRACTIONATED CRUDE-OIL SOLUTIONS 142

8.1 Introduction 142
8.1.1 Selection of model solvents and synthesis of model compounds *142*
8.1.2 Process conditions *143*
8.2 Fouling experiments: Investigating the effect of asphaltene concentration on fouling in 1-methylnaphalene 143
8.2.1 Sample preparation *144*

8.3 Effect of solvent aromaticity on fouling behaviour using asphaltene solutions 145
8.3.1 Preparation *145*
8.3.2 Experimental *145*
8.3.2 Fouling experiments using solutions of maltenes in dodecane 148
8.3.6 Fouling reactor modifications to enable wall surface analysis by SEM-EDX 150
8.4 Conclusions 152

CHAPTER 9 SYNTHESIS, CHARACTERISATION AND FOULING EXPERIMENTS OF MODEL ASPHALTENES 154

9.1 Introduction 154
9.2 Synthesis of alkylpyrene asphaltene models 155
9.2.1 Synthesis and characterisation *155*
9.2.2 Experimental section – Synthesis of pyrene models *156*
9.3 Asphaltene models using perylenetetracarboxylic diimide 157
9.3.1 Synthesis of symmetrical perylenetetracarboxylic diimides *157*
Figure 9.4 Solubility tests of perylene based compounds in various solvents *158*
9.3.2 Solubility vs temperature *159*
9.4 Fouling experiments with alkylpyrene model asphaltenes 160
9.4.1 Use of 1-butylpyrene and 1-decylpyrene solutions for fouling experiments *160*
9.4.2 Results and discussion *160*
9.4 Fouling of PDI-C_{12} solutions in 1-methylnaphthalene 160
9.4.1 Preparation *160*
9.4.2 FTIR data – PDI-C_{12} vs fouling products *162*
9.5 SEM images of PDI-C_{12} deposits 163
9.6 Conclusions 166

CHAPTER 10 CONCLUSIONS 167

10.1 Evaluating the research objectives 167
10.2 Future work 171
Further characterisation of existing deposits *171*
Fouling experiments on fractionated oil solutions *171*
Upgrades and modifications to the Taylor Coutte fouling reactor *171*
Further research on synthetic asphaltene model solutions *172*

REFERENCES 174

Chapter 11 Appendix **175**

List of Tables

Table 2.1 Typical elemental composition of crude oils (data from Mullins et al.[20]) 24
Table 2.2 Typical average properties of SARA fractions 26
Table 2.3 Model asphaltene structures used for investigated the phase behaviour and thermal characteristics of asphaltenes 46
Table 2.4 Key operating conditions for stirred batch fouling reactor as recommended by Bennett et al.126 54
Table 2.5 Advantages and disadvantages of different reactor configurations 55
Table 3.1 Paratherm® NF Physical Properties 71
Table 4.1 TGA program for proximate analysis 91
Table 4.2 Gas chromatography operating conditions 93
Table 5.1 Percentage elemental masses for crudes H and L as provided by oil supplier 98
Table 5.2 TGA mass proximate analysis of crude H and its fractions 107
Table 6.1 Observations from visual rheoscopic fluid dynamic investigations 118
Table 6.2 Furnace heating programs for various target reactor wall temperatures 120
Table 6.3 Mean reaction temperature difference between the wall surface and fluid bulk for reactions with dodecane and methylnaphthalene at 320 °C, 1500 rpm for 6 hours 123
Table 6.4 Initial Trials with Crude oil blended 1:1 Heavy/Light by weight. Experiments conducted for 6-hours under 30 bar pressure 125
Table 6.5 Deposit masses produced in fouling experiments for repeatability study for desalted crude oil with heavy:light ratio 3:2 at 320 °C, 1500 rpm, 30 bar pressure (RR denotes repeatability run). 130
Table 7.1 General conditions applied to all fouling experiments in chapters 7, 8 and 9 where deposit masses have been measured 136
Table 7.2 Average masses of fouling deposits: crude oil blend composition 137
Table 7.3 Deposit masses recovered from fouling experiments of 60:40 H:L crude oil blend at varying heated test time between 6 and 24 hours with associated errors. Wall Temperatures were maintained at 320 °C, rotation speed 1500 rpm. 139
Table 8.1 Properties of two key solvents used for fouling experiments 143
Table 9.1 Solubility tests of Perylene based compounds 157
Table 9.2 Deposit masses for PDI-C12 solutions in 1-methylnaphthalene 161

List of Figures

Figure 1.1 Simplified flow diagram of a typical crude oil distillation unit (Panchal and Huang Fu)..... 20
Figure 2.1 Laboratory SARA separation process..... 25
Figure 2.2 Hypothetical Island (a) and Archipelago (b) model asphaltene structures..... 28
Figure 2.3 The Modified Yen Model (from Mullins[17]) This depicts from single asphaltene molecules (approximate diameter 1.5 nm), aggregation leads to nanoaggregates (appoximate diameter 2 nm) which in turn aggregate together to form asphaltene clusters..... 28
Figure 2.4 Chemical structures of hopane (left) and cholesterol (right) 34
Figure 2.5 Nickel and vanadium bound porphyrins found in petroleum..... 34
Figure 2.6 Thermolysis mechanism of asphaltenes leading to phase separation and coke formation (by Wiehe et al) 35
Figure 2.7 Left C7-aspahtlenes and right C5-asphltenes - C7-asphaltenes appear glassy in contrast to the powdery texture of C5-asphaltenes. This reflects the more efficient stacking in the C7 fraction (from Langevin et al.)..... 36
Figure 2.8 scheme of a general multistep deposition process (source Watkinson and Wilson[68])..... 38
Figure 2.9 Structural Evolution of asphaltenic deposits with age (source Z. Fan & Wilkinson, 2009). 39
Figure 2.10 Four model compounds used in HRTEM studies: a = coronene, b = Naphtho[2,3-a]pyrene, c = perylenetetracarboxylic dianhydride (PTDA), d = N,N'-ditridecyl-3,4,9,10-perylenetetracarboxylic diimide (PTDI-C13)..... 47
Figure 2.11 Schematic of Microbomb reactor - Legend: [1] Thermocouple; [2] Pressure Transducer; [3] Union Tee; [4] Pressure Relief Valve; [5] Thermocouple; [6] Union Cross; [7] Ball Valve; [8] Needle Valve; [9] Heat Exchanger; [10] Vertical Pressure Extender; [11] (Source Khairul Rostani[128]) 49
Figure 2.12 Schematic Diagram of Fouling reactor (by Khairul Rostani) - [1] Nitrogen gas cylinder; [2] Ball valve; [3] Pressure transducer; [4] Ball valve; [5] Needle valve; [6] Sample cylinder; [7] Ball valve; [8] Needle valve; [9] Needle valve; [10] Ball valve [11] Needle valve; [12] Test section; [13] Thermocouple assembly; [14] Needle valve; [15] Pressure transducer; [16] Pressure relief valve; [17] Needle valve (Source Khairul Rostani[128])..... 50
Figure 2.13 Stirred batch fouling cell developed by Crittenden et al. (source Crittenden et al[117]) 52
Figure 2.14 Schematic diagram of Alcor HLPS 400 fouling system used for use with bitumen visbreaking products (source Ali et al.)..... 53
Figure 2.15 Schematic process flow diagram of the HiPOR fouling rig (source Coletti and Hewitt) ... 54
Figure 3.1 Schematic of Taylor Couette vessel body (not to scale) 58
Figure 3.2 Scale cross section through the assembled batch reactor cell excluding the motor unit. 1 – stainless steel head flange, 2 – mild steel wall body, 3 – stainless steel base flange, 4 – stainless steel

rotor, 5 – stainless steel rotor shaft, 6 – grub screw, 7 – stainless steel M6 x 25mm bolts, 8 – annealed copper gaskets, 9 – threaded motor port, 10 & 12 – ¼" Swagelok straight fitting with copper gasket, 11 - threaded inlet port, 13 – threaded top outlet port, 14 – lower outlet port, 15 – all stainless steel Swagelok bleed valve, 16 – Stainless steel reactor mounting assembly 59
Figure 3.3 Scale Top view of Taylor Couette reactor head unit: 1 – Stainless Steel head unit, 2 – threaded motor connection, 3 – threaded Inlet port, 4 – threaded top outlet port, 5 – Threaded bulk thermocouple connection, 6 – Hole for wall temperature thermocouple (drilled fully through head unit and to the middle of the wall body), 7 – recessed holes for M6 flange bolts, 8 – threaded connection to the mounting assembly 59
Figure 3.4 Magnetically sealed Motor Drive Unit from Autoclave Engineers (MAG3050) image with cross-sectional drawing superimposed onto reactor cross section for scale 60
Figure 3.5 Schematic of fouling reactor system with associated tubing and instruments. Purge/loading section (orange), purge/measurement section (blue), product collection section (green) 61
Figure 3.6 Scale Process flow diagram of the Taylor Couette cell batch reactor and purge, loading and product collection system: V1 – V6, V8 – V10: needle valves, A1 – A8: reduction adapters, Tee 1 – Tee 8: Tee fittings, P1 – P2 – pressure transducers, Ves 1 – Sample loading vessel, Ves 2 – Sample collection Vessel, RV – Pressure Relief Valve 62
Figure 3.7 Image of the batch fouling reactor system in steel cabinet: 1 - pressure logger, 2 - variable power supply, 3 - Temperature logger, 4 - sample loading port, 5 - sample loading vessel, 6 - motor, 7 - reactor, 8 - furnace, 9 product collection vessel, 10 - outlet valve 63
Figure 3.8 Schematic of the reactor lifting mechanism within the steel cabinet showing the lowered reactor inside the tube furnace (left) and the fully raised reactor in between experiments (right) ... 64
Figure 3.9 Top view of the steel cabinet showing reactor, furnace and lifting mechanism. The aluminium section slides on the white acetal polymer guides and is hoisted by a motor attached to a threaded bar which goes through the centre of the aluminium crossbeam. 65
Figure 3.10 Image of the partly constructed reactor detailing components of the reactor, furnace and lifting mechanism (note the reactor head viewed here was redesigned to better accommodate the motor and fittings) 65
Figure 3.11 Cross sectional profiles through the Taylor Couette cell reactor (left) and 1 inch heat exchanger tube (right). The steel wall is shaded grey and the brown fluid fills the annular section and inner tube section. Velocity profiles under turbulent conditions are shown for azimuthal flow in the Taylor Couette cell and axial flow in a pipe. 68
Figure 3.12 Model Predictions of the Temperature dependence on Reynolds Number for the Taylor Couette Reactor (TCR) at 823 rpm, 1646 rpm and 2470 rpm (tangential velocities of 1, 2 and 3 m/s) and Heat Exchanger Tube at 1, 2 and 3 m/s fluid velocity 71

Figure 3.13 Predictions of the fluid Reynolds number with tangential velocity for the Taylor Couette Reactor (TCR) and linear velocity in a Heat Exchanger Tube at three isotherms: 100, 200 and 300 °C. 72
Figure 3.14 Fluid Taylor number in the Taylor Couette reactor at varying temperatures for rotations speeds at 823, 1646 and 2470 rpm equivalent to 1, 2 and 3 m/s tangential fluid velocity..... 73
Figure 3.15 Model predictions for the temperature dependence on Reynolds number for the Taylor Couette Reactor (TCR) at 823 rpm, 1646 rpm and 2470 rpm (tangential velocities of 1, 2 and 3 m/s) and Heat Exchanger Tube at 1, 2 and 3 m/s fluid velocity 74
Figure 3.16 Model predictions for the dependence of wall stress on tangential velocity for the Taylor Couette Reactor (TCR) and Heat Exchanger Tube at three isotherms: 100, 200 and 300 °C. 74
Figure 4.1 Taylor Couette Reactor Operating Procedure 80
Figure 4.2 Product Recovery Procedure 82
Figure 4.3 Reactor Cleaning Procedure 84
Figure 4.4 representation of the XRF spectroscopy principal: a) an incident x-ray ejects an inner core electron, b) a higher energy electron jumps to fill the hole left by the ejected electron. This may occur from an adjacent orbital $\boldsymbol{K\alpha}$ or a higher orbital $\boldsymbol{K\beta}$. 88
Figure 4.5 Principal of the HPLC system - A: Helium carrier gas acts as the mobile phase, B: sample is injected into the column, c: sample components separate as they are carried through the capillary column in a temperature programmed oven, d: eluted compounds are detected (by flame ionisation detector), e: signal is processed by a recorder 93
Figure 5.1 Percent mass fractions of Crude H and L by analytical fractionation and large-scale fractionation methods 96
Figure 5.2 Density and API gravity of crude oils measured using pycnometer..... 97
Figure 5.3 Retention times of standard gas oil n-alkanes against boiling points..... 99
Figure 5.4 Gas chromatograph of crude L maltenes..... 100
Figure 5.5 Gas chromatograph of crude H maltenes 100
Figure 5.6 Boiling point fractions of Crudes H and L detected by gas chromatography..... 101
Figure 5.7 Synchronous UV-F spectra of whole Crude H and L dissolved in chloroform..... 102
Figure 5.8 UV-fluorescence spectra of crude H and its solubility fractions 103
Figure 5.9 FTIR spectra for whole crude oils H and L..... 104
Figure 5.10 FTIR spectra for crude H, and the maltenes and asphaltenes fractions derived from it 105
Figure 5.11 Normalised FTIR spectra of crude H and asphaltenes derived from it 106
Figure 5.12 Normalised weight-time TGA Plot for crude H and its fractions, averaged over two repeats with temperature on second y-axis 108

Figure 5.13 Derivative weight-time TGA Plot for Crude H and its fractions, averaged over two repeats with temperature on second y-axis 108
Figure 5.14 Normalised weight-time TGA plot for crude H, L and 3:2 H:L blend, averaged over two repeats with temperature on second y-axis 109
Figure 5.15 Derivative weight-time TGA plot for crude H, L and 3:2 blend and its fractions, averaged over two repeats with temperature on second y-axis 110
Figure 6.1 Batch fouling reactor with PMMA wall section installed 113
Figure 6.2 Calibration plot of motor input voltage against rotor rpm, measured using Olympus iSpeed-3 high-speed camera 115
Figure 6.3 Taylor vortices present the reactor annulus at 100-600rpm. Rotor rotates from right to left as viewed from front. (Still shown here at 400 rpm) 116
Figure 6.4 Still images of rheoscopic fluid under rotation inside the fouling rector with a PMMA body. a: 100rpm (1.67 s^{-1}), b: 200 rpm (3.33 s^{-1}), c: 400 rpm (6.67 s^{-1}), d: 750 rpm (12.5 s^{-1}), e, 1500 rpm (25.0 s^{-1}), f: 2500 rpm (41.7 s^{-1}). (Note: flange bolts in the wall -body are visible but not in the flow path) 117
Figure 6.5 Temperature profile of a 6-hour commissioning experiment with n-dodecane as the test fluid. Wall Temperature is maintained at 320 °C. Wall temperature T_{wall}, Bulk fluid temperature $T_{bulk,}$, Furnace set temperature $T_{furn\text{-}set}$ are displayed on the left vertical axis while the temperature difference between the wall and the bulk fluid ΔT is given on the right axis. 120
Figure 6.6 Temperature profile of the first 100 minutes of the earlier 6-hour experiment at 320 C. Wall temperature T_{wall}, Bulk fluid temperature $T_{bulk,}$, Furnace probe temperature T_{furn} are displayed on the left vertical axis while the wall/bulk temperature difference ΔT and the wall heating rate dT_{wall}/dt are given on the right axis. 121
Figure 6.7 Close-up of the steady state temperature profile the earlier 6 hour commissioning experiment at 320 °C. Wall temperature T_{wall} and Bulk fluid temperature $T_{bulk,}$ are displayed on the left vertical axis while the temperature difference ΔT is given on the right axis. 122
Figure 6.8 Temperature profile of the last 240 minutes of the earlier 6-hour experiment at 320 C. Wall temperature T_{wall}, Bulk fluid temperature $T_{bulk,}$, Furnace probe temperature T_{furn} are displayed on the left vertical axis while the wall/bulk temperature difference ΔT and the wall heating rate dT_{wall}/dt are given on the right axis. 122
Figure 6.9 Pressure-time profile for typical experiments with dodecane and 1-methylnaphthalene at 300°C and 1500 rpm. 124
Figure 6.10 Photos of the reactor wall surface after draining and rinsing with chloroform leaving the insoluble foulant adhered to the wall surface. Image A: experiment CR-03 after draining oil from the

reactor leaving behind the oil film and deposits Image B: - experiment CR-03 after rinsing with chloroform: salt deposits are clearly visible from the unprocessed crude oil. 126
Figure 6.11 Electrical Conductivity of residual water on repeated desalting of H:L crude blend 127
Figure 6.12 ICP-OES analysis of metal ions removed from crude oil in desalting water milligrams per litre of crude oil 128
Figure 6.13 A: (experiment CR-04) Reactor wall after repeat of the experiment under the same conditions but using desalted oil. Deposits are carbonaceous and salts are no longer visible. B: (experiment CR-05) Reactor wall after draining and rinsing with remaining chloroform. As a result of higher temp. and rotation speed, deposit rings are no longer apparent 129
Figure 6.14 Masses of chloroform insoluble foulant on for a repeatability study of crude oil at 320°C for 6 hours, 1500 rpm and 30 bar pressure 131
Figure 6.15 Masses of chloroform insoluble foulant on for the second repeatability study of crude oil at 320°C for 6 hours, 1500 rpm and 30 bar pressure, after changes to the cleaning method were applied 132
Figure 6.16 Modifications to reactor cell to enable inner wall surface analysis 133
Figure 7.1 Deposit mass as a function of blend composition: crude oil blend composition, in both total mass (mg) and miligrams of fouling per square meter of wall surface mg m^{-2} 137
Figure 7.2 Insoluble deposit masses for crude oil fouling experiments at 6, 12 and 24-hours including error bars. Total insoluble solids in wall and film was 15.0mg for 6 hours, 21.6 mg for 12 hours and 22.7 mg for 24-hour residence times. 140
Figure 8.1 Insoluble fouling deposits recovered from reactor for experiments ranging from 5% to 20% asphaltenes by weight dissolved in 1-mehtylnaphthalene. Logarithmic trends are plotted for the wall and film deposits, while total deposits (including those extracted from the bulk) scale approximately linearly so is plotted with a linear trend line. 144
Figure 8.2 Scatter plot of insoluble fouling deposits for solutions of 5% asphaltene. The solvents were binary mixtures of n-dodecane and 1-methylnaphthalene in varying proportions. Mean deposit masses for each composition are plotted as lines of the same colour. 146
Figure 8.3 Photographs of reactor interior walls after rinsing film with chloroform. Dodecane mass fractions (w_{dod}): a=0, b=0.5, c=0.6, d=0.67, e (no flash) & f (flash) =0.75. 147
Figure 8.4 Visible carbonaceous fouling adhered to rotor 5% asphaltene, w_{dod} = 0.75 148
Figure 8.5 Scatter plot of fouling deposit mass for dodecane/maltene mixtures. Mean deposit masses for each composition are plotted as lines of the same colour. 149
Figure 8.6 Scatter plot of deposits mass (mg) divided by mass of maltene starting material (g). Mean deposit masses for each composition are plotted as lines of the same colour. 149

Figure 8.7 SEM micrographs of a) the inner wall surface of an unused carbon steel sleeve, b & c) carbanaceous deposits from 3:1 Dod/malt mixture in different locations 151
Figure 9.1 Synthesis of 1-bromopyrene and 1-alkylpyrenes via 1-bromopyrene` 155
Figure 9.2 Reaction mechanism for the alkylation of 1-bromopyrene via lithium halogen exchange 155
Figure 9.3 Synthesis of Perylene diimides (N,N'-Bis(3,5-dimethylphenyl)-3,4,9,10-perylenetetracarboxylicdiimide - PDI-DMI, PDI-C3 – N,N'-bispropyl-3,4,9,10-perylenetetracarboxylic diimide, N,N'-bisdodecyl-3,4,9,10-perylenetetracarboxylic diimide – PDI-C12) from perylene tetracarboxylic dianhydride (PDA) 157
Figure 9.4 Solubility tests of perylene based compounds in various solvents 158
Figure 9.5 Temperature dependence of PDI-C12 solubility in 1-methylnaphthalene 159
Figure 9.6 Total deposit fouling masses in for PDI-C12 solutions 161
Figure 9.7 Fouling deposits visible on the reactor wall a) after draining from the cell and b) rinsing with chloroform leaving a cream residue. Fouling deposits are uniformly adhered to all outer surfaces resulting in elevated surface roughness 162
Figure 9.8 FTIR ATR Sectra for PDI-C12 and its fouling deposits 162
Figure 9.9 Fouled inner sleeve following heated fouling reaction with PDI-C12 in 1-methylnaphthalene for 12 hours at 320 °C. The left half has been fully washed with $CHCl_3$ until no red PDI-C12 starting material is visible. The right half was washed with heptane. The squares represent areas of the wall section which were cut out for SEM imaging 164
Figure 9.10 a-d Scanning Electron Micrograph of the PDI-C_{12} fouled surface. a) and b) show partially washed sleeve wall surface near the top of the reactor and c) and d) show the fully rinsed wall surface in the central section of the reactor sleeve 165
Figure 8.10.1 Branched alkyl substituted perylene diimide with good reported solubility 172
Figure 10.2 Naphthene diimide and tetrahydro-2,7-diazapyrene synthetic route from 1,4,5,8-naphthalene-tetracarboxylic dianhydride (molecular structures from Langford et al.189) 173

Symbols

β	Thermal expansion coefficient
ε	roughness height
η	radius ratio
ν	kinetic viscosity
ρ	Density
τ_w	wall shear stress
φ_{asp}	Volume fraction of asphaltene
ω	*angular velocity*
Γ	Aspect ratio
L	Length
ω	angular velocity

List of Abbreviations

d	cylindrical gap thickness
f_D	Darcy-Weisbach friction factor
u	(linear) velocity
u_{R1}	linear velocity at the rotor surface
$\bar{x}$	mean
D_h	Hydraulic diameter
G	Dimensionless torque
M_i	mass fraction of species i
R	Radius
Re	Reynolds number
Re_t	Tangential Reynolds number
P	Pressure
S_i	Solvent (i)
S_p	Cross-sectional area
T	Temperature
Ta	Taylor number
Ta_c	Critical Taylor number
V	Volume
ASTM	American Society for Testing and Materials
CII	Colloidal instability index
CNAC	critical nanoaggregate concentration
CVD	Chemical vapour deposition
Da	Daltons
DI	Deionised
Dod	n-dodecane
ESI	Electrospray ionisation
EDX	Energy dispersive x-ray (spectroscopy)
FID	Flame ionisation detector
FCS	Fluorescence correlation spectroscopy
FT-ICR	Fourier transform ion cyclotron resonance
FTIR	Fourier transform infra-red (spectroscopy)
HOMO	highest occupied molecular orbital
HCl	Hydrochloric acid
HRTEM	High Resolution Transmission Electron Microscopy
HLPS	Hot liquid process simulator
HPLC	High performance liquid chromatography
ICP	Inductively Coupled plasma
LDI	Laser desorption/Ionisation
LUMO	Lowest unoccupied molecular orbital
Malt	Maltene
MO	Molecular Orbitals
MS	Mass Spectrometry
MN	1-methylnaphthalene
NMR	Nuclear magnetic resonance

OES	Optical emission spectroscopy
PAH	Polyaromatic hydrocarbons
PHT	Preheat Trains
PDA	Perylene tetracarboxylic dianhydride
PDI	Perylene tetracarboxylic dicarboximide
PDI	N,N'-Bis(3,5-dimethylphenyl)-3,4,9,10 -perylene tetracarboxylic diimide
PDI-C_3	N,N'-bispropyl-3,4,9,10-perylene-tetracarboxylic diimide
PDI-C_{12}	N,N'-bisdodecyl-3,4,9,10-perylenetetracarboxylic diimide
PDI-C_{13}	N,N'-ditridecyl-3,4,9,10-perylenetetracarboxylic diimide
PTFE	Polytetrafluoroethylene
SE	Standard error
TCD	Thermal conductivity detector
TGA	Thermogravimetric Analysis
TEM	Transmission electron microscopy
TLC	Thin Layer Chromatography
TRFD	Time-resolved fluorescence depolarization
VPO	Vapor pressure osmometry
LIAD	Laser-induced acoustic desorption
WAT	Wax appearance temperature

Wall solids	Chloroform-insoluble deposits adhered to the wall surface
Film solids	Chloroform-insoluble deposits recovered from wetted film of the drained fouling cell
Bulk solids	Chloroform-insoluble deposits recovered from drained bulk fluid inside fouling cell

Chapter 1 Introduction

1.1 Energy outlook and Crude oil

World demand for energy is expected to grow between 0.3-0.7% per annuum between 2018 and 2050[1], and when forecasting oil demand over a period of decades ahead, multiple models need to be used. A number of outcomes are possible, as major global political efforts to decarbonise and transition away from reliance on coal, oil and gas as primary energy sources contrast against the rapid growth of demand from developing nations. The refence model of Global Downstream Liquids is predicted by McKinsey predict demand in 2050 to be approximately equal to that in 2020[2], whilst delayed transition scenarios place demand 15% higher than the current level, and an accelerated transition could see demand fall 22% from the 2020 level. Whilst significant efforts are being made to reduce global demand, transitioning current infrastructure to renewables will be a slow and lengthy process, and the demand for oil derived materials such as asphalt petrochemicals are unlikely to be impacted. Most striking to observe is the significant volatility in oil price. 2020 saw short-dated futures prices go negative (-$37.63) for the first time in history[3] and as supply outpaced buyers with facilities to store oil since demand collapsed as a result of the Covid pandemic and associated lockdowns. Over the following two years, Brent oil climbed back above $100/barrel, due economic normalisation and lately, geopolitical disruption due to Russia's invasion of Ukraine and restriction of hydrocarbon supplies to Western countries[4].

Whilst oil is projected to remain an intrinsic part of the global energy mix and important material feedstock, oil producers remain at the mercy of market forces, and often struggle to achieve consistent profits in a world where disruptive technology, consumer emotions and a changing political environment can turn favour away from conventional oil production. With the uncertainty this brings, improving process efficiency will remain a necessity to achieve profitability.

Many crude oil feedstocks in production such as heavy and sour crudes are associated with numerous processing difficulties. These oils are more viscous, and exhibit less stable phase behaviour when processing at high temperature, with a tendency to foul in the PHT heat exchangers. This has an enormous economic and environmental impact. Typically, heavy and sour crude oils are blended with lighter compatible oils to try to achieve a chemically stable feedstock with moderate rheological properties that allow for better processing characteristics. However, fouling remains a stubborn problem in the downstream oil industry.

1.2 Economic and Environmental Impact from Crude Oil Fouling

The overall impact to profitability and the environment is substantial. In 1995, Müller-Steinhagen estimated of the equivalent cost of heat exchanger fouling related costs to be $14bn (US currency at time of publication) in the United States alone[5]. The current economic cost is likely to be significantly greater. These costs arise from the following effects:

Energy Losses – Amorphous deposits build-up on heat exchange surfaces lowers the heat transfer coefficient and increases the effective thickness through which heat must flow across, resulting in a reduced overall heat transfer rate. In addition, the constricted tube cross section and increased surface roughness on the pipe surface results in a greater pressure drop[6] along the PHT and therefore more energy is required to pump oil through the process line. Consequentially more fuel may be consumed at the furnace to compensate for lost heat in the exchangers.

Environmental Impact – greater energy requirements for heating and pumping translates into greater CO_2 emissions for the refining process, and cost associated with those emissions (carbon credits). It was estimated in 2009, that 88 million tons of CO2 is emitted annually due to operational efficiencies due to fouling[7]. Cleaning also produces large quantities of contaminated waste which must be disposed of carefully, which itself represents significant cost.

Production Losses and Heat Exchanger Cleaning – Scheduled cleaning operations are usually contracted to independent firms at substantial cost and require periodic shutdown of the process line, resulting in loss of output and thus profitability. There is also additional cost with oil refining at sub-optimum conditions during the restart process.

and Maintenance Costs – Significant capital and maintenance expenses are associated with replaced tube bundles, heat exchanger repair, extra space requirements, anti-fouling equipment and additives, transport, and installation costs, and heat-exchanges are often overengineered to allow for fouling inefficiencies which develop during use.

1.3 Crude oil Preheat train Overview

Crude oil fed from storage tanks goes through several stages before it reaches the furnace for distillation. The PHT is the section of the process where crude oil is heated from ambient temperature

to between 230 – 300°C before being reaching furnace for distillation (Figure 1.1) The latter stage of the preheat train is where this research in fouling behaviour is focused.

Crude oil from storage tanks is fed into the process line at ambient conditions, passes through early stage heat exchangers (*E1* and *E2)* which use waste process heat further downstream in the refinery to raise the oil temperature to around 110-150 °C before reaching the desalter, where the oil is contacted with water to break any water/oil emulsion and remove dissolved salts which are extracted into the aqueous phase. Other inorganic species such as particulate matter (sludge), clays and sand present are also removed here. The oil then passes through a second train of heat exchangers to heat the crude oil to between 230 and 300 °C before reaching the furnace. It should be noted as illustrated in the diagram, that the hot stream entering the heat exchangers is not necessarily arranged by increasing temperature, but often matched to heat load and/or accessibility of the hot stream[8].

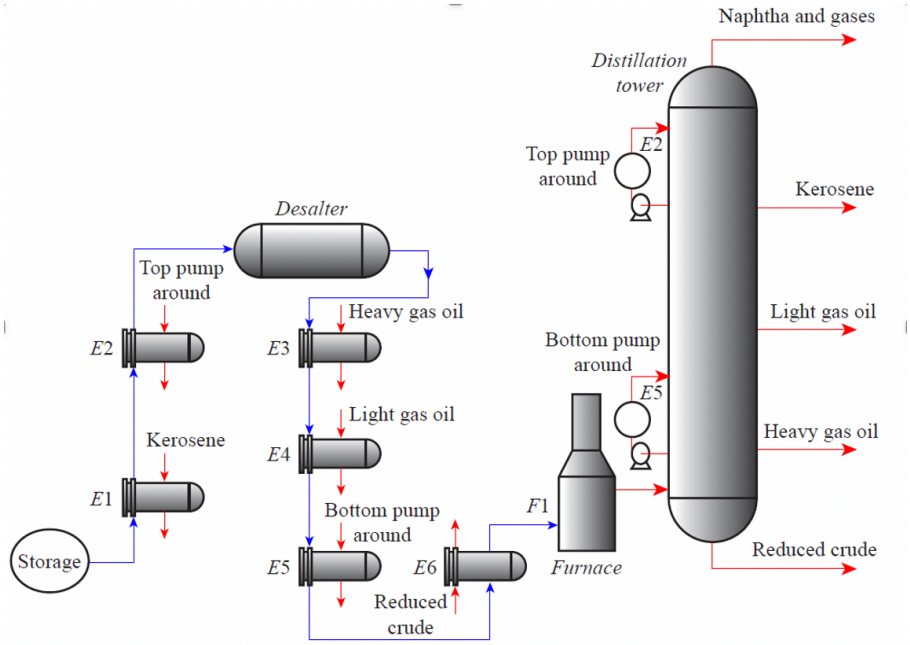


Figure 1.1 Simplified flow diagram of a typical crude oil distillation unit (Panchal and Huang Fu[9])

The type of fouling prevailing in the heat exchangers depends on its position along the heat exchange train. In the early heat exchangers *E1* and *E2*, the oil is at low temperature, and therefore sedimentation of inorganic silts and other particles, and crystallisation fouling from waxy constituents are likely, whilst thermally induced fouling is minimal. At low temperatures the viscosity is higher and therefore shear stress is higher at these regions, whilst momentum transfer is lower.

Downstream of the desalter unit, thermal effects begin to impact the oil, colloidal stability decreases at higher temperature which can result in aggregation and agglomeration of larger constituents such as asphaltenes and leading to precipitation at the wall surface of the heat exchanger tubes, corrosion

and other chemical reaction fouling at the wall surface is also more likely at higher temperatures. Fouling on the hot side of heat exchangers may also be a problem, especially on the shell side, where flow rates are lower.

As fouling deposits build up in the preheat train, the thermal and hydraulic efficiency of the system decreases, which results in the process oil arriving at the furnace at a lower temperature. Thus the furnace has must compensate for this by burning more fuel to raise the oil to distillation temperature, otherwise, the flow may need to be throttled to maintain operational conditions in the distillation unit. Distillate production volumes are reduced while fuel consumption is higher, negatively impacting system profitability. When operational conditions deteriorate sufficiently, heat exchanger units or even the distillation may need to be taken offline for cleaning depending on the refinery configuration, (also a costly and hazardous operation). Heat exchanger cleaning process and scheduling is in itself a matter for research and optimisation[10].

1.4 Research Objectives

This work is centred around the physicochemical properties of crude-oil and their fractions, and high temperature fouling processes that occur in PHT heat exchangers. The general aim of this research is to augment current understanding of fouling processes, provide greater insight into factors that affect fouling, and investigate how the chemical structure, composition and functionality affects fouling behaviour.

1. *Design, Construct and Commission a new fouling apparatus for studying crude oil fouling.*
   A laboratory scale apparatus to be constructed that allows for controlled processing of oils and other fluids at elevated temperatures which reflect PHT heat exchanger process conditions. In doing so, it will be necessary to develop a standard operation procedure and methods for sample preparation, recovery, cleaning, and product characterisation. The system must exhibit good control characteristics and be capable of producing repeatable data.
2. *Characterise the supplied crude oils and fractions thereof and provide a method for preparations of oils for use in fouling experiments*
   Fractionate the crude oil into maltenes and asphaltenes, characterise crude oils and their fractions using analytical techniques, develop methods for desalting and blending.
3. *Test the fouling characteristics of crude oils in a range of process conditions*.
   Prepared Crude oil blends are to be tested for fouling in the apparatus, considering the effect of process conditions and blend ratio. Deposits are to be characterised using analytical

techniques such as TGA and FTIR and the relationship between the oil blend/test conditions and the nature and amount of fouling deposits should be described.

4. *Prepare solutions of asphaltenes and maltenes in high boiling temperature solvents and investigate fouling behaviour of these solutions*

   Model oil solvents should be selected with chemical and physical characteristics representative of the oils from which they came, also considering the classically defined SARA oil solubility fractions. Solvent selection must take into consideration boiling temperature, reactivity, and rheological properties. Fouling experiments will be conducted to investigate the effect of solution composition on fouling behaviour. The masses of fouling deposits should be measures and nature of the deposit characterized and compared with those derived from crude oil blends performed earlier.

5. *Synthesis of model asphaltene compounds, solution properties and fouling experiments using model asphaltene solutions*

   Model asphaltene targets are to be selected, synthesised, characterized, and prepared as solutions in suitable high boiling-point solvents for fouling experiments. Fouling experiments of the synthetic model-asphaltene solutions are to be performed and validated for use as synthetic crude oil models in fouling research. The nature and amount of any fouling deposits should be compared with those produced by fractionated oil solutions and natural crude oil blends.

6. *Use the output of the experimental fouling work to describe the learning outcomes from the presented research*

   Describe the main findings from experimental work and evaluate of the effectiveness of the research approach and evaluate the appropriateness of synthetic and modified solutions as models for natural crude oil blends, making recommendations for further study.

1.5 Structure of the thesis

The thesis is composed of nine chapters:

Chapter 1 Introduces the problem and the impact on the industry and the environment, with the scope and aims also provided here.

Chapter 2 provides a detailed background and literature review on crude oil composition and phase behaviour, fouling phenomena and mitigation strategies.

Chapter 3 outlines the design specification for the necessary fouling apparatus, giving examples of prior designs used within the research group. The design and construction are presented here along with predictive a model of the test fluid hydrodynamics during operation.

Chapter 4 describes experimental methods employed relating to the desalting, blending and fractionation of crude oils, the standard operating procedure for the fouling apparatus, product recovery and cleaning procedure. The analytical techniques employed in this work are also outlined here.

Chapter 5 presents the commissioning trials of the fouling apparatus using both non-fouling and fouling fluids, focusing on velocity calibration, hydrodynamics visualisation, thermal effects and experimental repeatability.

Chapter 6 explores the chemical and physical properties of the BP supplied crude oils and the asphaltenes and maltenes fractionated from the heavy crude. Characterisation is achieved through various analytical techniques including pycnometry, Elemental analysis, GC simulated distillation, TGA, UV-Vis and FTIR spectroscopy.

Chapter 7 presents experimental fouling of crude oil blends, exploring the effect of process conditions and composition (heavy:light oil blend ratio) on production of deposits on the reactor wall surface.

Chapter 8 investigates solutions of asphaltenes and maltenes in two high boiling temperature solvents, 1-methylnaphthalene and n-dodecane. Fouling experiments are presented, exploring the effects of asphaltene concentration in 1-methylnaphthalene, solution stability in binary mixtures of 1-methylnaphthalene and n-dodecane, and solution stability of maltenes/dodecane mixtures.

Chapter 9 presents the synthesis and characterisation of proposed model asphaltenes based on alkyl-pyrenes and perylene diimides. Solubility of model asphaltenes are investigated in a range of solvents, and fouling experiments are presented.

Chapter 10 presents the conclusions from this work and recommendations going forward for further research.

Chapter 2 Background/Literature Review

2.1 Chemical composition of crude oil

Crude oil, is a complex ill-defined mixture principally of hydrocarbon organic molecules that derive from the controlled transformation of degraded organic matter fixed in a geological formation over time. From and elemental breakdown, crude oil has a fairly narrow composition range: see Table 2.1.

Table 2.1 Typical elemental composition of crude oils (data from Mullins et al.[20])

Element	Typical Composition (%)
Carbon	83 – 87
Hydrogen	10 – 14
Nitrogen	0.1 – 2.0
Oxygen	0.05 – 1.5
Sulfur	0.05 to 6.0
Metals	<1000 ppm

However, these elements give rise to a vast number of complex chemical structures. For example, using powerful FT-ICR mass spectrometry[11], over 100,000 different compounds can be identified in given crude oil sample[12], and thus consequentially the range of physical properties that derives from different oil sources can be immensely varied. This makes the chemical composition of an oil sample difficult to describe.

One of the challenges in understanding the complex interactions that occur in oil at high temperatures is the necessity to first understand the chemical composition of the oil which is undergoing the high temperature processing. This is itself is a formidable task, as crude oil is both highly complex and highly variable in composition in different geological locations, age even depth of an individual well. Oil recovered from these formations may also differ depending on the extraction technique.

2.2 SARA fractionation analysis

A frequently used method of describing crude oil composition is by fractionation according to solubility class. One classical method for characterising crude oil constituents is the SARA

fractionation analysis. In this method, crude oils are separated into 4 major groups by means of their polarity and polarizability, and SARA acronym represent the four fractions which derive from this method: Saturates, Aromatics, Resins and asphaltenes (see Figure 2.1). These groups roughly describe the chemical structure and functionality (as described in Table 2.2); however, as it is a solubility-based separation the boundaries are not rigidly defined. The separation methodology is outlined below (ASTM D6560, ASTM D2007)[13]:

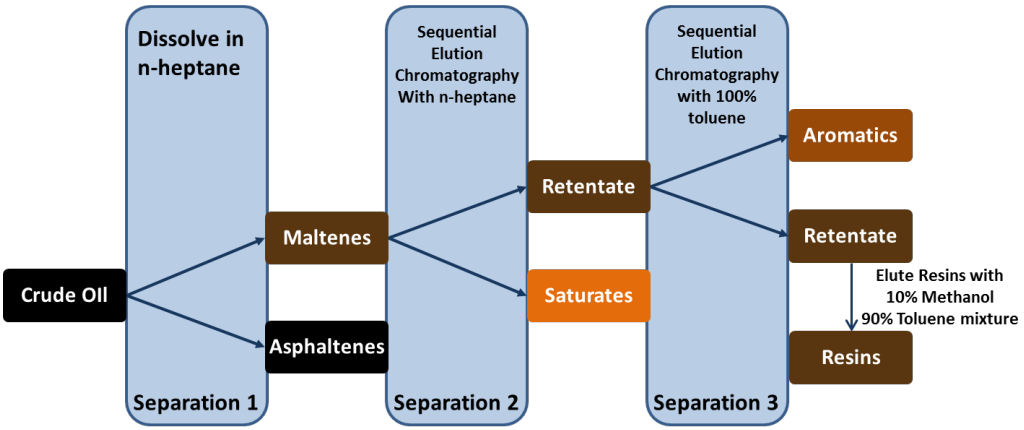
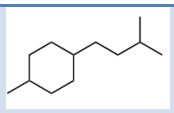
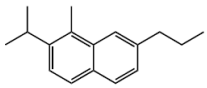
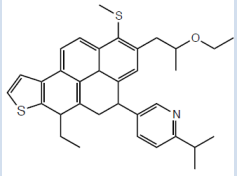
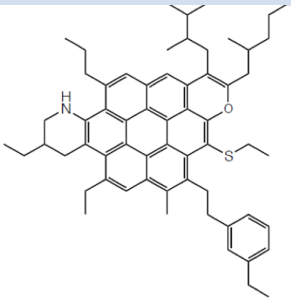


Figure 2.1 Laboratory SARA separation process

First, crude oil is dissolved in n-heptane under reflux and hot filtered. The washed and dried residue left behind is the asphaltene fraction. The solvent is then removed from the filtrate by rotary evaporation to leave behind the n-heptane soluble maltene fraction.

The maltene fraction contains the saturates, aromatics and resins, which may then be separated by sequential elution column chromatography on a silica or clay gel bed. First the maltene fraction is eluted first using n-heptane. The eluent is the saturates fraction and the remaining column adsorbed fraction contains the aromatics and resins. Next the solvent is switched to toluene which elutes the aromatics fraction. The remaining retentate (resins) is then finally eluted with a 10:90 methanol:toluene mixture. A number of alternative separation methods are known in the literature including Thin Layer Chromatography with Flame Ionisation Detector (TLC-FID) and high-pressure chromatography (HPLC)[14], although each technique produces slightly different fractionations[15]. Sometimes, the asphaltenes are separated using refluxing n-pentane instead of n-heptane. They are called C5-aspahltenes and C7-aspahltenes respectively.

Table 2.2 Typical average properties of SARA fractions

Fraction	Typical Molecular weight	Polarity	Aromatic	Other	Hypothetical Structure
Saturates	~ 100 - 400	Non/Low	No	Cyclic & Aliphatic	
Aromatics	100 - 500	Low/Med	Yes 1 or 2 rings	Benzene & Derivatives	
Resins	250 - 750	Med/High	yes Med/Large PAHs	Contains Heteronuclear Atoms	
Asphaltenes	500 - 1000	High	6-10 aromatic rings 1 PAH on average	High Heteronuclear Content	

2.2.1 Saturates

Saturates are the least polar group of compounds derived from crude oil. They are soluble in n-heptane but not in aromatic solvents and generally contain saturated aliphatic hydrocarbons. Their structure may contain cyclic (napthenic) and acylic alkanes (paraffinic) with or without branching. They typically do not contain aromatic or double bonds, however as this is a solubility separation some may be present. They typically represent the lightest average molecular weight; however long chain paraffinic waxes are also found in this class.

2.2.2 Aromatics

The aromatics are the fraction which elutes from silica gel in toluene but not n-heptane. They generally contain aromatic substituents and thus have delocalised pi electron making them more polar than the Saturates fraction. They may also contain aliphatic groups, or heteroatoms such as sulphur, nitrogen and oxygen.

2.2.3 Resins

Resins are the retentate left adhered to the gel column after eluting with n-pentane and toluene. This greater affinity to the gel column is a result of their greater polarity, and resins tend to contain multiple

aromatic groups which may be fused (clustered) together, and generally contain a higher proportion of heteroatoms than the aromatic fractions and have a higher average molecular weight than the former category.

2.2.4 Asphaltenes

These are the organic fraction which is insoluble in hot n-pentane but soluble in hot toluene, as defined by the ASTM[16]. They are the most polar class of compounds hence their insolubility in non-polar solvents. They are also the largest and chemically most diverse class of compounds, generally containing extended fused aromatic ring networks with peripheral alkyl substituents, often numerous heteroatoms and can contain electrostatically coordinated metal ions. Their pi aromatic cloud extends over a large area of the molecule and asphaltenes have a strong tendency to attract to each other leading to aggregation and agglomeration, leading to precipitating out of the oil leading to fouling. For this reason, asphaltenes have been the focus of extensive research to understand how high temperature processing of crude oil can lead to instability and fouling.

2.3 Asphaltene structure

Characterising asphaltenes is not a simple task, due to their vastly variable chemical structure and tendency to aggregate, often giving rise to false interpretations of size, molecular weight and chemical properties[17]. Molecular weight has previously been estimated at anything between 400 to 10^9 Da![18] Asphaltenes have a significant effect on the behaviour of crude oils and thus a good understanding of their chemical and physical properties is important.

2.3.1 Island and archipelago models

For considerable time, the size of asphaltenes and aspects of their structure remained debated. Two models were proposed, the Island model in which asphaltenes are small monomeric molecules with predominantly only one PAH centre and pendant alkyl moieties, or the archipelago model whereby several PAH moieties were linked together by their alkyl substituents.

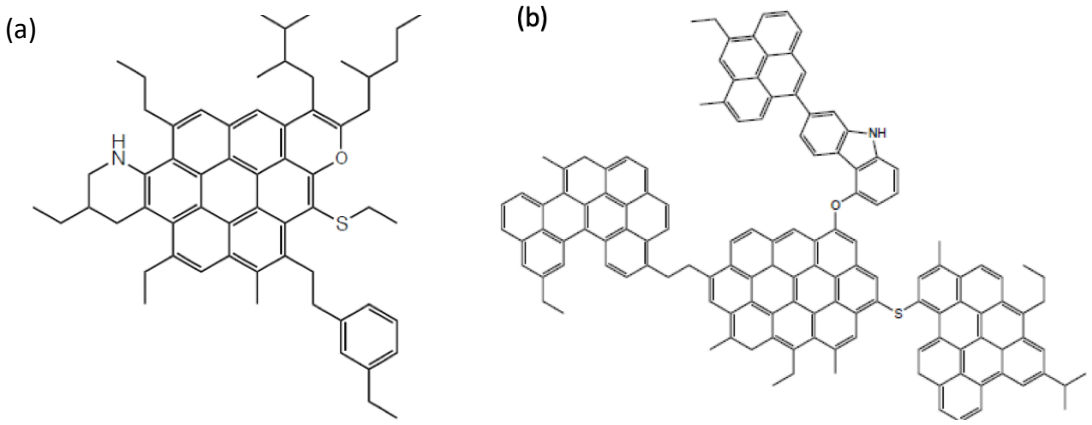


Figure 2.2 Hypothetical Island (a) and Archipelago (b) model asphaltene structures

2.3.2 Asphaltene/oil phase behaviour - The modified Yen model

The Yen model was developed in 1967 in order to describe the structural features in asphaltenes such as fused aromatic ring groups (or polycyclic aromatic hydrocarbons - PAHs), alkyl substituents, porphyrins moieties and PAH stacks. Development of the model to include colloidal properties and physical behaviour led to the modified Yen Model[19] (see Figure 2.3).

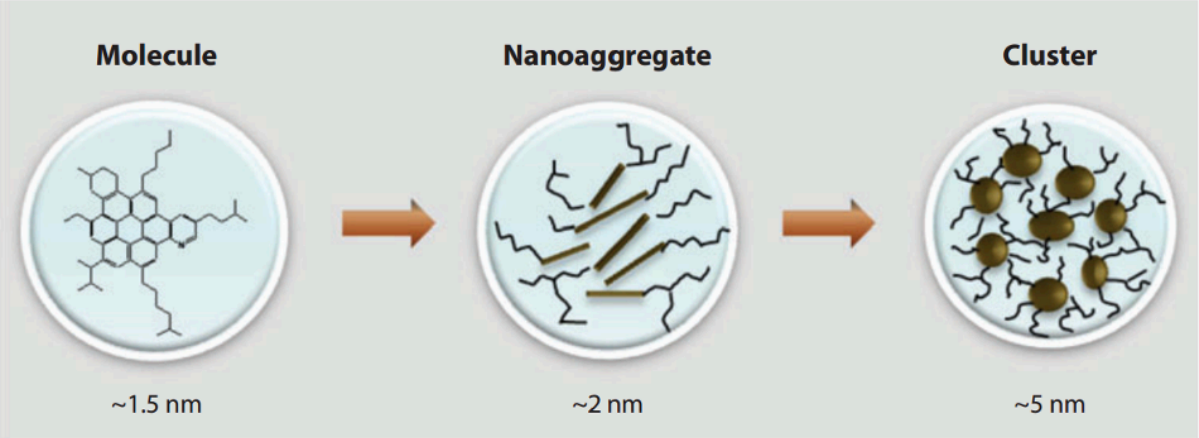


Figure 2.3 The Modified Yen Model (from Mullins[17]) This depicts from single asphaltene molecules (approximate diameter 1.5 nm), aggregation leads to nanoaggregates (appoximate diameter 2 nm) which in turn aggregate together to form asphaltene clusters

Asphaltenes molecules contain large PAH moieties. At very low concentrations they exist as individual monomers in solution; however, in order to reduce their free energy, the aromatic regions tend to order together while the peripheral alkyl substituents extend out into the continuous phase. The entropy gains from mixing outweigh the thermodynamic gains from association.

In higher concentrations, the addition of an antisolvent or changes in the physical conditions, the entropy of mixing is not sufficient to overcome the thermodynamic gains from pi-pi association. Above a certain concentration or critical nanoaggregate concentration (CNAC), individual monomers stack together in order to lower their free energy, forming nanoaggregates of an average of 5 monomers. They do not behave like surfactants[20] due to the multiple substituents around the PAH centre. It is also incorrect to describe asphaltenes aggregates as micelles, as this implies a finite aggregation number, instead asphaltene clusters grow as dimers, trimers etc.

At still less favourable conditions, the nanoaggregates themselves flocculate together to form clusters of 6 nanoaggregates on average. The formation of large clusters eventually leads to phase separation, where they precipitate as a highly viscous semisolid phase, where they behave as fractal colloidal structures because their high viscosity prevents them from condensing into lower surface area morphologies[21,22]. This semisolid asphaltene phase is thermodynamically a liquid (or glass) with the solvent incorporated into the phase (in certain conditions or at high temperatures) and exhibits coarsening and coalescence rather than colloidal aggregation[23]. Coarsening or digestion occurs when fresh precipitates from an unstable solution in its precipitating solvent grow while smaller particles shrink and disappear, it is a thermodynamic process that minimises the surface energy if those precipitated particles and is analogous to Ostwald ripening in emulsions.

2.4 Effects of asphaltenes on viscosity

It is well known that dispersions of solid particles in a liquid have a significant impact on fluid viscosity. Likewise, asphaltene concentration has been found to have a profound effect on crude oil viscosity[24]. Gu et al. studied the effects of asphaltene concentration on viscosity of reconstituted crude oils that had first been fractionated by n-heptane precipitation in the range of 0 – 16 % by weight. He found three regions of viscosity behaviour. For this particular system, low volume fractions ($\varphi_{asp} < 0.065$) the relative viscosity increases slowly with volume fraction, the interactions between asphaltenes are minor and increased viscosity is associated with long range hydrodynamic interactions between asphaltenes and the maltenes. Then in the range of $0.065 < \varphi_{asp} < 0.122$, the short range asphaltene inter-particle interactions become more pronounced, and viscosity against φ_{asp} deviated from its linearity and viscosity increases at a higher rate. The deviation is more pronounced at lower temperatures. At $\varphi_{asp} > 0.122$, the asphaltene fraction increases the most quickly and is very temperature sensitive with an inverse relationship. The asphaltene particles become entangled at high volume fractions and the strong inter-particle interactions are evident but the increased viscosity dependency on φ_{asp} and temperature. Whilst these findings are very useful for understanding how

composition and temperature affect the phase behaviour little is known experimentally of the phase behaviour at high temperature.

Non-Newtonian behaviour has been observed in crude oils containing high wax or asphaltene content[25,26]. Shear thickening is a common behavioural trait of colloidal systems and stabilised suspensions as is the case with high asphaltene crudes. Heavy oils behave as viscoelastic materials, and therefore shear modulus and the viscosity are coupled. Shear thinning has also been observed for heavy oils at low temperature and high shear rates[27].

2.5 Asphaltene solubility and colloidal stability models

Asphaltenes, by definition, are a solubility class. They are soluble in toluene but insoluble in n-heptane. As such there is a balance of forces that is dictated by the chemical interactions between asphaltene molecules and the solvent. In stable solvated asphaltene oil solutions, the attractive force of the π-ring stacking behaviour of the aromatic groups is balanced by the steric hindrance and solvation enthalpy of asphaltene aliphatic substituents in the surrounding solvent preventing agglomeration in stable systems. Without asphaltenes' aliphatic substituents, such π-bonding attractions would result in aggregation leading to precipitate out in solutions with lower aromaticity. Temperature and pressure are also critical to asphaltene stability; depressurisation on extraction may also precipitate asphaltenes in some oil solutions.[28]

Fogler et al. explained the effect of temperature on solubility of asphaltenes as the product of two competing factors[29]. First, the higher kinetic energy overcomes the asphaltene intermolecular interactions and solubility increases. This would lead to fewer nanoaggregates at higher temperature, the second is a result of the variation of liquid composition upon heating. The thermal expansion of the lighter solvent fractions reduces the solubility parameter of the mixture decreasing the solubility of the asphaltenes so overall, at higher temperature, asphaltenes are less soluble as has been observed in precipitation studies[29]. Lambourn et al. reported a solubility maximum of asphaltenes at 140 ˚C which then declined at higher temperatures[30].

SARA fraction oil stability models

Several models for crude oil stability have been defined in the literature based on the relative weight percent of SARA solubility fractions[31]. The simplest being the Stability Index (SI) based on the mass ratio of asphaltenes:resins. Oils with SI > 0.35 are generally considered unstable.

Colloidal instability index (CII)

A more widely used approach to assess crude oil stability assumes oil to be stabilised in colloidal systems. This uses the Colloidal Instability Index (CII), as suggested by Yen et al. This method considers the weight percent of each of the four SARA fractions, applying the general hypothesis that in a given crude oil sample, higher concentrations of asphaltenes and saturates are destabilising, whereas higher concentrations of Aromatics and Resins are stabilising. Saturates are a poor solvent for asphaltenes since the non-polar molecules do not pi-coordinate to the asphaltenes, whereas aromatics and resins do π-coordinate to and stabilise the aromatic cores of asphaltenes.

$$\mathrm{CII} = \frac{\text{Saturates (\%)} + \text{Asphaltenes (\%)}}{\text{Aromatics (\%)} + \text{Resins (\%)}} \qquad 2.1$$

CII has been extensively applied for crude oil blending. Higher index suggests a lower stability. Asomaning and Watson defined that above 0.9 is generally considered unstable, crude oils with CII ≤ 0.7 are considered stable and those with CII = 0.7 – 0.9, have uncertain stability.[32] CII should however be applied in conjunction with other empirical analysis and may not be applicable to some oils. For example, those with no asphaltenes may have a high CII and still be stable. This model also does not consider changes in stability under different physical conditions. It should also be noted that since SARA fractionations are a solubility class, the compositions of asphaltenes from different oil origins may have very different properties and may behave unexpectedly at high temperature.

Colloidal stability index (CSI)

The CSI is a development of the above CII model, and additionally factors in the polarity of the components of oil.[33] The model assumes that unstable oils are likely to be more polar than those that are stable using dielectric constant (ε) of each of the SARA fractions.

$$\mathrm{CSI} = \frac{\varepsilon^{sat} \times \text{Saturates (\%)} + \varepsilon^{asp} \times \text{Asphaltenes (\%)}}{\varepsilon^{aro} \times \text{Aromatics (\%)} + \varepsilon^{res} \times \text{Resins (\%)}} \qquad 2.2$$

where ε^{sat}= 1.921, ε^{asp}= 5.5, ε^{aro} = 4.7, ε^{res} = 2.379

2.6 Heteroatom effects

2.6.1 Heteroatoms present in crude oils

Nitrogen, oxygen, sulphur, and a number of metals are naturally present in crude oil as well as carbon and hydrogen as shown in Table 2.1. Several species may lead to fouling by deposition/precipitation or reaction. Many species increase the polarity of organic molecules (sulphur has a negligible effect)

and many metals, metal oxides, sulphides and carbides potentially present in the PHT lines may act as active catalysts and contribute to fouling, however just as important as the elemental content is the location and form in which heteroatoms exist. A recent molecular dynamics simulation study by Ramirez et al. found that replacement of carbon atom the asphaltene polyaromatic core with a single heteroatom (S, N or O) showed a higher aggregation tendency, increasing the planarity and polarity of the aromatic cluster and increasing the interaction energies with other asphaltene molecules.[34] Sulphur was found to form larger more stable aggregates than oxygen and nitrogen atom replacements.

Sulphur – often the most abundant heteroatom in crude oil but may vary considerably in occurrence, from 0.5 – 6 % by weight. Marine crudes often have high sulphur content (4.5% or more) and many oils must be desulphurised to meet European standards for use as liquid fuels[35]. The sulphur may be organic (thioethers, or aromatic such as thiophene moieties), or inorganic such as hydrogen sulphide gas dissolved in oil which is both corrosive to steel and toxic to humans[36]. Asphaltenes usually contain large proportions of aromatic sulphur. These may undergo oxidative ring opening mechanisms as exploited in desulphurisation techniques[37,38]. Sulphurous compounds are highly problematic (particularly H_2S) which are known to cause corrosion fouling on heat exchanger walls by reacting to form iron sulphide (FeS)[39]. Hydrogen sulphide is also responsible for poisoning catalysis in refinery processes[40].

Oxygen - Oxygen compounds (like other heteroatoms) are mainly found present in resins and asphaltenes. Carbonyls (ketones, carboxylic acids and esters) are the major bonding form of oxygen although phenols, furan derivatives are also present[41].

Poor storage conditions in the storage tanks or elevated temperatures in the presence of oxygen can destabilise crude oil and lead to oxidation reactions[42]. Autoxidation forms polyperoxide gums via a free radical polymerization mechanism[43] and are highly unstable products themselves.
Naphthenic acids (saturated cyclic organic acids) are often found in crude oils, and are corrosive to refinery equipment.[44] The acid content of crude oils can be determined by potentiometric titration (ASTM D664[45]).

Nitrogen – Accounting for 0.1-2% crude weight, nitrogenous species are generally aromatic, and can be either basic or very weakly acidic. Basic nitrogen moieties found in crude oil include pyridines, quinolines, phenanthridines, while the protonated (and very slightly acidic) nitrogens include indoles, carbazoles, benzcarbazoles. Aromatic nitrogen compounds are more electrophilic than their carbon

equivalents, and therefore they are generally more susceptible to thermolysis. Gray et al found thermal cracking coke yields in model compounds containing nitrogen to be 10x greater than their carbon counterparts. Porphyrin rings are also a notable source of nitrogen in oil.

Basic nitrogen has been observed to have both advantageous and negative effects, depending on the composition of blended oils. Basic nitrogens can react react with organic acids present in some oils (particularly those exposed to oxygen) forming organic salts which may phase separate, resulting in fouling[46]. A different study reported an anti-fouling effect in crude oils proposed that crude oils with a basic nitrogen content of >200 mg/kg will not foul, whereas crudes with less than 100 mg/kg exhibited heavy fouling.[47]

2.6.2 Metals

Nickel and vanadium are always present in crude oil, serving as a reminder of the biogenic derivation of oil. They can be fairly abundant (V up to 1200ppm, Nickel up to 150ppm), although other metals are also found in trace quantities. They are considerably problematic further downstream where they encourage coke formation in fluid catalytic cracking[48]. Mullins and co-workers noted that the concentration of metal species in an oil sample can be correlated to the amount of porphyrin[99].

2.6.3 Salts, sediments and corrosion products

Crude oil is often extracted with droplets of water or brine solution containing dissolved salts. Other mineral impurities may cause problems in the process line. Inorganic salts, silicates, carbonates are generally present upstream of the desalter, and after demineralisation, trace quantities may still remain leading to fouling reactions[49]. For example during flash vaporisation, salts can be hydrolysed to corrosive HCl[50].

2.6.4 Porphyrins and other biomarkers

Crude oil is the fragmented and defunctionalised remains of organic matter locked in geological landforms, and some of these structures remain as biomarkers of former life. Terpanes and hopanes are biomarkers found in crude oil[51] as defunctionalised aliphatic skeletons of biosynthesised isoprenoids. Hopanes are related to sterols such as cholesterol see Figure 2.4:

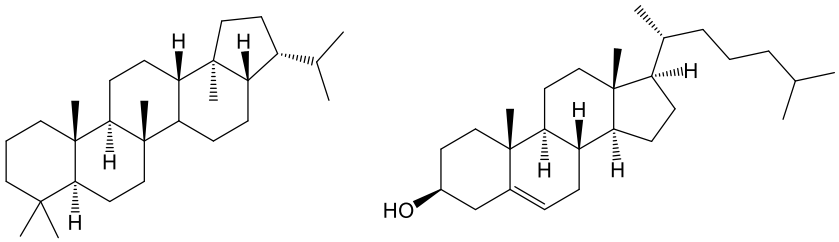


Figure 2.4 Chemical structures of hopane (left) and cholesterol (right)

Porphyrin is a complex organic molecule found in all forms of life yet remains in-tact in crude oil due to its structural rigidity and strong bond energy from aromatic stabilisation. It very strongly chelates metal ions in a tetradentate coordination mode[52,53] (Figure 2.5).

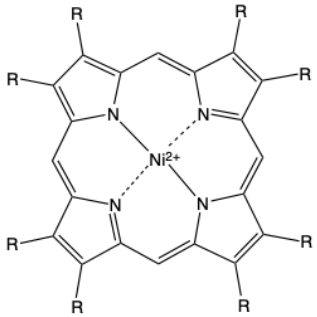


Figure 2.5 Nickel and vanadium bound porphyrins found in petroleum

2.7 Crude oil compatibility

Typically, before a crude oil is blended or subjected to refined, it is subjected to tests to determine whether blending will result in asphaltene precipitation and how likely oil is to foul when subjected to heating. The insolubility number and the solubility blending number are determined. Flocculation tests determine the point of incipient asphaltene precipitation by blending oils with binary solvent mixtures of toluene and n-heptane of varying proportions. A crude blend is incompatible if the average solubility blending number is less than the maximum insolubility number of the oils to be blended[54]. A similar test for oil incompatibility called the Heptane Dilution Test, determines the volume required for asphaltene precipitation to occur on titrating with n-heptane antisolvent, and is found to have more consistent results for low asphaltene concentrations.

2.8 Thermal cracking mechanism leading to coke formation

As described earlier, thermal cracking of non-volatile compounds found in oil such as resins and asphaltenes lead to coke formation at elevated temperatures. The mechanism for thermal cracking

(thermolysis) of asphaltene molecules in oil is illustrated in Figure 2.6. Asphaltene molecules contain a thermally stable PAH core with thermally labile pendent aliphatic groups. At high temperature, the aliphatic groups undergo thermolysis producing radical atoms. In oil these radical atoms abstract protons from hydroaromatics (and other neighbouring molecules with low pKa) terminating their reactivity, exposing the aromatic core which is also now less soluble. This increases the free energy, promoting aggregation and eventually phase separation. To minimise their surface free energy, the aromatic ring groups associate by pi bonding interactions. This new anisotropic intermediate is often referred to as a carbonaceous mesophase and is found surrounded by an isotropic liquid matrix[55]. When further thermally labile groups are broken off, the asphaltene aggregate phase contains very few radical terminating species and thus asphaltene polymerisation leads to solid coke formation.

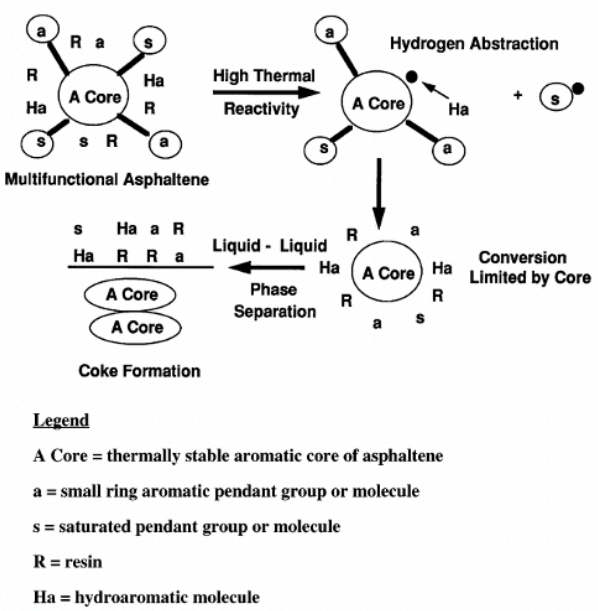


Figure 2.6 Thermolysis mechanism of asphaltenes leading to phase separation and coke formation (by Wiehe et al[56])

Thermal cracking mechanisms of archipelago type model asphaltenes have been investigated by Murray et al[57]. Cracking kinetics and coke yield was measured using Thermogravimetric Analysis (TGA) and micro reactor experiments.

Normally, surface temperatures of heat exchanger walls are less than that where thermal cracking reactions are significant. For example, in pitch, at around 350-500°C carbonaceous mesophase production becomes significant[58], however in the later heat exchangers of the PHT, temperatures approach that found in thermal cracking so is possible to occur on a small scale in particularly thermally sensitive compounds found in oil. This, combined with long operation times between shutdown for cleaning leads to the significant feasibility that thermolysis plays a significant role in heat

exchanger fouling. Studies of aged heat exchanger deposits clearly show that thermal cracking/polymerisation mechanisms are significant[59].

2.8.1 Role of resins in stabilising asphaltenes

The classic colloidal model of crude oil defines the fraction of 'surfactant resin' stabilising asphaltene colloidal systems in a continuous solvent phase of aromatics and saturates. Yet the Modified Yen Model does not explicitly define any role the resins play within crude oil behaviour. Asphaltene aggregation studies in toluene have demonstrated the same phase behaviour in the absence of resins, however, the addition of resins to asphaltene solutions has also been shown to stabilise asphaltenes and impede the onset of flocculation[60].

In terms of size and structure and polarity, resins have physical and chemical characteristics that are intermediate between asphaltenes and lighter solvent molecules such as aromatics and saturates. C5 asphaltenes (deposited with pentane) have a more powdery appearance, compared to C7 asphaltenes which are more "glassy" see (Figure 2.7). Pentane is even less compatible solvent with the polar asphaltenes and resins, and as such will also deposit some C7 resins. These compounds which are on border of the solubility class may be termed as heavy resins or light asphaltenes.

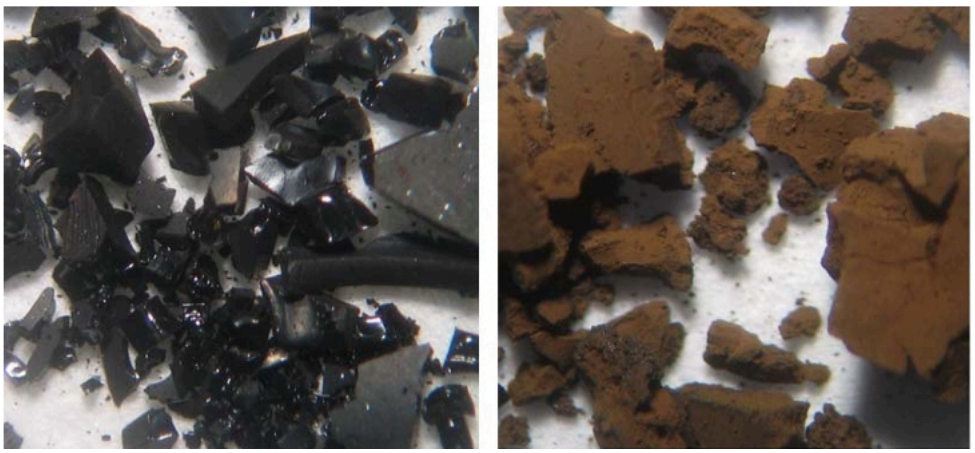


Figure 2.7 Left C7-aspahtlenes and right C5-asphltenes - C7-asphaltenes appear glassy in contrast to the powdery texture of C5-asphaltenes. This reflects the more efficient stacking in the C7 fraction (from Langevin et al.[61])

High resolution SEM and TEM microscopy of asphaltenes precipitated with C_5,, C_7, and C_{10} asphaltenes revealed denser packing and lower particulate circularity of the higher alkane asphaltenes resulted in reduced interparticle spacing and overall greater crystallinity61.

2.9 Crude Oil Fouling Research

2.9.1 Fouling mechanisms

Four fouling mechanisms can be applied to the crude oil heat exchanger train: particulate fouling, chemical reaction fouling, crystallisation fouling and corrosion fouling[62]. The relative significances of these mechanisms is dependent on the composition and conditions.

Particulate fouling

Particulate or precipitant fouling is the deposition of insoluble material on the tube surface. The mechanism of asphaltenes destabilisation and precipitation is described below under 'Chemical reaction fouling'. This is generally the most prominent mechanism, especially for oils with high asphaltene content. Deposition onto the surface relies on the collisions of fractal semisolid phase on the surface which is an equilibrium-governed process in the boundary layer. Removal of the phase separated material back into the bulk fluid may take place if the adhesion energy is low (physisorbed rather than chemisorbed (chemical reaction)) and the Reynolds number is sufficiently high. Gum formed by autoxidation reactions is a polymeric semisolid which may also contribute to deposition[63].

Crystallisation fouling

Crystallisation fouling in oil process systems may occur as organic wax crystallisation fouling at low temperature[64] or inorganic crystallisation fouling at high temperature[65]. In the former, oil below its Wax Appearance Temperature (WAT) may crystallise and deposit in the early heat exchangers. Wax appearance is unlikely in PHT heat exchangers and since it is only possible at low temperatures but may be a problem in cold ambient environments in the initial stage of refinery process systems. Kok et al. reported wax appearance of a range of crudes between 14 and 37 degrees Celsius[66]. In inorganic crystalisation fouling, as the crude oil temperature rises, inorganic salts present in brine-oil emulsions may become supersaturated and precipitate as scale deposits on the surfaces prior to the desalter. A faulty/ineffective desalter with incomplete removal will lead to significant fouling if salt particles and ions persist at the hot end of the PHT[67].

Corrosion fouling

Corrosion fouling, a type of chemical reaction fouling, comprises specifically the reactions that take place with the metal tube wall material and produce fouling. H_2S is a notorious example of a corrosive constituent of crude oil and may also be formed from the cracking of aliphatic sulphides. It readily

reacts with iron to form iron sulphide (FeS) which is brittle yet thermodynamically stable. Organic acids such as naphthenic acids in crude can also contribute to corroding heat exchanger metal surfaces[44].

Chemical reaction fouling

There are a vast number of reactions that could potentially occur during oil processing at high temperature. This principally breaks down into organic fouling derived from hydrocarbons and inorganic fouling derived from salts and complexated metals present in oil. The types of reactions that dominate depend on the composition, the physical conditions and the loci of those reactants. In a heat exchanger they may take place in the bulk, the thermal boundary layer, or at the wall surface (see Figure 2.8).

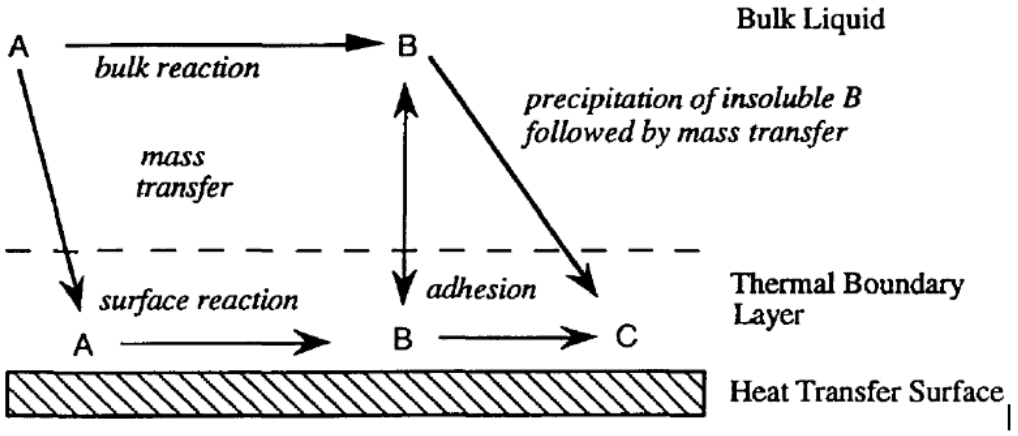


Figure 2.8 scheme of a general multistep deposition process (source Watkinson and Wilson[68])

A product species of a reaction that occurs in the bulk may remain entrained in flow and not produce fouling, or it may diffuse to the thermal boundary layer. Here it may adhere to the surface in a non-reactive way, or it may react with the surface (as in the case of naphthenic acid reaction with metal forming ionic salts[44]). The adhered species may subsequently desorb back into the bulk or remain at the surface where it may react again further making it irreversibly adhered onto the surface. The mass transport (diffusion kinetics) is important when considering overall reaction kinetics. A review by Watkinson and Wilson[68], categorises 3 general classes of reactions:

1) Autoxidation
2) Polymerisation
3) Thermal Decomposition

Autoxidation can be a problem if exposed to air during the storage of crude oils and petroleum products. Whilst oil flows through the preheat train in a closed system, oxygen gas may be dissolved in the crude oil in low concentrations, and oxidation reactions may be more problematic at elevated temperatures. Autoxidation reactions have been shown to occur with even unreactive n-alkanes at temperatures below 250°C[69]. However, autoxidation may not necessarily cause significant fouling, since the low residence times through the preheat train may not be sufficient to form gums capable of depositing and leading to fouling.

Since efforts are usually made to process oil in deoxygenated systems, polymerisation and thermal decomposition reactions may be more prominent thermal reaction pathways leading to fouling. Large insoluble molecules can be formed in polymerisation reactions causing precipitation and fouling. Olefins, if present in feedstocks are highly susceptible to thermal cracking produces by radical mechanisms.[70] Styrene has been used as a model by Crittenden to study chemical reaction fouling kinetics.[71] Fouling rate models of this kind are of semi empirical Arrhenius type and relate the Reynolds number, activation energy and film temperature to the fouling rate for a plug flow system.

2.9.2 Ageing

Fresh deposits undergo a complex thermal ageing process which leads to the formation of very hard and stable graphite-like material over long operating times[72] illustrated in Figure 2.9.

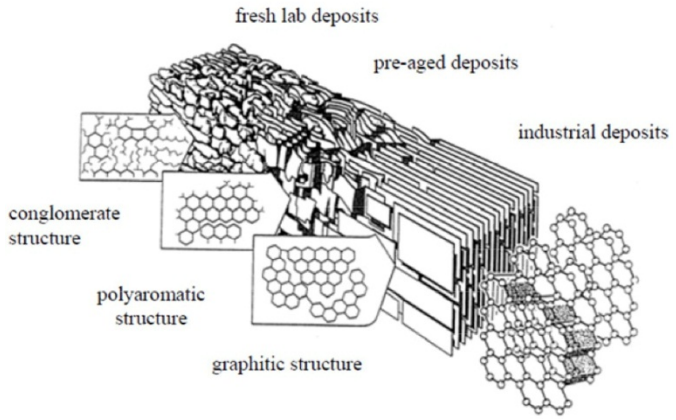


Figure 2.9 Structural Evolution of asphaltenic deposits with age (source Z. Fan & Wilkinson, 2009)

This gradual coking mechanism is a thermodynamic effect that arises from cracking of fresh organic precipitates and has been investigated by authors such as Cesti and co-workers.[73] Deposit material

undergoes thermal cracking at the hot surface. Some of the lower energy aliphatic bonds undergo radical bond breaking enabling the PAHs to recrystallise, aligning more efficiently, whilst some of the asphaltene's pendant aliphatic groups sterically packed into appropriate steric conformations undergo intramolecular cyclisation/aromatization reactions. The thermally insulating properties of the deposit mean that local surface temperatures are significantly higher and further radical thermolysis reactions take place, breaking C-H bonds and forming C-C bonds with neighbouring PAHs until the molecular structure resembles a fragmented graphite structure, which is now thermally stable and very challenging to remove.

Thermal decomposition gains significance latter end of the PHT and is more prevalent in oil streams with higher heteronuclear content[68]. For fouling involving asphaltenes, the interplay between asphaltene phase stability, precipitation processes and radical thermolysis is still an active topic of research.

Precipitation onset time

An induction period is often associated with fouling experiments when no fouling is observed on clean smooth surfaces. When the surface is smooth and clean, particles that diffuse through the boundary layer to the wall surface may bind with a weak electrostatic binding force (physisorption). In highly turbulent flows, the boundary layer thickness is small and the attraction may be overcome by shear forces by the fluid. Alternatively, if particles adhere to the surface by chemical reaction (chemisorption), the binding force is strong, and shear forces may not be sufficient to re-entrain particles into the bulk flow. However, once a precipitate has begun to adhere to the surface the increased heterogeneity and reduced energy barrier to binding results in increased fouling rate. A number of models have been proposed to describe this fouling onset kinetics[74,75]. It is generally thought that the initial particles that do adhere to the surface act as "seeds" for attracting further foulant around them[74], in a similar way that crystallisation be delayed in a supersaturated solution until a suitable nucleation site initiates crystal growth. This is certainly true of crystallisation fouling, but also true of organic asphaltenic fouling, since π-stacking of aromatics lowers the free energy of the system.

Crude oil composition and solution stability are important factors in determining fouling onset, as this will govern the type of fouling likely to occur and the free energy of the system which in turn impacts the fouling kinetics. During the induction period, a fouling crude oil liquid phase is only metastable,

i.e. thermodynamically unstable but limited by kinetics, the onset time may be related to the solution stability at ambient conditions. i.e. the onset time will be less for unstable crude mixtures.

The induction time is also related to the process conditions such as surface temperature, as asphaltene solubility and liquid viscosity are decreased at higher temperature, less stable nanoaggregates which flocculate together into clusters faster leading to phase separation, and therefore result in a reduced fouling induction time.

2.9.3 Hydrodynamic effects due to fouling

As a the foulant thickness of a tube inner surface increases the flow cross section will inevitably decrease, increasing the fluid velocity at this location. When suspended particles adsorb to the surface the likeliness of adhesion to the existing layer will decrease with the higher resultant shear stress and the fouling rate falls off as long as the total mass flow rate remains constant. However, if the increased pressure drop due to fouling reduces the overall mass flow rate, the lower fluid velocity will result on continued build-up of the foulant layer. Studies by Crittenden et al.[76] have shown fouling rates of both oil and styrene to be highly dependent on fluid velocity, with apparent activation energies shown to be increasing with increasing linear velocities in a parallel tube test apparatus.

2.9.4 Thermal effects due to fouling

The soft fouling deposit layer which builds up on heat exchanger surfaces have a lower thermal conductivity than the tube wall which has a negative impact on the heat exchanger performance. Since fouling layers are usually thin, the fouling resistance is often modelled as a single layer and its fouling resistance R_f given by:

$$R_f = \frac{\delta}{\lambda_f} \qquad 2.3$$

where the δ = deposit thickness and λ_f = thermal conductivity of the foulant layer. Ageing, as noted above results in a change in physical nature for the fouling deposit and thus the thermal conductivity is also a function of both the chemical nature (inorganic/organic) and the thermal history of the deposit for a given thickness.

A number of fouling models considering kinetics and thermo-hydraulic have been developed to analyse and predict the effect of fouling on heat exchanger performance.[77,78,79,80] The Hexxcell model developed by Coletti and Macchietto is an industrial scale model integrates multiple aspects that impact heat exchangers undergoing fouling[81]. It takes into account the rates of processes leading to

fouling deposition, temperature distributions and deposit thickness profile and the effect of flow on deposition and re-entrainment of deposits.

2.9.5 Fouling mitigation strategies

Owing to the persistence of the fouling problem, and detrimental effects on refinery performance, a broad range of strategies have been developed that focus on different aspects of the problem.[82]

Surface modifications

Steel tubing is a good material in terms of mechanical stability and thermal conductivity, however an active steel surface exhibits significant reactivity, especially in nickel-containing alloys. While nickel alloys increase the strength of steel alloys, it is also known to catalyse the formation of coke from petrochemical media such as heavy oils[83]. Carbon steel heat exchangers are often passivated before entering service, to prevent atmospheric rust corrosion forming prior to entering service[84].

Electropolishing – Polishing reduces the roughness of the tube heat exchanger surfaces, lowering the coefficient of friction and prevents particulates from adhering in valleys of an uneven surface.

Barrier Coatings – A number of commercial coatings have been developed to control the surface properties of process equipment by lowering chemical reactivity and reducing surface energy to prevent particulate adhesion on coated surfaces and reaction of gases (such as H_2S) with the bare metal surface[85]. Two such silicon-based coatings developed by SilcoTek have been utilised in the oil and gas industry. Siloklean, an amorphous silicon coating, originally developed to passivate the inner surface of gas chromatography columns, is coated by a chemical vapour deposition (CVD) process from the thermal degradation of SiH_4.[86] A more recent coating (Dursan) applies a similar CVD deposition treatment which is then further processed by addition of a fluorinated functional group, which is reported to be more durable and significantly lower the surface energy, also reducing the coefficient of friction, leading to greater pumping efficiencies[87]. The downside to coating heat exchanger tubes and shell surfaces is a substantial increase in cost, 3.5x total cost of an untreated 304 Stainless steel tube[85]. Coatings may also degrade over time, diminishing the beneficial impact.

Heat exchanger design and overall fluid process

Mitigation strategies include the heat exchanger thermal design parameters (reducing the temperature differential between the tube wall and the process fluid), configuration (avoiding “dead zones”) and material choices can all be selected or designed to reduce the likelihood of fouling, and also the ease of cleaning. Additionally, effective processing and control of the upstream process fluid,

correct blending procedures, H_2S off-gassing, desalting (salt removal and emulsion breaking) and effective integration of heat exchangers to avoid processing oils above or near fouling thresholds.

Chemical additives

These can broadly be split into dispersants and inhibitors. Both work by lowering the free energy of the oil system and prevent phase separation (and hence fouling). Dispersants change the polarity of nano-aggregated asphaltenes, helping to disperse into the solvent phase and break up. Inhibitors act as resins, stabilising asphaltene nanoaggregates and preventing phase separation. A number of non-ionic and ionic dispersants have demonstrated good dispersive action on asphaltene aggregates[88].
A number of soluble amphiphilic oils have been investigated as fouling inhibitors in the PHT[89,90]. Overall, whilst effective in principle, the downside is that chemical additives significantly increase cost of production, so a focus on blending and process optimisation is a preferred option in operating refineries.

2.10 Characterisation of asphaltenes

2.10.1 Mass analysis

Mass analysis has long been a problem when characterising the large polar non-volatile asphaltenes present in oil. Nanoaggregation of asphaltenes and clusters with strong pi bonding attractions often lead to overestimation of asphaltene molecular weight The development of new mass spectroscopy techniques and agreement with other mass and size analysis methods has led to the converged mass estimation of asphaltenes having a mass on average of 750 Da and mass range of approximately 500 – 1000 Da[17].

2.10.2 Mass spectrometry

A number of mass spectrometry approaches have been reported, however the volitilisation approach for MS analysis is critical to obtain reliable mass analysis. Low resolution techniques employing thermal volatilisation tend to provide lower asphaltene masses, as only lighter asphaltenes may be volitilised and heating to higher temperatures >300°C results in significant fragmentation, leading to misrepresentation of asphaltenes parent ions and the mass distribution. Soft ionisation methods involving Electrospray ionisation (ESI)[100] and matrix assisted laser desorption ionisation (MALDI-TOF)[91] MS can minimise fragmentations, and have been extensively used for analysis of biopolymers.

Fourier transform ion cyclotron resonance mass spectrometry (FT-ICR MS) is a broadband high resolution MS detection method for of asphaltenes, and is able to identify uniquely many thousands of elemental compositions in a single mass spectrum.

2.10.3 Other mass analysis techniques

Time-Resolved fluorescence depolarization (TRFD) studies has enabled the archipelago model to be substantially disproved and the island architectural model is currently accepted. In this technique asphaltenes in a solution of toluene are excited and polarised by a polarised laser. The excited asphaltenes fluorescence back to their ground state and while doing so, also lose their polarisation of the fluoresced light by rotational diffusion. The rotational correlation time is positively related to the molecular size and so small size short wavelength fluorophores rotate much faster than larger and longer wavelength fluorophores. If smaller fluorophores were cross linked to larger ones as in the archipelago model, expected depolarisation times and rotational diffusion constants would be considerably longer. Numerous studies on asphaltene extractions in solution have shown the molecular size to be on the order of 500-1000 Da and so contain mostly single fluorophores[92,93].

2.10.4 Translational diffusion measurements

Fluorescence correlation spectroscopy (FCS) using confocal microscopy of ultra-dilute asphaltene solutions has been used to determine diffusion coefficients by measure time fluorescence intensity fluctuations elicited from asphaltenes diffusing into and out of the confocal volume**.** The molecular size can be related to the diffusion constant. Small values were also obtained rotational diffusion constants indicating no internal core of fluorophores groups within asphaltenes.[94]

Nuclear magnetic resonance (NMR) has been employed investigate spin relaxation and translational diffusion constants, and are in agreement with FCS studies (r = 1.2 nm (monomers) and 3.4 nm (nanoaggregates)). By studying the spin echo signal of asphaltenes at varying and temperatures concentrations around the aggregation concentration the critical nanoaggregate concentration (CNAC), enthalpy (-15 kJ/mol) and entropy (35 J/mol K) of nanoaggregation were determined for asphaltene extracts in toluene.[95]

2.10.5 Molar concentration measurements

Vapor Pressure Osmometry (VPO) has been used extensively for measurements of asphaltene molecular weights due to its simplicity, providing a number average molecular weight.[96] This provides accurate measurements for low polarity lower molecular weight compounds, but poor results for polar asphaltenes due to aggregate formation leading to high reported molecular weights up to 10^5 Da.

2.11 Characterisation of asphaltene structure

In order to understand the function asphaltenes play in oil systems, the structure must be understood. Because of the many variant chemical features of asphaltenes, many characterisation techniques have been employed to define these structural features and constrain the proposed definitions of petroleum asphaltene molecules. Polyaromatic ring groups (PAH moieties are the main structural feature of asphaltene molecules. The average number of fused rings in an asphaltene molecule has been estimated by NMR and optical fluorescence spectroscopy.

The fluorescence optical spectra of asphaltenes are inherently related to the conjugation of delocalised pi electrons. Fused aromatic rings, as well as adjacent double bonds and some heteroatoms can conjugate together to form large pi bonding molecular orbitals (MO). They may be excited by photon absorption, and fluoresce to the ground state at characteristic wavelengths depending on the size of the delocalised pi system. The number of aromatic rings may be estimated by the fluorescence emission wavelength. Comparing theoretical MO calculations to optical spectra, asphaltene ring systems predominantly found to consist of 4 – 10 rings[97,98]. In petroleum systems, 6-8 rings are most predominant.

Nuclear magnetic resonance (NMR) provides information on the electronic environment of spin active nuclei from which it is possible to quantify the distribution of carbon and hydrogen according to structural type. From ^{1}H-NMR, we can quantitatively determine the relative amounts hydrogen atoms bonded to aliphatic and aromatic carbon atoms. ^{13}C-NMR shows that approximately 40-50 % of carbon found in petroleum asphaltenes is aromatic[99]. Therefore aliphatic substituents also make up a major portion of asphaltene structure. Also by analysing the ratios of aliphatic to aromatic carbons in the ^{13}C-NMR spectra, it is also possible to estimate the average number of aromatic and aliphatic carbons per molecule, and average number of rings per molecule[100,101]. Through Infrared and NMR studies, it is believed, alkyl substituents of asphaltenes thought to be on average 4-5 carbons long[102]

2.12 Organic compounds as asphaltenes models

The use of synthetic crude oils containing asphaltene like models overcomes the challenges arising from the variability of crude oils, and may enable a pathway to better understanding fouling mechanisms and how industry may take steps to mitigate this phenomena leading to more efficient fluid processing and better profitability. Thermal cracking kinetics and mechanisms have been researched for a handful of asphaltene like structures[57], and the association/aggregation of these molecules in solid or gas phase, and light solvents at moderate temperatures, but these studies lack realistic physical solution properties that allow direct comparison with actual fouling of crude oil in refinery heat exchangers. There is an opportunity therefore to research fouling behaviour on asphaltenes-like synthetic models compounds in solution which may be representative of industry conditions, so this is a novel and potentially rewarding avenue of research to explore.

Since asphaltenes possess the ability to form π-bonded stacking nanoaggregates, It has been demonstrated that the aliphatic substituents bonded to the PAH centre, and the steric hindrance to stacking this induces, is a necessary structural feature to demonstrating interaction characteristics of the asphaltene fraction[99], as large PAHs without aliphatic substituents are not soluble in toluene and will not exhibit similar phase behaviour as real asphaltenes.

A number of studies have aimed at understanding the complex thermal and phase behaviour of asphaltenes, and various molecular structures have been employed for this purpose (see Table 2.3)

Table 2.3 Model asphaltene structures used for investigated the phase behaviour and thermal characteristics of asphaltenes

PAH ring number	Model Asphaltene Architecture	Research Area	References
1	Benzene or derivatives	Bulk and Solution pyrolysis	103
2	Napthalene or derivatives	Bulk and solution Pyrolysis	104
3	Benzoquinoline-Cholostane derivatives	Bulk Pyrolysis	105
4	Pyrene and derivatives (island and archipelago models)	Solution aggregation behaviour Bulk and solution Pyrolysis	106107,108,109
5	Perylene and derivatives	Interfacial behaviour and emulsion stability Solution aggregation behaviour	110,111
7	Coronene	Solution aggregation behaviour	111

High Resolution Transmission Electron Microscopy (HRTEM) has been employed[111] to study stacking behaviour of asphaltenes and PAH model compounds (Figure 2.10) in toluene.

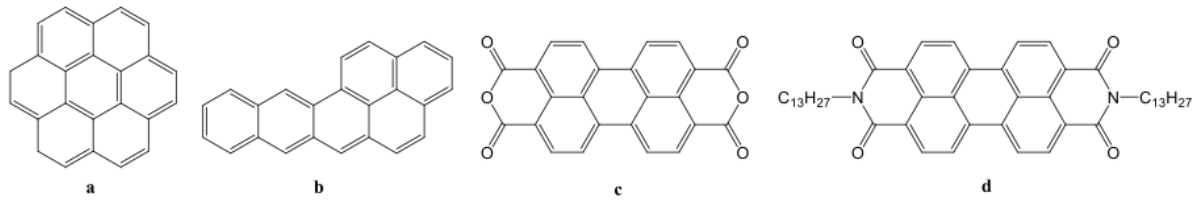


Figure 2.10 Four model compounds used in HRTEM studies: a = coronene, b = Naphtho[2,3-a]pyrene, c = perylenetetracarboxylic dianhydride (PTDA), d = N,N'-ditridecyl-3,4,9,10-perylenetetracarboxylic diimide (PTDI-C13)

2.12.1 Use case for model asphaltene compounds to assist fundamental understanding of the crude oil fouling processes

1) **Control**:
   a) **Composition** - The main benefit of using model compounds is the extra control afforded by being able to specifically control all aspects of the fluid composition: such as the molar/volume/mass fraction of each component, and the chemical features of each component - functional groups and architectural structures. The physical properties of a fluid mixture are a direct result of its composition at a given temperature, so it is possible to design a fluid system to exhibit desired physical properties by this control.
   b) **Structure –** The structural architecture and functional groups can be manipulated in the test models compounds by modifying the synthesis to include a range of "R"(side chains) groups with tunable properties.
2) **Reaction kinetics** - Real oil solutions have a range of compositions, functional groups and structures. Reaction kinetics will be different for each oil sample and asphaltenes controlled systems using model compounds
3) **Minimise unknown/unwanted or competing side reactions –** Using model compounds limits unwanted side reactions occurring such as corrosion fouling with unintended species such as H2S or trace metal species. In this kind of study the reactions of a known compound or group of compounds can be implemented.

The difficulty in understanding and predicting fouling behaviour of crude-oil can in part be attributed to the multitude of unknowns about the compositional make up which in turn leads to unknown and

unpredictable phase behaviour. i.e. behavioural trends for one oil can be completely different to that of a second oil, and this ultimately is dependant on the oil composition.

An improved understanding in the molecular architectures of asphaltenes has helped to allow the use of better chemical model compounds to observe the behavioural properties that these molecules exhibit. Most of the work has focused on the phase behaviour of asphaltenes solutions in light solvents or in the gas phase, and some studies have been done on the thermal cracking of asphaltene models, but there is a lack of research using synthetic model asphaltene solutions to study fouling behaviour in solutions and under the thermal and dynamic conditions which can realistically be expected in the PHT refinery. This work aims to demonstrate fouling behaviour of structurally analogous models in a realistic physical and solution environment where fouling occurs, observe the nature of those fouling deposits, and compare this behaviour to crude oil and their deposits.

2.13 Laboratory scale crude oil fouling research

Crude oil fouling has been investigated by numerous research groups in the past[112-125]. This section presents some examples of laboratory scale systems used for crude oil fouling research and presents a basis for the design of the fouling apparatus purposefully designed and commissioned by the author for purpose of this research work.

Crude oil fouling in refinery heat exchangers typically occurs over long durations, often months between cleaning intervals. For practical purposes, laboratory experiment durations must be sped up to the order of hours such that sufficient experiments may be performed during the research duration to facilitate the production of insightful data across a range of process conditions and fluid compositions but must also be sufficiently long in duration to produce fouling deposits for analysis and characterisation.

2.13.1 Crude oil fouling systems without dynamic flow

Previous research in Dr. Millan's research group at Imperial College by S. Venditti[112] and K. Rostani[113] has utilised laboratory scale fouling apparatuses for studying batch crude oil fouling. The first equipment utilises a batch micro-bomb reactor as shown in which was designed and commissioned by S. F. Zhang[114] composed of Swagelok® fittings. An end-capped Swagelok® union-tee containing oil samples was pressurised via a Nitrogen cylinder and heated in a fluidised sand bath whilst shaking using an oscillating agitator to improve thermal homogeneity. The tee connects via a long tube and

small water-cooled heat exchanger to a K-type thermocouple, pressure transducer, pressure-relief valve and nitrogen line. This apparatus was designed to operate at up temperatures up to 500 °C and 200 bar pressure.

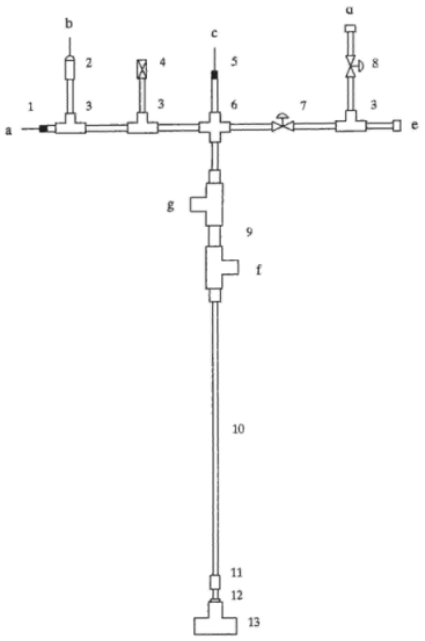


Figure 2.11 Schematic of Microbomb reactor - Legend: [1] Thermocouple; [2] Pressure Transducer; [3] Union Tee; [4] Pressure Relief Valve; [5] Thermocouple; [6] Union Cross; [7] Ball Valve; [8] Needle Valve; [9] Heat Exchanger; [10] Vertical Pressure Extender; [11] (Source Khairul Rostani[128])

Crude oil fouling experiments were conducted in the microbomb reactor at 250 – 400 °C and 60 – 80 bar pressure. The high pressure was necessary to minimise vapour loss from the liquid sample as a result of having a two-phase system at high temperature. At 40 bar, around 20 % w/w of sample was lost due to volatilisation. At 80 bar, considerably higher than most refineries, still 2-6 % w/w was lost.

This work was followed on by Kairul Rostani using a new experimental setup, which aimed to address the limitations of the microbomb reactor due to oil volatilisation at the nitrogen-oil interphase. A flow sheet of the reactor is shown in Figure 2.12:

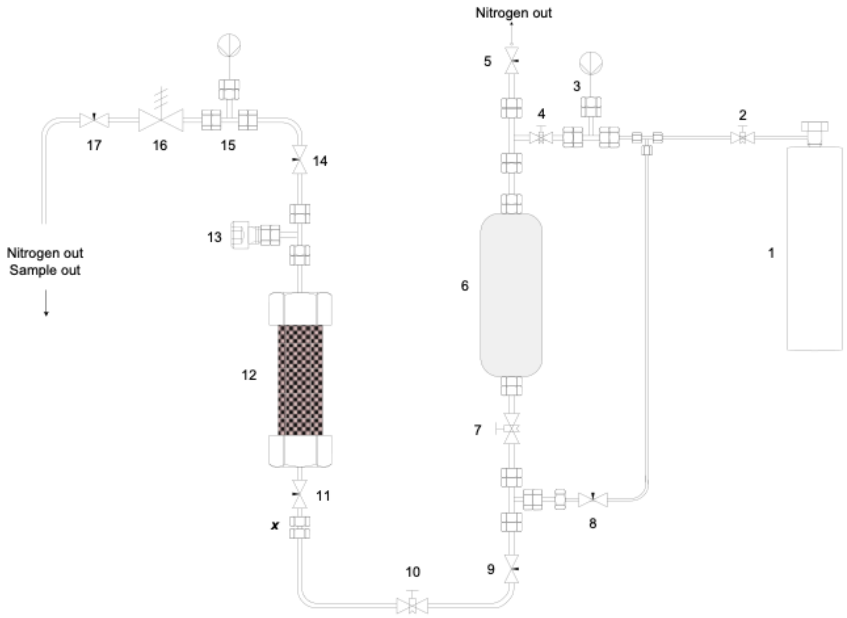


Figure 2.12 Schematic Diagram of Fouling reactor (by Khairul Rostani) - [1] Nitrogen gas cylinder; [2] Ball valve; [3] Pressure transducer; [4] Ball valve; [5] Needle valve; [6] Sample cylinder; [7] Ball valve; [8] Needle valve; [9] Needle valve; [10] Ball valve [11] Needle valve; [12] Test section; [13] Thermocouple assembly; [14] Needle valve; [15] Pressure transducer; [16] Pressure relief valve; [17] Needle valve (Source Khairul Rostani[128])

The reactor test section consists of a steel tube filled with the sample fluid with no gas phase and heated using a coiled electrical heating tape supplied by Omega. The process line contains a hot section (heated test section, thermocouple, pressure transducer, pressure relief valve) and a cold section (sample loading and purging line). The crude oil sample is first filled into the sample cylinder. The whole system is then purged with nitrogen and the sample fluid degassed by bubbling nitrogen up through fluid in the vessel. The fluid loads into the heated section by differential pressure provided by a nitrogen cylinder. Once the hot system side was loaded with the sample fluid and pressurised, the valve separating the hot and cold sections was closed and the test section heated to the operating temperature for the duration of the experiment and maintained using a ring thermocouple around the outside of the tube.

This one phase heated test section solved the problem of liquid volatilisation, however fluid dynamics inside the test section was governed by convective mass transfer during heating, and when held at steady state, the uniform temperature results in a mostly static fluid. This differs strongly from refinery process conditions which under turbulent flow in heat exchanger tubes exerts a shear stress at the wall. Fluid motion inside the test section has a profound effect on fouling at the wall surface. The

apparatus developed for this project considers both these limitations, to better replicate refinery conditions for fouling experiments.

As discussed in section 2.9, when asphaltene precipitation occurs in the bulk liquid phase and is carried through to the distillation furnace, they do not pose a problem in the PHT. Likewise, when asphaltenes deposit on the exchanger tube walls but and are removed back into the bulk liquid and remain entrained in the flow, again also fouling build up does not occur and entrained particulate material will carry through to the furnace. However, when asphaltenes deposit and are not removed on the tube walls, the result is an irreversibly detrimental effect on the heat transfer rate and pressure drop across the system. In a static system, there is no shear stress present to enable dislodging of adhered deposits. The only force acting to remove the deposit is equilibrium diffusion. Fouling rates have been shown to decrease with increased wall stress, a function of flow velocity[115,116].

This is why a static system is not appropriate for studying fouling on heat exchange surfaces. As the shear stress induced removal force must be replicated in an experimental system to be a valid representation of fouling in a heat exchange system, otherwise giving rise to greater attached deposits than in the refinery. It then is also possible to analyse the suspended foulant in the bulk phase and compare to the adhered foulant, whether corrosion products (e.g. FeS) are contributing to precipitate adhering, or if fouling is primarily a deposition governed process.

2.13.2 Crude oil fouling systems with dynamic flow

Stirred batch cells

Crittenden et al. have reported the development and use of a versatile closed cell oil fouling apparatus,[117] (see Figure 2.13). The cell features a heated test probe mounted from the base of the cell, an inverted cup-shaped stirrer with coupled motor axially mounted to the top of the cell, and a coiled cooling loop in the annular space to remove heat from the bulk fluid allowing control of the temperature difference between the hot test surface and the bulk fluid.

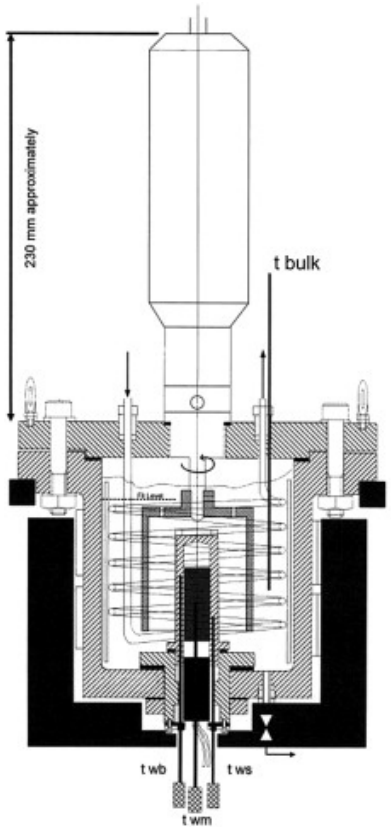


Figure 2.13 Stirred batch fouling cell developed by Crittenden et al. (source Crittenden et al[117])

The cell is designed with a 1L oil capacity and operates in two phases with a nitrogen blanket above the liquid, and the stirrer is rotated at between 50 and 400 rpm, temperatures up to 450 °C and pressures up to 30 bar. Presumably the impellor frequency is set below that which the gas phase would become entrained as bubbles in the liquid phase. Heat input into the cartridge heater and flow rate of the cooling fluid are independently controlled, along with three thermocouples in the heater probe wall and one in the annular fluid space to monitor and control the thermal parameters of the system to achieve steady state heat transfer conditions. The test probe is fitted with a new carbon steel flange for each experiment for repeatability and may be switched out for testing other materials or surface conditions. Fouling tests typically last lest than 10 hours. Indirect in-situ measurement of the deposit formation was achieved by observing the change in heat transfer between the heated probe and the bulk fluid, and correlating the fouling resistance to the average deposit thickness. Experimental studies by young et al concluded that fouling rate increased with surface temperature and decreased with an increase in fluid shear rate[118].

Another cylindrical stirrer batch cell rig been developed by Krishnaswamy et al. for crude oil fouling studies. The autoclave is heated by a ceramic band heater and the oil agitated by means of an axial flow impellor. The boiling was limited by an overpressure of nitrogen gas at 8 bar, with a reflux condenser fitted to the head of the cell, and the system held at between 275 – 300 °C for 80 hour

residence times per test run. Fouling deposits were collected on a series of 1 - 12 carbon steel test coupons 75 x 12 x 1 mm fixed inside the autoclave cell but are not heated directly. Deposits were characterised with TGA, elemental analysis, XRD and SEM/EDX[119].

Plug flow fouling systems

A commercial single pass PFR type system named the hot liquid process simulator (HLPS) intended for studying fouling heat exchanger performance and fouling tendencies is available by Alcor[120] and has been used by a number of researchers for oil fouling studies[121,122,123] (see Figure 2.14). Industry-Recommended Procedures for Experimental Crude Oil Preheat Fouling Research) The system is highly adjustable, but a standard configuration flows test fluid across the annular space across a cartridge heater, whilst data on the heat transfer coefficient and pressure differential may be logged in real time.

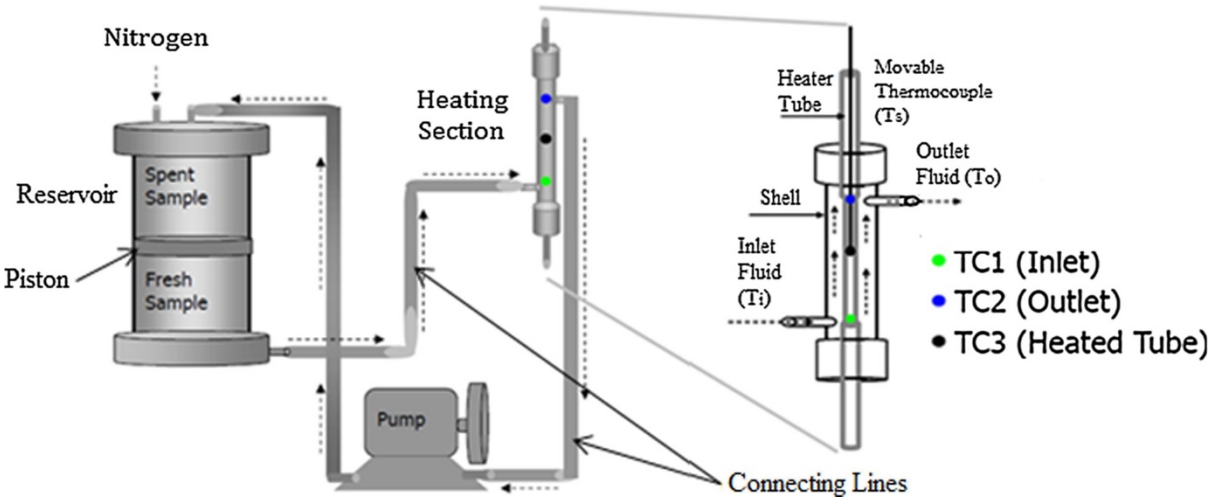


Figure 2.14 Schematic diagram of Alcor HLPS 400 fouling system used for use with bitumen visbreaking products (source Ali et al.[123])

HIPOR, a pilot scale crude oil fouling rig has been developed by Hewitt and Macchietto et al.[124,125] at Imperial College London, which operates a as recirculated (PFR type) system (see Figure 2.15) with two parallel test sections and heated by resistive joule heating, a tubular flow test section, and an annular flow test section. A secondary cooling loop removes excess heat from the system during operation. Differential pressure and differential temperature measurements across the test sections allow online heat exchanger performance data to the data acquisition system, operated via a customised LABVIEW software system. An additional sensing design feature called the 'dynamic thickness gauge' has been incorporated into the annulus test section which enables online axial temperature measurement. The inside the inner tube of the annulus test section contains a radiation equilibrium thermocouple mounted to a sliding ceramic piston which can traverse the length of the

test section during operation, collecting temperature profile data along the section length at intervals during the test runs providing information on changes in the temperature profile and fouling deposit thickness on the oil side of the heated surface.

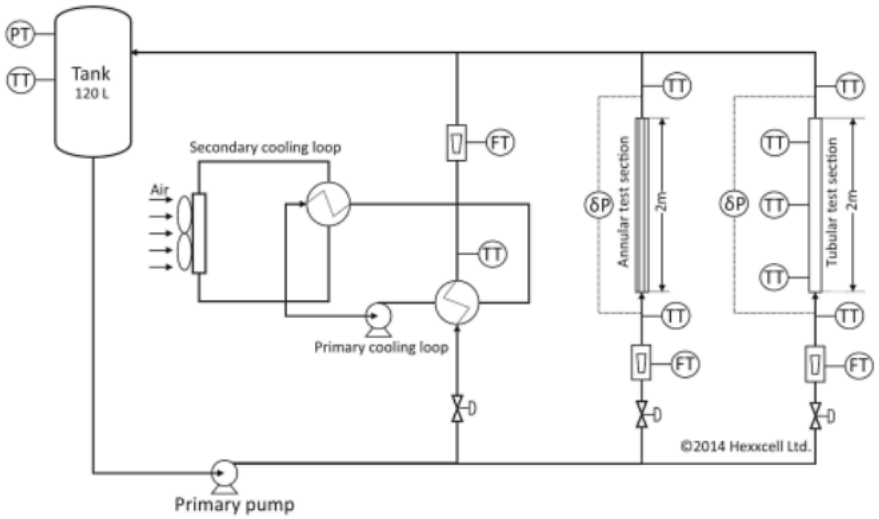


Figure 2.15 Schematic process flow diagram of the HiPOR fouling rig (source Coletti and Hewitt)

The system processes 50-60 litres of oil in a typical run at temperatures up to 300 °C and up to 30 bar for and durations reported up to 72 hours, and provides high fidelity processing conditions for fouling research when large volumes of crude oil are available.

2.13.3 Recommended process conditions and the pros and cons of various configurations

In the refinery heat exchanger train, typically, process crude oil flows through a series of shell-and-tube heat exchangers under high pressure. With both previous experimental setups, the flow element is not replicated this is an important factor missing when attempting to match refinery conditions. While refineries pass vast volumes of fluid through the process line in a single pass, laboratory scale equipment must process much smaller volumes. Bennett and coworkers[126] provided suggestions for recommended process conditions for undertaking crude oil fouling research. These are summarised in

Table 2.4 below:

Table 2.4 Key operating conditions for stirred batch fouling reactor as recommended by Bennett et al.126

Surface Temperature	260 – 320 °C
Operation Pressure	2-7 MPa
Linear Fluid Velocity	1-3 m s^{-1}
Metallurgy in order of decreasing fouling propensity	Carbon steel, low chrome steel, stainless steel

Generally, fouling apparatuses considered above can be generalised into three configurations, stirred batch apparatus, a recirculated PFR (Plug flow reactor) type apparatus and a single pass PFR type apparatus. The advantages and disadvantages of these are summarised in Table 2.5:

Table 2.5 Advantages and disadvantages of different reactor configurations

Reactor Type	Advantages	Disadvantages
Stirred Batch Cell Apparatus	• Long experimental times possible • Small sample volumes are possible • Fouling occurs only in the reactor • Simpler design	• Fixed fluid volume so reactants diminish with time (batch reaction dynamics) • Heat exchanger flow dynamics not replicated
Recirculated Plug flow apparatus	• Long experimental times possible • Heat exchanger dynamics replicated	• Fixed fluid volume so Reactants diminish with time (batch reaction dynamics) • Fouling may occur outside the PFR • Larger volumes consumed • More complex design
Single Pass Plug flow apparatus	• Heat exchanger dynamics replicated • Reactants entering heated test section do not diminish with time	• Flow rate (and Re) are low • Short experimental times or much larger volumes consumed

Each of these configurations was considered in the initial design stage for the development of the laboratory scale fouling equipment. Details are provided in Chapter 3.

Chapter 3 Design, Development and commissioning of a Stirred Batch Fouling Apparatus

3.1 Introduction

This chapter discusses the development of experimental equipment built for testing the fouling behaviour of crude oils and related solutions in an environment whose process conditions may be compared to heat exchangers in refinery process lines. Within the chapter, the author discusses the design, safety considerations, construction process and equipment testing and commissioning leading to a procedure for sample preparation, operation of the equipment, sample collection and processing for fouling experiments.

3.2 Reactor design process

One defining feature of the current work is the investigation of crude oil fouling with respect to its chemistry. Model compound solutions and fractionated crude oils play a significant role in the experimental outline of the research work. Considering the significant chemical costs and large processing time for the preparation of these solutions, sample test volumes above all else must be kept within workable limits. Therefore, fluid test volume per experiment was limited by design to under 100 mL per experiment. Consideration was given regarding expected fouling residence times, sample volumes, where fouling may occur, design complexity and whether to flow fresh feed continuously or use a fixed volume of fluid.

After considering several designs and configurations as summarised in Table 2.5, a stirred batch apparatus was chosen. The low volumes possible, ability to perform long times and produce highly turbulent flows with an integrated stirrer outweigh the shortfalls of having batch reaction dynamics instead of a continuous fresh feed and different geometry to the plug flow geometry found in shell and tube heat exchangers. In recirculated systems, fouling deposition may also occur outside the heated test section, for example in sections of lower temperature or lower fluid velocity such as the fluid tank, this would not be a problem in a batch cell where all the sample fluid is under uniform conditions.

3.3 Details of the reactor design

3.3.1 Radiant heated Taylor-Couette Cell apparatus

The batch-fouling apparatus has the form of a Taylor-Couette cell: a cylindrical vessel and a coaxially mounted cylindrical rotor with head and base units on the ends, in which the fluid fills the annulus between the two cylinders (see Figure 3.1 and Figure 3.2).

The top and bottom flanged bodies are secured to the central wall section by six M6 stainless steel bolts and sealed by annealed copper gaskets. A variable speed commercial DC servo motor drive unit mounts coaxially to the head unit of the reactor and connects the drive shaft to a stainless-steel cylindrical rotor via a grub screw and is controlled by a variable power supply. The motor has a sealed magnetic coupling to transfer torque to the cylindrical rotor. The head unit has inlet and outlet ports (1/4" Swagelok fittings) and a further threaded port that attaches a K-type thermocouple for measuring bulk fluid temperature positioned at the midpoint of the reactor body, equidistant between the reactor body wall and the rotor. The body wall temperature is measured via a thermocouple inserted into a hole drilled in the wall body to the midpoint of its length. The base unit contains a threaded port for a liquid outlet via an all-stainless-steel bleed valve designed to withstand the high temperature and pressures during an experiment.

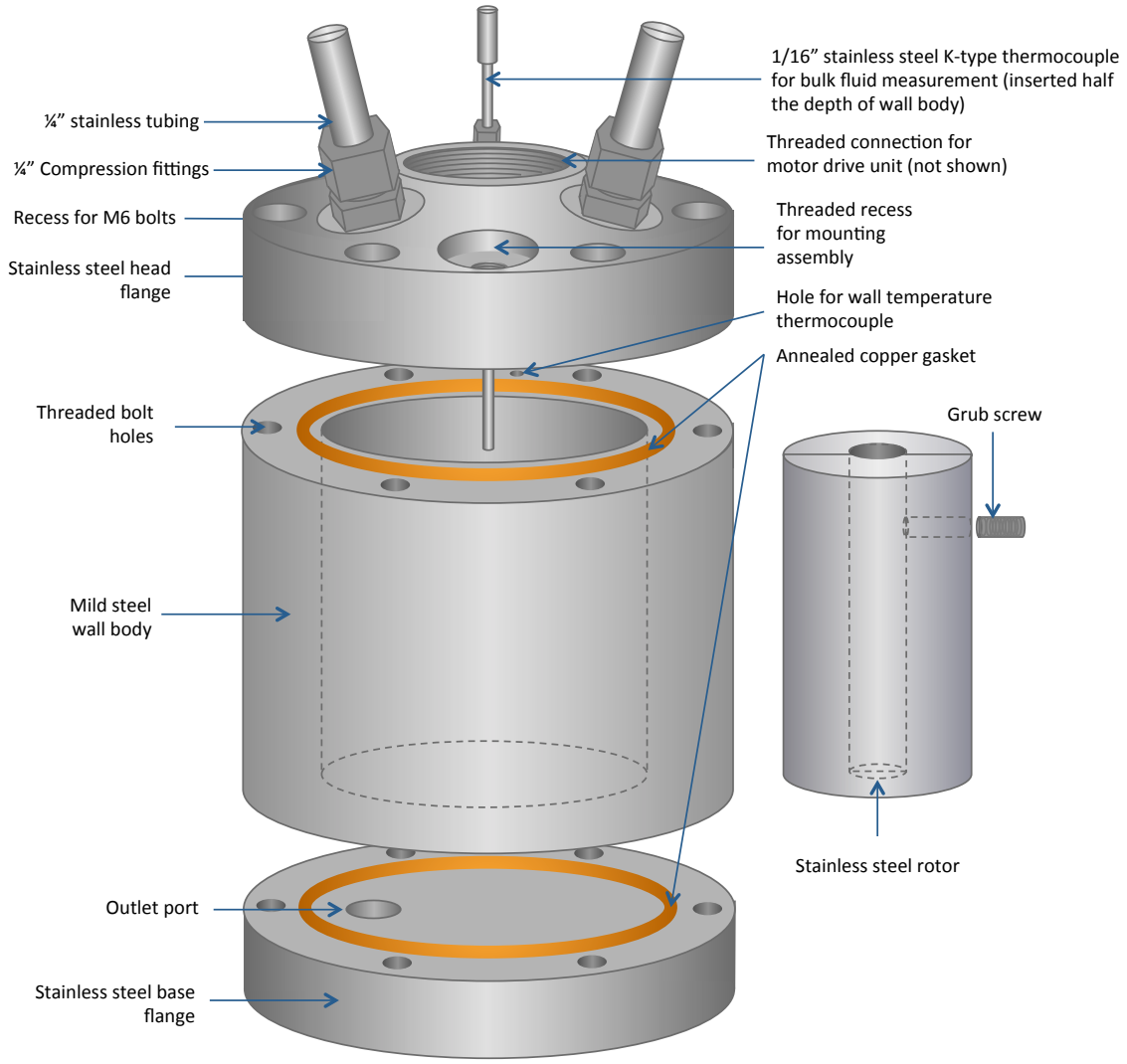


Figure 3.1 Schematic of Taylor Couette vessel body (not to scale)

The cross-sectional drawing (Figure 3.2) shows the reactor components and void spaces. The annular fluid space is defined by the inner cylinder, outer cylinder and top and bottom flanged bodies. During operation, the void is completely filled by liquid, i.e. one single phase thereby preventing flashing problems present with the earlier micro-bomb reactor. A small gap (2 mm each) above and below the rotor is maintained to allow for rotation of the shaft within its enclosure. A stainless-steel mounting assembly is attached to the reactor head unit for securing the reactor in place. Detail of the reactor head unit can be seen in the scale top view Figure 3.3.

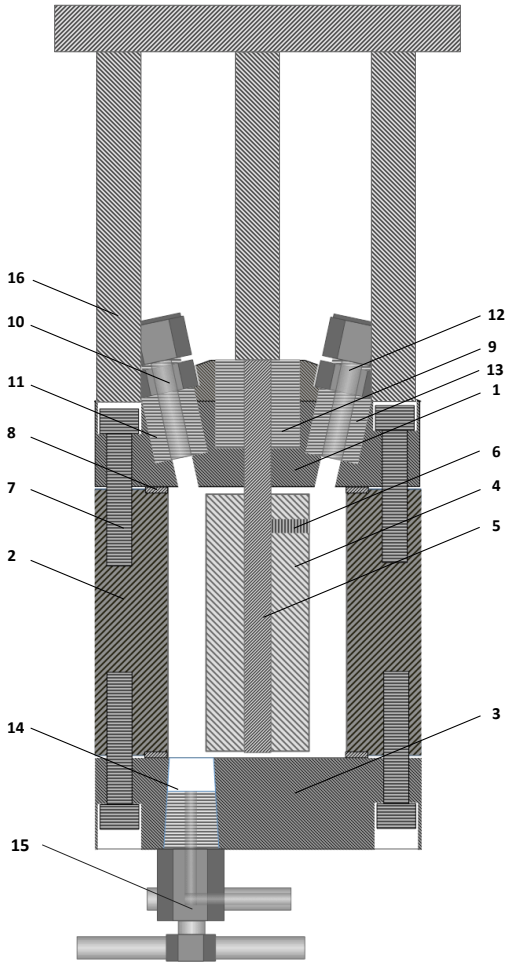


Figure 3.2 Scale cross section through the assembled batch reactor cell excluding the motor unit. 1 – stainless steel head flange, 2 – mild steel wall body, 3 – stainless steel base flange, 4 – stainless steel rotor, 5 – stainless steel rotor shaft, 6 – grub screw, 7 – stainless steel M6 x 25mm bolts, 8 – annealed copper gaskets, 9 – threaded motor port, 10 & 12 – ¼" Swagelok straight fitting with copper gasket, 11 - threaded inlet port, 13 – threaded top outlet port, 14 – lower outlet port, 15 – all stainless steel Swagelok bleed valve, 16 – Stainless steel reactor mounting assembly

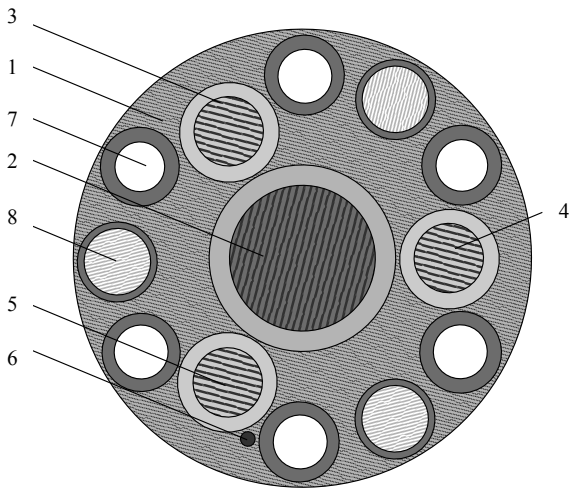


Figure 3.3 Scale Top view of Taylor Couette reactor head unit: 1 – Stainless Steel head unit, 2 –threaded motor connection, 3 – threaded Inlet port, 4 – threaded top outlet port, 5 – Threaded bulk thermocouple connection,

6 – Hole for wall temperature thermocouple (drilled fully through head unit and to the middle of the wall body), 7 – recessed holes for M6 flange bolts, 8 – threaded connection to the mounting assembly

3.3.2 Stirring

The motor drive unit (Figure 3.4) is powered by a 1/10 horsepower DC servo motor from Autoclave Engineers (Mag3050) with all stainless-steel construction and graphite bushings. The motor is sealed from the rotor and uses magnetic couplings to transfer torque. The motor unit screws onto the head of the reactor and is sealed using a copper gasket.

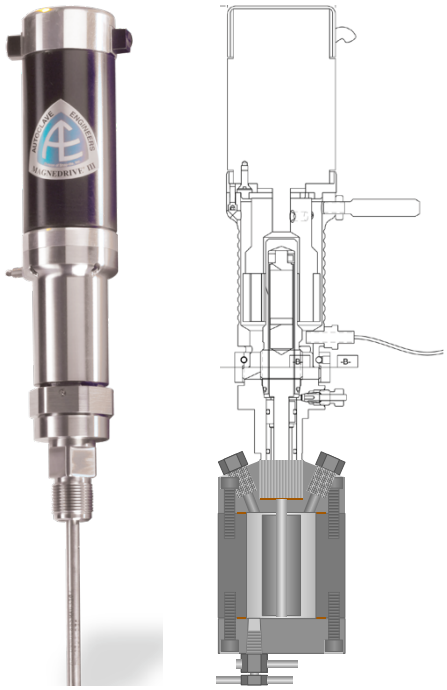


Figure 3.4 Magnetically sealed Motor Drive Unit from Autoclave Engineers (MAG3050) image with cross-sectional drawing superimposed onto reactor cross section for scale

3.3.3 Heating

During operation the Taylor Couette reactor is heated in a vertical cylinder furnace (Carbolite VST 12/200) with a ceramic tube (60% alumina from Multi-lab) installed to electrically insulate the heating element from the steel reactor whilst helping to provide even heat distribution. The top of the furnace is packed with ceramic fibre wool to limit convective heat losses. Temperature inside the furnace is controlled by a proportional integral derivative (PID) controller and adjusted manually from the power control box. The operator controls the furnace temperature to achieve the desired wall surface temperature (monitored using a separate thermocouple and data-logging software). There is also an in-

built over-temperature protection system consisting of a secondary thermocouple which cuts the power if the furnace exceeds a pre-set temperature (set to 650 °C), in the case of a faulty temperature sensor.

3.3.4 Gas purging, loading, measurement and product collection

The process lines connected to the reactor are comprised of three sections: purge/loading, purge/measurement and product collection (see Figure 3.5). The purge/loading and purge/measurement sections enable the user to dry and purge the process line with an inert gas supply (N_2), load the sample fluid into the vessel and slowly force the liquid from the sample vessel into the reactor by differential pressure. Ambient air is displaced with nitrogen by repeatedly pressurising from the supply bottle and venting before the sample fluid loads into the reactor.

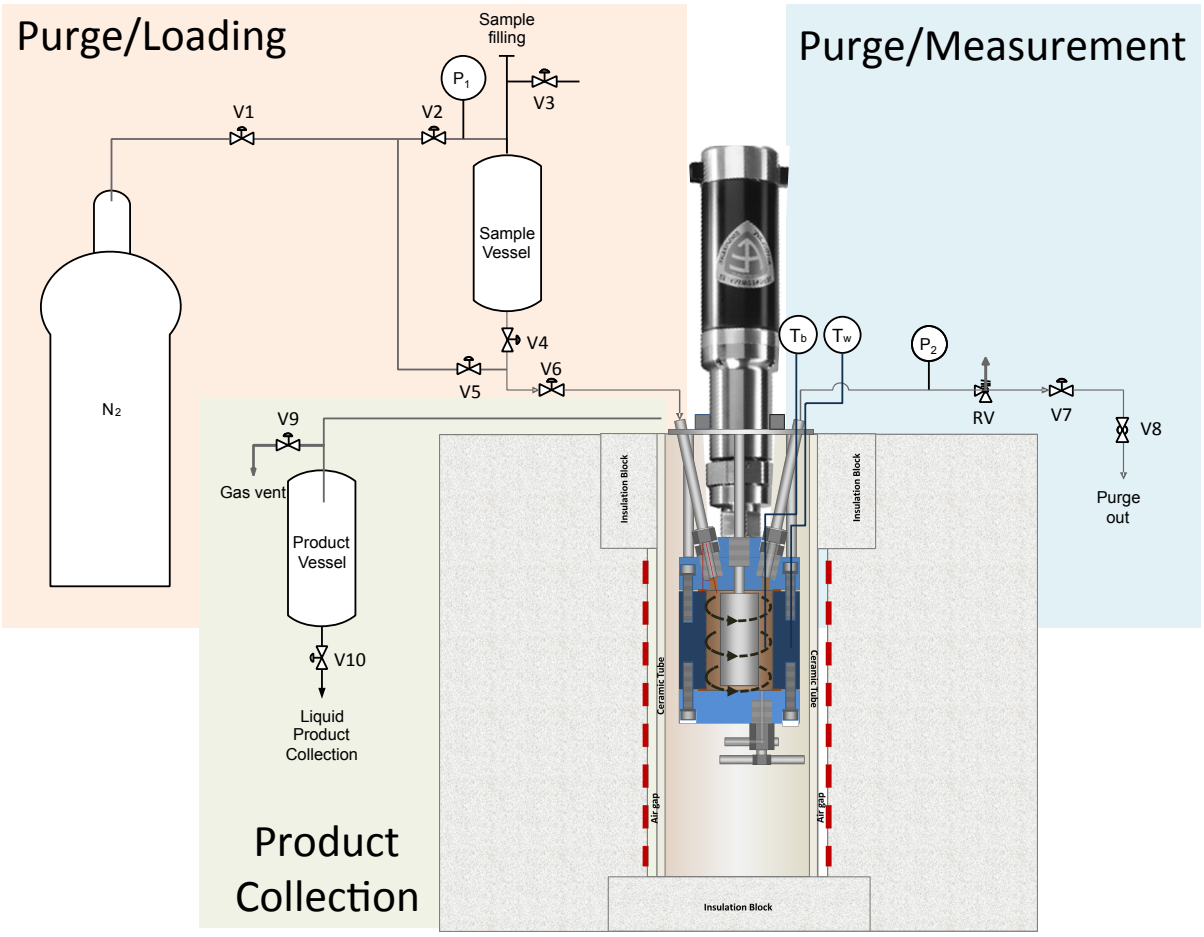


Figure 3.5 Schematic of fouling reactor system with associated tubing and instruments. Purge/loading section (orange), purge/measurement section (blue), product collection section (green)

The scale process flow diagram (Figure 3.6) shows labelled fittings for the construction of the fouling reactor system. Test fluid is filled into the sample vessel by removal of the plug on Tee4, injecting the sample liquid via syringe and blunt needle. The system is purged with nitrogen and the sample liquid

is transferred into the reactor by pressure gradient from the inert gas supply under slow rotation of the inner cylinder. This rotation is important to help liquid to fill the void under the rotor and encourage bubbles to the surface. A one-phase system can be achieved by expelling the nitrogen gas from the outlet until the entire line is filled with liquid. Pressurising the system to full operational pressure (30 bar) will collapse any remaining potential gas bubbles remaining.

The batch reactor connects to the purge/loading system via the inlet and top outlet ports using stainless steel braided flexible hoses. The bleed valve is located on the underside of the reactor base. At the end of an experiment, the reactor is raised out of the furnace and the bleed valve connects to the product collection section of the process line. Fluid is transferred to the product vessel; excess gas is vented and the liquid product is collected into a sample container for subsequent analysis.

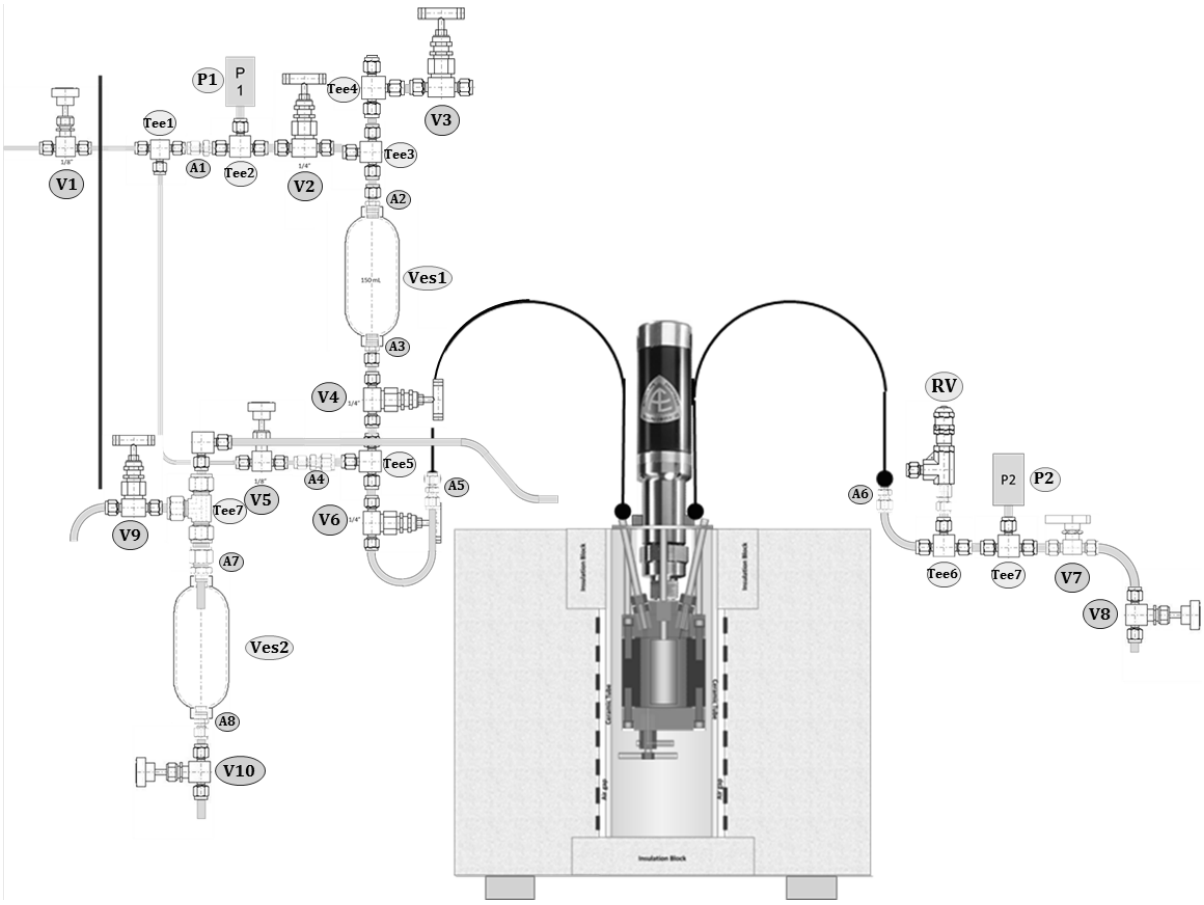


Figure 3.6 Scale Process flow diagram of the Taylor Couette cell batch reactor and purge, loading and product collection system: V1 – V6, V8 – V10: needle valves, A1 – A8: reduction adapters, Tee 1 – Tee 8: Tee fittings, P1 – P2 – pressure transducers, Ves 1 – Sample loading vessel, Ves 2 – Sample collection Vessel, RV – Pressure Relief Valve

A photograph of the assembled fouling test apparatus is given below in Figure 3.7, including motor speed control, pressure and temperature logging assemblies. The assembly can be seen inside its steel containment box.



Figure 3.7 Image of the batch fouling reactor system in steel cabinet: 1 - pressure logger, 2 - variable power supply, 3 - Temperature logger, 4 - sample loading port, 5 - sample loading vessel, 6 - motor, 7 - reactor, 8 - furnace, 9 product collection vessel, 10 - outlet valve

3.3.5 Pressure measurement and safety considerations

The liquid pressure in the reactor is measured using a pressure transducer P2 and a pressure relief valve RV protects against over-pressurisation in the system. During operation, needle valve V6 connecting the reactor to the liquid supply vessel is kept open. An excess of the working fluid is present in the inlet/outlet lines and in the supply sample vessel Ves1. At the end of the experiment, V6 is closed to prevent fresh liquid from the Ves1 from flowing back into the reactor as the reactor cools and the fluid contracts so preventing contamination of the heated fluid.

The whole process system, reactor and furnace are housed in a cabinet built from 3 mm thick steel sheets with shatterproof polycarbonate windows. The cabinet is ventilated with an in-line ducted fan that runs to the laboratory extraction system creating a reduced pressure inside the cabinet and preventing any gas or liquid fumes from escaping into the laboratory workspace. The unit is highly fire resistant as there are no flammable materials inside the cabinet other than the sample fluid, and the small working volumes (~75 mL) would very likely not cause any runaway fire.

The system pressure operates at 30 bar pressure (3 MPa) for all experiments. The relief valve is calibrated to 50 bar and during commissioning the system pressure was raised up to 70 bar to check for leaks before tuning the relief valve down to 50 bar. Additionally, the experiments are endothermic in nature and do not release noticeable gas so the risk of over-pressurisation is minimal.

3.3.6 Lifting mechanism

The reactor and motor drive are heavy, so for safety, operator convenience and ensuring the reactor is repeatedly held in the same location for each reaction, a robust lifting mechanism was constructed within the steel cabinet, see Figure 3.8 and Figure 3.9.

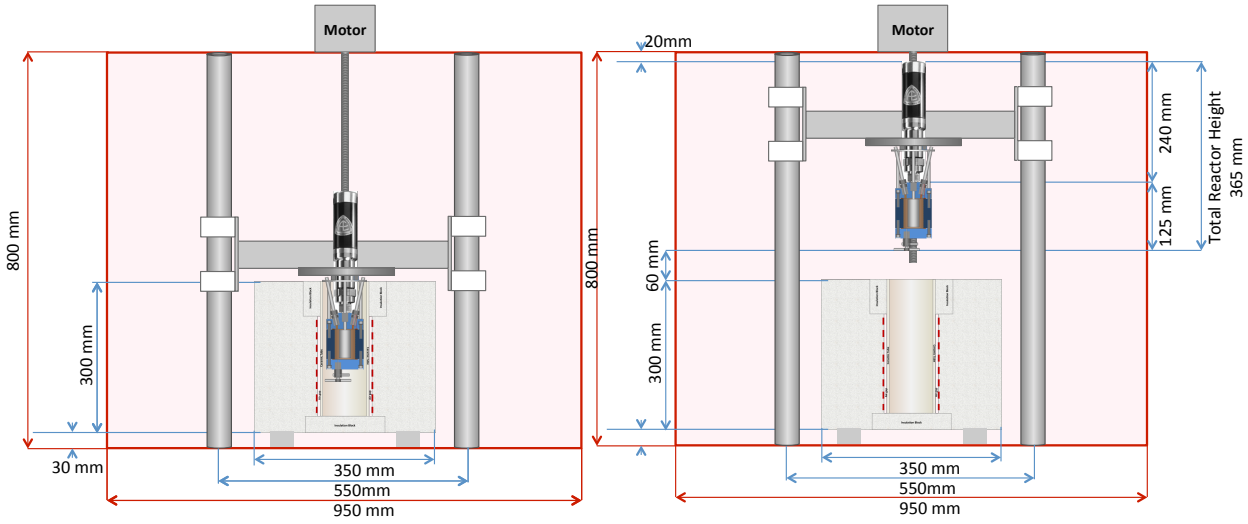


Figure 3.8 Schematic of the reactor lifting mechanism within the steel cabinet showing the lowered reactor inside the tube furnace (left) and the fully raised reactor in between experiments (right)

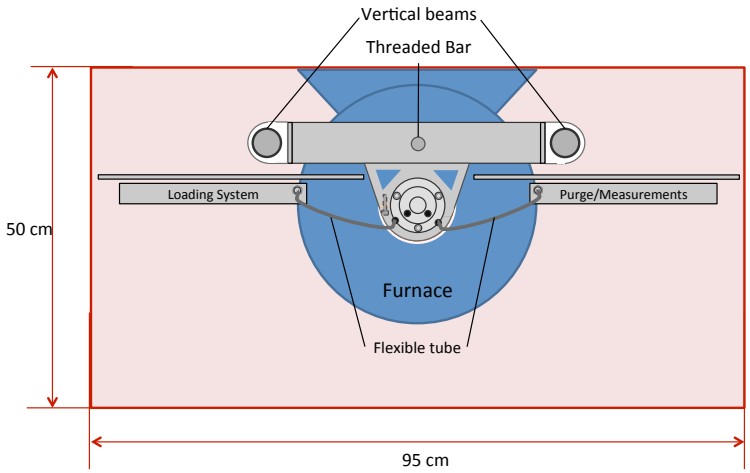


Figure 3.9 Top view of the steel cabinet showing reactor, furnace and lifting mechanism. The aluminium section slides on the white acetal polymer guides and is hoisted by a motor attached to a threaded bar which goes through the centre of the aluminium crossbeam.

A pair of vertical steel tubes guide the horizontal aluminium beam attached to pairs of acetal guides (see Figure 3.10). The beam is hoisted by a threaded bar driven by a geared motor on top of the cabinet. A support fixture clamps the mounting assembly firmly in place, which in turn suspends the reactor into the furnace. The upper and lower lifting heights are limited by high and low level micro-switches which ensure the reactor is always suspended in the furnace in the same position each time it is lowered.

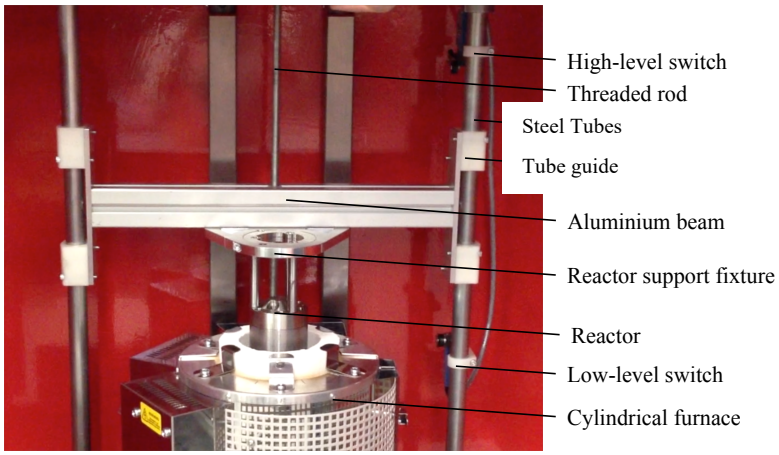


Figure 3.10 Image of the partly constructed reactor detailing components of the reactor, furnace and lifting mechanism (note the reactor head viewed here was redesigned to better accommodate the motor and fittings)

3.3.7 Thermal expansion considerations

During warm-up of the system to operating temperature, both the fluid and the Taylor Couette cell expand, both the thermal expansion coefficient of the test fluid is far greater. The open system design allows excess fluid to flow back into the liquid vessel. For safety reasons a predetermined minimum gas volume is maintained in the sample vessel before heating to allow the liquid to fill the space during expansion.

During heating the thermal expansion of the crude oil inside results in an increased volume of liquid inside the system. This excess liquid expands back into the sample vessel and the gas volume above it decreases, so acting as a buffer to the expanded liquid. In the event of pressure build up or gas evolved from cracking reactions, the pressure would increase up to a maximum of 50 bar. Above this pressure excess liquid would be expelled from relief valve to relieve the pressure.

Internal volume of the Taylor-Couette cell annulus at ambient temperature is given by:

$$V_{annulus} = \pi L({R_2}^2 - {R_1}^2) = 50.47 \text{ mL} \quad 3.1$$

The reactor is intended to operate at temperatures up to 320 °C. The volume expansion for n-dodecane can be given by equation 3.2:

$$\Delta V_{annulus} = \frac{\rho_1}{\rho_2} \cdot V_{annulus} \quad 3.2$$

Where ρ_1 and ρ_2 are the densities of the fluid at full temperature and ambient temperature respectively. The steel reactor body also undergoes a thermal expansion (volumetric thermal expansion coefficient β for carbon steel = 32.4×10^{-6} m·($m^{-1}K^{-1}$)) thus the reactor annulus volume at 320°C can be calculated by:

$$\Delta V_{annulus} = V_0\beta(T_2 - T_1) = 50.5 * 32.4 \times 10^{-6} * 300 = 0.49 \text{ mL} \quad 3.3$$

Therefore, at 320 °C, $V_{annulus}$ = V_0 = 51.0 mL.

Dodecane has the highest thermal expansion of all fluids intended for use in the Taylor Couette reactor. The density of n-dodecane has been predicted using NIST REFPROP[133] for temperatures from 20 °C (751.5 kg/m^3) to 320 °C (495.8 kg/m^3) and 30 bar pressure (3 MPa). The 51mL volume of n-dodecane which is present in the reactor at 320 °C is equivalent to 33.6 mL n-dodecane at ambient temperature $\left(\frac{\rho_1}{\rho_2} \cdot V_{annulus} = \frac{495.8}{751.5} * 51.0\ mL\right)$, so upon heating, 17.4mL dodecane is expelled from

the reactor upon heating. Fluid expansions for crude oils are similarly calculated in appendix 11.6.1 using data from the US Dept. of Commerce, Beaureu of standards.[134]

The volume above the reactor including the sample vessel and tubing is approximately 150 mL. If the 17.4 mL sample fluid is displaced from the reactor upon heating, the reduction in volume would result in an increase in pressure of 13%. Therefore, initial pressurisation at ambient temperature will need to be less than the target operational pressure after accounting for heating the sample. The ambient starting pressure required to achieve 30 bar pressure at operating conditions $P_2 = \frac{V_1}{V_2} \cdot P_1 = 26.5\ bar$, so this is a first starting pressure for commissioning tests. Additionally, having a significant gas volume above the fluid provides a buffer for the sample fluid to expand into without activating the relief valve, which is not wanted, as this will draw liquid out of the reactor into the effluent tubing, which could affect results.

3.4. Hydrodynamic properties: comparison between the Taylor Couette reactor and a heat exchanger tube

3.4.1 Fluid velocity

Linear fluid velocities of crude oil in industrial heat exchanger tubes are generally in the region of 1 – 3 m s^{-1} and in the turbulent regime for all but the earliest heat exchangers of the process line (i.e. when the feed is cold). The focus of this work is fouling phenomena at the hot end of the heat exchanger train.

Shell and tube heat exchangers in chemical processing industries generally use tubes diameters from 3/8" to 1.5", most commonly 3/4 or 1" OD, the latter being preferable for fouling services[135]. Thus, assuming a standard 1" OD, 0.083” wall thickness and thus an inner radius of 0.417” (10.6 mm).

The geometry of a Taylor Couette cell is characterised by the radii of the outer (R_2) and inner (R_1) cylinders and its axial length L (see Figure 3.11)[136]. The cylindrical gap thickness $d = R_2 - R_1$ = 0.0084 m and radius ratio $\eta = \frac{R_1}{R_2}$ = 0.58 in this case. The aspect ratio (Γ) is the ratio of the axial length to cylindrical gap thickness $\Gamma = \frac{L}{d} = 7.14$ in this case.

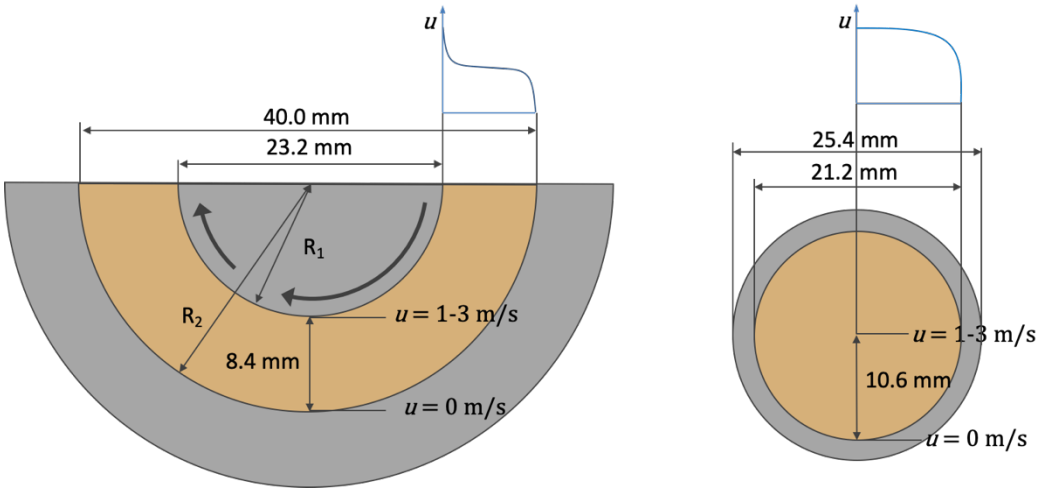


Figure 3.11 Cross sectional profiles through the Taylor Couette cell reactor (left) and 1 inch heat exchanger tube (right). The steel wall is shaded grey and the brown fluid fills the annular section and inner tube section. Velocity profiles under turbulent conditions are shown for azimuthal flow in the Taylor Couette cell and axial flow in a pipe.

The design requirement for rotational velocity mandates that the inner cylinder surface must also be in the region of 1 - 3 m/s (equivalent to the bulk fluid velocity in a tube). The annular gap within the reactor *(R_2 - R_1 = d)* = 8.4 mm. Both Taylor Couette cell and tube satisfy the boundary conditions where the maximum fluid velocity is between 1 and 3 m/s and no-slip condition at the wall.

Having defined the inner cylinder dimensions, with a radius R_1 of 11.6 mm, the rotation speed in rpm required to achieve the minimum tangential velocity u_t at the rotor surface of 1 ms^{-1} is given by:

$$u_t = \frac{30u_{R1}}{\pi R_1} = 823\ rpm \qquad 3.4$$

where: u_{R1} = rotational velocity at rotor surface (m/s)

The motor drive unit is capable of rotational speeds of up to 2500 rpm, so this satisfies the flow speed requirement, 1-3 m/s thus representing 33 - 99% of the motor speed range.

Fluid flow can be characterised by the geometric parameters mentioned above, physical properties of the fluid and the rotational speed of the inner cylinder. To compare the states of flow between a heat exchanger tube and the Taylor Couette reactor in turbulent flow, two rheological properties, Reynolds number *Re* and wall shear stress τ_w will be determined for both cases. Taylor number will also be determined for the Taylor Couette reactor.

3.4.2 Flow Behaviour in a steel heat exchanger tube

Reynolds number in a tube is given by the equation:

$$Re = \frac{uD_h}{\nu} \quad 3.5$$

where u = mean fluid velocity (m/s) D_h = hydraulic diameter (m), ν = kinematic viscosity (m^2/s)

The mean wall shear stress τ_w (Pa) may be expressed in terms of the Darcy-Weisbach equation[137]:

$$\tau_w = \frac{1}{8} f_D \rho u^2 \quad 3.6$$

where: ρ = fluid density (kg/m^3)

The Darcy-Weisbach friction factor f_D measures of the resistance to flow in a pipe and is given by $f_D = 64/Re$ for laminar flows[138]. For turbulent flows it is a function that depends on the pipe, the fluid and its velocity. For fully developed turbulent flows it may be solved using the Colebrook Equation or using the Moody chart (appendix 11.3.1)[139,140], both relate the relative roughness $\left(\frac{\varepsilon}{D_h}\right)$ and Re to f_D.

In a typical 1" OD drawn steel tube, the roughness height (ε) may be 0.015 mm[141] and hydraulic diameter D_h is 21.2 mm so the relative roughness $\left(\frac{\varepsilon}{D_h}\right)$ = 0.00071. The friction factor can also be modelled at this relative roughness by the Blasius correlation for smooth pipes $f_D = (100Re)^{-0.25}$ for Reynolds numbers between 3,000 and 2 x 10^4. At higher Reynolds numbers (between 2 x 10^4 and 2 x 10^6), a different correlation should be used where $f_D = \frac{0.184}{Re^{0.2}}$.[142]

3.4.3 Flow behaviour in the Taylor Couette reactor

The main dynamic variable is the angular velocity (ω /rad s^{-1}) of the inner cylinder: This may be calculated from the rpm as follows:

$$\omega = \frac{\pi \cdot rpm}{30} = \frac{u_i}{R_1} \quad 3.7$$

u_i = velocity at inner cylinder surface (ms^{-1})

The tangential Reynolds number (Re_t) at the surface of the inner cylinder can be defined as

$$Re_t = \frac{\omega R_1 D_h}{\nu} \quad 3.8$$

where: ν = kinematic viscosity (m^2/s) D_h = Hydraulic diameter (m)

$$D_h = \frac{4S_p}{P_m} = \frac{2\left(R_2^2 - R_1^2\right)}{R_2 + R_1} = 0.0168 \text{ m} \quad 3.9$$

Where: S_p = cross sectional area = $\pi(R_2^2 - R_1^2)$

P_m = Wetted Perimeter = $2\pi(R_2 + R_1)$

The Taylor number *Ta* determines the significance of the centrifugal forces relative to viscous forces and which give rise to the vortex flow above a critical Taylor number Ta_c and may be calculated from the following equation:[143]

$$Ta = \frac{2(1-\eta)}{1+\eta} Re^2 \qquad 3.10$$

It should be noted that several other definitions for the Taylor number are used in the literature. One frequently used definition[136] takes into account the hydraulic diameter $Ta = (\omega^2 R_1 (D_h/2)^3/v^2)$, another such definition[145] is Ta = $(\omega^2 R_1 (d)^3/v^2)$, however all give rise to values in the same order of magnitude. The critical Taylor number as cited by Roberts et al[146] is 2336. The Taylor number ratio Ta/Ta_c is often used as a metric to describe vortex flow. Vortex flow generally becomes turbulent above approximately $1000Ta_c$. [147]

Wall shear stress is given as:[148]

$$\tau_w = \frac{G\mu^2}{2\pi {R_2}^2 \rho} \qquad 3.11$$

where, μ = dynamic viscosity (Pa.s) G is the dimensionless torque

For *Re* > 10 000, $G = \left[\frac{0.23 \cdot \eta^{1.5}}{(1-\eta)^{1.75}}\right] Re^{1.7}$

For *Re* ≤ 10 000, $G = \left[\frac{1.45 \cdot \eta^{1.5}}{(1-\eta)^{1.75}}\right] Re^{1.5}$

3.4.4 Hydrodynamic prediction for Paratherm® NF - heat transfer oil

For the commissioning process, a commercial non-fouling heat transfer oil Paratherm NF is used. Paratherm is a purified and hydrotreated mineral oil with fluid properties similar to a medium crude oil with well-defined physical properties and is stable at temperatures exceeding 340 °C.

Calculations of Re, Ta and τ_w are useful for predicting hydrodynamic conditions for the Taylor-Couette reactor and for comparisons with heat exchanger tubes. Physical properties[149] are given in Table 3.1:

Table 3.1 Paratherm® NF Physical Properties

Dynamic Viscosity at 20 °C /Pa.s	37.46×10^{-6}
Density at 20 °C /kg m^{-3}	883
Flash Point (ASTM D93) /°C	149
Boiling Point (at 101 kPa) /°C	371
% Volume expansion per 100°C	9.9
Average Molecular Weight	340

For the purpose of comparison, the tangential velocity u_t of the Taylor Couette rotor was compared against an equivalent linear fluid velocity in a typical heat exchanger tube. A rotation speed of 823 rpm (13.7 s^{-1}) corresponds to 1 m/s. 1646 rpm (27.4 s^{-1}) corresponds to 2 m/s and 2470 rpm (41.2 s^{-1}) corresponds to 3 m/s. Results are given below in Figure 3.12 and Figure 3.13:

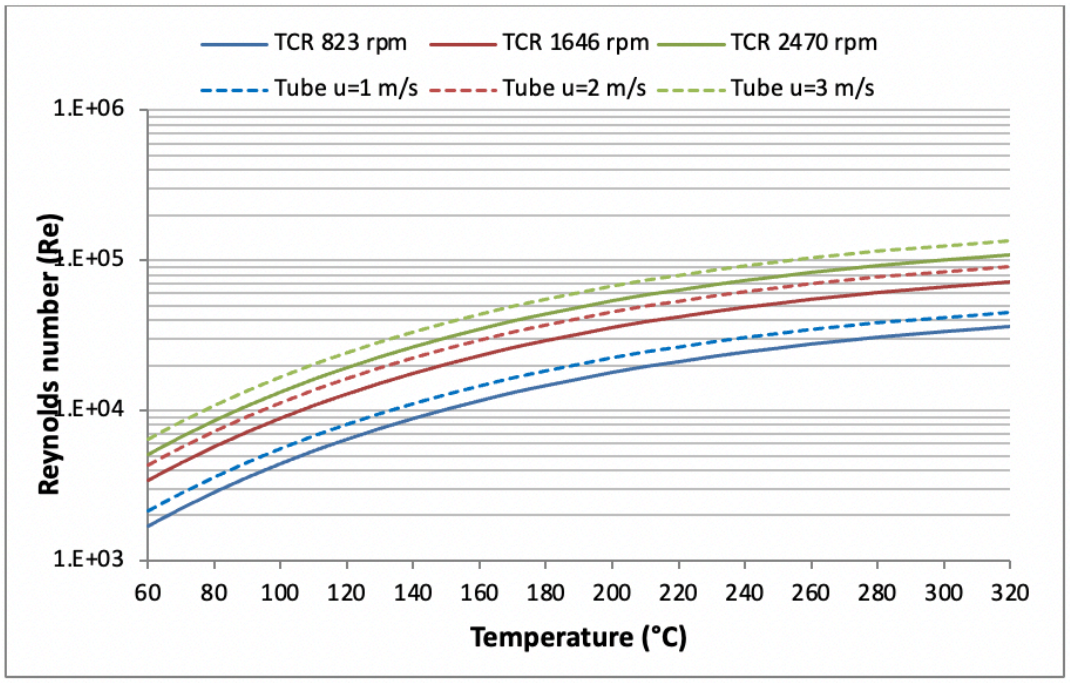


Figure 3.12 Model Predictions of the Temperature dependence on Reynolds Number for the Taylor Couette Reactor (TCR) at 823 rpm, 1646 rpm and 2470 rpm (tangential velocities of 1, 2 and 3 m/s) and Heat Exchanger Tube at 1, 2 and 3 m/s fluid velocity

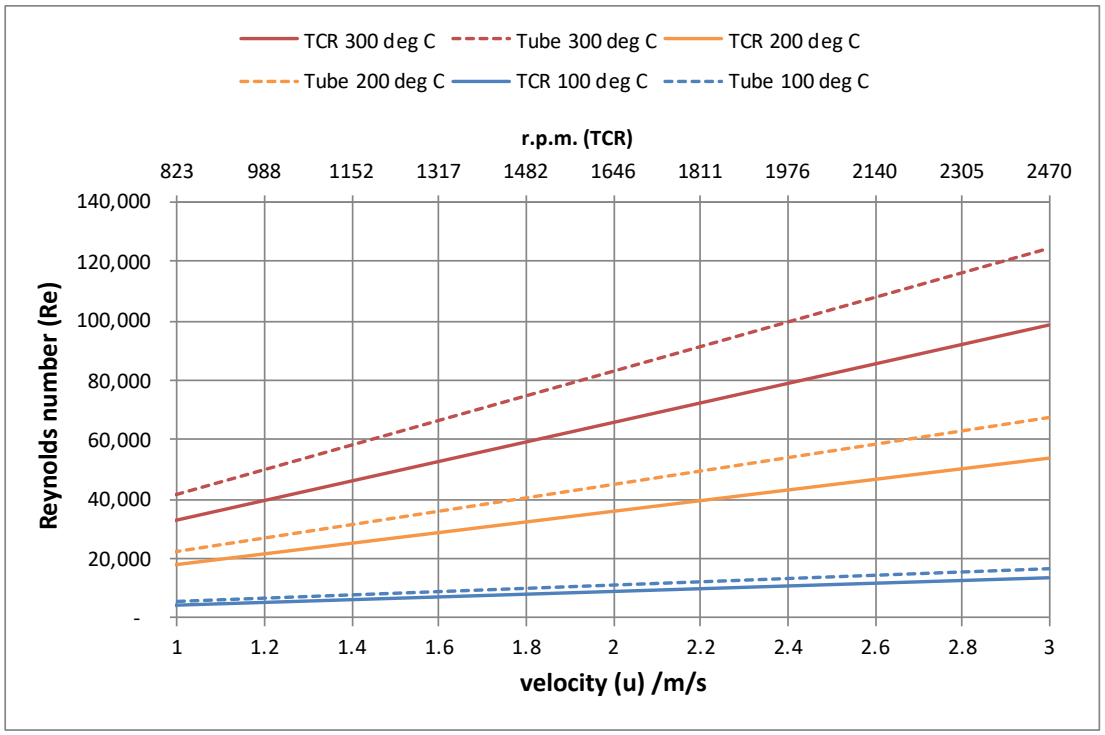


Figure 3.13 Predictions of the fluid Reynolds number with tangential velocity for the Taylor Couette Reactor (TCR) and linear velocity in a Heat Exchanger Tube at three isotherms: 100, 200 and 300 °C.

As expected, Reynolds numbers increase with higher temperature (and correspondingly lower viscosity). Re also increases with higher fluid velocity for both TCR cell and tube flow. Reynolds numbers are relatively higher for the tube relative to the reactor. At expected operating conditions of between 1 and 3 m/s at 300 °C, Re is in the highly turbulent regime: 4.2 - 13.5 $\times$ 10^4 in the tube, 25 % higher than the Taylor Couette Reactor at 3.3 - 9.9 $\times$ 10^4 at all velocities. Whilst the difference is significant, they are in the same order of magnitude for reasonable comparison.

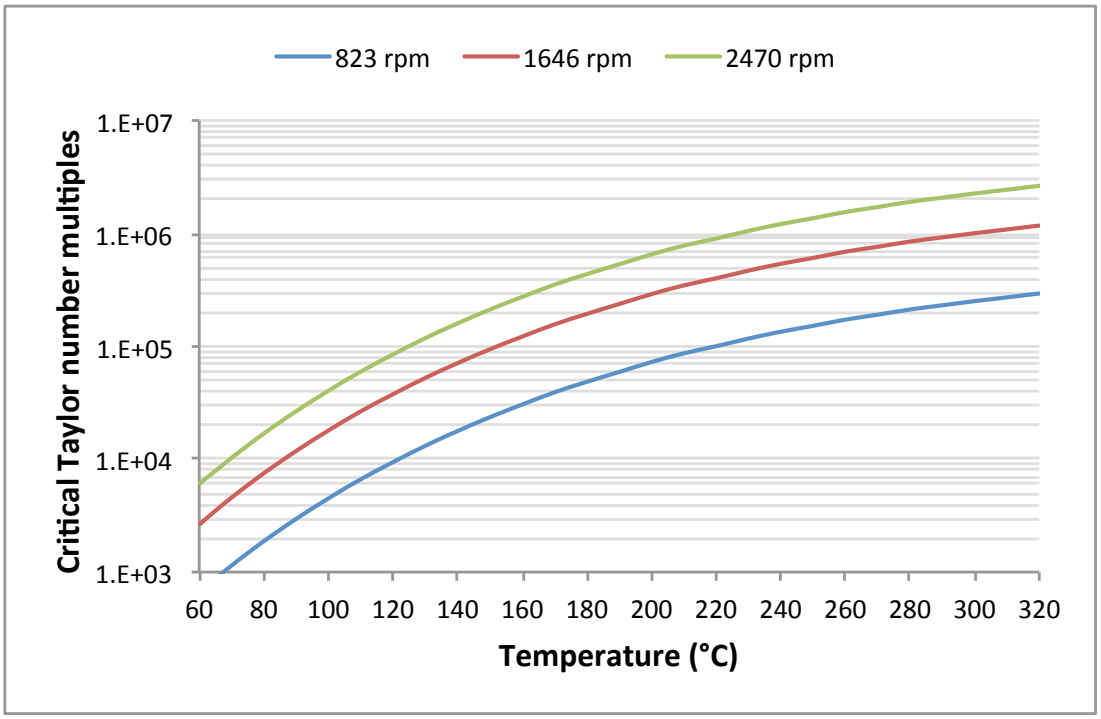


Figure 3.14 Fluid Taylor number in the Taylor Couette reactor at varying temperatures for rotations speeds at 823, 1646 and 2470 rpm equivalent to 1, 2 and 3 m/s tangential fluid velocity

Taylor numbers are in range of 5.9×10^8 to 5.3×10^9 at 300 °C, highlighting strong centrifugal forces relative to viscous forces in the reactor. Dividing by Ta_c gives the critical Taylor multiple[143]. At 300 °C, this is between 2.5×10^5 Ta_c and 2.3×10^6 Ta_c highlighting turbulent instabilities caused by centrifugal forces; any Taylor vortices are highly turbulent in these conditions. Wall shear stresses are predicted as a function of temperature and velocity for the Taylor Couette reactor and heat exchanger tube in Figure 3.15 and Figure 3.16

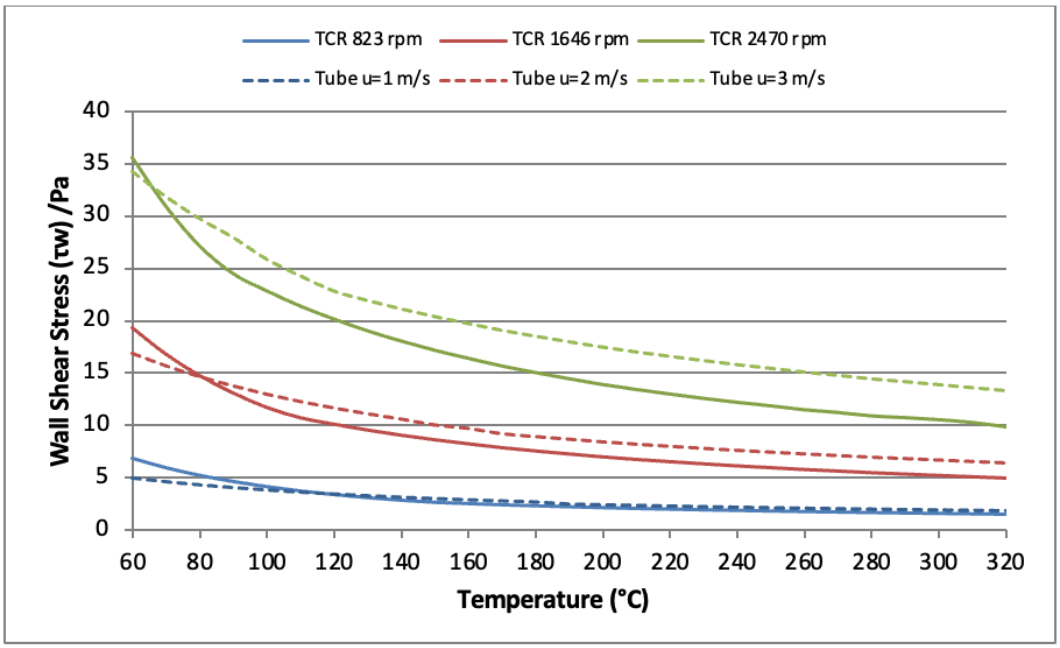


Figure 3.15 Model predictions for the temperature dependence on Reynolds number for the Taylor Couette Reactor (TCR) at 823 rpm, 1646 rpm and 2470 rpm (tangential velocities of 1, 2 and 3 m/s) and Heat Exchanger Tube at 1, 2 and 3 m/s fluid velocity

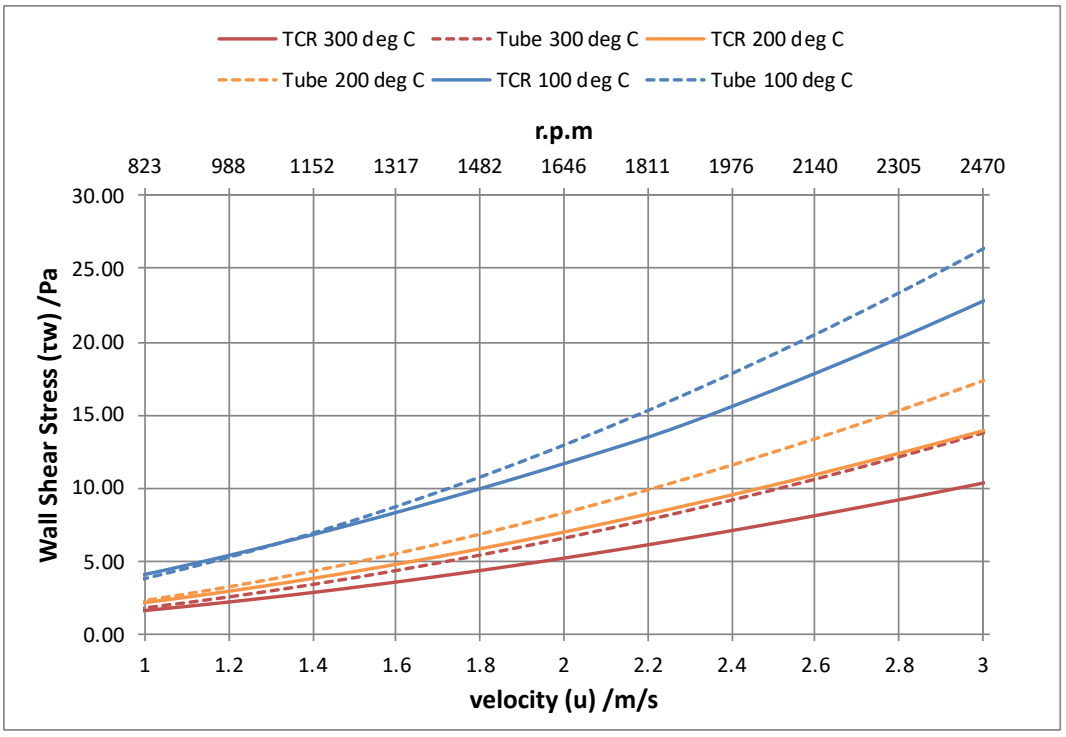


Figure 3.16 Model predictions for the dependence of wall stress on tangential velocity for the Taylor Couette Reactor (TCR) and Heat Exchanger Tube at three isotherms: 100, 200 and 300 °C.

As expected, wall shear stress decreases with increasing temperature due to reduced viscosity, and increases with fluid velocity for both the Taylor Couette reactor and tube. Again, the tube generally

exhibits higher wall stresses than the reactor for the same tangential flow rate. There is an exception at lower temperatures where the reverse is true.

This inflection of wall shear stress at relatively low temperatures is governed by the different powers applied to viscosity between the reactor and the tube. In the tube, τ_w relates the viscosity by the friction factor f_d. while in the Taylor Couette reactor, τ_w relates to the square on the viscosity and the dimensionless torque G, which is also dependent on viscosity. However, during operation (at high temperatures), the wall shear stress is always higher in the tube than the reactor. For velocity ranges between 1-3 m/s at 300 °C, τ_w is between 1.9 and 12.9 Pa in the tube, 20 - 25 % higher than in the Taylor Couette Reactor at 1.6 - 10.5 Pa.

3.5 Conclusions of reactor dynamic model

Predictions of fluid flow characteristics have allowed for comparison between the Taylor Couette fluid system and a real heat exchanger tube typically found in a refinery. Hydrodynamic parameters have been calculated for a non-fouling fluid with characteristics equivalent to a medium crude oil at rotational velocities from 1-3 m/s and temperatures from 60 - 320 °C, although fouling experiments will take place principally at the upper end of this range. Reynolds numbers Re_t at 300 °C are in the order of 3 - 10 $\times 10^4$, wall shear stress τ_w in the region of 1.6 - 10.5 Pa, and Taylor numbers in the order of 10^5 - 10^6 Ta_c are well beyond those expected of stable vortex flow. The laboratory-scale fouling reactor has good comparability to a real heat exchanger tube. Whilst at given tangential velocities Reynolds numbers and wall shear stress in the reactor are lower than equivalent linear fluid velocities than the tube (varying 20-25%), they are on the same order of magnitude, and rotational velocities can be adjusted to achieve a target Reynolds number or wall shear stress if required. For the scope of this project, the reactor is intended to operate in the highly turbulent regime well beyond stable and wavy vortex flow, averaging wall shear stresses axially and azimuthally over the long experimental durations.

Chapter 4 Experimental Methods

4.1 Introduction

This section describes the experimental methods developed and utilised for the preparation and fractionation of crude oils, operation of the Taylor Couette fouling apparatus, subsequent recovery and analysis techniques and procedures of recovered test samples.

4.2 Crude oil Preparation Techniques

Crude oil received from BP exists in its raw extracted from. Whilst H_2S has been off-gassed before delivery, most raw crude oil usually exists as a water-in-oil emulsion containing dissolved salts which are have a high propensity to foul in heat exchangers. In refineries, crude oil is first blended before passing through a desalting step before entering the heat exchanger network. Since this work is focussed on fouling occurring in this heat exchange network, the crude must be desalted prior to fouling experiments in the Taylor-Coutte cell.

This chapter describes two methods for fractionation into Maltenes and C-7 asphaltenes. A method utilised for fractionation on large scale, which relate to fouling experiments on fractionated crude oils and solutions thereof. Secondly an analytical fractionation method is used for analysis of crude oils prior to and post fouling experiments.

4.2.1 Oil Blending

As per BP recommendations, crude oil was blended by addition mass heavy oil into the light oil to prevent asphaltene precipitation. Heavy crude oil was first warmed to 50 °C to reduce the viscosity and mixed, using a clean steel rod. Light oil was weighted out and added to a clean glass flask with magnetic stirrer. Heavy crude oil was slowly added to the light oil under mixing until the correct mass of heavy oil was added and stirring continued for 1 hour.

4.2.2 Desalting Method for crude oil used in fouling experiments

Deionised water and crude oil were measured out in volume ratios of 1.5:1. The water was heated to boiling in a conical flask. While stirring vigorously, crude oil was slowly added to the water flask. The flask was sealed, and temperature was held at 85°C under rapid stirring for 6 hours, maintaining an emulsion of the two phases. The stirrer was then stopped, and heating switched off, allowing the mixture to phase separate and cool overnight. The oil layer was removed by separation funnel and

decanted into vials for centrifugation at 2000 rpm for 10 minutes. The vials of oil were combined into a flask and any remaining water discarded.

4.2.3 Large Scale Crude oil Fractionation

Separation: BP heavy oil was fractionated with n-heptane to produce asphaltenes and maltenes for fouling experiments. The method was adapted from ASTM D6560 to allow separation of sufficiently large quantities of maltenes and asphaltenes without excessive consumption of heptane. Heavy crude oil was warmed to 60°C and stirred to ensure homogeneity before sampling. N-heptane was warmed to 90°C in a closed conical flask and heavy crude oil was poured into heptane in a ratio of 7:1 n-heptane to crude oil whist stirring. The mixture was stirred at this temperature for 1 hour before cooling to room temperature and stirring for a further 3 hours. The resultant mixture was then transferred into vials and centrifuged for 10 minutes at 2000 rpm. The supernatant heptane/maltene was collected in a separate container. N-heptane was again added to the precipitated asphaltenes in a mass ratio of 30:1 to wash residual maltenes from the precipitate. The mixture was then vigorously agitated for 1 hour, centrifuged again for 10 minutes at 2000 rpm and the supernatant added to the previous supernatant. Asphaltenes were then dried at 60°C, crushed and mixed together to a uniform black powder, and sealed to prevent moisture from adsorbing into the powder.

Asphaltene homogenisation and desalting: Asphaltenes may at this stage contain salts from the original oil sample and combined vials of asphaltenes needed homogenisation before use, so asphaltenes were added to a cellulose thimble and extracted into chloroform via Soxhlet apparatus. The chloroform was distilled off and the resultant asphaltenes were dried in an oven at 60°C for 3 days until no further mass loss was detected.

Workup and desalting maltene fraction: Heptane was removed from the supernatant by rotary evaporator at 140°C at ambient pressure until no further liquid was lost. The evaporated heptane was then recycled for further fractionations. The maltene fraction was then desalted by mixing with 1.5 volumes of deionised water and heated to 85 °C stirred vigorously for 6 hours, then left overnight to separate and the oil layer collected via separation funnel.

It should be noted that the recovered maltene fraction contained considerable residual heptane even after ambient pressure rotary evaporation at 125 °C for 4 hours. Vacuum was not applied in the evaporator as the equipment did not have pressure control and more aggressive evaporation would lead to loss of other volatile compounds intrinsic to the maltene fraction. The residual heptane

concentration in the prepared maltene sample was determined by GC-FID to contain 222 mg/ml (see appendix 11.4.1 for GC calibration).

4.3 Taylor Couette Reactor Standard Operation Procedure

4.3.1 Start-up Procedure

Refer to Figure 3.8 in Chapter 3 for the annotated reactor flow diagram. The schematic for the operational procedure is given in Figure 4.1.

Dry process line System: Any remaining solvent had to be removed before use. With valve V3 was closed and V2, 4, 5, 6, 7 and V8 open, V1 was opened to allow a steady flow of N2 gas for 15 minutes and then closed again.

Loading Test fluid into reactor: Valve V4 was closed and the Plug removed from the top (tee4). Sample fluid was loaded into the sample cylinder by syringe and the plug replaced.

Pressure test: The exit valve V8 was closed and the system was leak tested at 30 bar pressure, checking P1. If pressure dropped, the leak was located using soap solution and the joint remedied. After successful leak test was complete, V8 was opened to relieve the pressure to ambient before closing again.

Purge with N2: The system was then purged with N_2 gas by pressurising with nitrogen via V1 to 435psi (30 bar) then closing and carefully opening V8 to relieve the pressure and closing again. This procedure was repeated two further times. Air is diluted in the system to a ratio of 1/30 each time resulting in approximately 1ppm of the original air in the system.

Start motor rotating slowly: The Motor power Supply was switched on and set to 5V for slow rotation of the rotor to help mitigate bubbles during filling.

Load Test Fluid into Reactor: Valves V5, 6 and 7 were closed leaving only V2 open. V1 was slowly opened until P1 displayed 100 psi. V4 was opened followed by slowly opening V6, slowly transferring fluid into the reactor allowing P1 to decrease in pressure by approximately 2 psi per second whilst monitoring increase in P2 until the pressures in P1 and P2 equalised.

Degas Outlet Line: Valve V7 were slowly opened and then closed, allowing the fluid to pressurise the tube section between V7 and V8. V8 was opened to release the pressurised gas from this isolated tube section. This was repeated until all the gas had been released from the system and the sample liquid flowed from the exit stream. V7 and V8 were then kept closed.

Pressurise Reactor with N_2: V1 was opened until pressure readings in P1 and P2 achieved the required system pressure before heating. Set motor to operational speed.

Set Motor to Operational Speed: The motor power supply voltage was increased to achieve the operating rotational speed according to the speed calibration. (1500rpm = 31.4 V)

Begin Data Logging: The computer was switched on and data logging software loaded. Recording was commenced, recording temperature readings every 5 seconds. Pressure, furnace set temperature and measured furnace temperature were recorded in the log-book.

Run Experiment: The furnace was switched on. The reactor was operated according to commissioning recommendations in Chapter 4. The experiment was maintained under constant conditions for the duration of the run, not allowing the wall temperature to deviate more than 1% from the difference between ambient and operational temperatures. i.e. 3 °C for ΔT = 300 °C.

End Experiment: After the reaction time was complete, valve V6 was closed to prevent backflow of fluid into the reactor upon cooling, the furnace was switched off and the reactor was raised out of the furnace to its maximum height for cooling. The cabinet must be kept closed during this time as convection currents from the furnace tended to blow mineral fibres around the cabinet posing an inhalation risk.

End Data Logging: After the reactor had cooled to ambient temperature, the data logging was stopped, saved and the computer switched off.

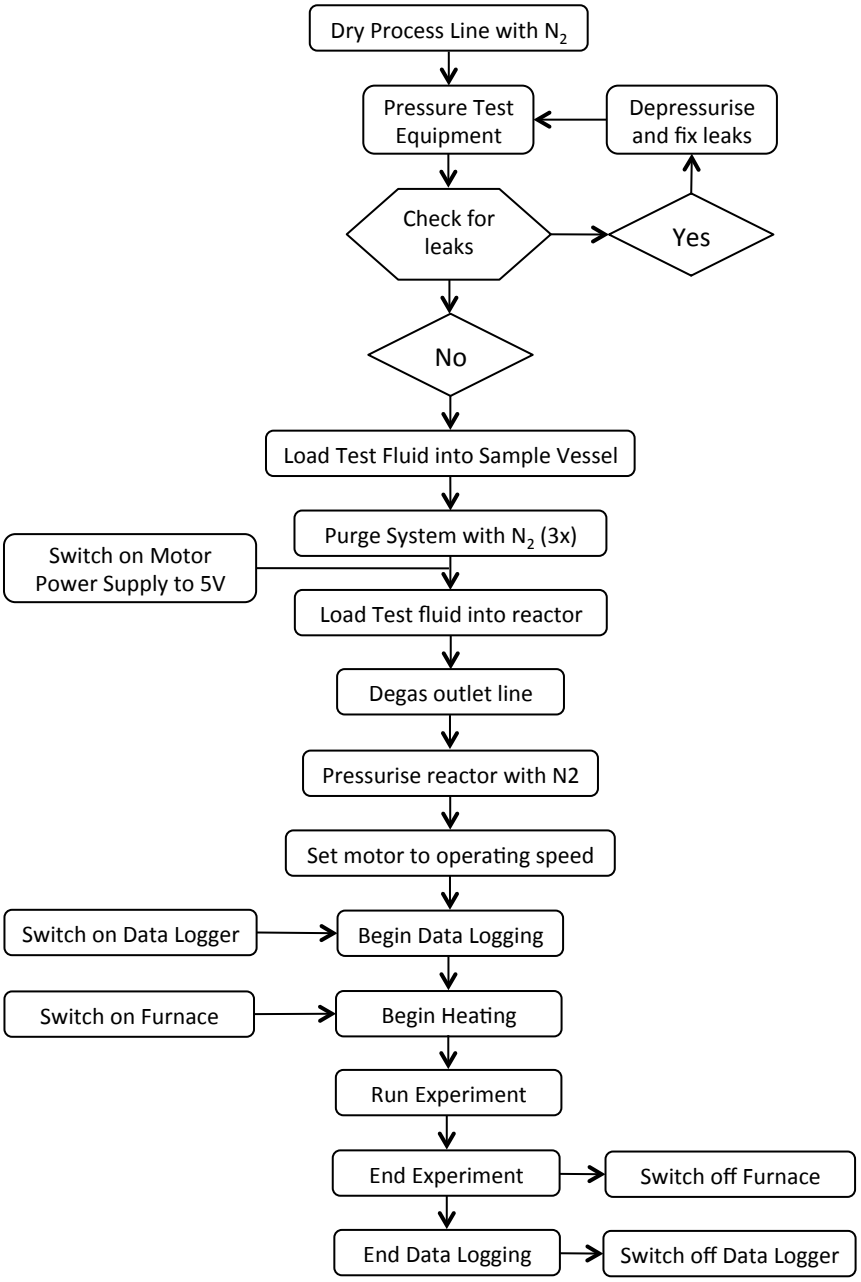


Figure 4.1 Taylor Couette Reactor Operating Procedure

4.3.2 Reactor Products Recovery Procedure

The procedure for the recovery of experimental products is illustrated in Figure 4.2. Once a reaction has cooled to ambient temperature overnight, the mineral wool insulation was removed from the reactor and loose fibres brushed away to prevent contamination during product recovery. The motor is stopped, and its controller switched off before removal of the liquid. Residual pressure in the reactor should be less than 100 psi, if not V8 is opened to reduce pressure to 100 psi recovering liquids. The Collection procedure is as follows:

1. The bleed valve was carefully opened, and the bulk liquid products filled into a pre weighed 60 mL glass vial. The mass of the bulk liquid fraction was recorded.
2. The six reactor bolts securing the top flange unit to the rest of the body were removed and the lower part of the reactor detached from the system and clamped in a vice.
3. The walls of the reactor were carefully washed with chloroform, trying as far as possible to avoid dislodging the fouling solids from the wall surface. The soluble liquid film fraction was filtered and transferred into a separate pre-weighed 30 mL vial. The soluble liquid fraction may contain some solids dislodged from the wall on washing with chloroform. The solution was vacuum filtered through a PTFE filter with a 1 µm pore size from Whatman and washed with chloroform. The soluble film solution was collected in a container. Solids were then dried in an oven for 3 hours at 60 °C and the mass added to that of the wall solids fraction. The soluble film fraction was dried under nitrogen gas flow until the change in mass was >1% in 1 hour.
4. The insoluble fouling solids attached to the wall were removed by washing with a nylon brush and chloroform, the suspension was transferred into a separate vial and the chloroform removed by drying under N_2 gas, then transferred into an oven for 3 hours at 60 °C before weighing.

   The reactor was then cleaned in preparation for the next experiment.

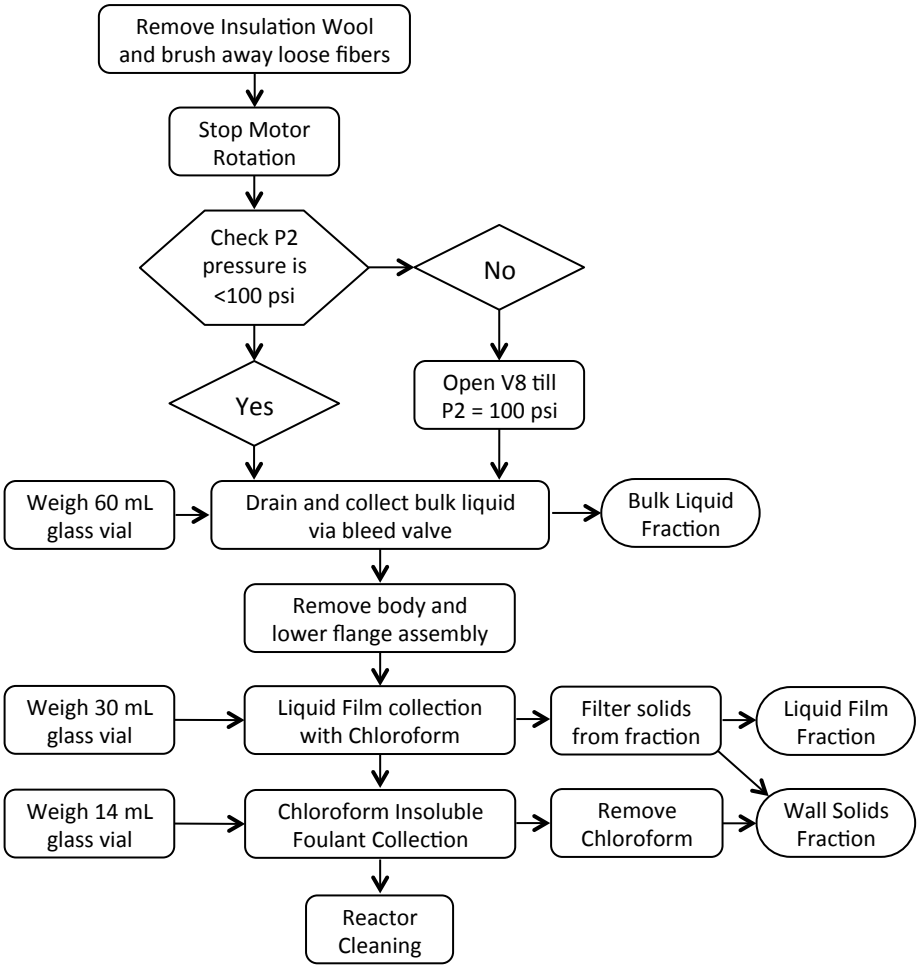


Figure 4.2 Product Recovery Procedure

4.3.3 Reactor cleaning procedure

Once the recovery procedure was complete, thorough cleaning was crucial in achieving reliable data, as any foulant left remaining from previous experiments could act as nucleation sites leading to stronger fouling in subsequent experiments, additional to the extra mass of the un-removed material. The cleaning method was developed and revised after trial experiments (see Figure 4.3), which previously exhibited erratic masses of foulant material.

The lower reactor body was clamped in a vice and the lower flange base was first detached from the wall section by removing the m6 Allen bolts. Each section was cleaned separately. An organic vapour mask must be used for the entire cleaning process where oil and solvent vapours are exposed outside of the fume hood. This includes cleaning the tube system and reactor cabinet.

Lower flange: The bleed valve was dismantled and cleaned using cotton buds and chloroform to remove oil and solids. The inside surface was sanded with 800 followed by 1200 grit wetted alumina paper before rinsing with deionised water, acetone and dried in an oven at 60°C, leaving a shining metallic inner surface.

Wall body: The reactor wall body was turned on its side and the inside surface sanded with 800 grit wetted alumina paper by rolling on a table surface until the inner surface is bright, this was repeated with 1200 grit alumina paper, rinsed with deionised water and acetone and dried in an oven at 60 °C, leaving a shining inner metallic surface. Rolling with abrasive paper leaves fine surface scratches in an azimuthal direction only.

Tube system: A polypropylene flask was positioned under the suspended reactor top flange and rotor to collect waste oil and solvent. Valves V2, 4 and 6 were closed and V3 and 5 opened. The plug on tee 4 was removed and 50 ml chloroform was filled into the sample vessel using a syringe and needle. V1 was opened slightly and V4 carefully opened slightly until N2 gas could be heard bubbling up through the chloroform in the vessel to wash the vessel of residual oil. After a minute, V1, 3, 4, and 5 were closed and V2 opened. V1 was opened until P1 displayed 50 psi. V4 was opened followed carefully by V6 to force the solution out of the reactor inlet line into the propylene flask below. This process was repeated two further times or until the solution showed no further oil being washed from the system. V1 was then opened for 5 minutes to dry any remaining solvent from the line. The reactor outlet line was cleaned by connecting the outlet next to V8 to a 20mL syringe filled with chloroform via silicone tubing and forcing the chloroform up through to the reactor outlet into the flaks below. This was also repeated twice more or until the outlet line showed no remaining trace of oil in the solution.

Top flange: The underside of the top flange and rotor were washed with chloroform. The tube ports were cleaned with cotton buds and chloroform to remove any oil and deposits. The inner surface of the top flange was sanded with wetted 1200 grit abrasive paper leaving bright steel. The rotor was similarly cleaned with 1200 grit abrasive paper, with slow rotation at 8V. After this, the top flange and rotor were rinsed with water followed by acetone to remove any remaining particles, and dried with compressed air.

Reassembly: The wall and bottom flange sections were removed from the oven and the wall clamped in the vice. The bleed valve was reassembled, and two sections were bolted together using new stainless steel bolts and a new copper gasket. The lower reactor unit was then reassembled to the top flange again with new copper gasket and new bolts. Valve V3 was closed, and V2, 4, 5, 6, 7 and 8

opened, and V1 opened to dry the entire line for 15 minutes prior to loading the reactor for a new experiment.

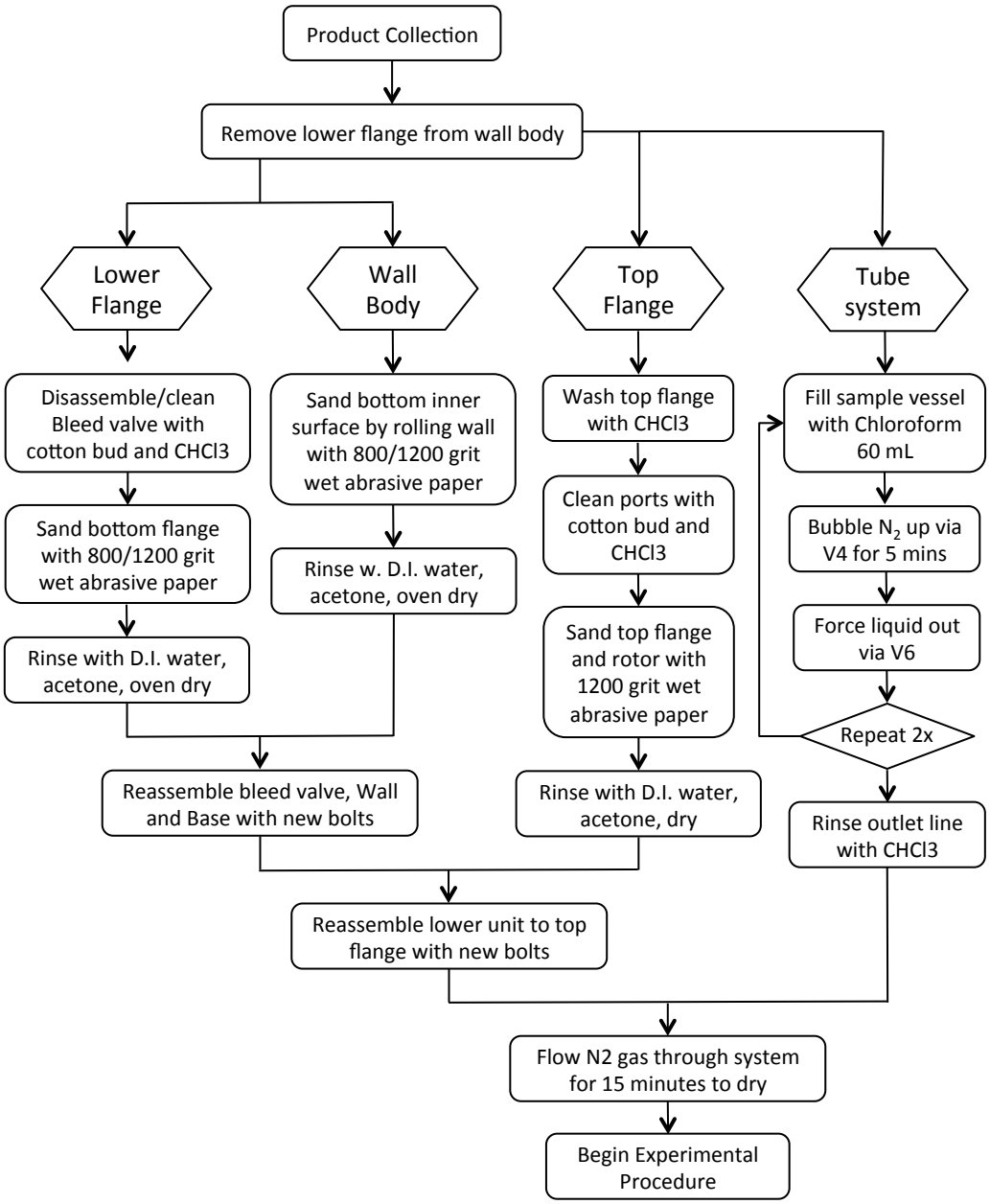


Figure 4.3 Reactor Cleaning Procedure

4.3.4 Mass analysis of insoluble reaction deposits

Whilst organic fouling deposition process is a continuous process which may contain include the precipitation of soft "gum like" material which may be resolubilised by conventional solvents, the insoluble deposits, which may be inorganic as well as organic, have been considered in the quantification of fouling deposits for this section which may be organic as well as inorganic. Insoluble

foulant mass is collected from the wall surface of the heated cell as well as that recovered from the liquid film of the wall surface after draining oil from the reactor. Insoluble fouling material entrained in the bulk fluid are not considered deposits but may also be a problem in industrial applications further along the refinery process train.

Insoluble wall and film solids: As described in parts 3 & 4 of section 4.3.2, deposits were collected from both the reactor walls through cleaning using a chloroform solvent and nylon brush, and in the wet oil film layer by rinsing only with chloroform.

Bulk fluid solids: Insoluble deposits may also be present in the bulk crude oil. This may be due to insoluble particles in suspension in the oil originating before the reaction or formed as a result of fouling processes on the surface, followed by removal through shear forces due to the fluid rotation. In refinery systems, this may contribute to fouling further down the process or may be carried through to the distillation furnace, and not represent a problem to the heat exchanger network. Throughout the commissioning trials, it was found that the high viscosity of the crude oils and presence of suspended particulates made filtering solids via membrane filter impractical. Even with fluid dilution with chloroform to lower the fluid viscosity, membranes pores were consistently blocked by particulates making filtering even under high vacuum impossible. Filtration was also attempted with Whatman grade 1 filter paper, although the same problem persisted.

As a result, a separation method using centrifugation was developed for the removal of bulk crude oil particulates. This again required dilution with a fully miscible solvent to decrease the fluid viscosity and aid separation. Crude oils are fully soluble in both toluene and chloroform, however, dilution with chlorinated solvents such as chloroform (1.49 g/mL^{-1}) and dichloromethane (1.33 g/mL^{-1}) would result in the overall fluid density being greater than the suspended organic solids, making a centrifuge-based separation impossible. Toluene was chosen due its lower fluid throughout the commissioning trial as its density (0.867 g/mL^{-1}) is lower than the oil blends used.

Method: Toluene was added to a 120 mL vial of the spent bulk crude oil in a 1:1 mass ratio and mixed thoroughly and placed in a MSE Centaur 2 centrifuge. The vial was centrifuged at 2000 rpm for 15 minutes and the supernatant removed. 6 mL toluene was added to the vial and sonicated for 5 minutes to create a suspension before transferring to a pre-weighed 14 mL glass vial. The 120 mL vial was washed three times with 2 mL toluene or until clear and the solution added to the 14 mL vial. The vial was centrifuged for 10 minutes at 2000 rpm. The supernatant was removed, and the residue washed with a further 6 mL toluene, sonicated, and centrifuged as before, and this process repeated

until no further oil could be removed from the residue (usually three washes). The resulting solids were oven dried at 80 °C until no further mass change was detected.

4.3.5 Deposit recovery and quantification from bulk fluid

During commissioning trials, filtration of the bulk crude oil was found to be very difficult due in part to the high viscosity of the fluid and in part to waxy compounds and fine particulates obstructing the pores of the filter and preventing fluid from passing through. Heating and diluting the oil with solvent helps to reduce the viscosity but again the filter quickly become blocked making filtration impractical. Centrifugation was determined to be the preferred method for separation of particulates from the bulk fluid. Vacuum filtration as a method for separating suspended solids from the liquid phase proved highly problematic as pores of <1μm are easily blocked making separation impossible and using larger pored membranes did not provide effective filtration.

Solubility of crude oils was tested with both toluene and chloroform. Both were found to solubilise the supplied crude oils completely. Chloroform cannot be used for separation of solids in suspension by centrifugation because the solvent density is higher than the carbonaceous solids produced in fouling tests and so they would remain in suspension after centrifugation. Toluene however is an acceptable solvent as the oil is fully solubilised, but the density is lower than the carbonaceous solids allowing them to be separated by centrifugation.

4.3.6 Analytical asphaltene fractionation

Soluble organic products from the film and bulk fractions were fractionated using a method adapted from ASTM method D3279[150] and used previously in the theses from Puron and Arcelus-Arrillaga[151]. 0.5 ± 0.05g organic samples were accurately weighed into a 14 mL glass vial and 7 mL n-heptane was added. The vial was vigorously agitated for 60 minutes in a Vortex Genie 2T shaker, before centrifugation in a MSE Centaur 2 centrifuge for 20 min at 2000 rpm. The supernatant was pipetted into a separate weighed vial for maltenes. A layer of precipitated solids was left remaining in the vial. A second volume of 7 mL n-heptane was added, and the process of agitation, centrifugation and removal of the supernatant was repeated. The removed supernatant layer was added to the maltene vial. The two fractions were dried by flow of N_2 gas. The asphaltene layer was placed in an oven at 60 °C for 3 hours and weighed. The maltene layer was dried until weight changed less than 1% in 1 hour. The maltene fraction was analysed by simulated distillation using the GC-FID (see section 6.2.5).

4.3.7 Repeatability and error estimation

The main issue for experimental data performed with the fouling reactor as described in detail in chapter 6 was the challenge of producing repeatable data for a given set of parameters and fluid composition. This is likely to the large number of preparatory operations that need to be executed with consistency, manual control of the reactor conditions during an experimental run. Significantly, deposits may act as nucleation sites for further deposition and not all areas of the reactor and tube system are easily accessible for physical cleaning. Heavy fouling experiments generally tended to show more divergent deposit masses between, possibly for the previous reason. Aiming to minimise experimental error, where possible, each experiment was performed a minimum of two times for every composition or process condition, with the aim being to have two concordant results which were then averaged. Where results vary significantly usually >30% the experiment was repeated, and anomalous data discarded. This was a common occurrence when a low fouling experiment followed a high fouling experiment. Because of this inherent difficulty of obtaining repeatable data, three experiments per set of conditions/composition was targeted for fouling experiments, however later in the project timeline two fouling of reasonable agreement were conducted for greater throughput of the experimental plan.

4.4 Characterisation techniques

4.4.1 X-Ray fluorescence spectroscopy

X-ray fluorescence is a non-destructive analytical technique for quantification of elements with atomic number greater than 10 (Ne) in liquid and solid samples and has been used to measure metals and inorganics present in crude oil[152]. The ASTM provides an XRF method for quantifying sulphur content[153]. X-rays are fired at a liquid of fine powder sample knocking out inner core electrons vacancy in the atomic orbital. Electrons from a higher orbital fall to fill the vacancy and in doing so emit a photon via secondary fluorescence of a charismatic frequency that corresponds to the energy gap between the orbitals (Figure 4.4). The intensity of the light emitted corresponds to the concentration of that element in the sample. Elements in third row of the periodic table and below are detectable, however lighter elements require a different technique such as combustion microanalysis. Preparation is quick as samples need only to be homogenised, but masses required may be too large for foulant deposit analysis.

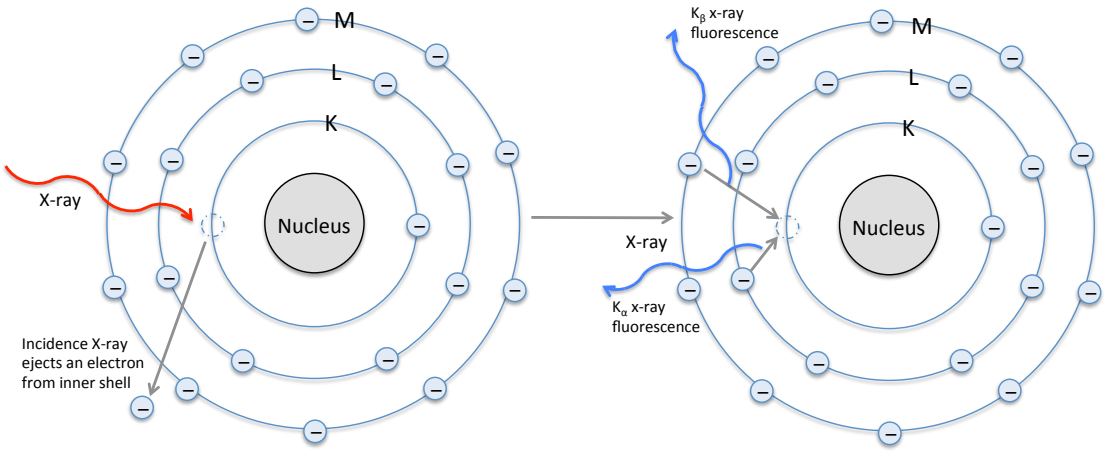


Figure 4.4 representation of the XRF spectroscopy principal: a) an incident x-ray ejects an inner core electron, b) a higher energy electron jumps to fill the hole left by the ejected electron. This may occur from an adjacent orbital K_α or a higher orbital K_β.

X-Ray fluorescence analyses were performed with a Bruker AXS S4 Explorer with a Rhodium source and operating power of 1kW. Samples were stirred (Liquid) or ground and mixed before analysis. They were placed in PTFE cups over a 4µm thick polypropylene film and spread evenly to minimise heterogeneity in the sample.

4.4.2 Scanning electron microscopy with energy dispersive x-rays

SEM uses the same principle of x-ray fluorescence, as earlier, however when combined with SEM, this provides high resolution images of the surface topology of solids and coupled with surface elemental analysis of non-volatile solids by energy dispersive X-ray spectroscopy (EDX), and has beenpreviously reported in literature for oil deposit characterisation[154].

This has been employed within this research work for fouling deposit characterisation. SEM experiments were conducted in a JEOL JSM 6400 microscope with an Oxford Instruments EDX analyser. Samples of 8 x 8 mm steel sections were cute from removed sleeves containing surface deposition and were either directly imaged or gold coated to improve conductivity for samples with a thicker deposit layer. Elemental analysis was qualitatively analysed at various loci within the sample images.

4.4.3 UV fluorescence spectroscopy

In Ultraviolet Fluorescence Spectroscopy, ultraviolet and visible light excites electrons in aromatic π orbitals present in an analyte solution. When these excited electrons fall back to the ground state they fluoresce light at a longer wavelength characterised by the LUMO-HOMO energy gap. By analysing the fluorescence emission spectrum, it is possible to gain an understanding of the abundance and types of functional groups present in organic molecules capable of fluorescing. UV Fluorescence spectroscopy can be used to probe aromatic structures in an organic sample. Larger sets of π conjugated electrons in an aromatic system absorb light at a longer wavelength. Synchronous UV-F spectroscopy allow qualitative description of the size of poly aromatic hydrocarbons (PAH)[155]. UV-F can be used in a static mode or combined with a dynamic separation method as size exclusion chromatography, or similar liquid chromatographic method[156].

For analysis of model compound solutions, absorbance is correlated to concentration for "synthetic asphaltene" solution against a reference cell of the solvent. This allows for the measurement of changes asphaltene solution concentration over the experiment time.

Analysis was performed using a Perkin Elmer Lambda 40 UV/VIS Spectrometer in a quartz cell with 1cm path length. Samples were diluted till absorbance was measured at between 0.1 and 0.9.

4.4.4 Combustion microanalysis

Combustion Microanalysis, also known as elemental analysis, is used for measuring the content of carbon, hydrogen, nitrogen and sulfur in organic samples[157,158,182]. In this technique, a sample is first completely oxidised at high temperature into their combustion products, CO_2, H_2O, NO_2 and SO_2. Gas products are swept out of the combustion chamber with helium over a reduction furnace of copper to remove excess oxygen gas and convert NO_2 to N_2 gas. The gases pass through absorbent traps and then into a gas chromatography column with thermal conductivity detector (TCD).
For crude oil and foulant analysis, C/H ratios can be used to indicate whether the deposit is waxy (H/C approaching 2:1) or asphaltenic in nature (H/C of 1-1.2:1). The presence of heteroatoms such as Nitrogen and Sulphur in the foulant material can provide information to whether these elements were responsible for the reactivity.

4.4.5 Inductively coupled plasma with optical emission spectroscopy (ICP-OES)

Inductively Coupled Plasma is an analytical technique for the determination of trace metals and other elements in a sample providing they can be solvated. A solution containing dissolved metals and other elements is nebulised into an aerosol and passed through an argon plasma heated by radio frequency induction where molecules dissociate into atoms and loose electrons. The ions recombine and re-ionise repeatedly emitting radiation with a frequency characteristic to that element. The intensity of the emission corresponds to the concentration in the sample. The light is diffracted and detected in an optical spectrometer. The technique characteristically has a low level of background noise and is can be used to detect most cations and most anions extracted from crude oil brines[159].

Samples were analysed using ICP-OES by MEDAC Ltd. Solutions were prepared by microwave digestion using HNO_3 /H_2O_2 to produce the analyte for injection and concentration was determined against a 1000 ppm calibration.

4.4.6 Fourier transform infra-red spectroscopy (FTIR)

Infrared light excites vibrational modes of bonds present within the analyte molecules. The stretching frequency of individual bonds in the molecules corresponds to a characteristic wavelength absorbed, allowing for the analysis of what types of bonds and thus what functional groups are present in molecules in the analyte. The use of an attenuated total reflectance ATR prism allows preparation free detection sample by an evanescent wave that extends into the sample by total internal reflectance infrared light. Mid FTIR spectroscopy has previously been applied for analysis of crude oils and fractions thereof by absorption or transmittance[100]. This method gives qualitative data but it can be

applied to crude oil to determine organic functional groups present in crude oil and deposits for example whether deposits are waxy (C-H stretch) or aromatic (C=C stretch) and heteroatom bonds can also be determined.

Samples were analysed using a Perkin Elmer 100 FTIR Spectrometer with a Pike Miracle ATR detector using a crystal of ZnSe. Samples were scanned 4 times between wavenumbers 4000 and 600 cm^{-1} with intervals of 1 cm^{-1}.

4.4.7 Thermogravimetric analysis (TGA)

Thermogravimetric Analysis (TGA) reveals information on the thermophysical behaviour, providing a proximate composition of a substance. An accurately weighed sample is heated in a crucible under either an inert or oxidising atmosphere under a controlled heating programme. The mass change is recorded as a function of time or temperature, and may be used to determine the volatile loss, fixed carbon content, and total ash content. Cracking kinetics may also be investigated using this technique[160,161,162].

TGA proximate analysis for coal and coke materials may be determined by ASTM method D7528[163].

Analysis was performed in a Perkin Elmer Pyris 1 TGA. 3 ± 0.5 mg of sample was used for each analysis. The TGA method is derived from ASTM D7528 for the sample matter and modified from the program previously used by Rostani[128] (Table 4.1). Before heating to pyrolysis temperatures, the sample is held at 105 °C for 30 minutes under nitrogen flow to evaporate any moisture or residual solvents from solid samples. In organic liquid samples this weight loss is considered the 'light volatiles' fraction from evaporation.

Table 4.1 TGA program for proximate analysis

Step	Operation
1	Hold at 30 °C with nitrogen flow at 100 mL/min for 10 minutes to allow the mass to stabilise
2	Heat from 30 to 105 °C at 15 °C/min
3	Hold at 105 °C for 30 mins
4	Heat from 105 to 900 °C at 15 °C/min
5	Hold for 30 mins
6	Cool from 900 °C to 850 °C at 15 °C /min
7	Hold for 10 minutes
8	Switch gas from Nitrogen to air at 40 mL/min
9	Hold for 30 minutes

The fraction of light volatiles in the analysis sample is given by:

$$L.Volatiles\ \% = [(W - B)/M_0] \quad 4.1$$

where: M_0 = mass of the sample at the start of the analysis

M_{Dry} = mass of the sample after drying at 105 °C

The percentage of volatile matter in the sample, is given by:

$$Vol\ \% = \left[\left(M_{Dry} - M_1\right)/M_0\right] \times 100 \quad 4.2$$

where: M_1 = mass of sample after step 7, (heating in nitrogen)

The percentage ash in the sample, is given by:

$$Ash\ \% = [M_2/M_0] \times 100 \quad 4.3$$

where: M_2 = mass of sample after heating in air at 850 °C

The percentage fixed carbon in the sample M_{FC}, is given by:

$$M_{FC} = [(M_1 - M_2)/M_0] \times 100 \quad 4.4$$

4.4.8 Gas chromatography - flame ionisation detection (GC-FID)

Capillary gas chromatography is useful for separation and analysis of complex organic mixtures. Injected samples are volatilised and carried by an inert gas through a fused silica-lined column under a controlled temperature program. Sample molecules interact with the silica walls to different extents depending on their polarity separating out and eluting at different retention times. Quantitative detection is possible using a flame ionisation detector (FID) or similar technique (Figure 4.5). For petroleum analysis, this technique is useful for volatile components up to approximately 450 atomic mass units (amu)[164], however non-volatile compounds are not detected and may be retained in the column causing damage. Petroleum samples must therefore be fractionated before use to remove non-volatile asphaltenes before analysis.

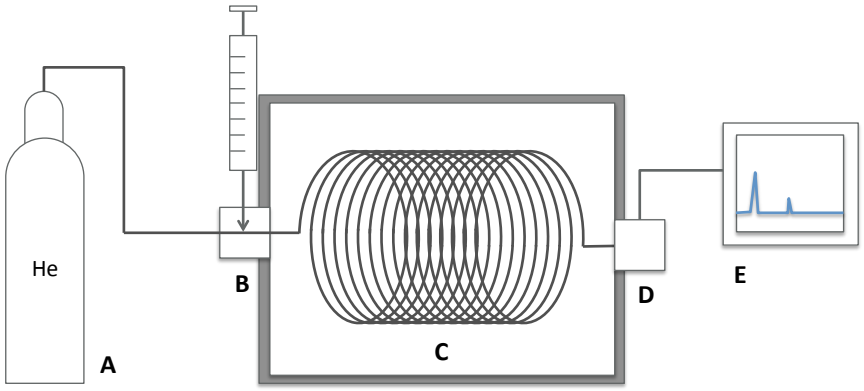


Figure 4.5 Principal of the HPLC system - A: Helium carrier gas acts as the mobile phase, B: sample is injected into the column, c: sample components separate as they are carried through the capillary column in a temperature programmed oven, d: eluted compounds are detected (by flame ionisation detector), e: signal is processed by a recorder

Gas chromatography may also be hyphenated with mass spectroscopy GC-MS. This powerful technique provides mass analysis of the eluting peaks and fragment signals can be matched with a database for full structural characterisation. However molecular isomers may not be differentiated with this technique. GC-MS is particularly useful when considering fouling reactions of synthetic and semisynthetic crude oil mixtures. Identifying reaction products from a limited number of compounds allows a better understanding of fouling process.

Model compounds and crude oil maltenes were analysed with a Perkin Elmer Clarus 500 GC with SGE HT5 silica lined capillary column and FID detector. This is a high temperature capillary column suitable for simulated distillation analysis using ASTM D2887[165]. This method determines the boiling range distribution of components within the sample against a known calibration standard with boiling points between 55 and 538 °C. Samples were prepared with $CHCl_3$ as a solvent and diluted to obtain peak intensities less than 20% of the detection limit. Helium was used as the carrier gas. A calibration was made using a gas oil standard obtained from Sigma-Aldrich at varying concentrations. GC analysis using synthetic compounds was done using an ramped heating method developed within the research group as previously reported[151]. Conditions are given in Table 4.2:

Table 4.2 Gas chromatography operating conditions

Method	Model organic compounds	ASTM D2887 for maltenes
Column	SGE HT5	SGE HT5
Carrier gas	He	He
Gas flowrate /mL min^{-1}	20	10

Injector temperature /°C	300	350
Detector temperature /°C	380	370
Split	1:20	1:20
Oven heating program	Start with oven at 50 °C Heat at 5 °C/min to 100 °C Hold for 1 min Heat at 10 °C/min to 320 °C Hold for 10 minutes	Start with oven at 35 °C Hold for 1 min Heat at 15 °C/min to 350 °C Hold for 2 mins Heat at 15 °C/min to 380 °C Hold for 10 minutes
Total time /mins	43	34.87

Chapter 5 Characterization of Crude oils

5.1 Introduction

Refinery process equipment is designed to handle crude oils within a range chemical and physical properties. The variable nature of crude oil causes challenges for refineries, who may receive oil from different sources; even oil produced from a single geological formation can exhibit wide variations in properties over time and spatial distribution[167]. Consistency is achieved through blending strategies; however, this requires a thorough understanding of the incoming crude oils to achieve a blend with the correct characteristics without destabilising the oils' complex phase behaviours and lead to fouling behaviour in the process equipment.

Two crude oils with very different characteristics were provided by BP for the purpose of this research. One crude oil is higher density and viscosity, and shall be referred to as Crude H, the other oil is considerably lower density and more volatile and shall be referred to as Crude L. This chapter presents the characterisation of the supplied crude oils by their chemical and physical properties, employing various analytical and preparative techniques, commonly used in industry.

In the second part of the chapter, the desalted and blended crudes were blended and used in the Taylor-Couette reactor for fouling experiments. Crude oil blend ratio, residence time and
focusing on the fouling behaviour of the supplied crude oils.

The oils are blended according to the methodology in Section 4.2.1. for use in fouling experiments. The analytical techniques described in Chapter 4 have been employed for this characterization. These include solvent-based fractionation, elemental analysis, gas chromatography, UV-fluorescence spectroscopy, Fourier transform IR spectroscopy, thermo-gravimetric analysis, density measurements by pycnometer and rheology characterisation.

5.2 Crude Oil Analysis

All crude oils and fractions thereof described in this section have been desalted prior to analysis using the methodology described in Section 4.2.2.

5.2.1 Solvent fractionation and mass balances of crude fractions

Crudes H and L were fractionated into maltenes and asphaltenes, both on a small scale for analytical purposes and on a larger scale for preparation of fractionated oils for fouling experiments in section 7. Fractionation methods were derived from ASTM D6560 as described in sections 4.2.3 and 4.2.4. The analytical method is a relatively quick procedure that is appropriate for small volumes where the ratio of heptane to oil is much higher. For analytical purposes the method in 4.2.4 is used, however this method was not practical for the large-scale fractionation as impractically large quantities of solvent would be required. Therefore it is necessary to compare the difference in these two methods. Crude L contained almost no asphaltenes and consequently was not fractionated on a large scale. Crude H also was fractionated to the method defined for the large-scale fractionation in section 4.2.3.

The mass balance of solubility fractions for crude L and crude H is given in . A scaled down repeat of the large-scale fractionation method was made for analytical purposes but maltenes were dried under nitrogen flow instead of rotary evaporation. The large-scale fractionation method contained significant residual heptane leading to a recovered total mass greater than 100%. Drying under vacuum more effectively removed heptane solvent and allowed for a direct comparison of the two methods.

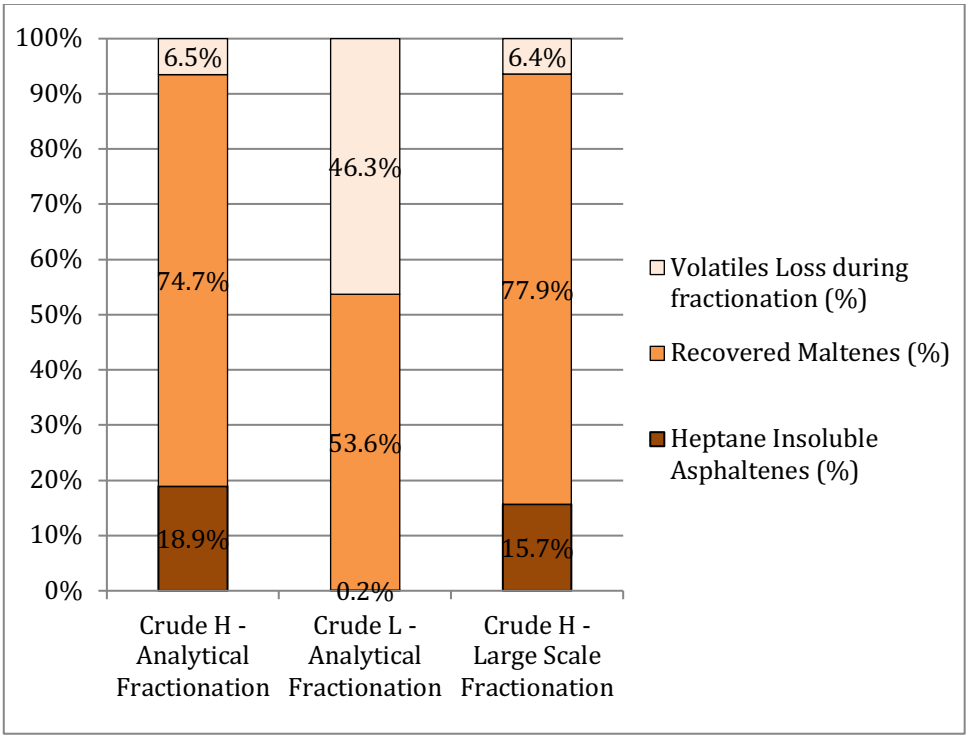


Figure 5.1 Percent mass fractions of Crude H and L by analytical fractionation and large-scale fractionation methods

Crude L, being highly volatile lost a large mass fraction (46.3%) during the drying stage under N_2 gas flow. Only 0.2% mass was recovered as heptane insoluble fraction, the remainder was the recovered maltene fraction. Crude H asphaltenes contains a significant asphaltene content (18.9% by analytical method and 15.7% by large scale method). The difference can be attributed to both the lower oil to heptane ratio for the large-scale method leading to more 'marginal asphaltenes' in the maltene fraction. Both methods lost similar volatiles by evaporation (6.5% and 6.4%).

5.2.2 Density

Density was measured using a pycnometer for desalted crude oils H and L as well as crude oil blends used for fouling experiments according to ASTM 1480[168].

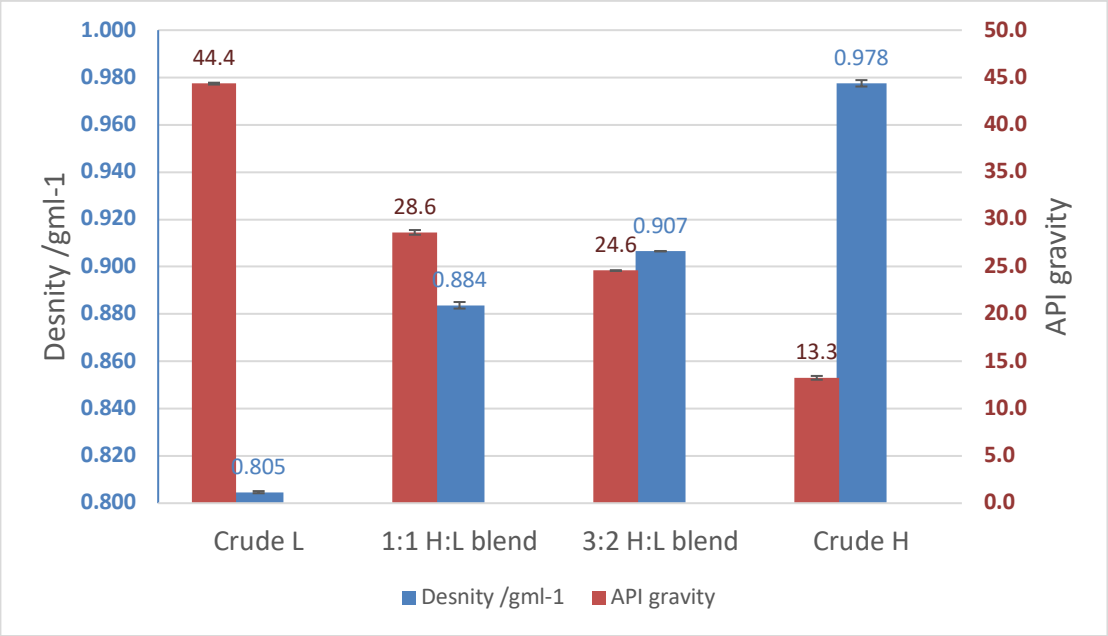


Figure 5.2 Density and API gravity of crude oils measured using pycnometer

Crude H and L have very significantly different densities. Crude H is a heavy oil with API of 13.3 (0.978 g mL^{-1}) and Crude L is a light oil with API 44.4 (0.805 g mL^{-1}). Desalted blends of 1:1 and 3:2 used in fouling experiments may be characterised as medium oils with API gravity of 28.6 and 24.6 respectively.

5.2.3 Elemental analysis (EA)

Elemental analysis was performed by MEDAC Ltd by Combustion microanalysis and ICP-OES.

Flash dynamic combustion microanalyses were determined using a Thermo Scientific FlashEA 1112 with a TCD analyser to obtain elemental mass percentages of C, H, N, O and S (see Table 5.1). The

method is described in section 4.4.4. Nickel and Vanadium were measured using ICP-OES.

Table 5.1 Percentage elemental masses for crudes H and L as provided by oil supplier

Element	Crude H	Crude L
C (% mass)	83.83	85.57
H (% mass)	11.38	13.87
N (% mass)	0.63	<0.10
O (% mass)	2.73	0.50
S (% mass)	1.46	<0.10
Ni (ppm)	25	2
V (ppm)	30	<1
H/C atomic ratio	1.61	1.93
H/C mass percent	95.2	99.4

Elemental mass analysis exhibits a typical elemental composition for crude oils. Heteroatom abundance is relatively higher for crude H and scarce for crude L. For crude H, oxygen content is high (2.73 %) and nitrogen and sulphur contents are moderate (0.63 % and 1.46 % respectively). Nickel and Vanadium generally found in the form of porphyrin biomarkers are moderate in crude H. Hydrocarbon content in crude L is almost complete (99.4 %) and notably lower in crude H (95.2 %) more typical for a heavy oil. H/C atom ratio is high for crude L (1.93), suggesting a very high paraffinic content. Crude H is notably lower (1.61), indicating significant aromatic content.

5.2.4 Characterization by GC-FID

GC analysis was performed on desalted Crude L and the maltenes fraction from Crudes H and using ASTM D2887 method described in Section 3.3.9. Maltene fractionation is important prior to analysis to remove the heavier non-volatiles that will not be detected and can become retained in the column. ASTM D2887 Reference Gas Oil provided by Sigma-Aldrich was used as a calibration standard to relate real boiling points of the n-alkanes within the oil with their retention times in the column and relating this to the oven temperature so that real boiling points can be related to oven temperature; see Figure 5.3.

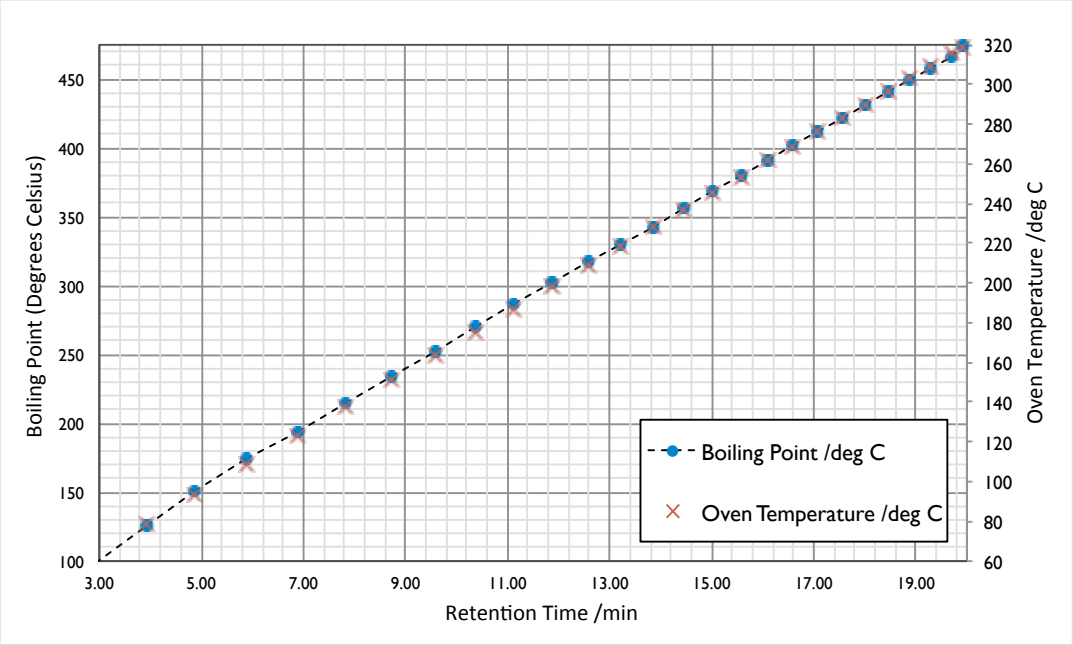


Figure 5.3 Retention times of standard gas oil n-alkanes against boiling points

A signal integration algorithm using the same gas oil standard was developed in the research group[169] according to the method described in ASTM D2887 for the calculation of boiling point fractions (Heavy Naphtha - <205 °C, Kerosene - 205-260 °C, Diesel - 260-340 °C, Gas Oils - 340-425 °C) and residue - >425 °C) by integration of the GC signal between retention-times correlating to boiling points of those fractions. From this a simulated distillation of the crude oil samples is generated. Signal generated less than 3.3 minutes elution time is ignored as carrier solvent and possible residual n-heptane from the fractionation process.

Chromatograms for Crude H and Crude L are given in Figure 5.4 and Figure 5.5. n-Alkane peaks were assigned by repeating chromatograms of the oils with "spiked" addition of n-dodecane (C_{12}) and, n-eicosane (C_{20}) and tricontane (C_{30}) to the injection samples. n-Alkanes were determined as prominent peaks corresponding to regular retention times intervals.

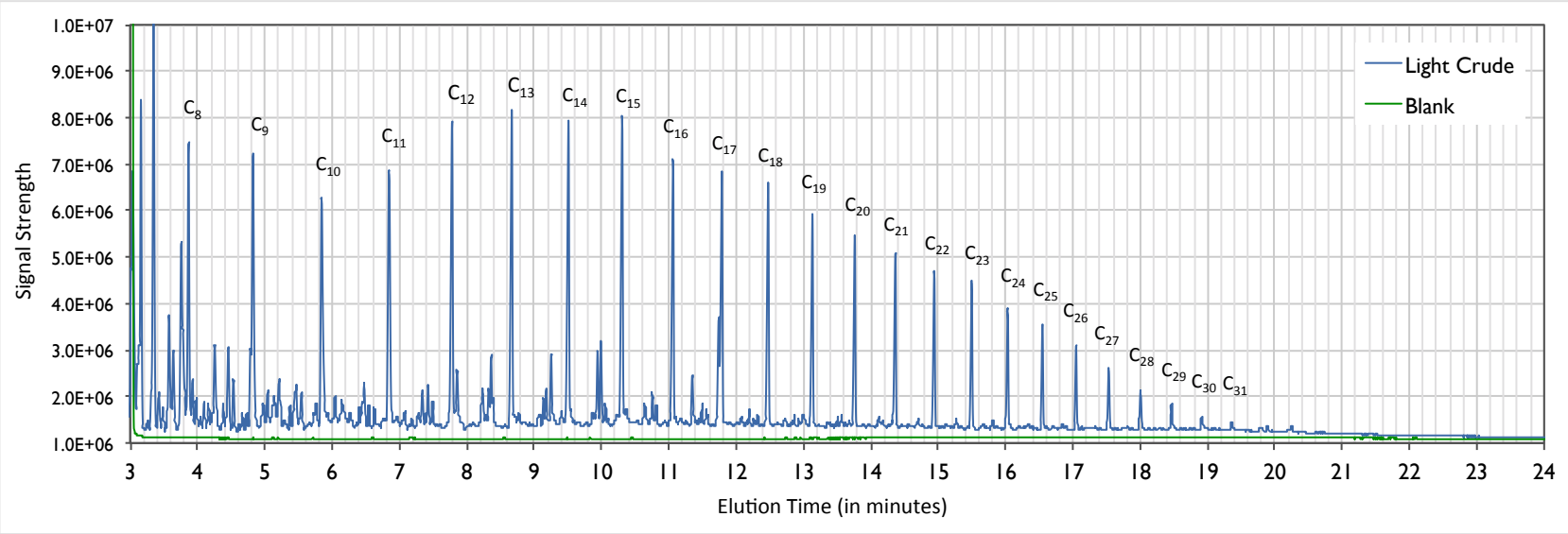


Figure 5.4 Gas chromatograph of crude L maltenes

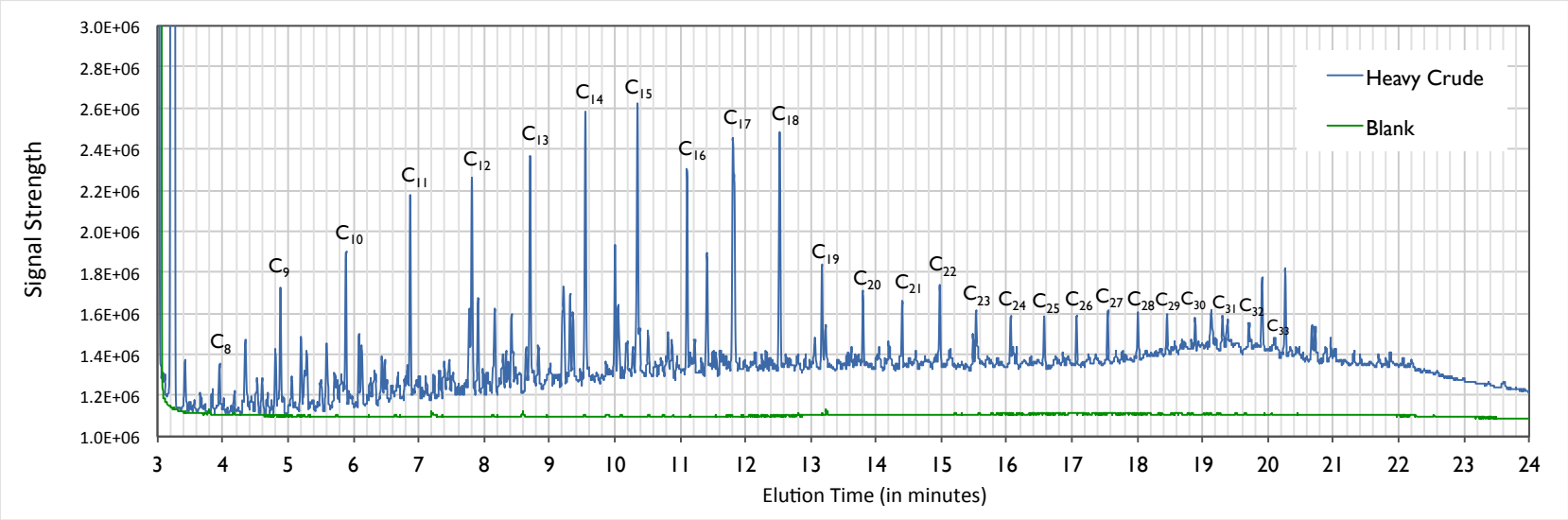


Figure 5.5 Gas chromatograph of crude H maltenes

The Crude L chromatograph showed a signal characteristic of a highly paraffinic oil. Strong peaks correspond to n-alkanes from C7 to approximately C31, with a baseline relatively close to the blank. Crude H also showed displayed n-alkane peaks from C8 to around C33, although less prominent than in the Crude L chromatogram. The baseline is also significantly raised from that the blank at long elution times indicating greater proportion of chemically distinct low volatility molecules. The boiling point distribution obtained from simulated distillation for the desalted maltenes from crude H and L are given in Figure 5.6.

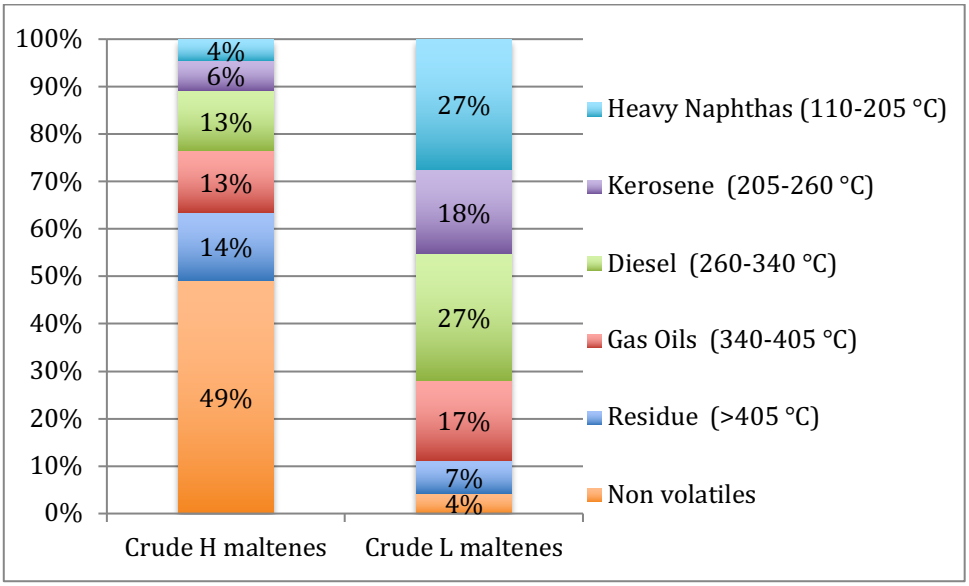


Figure 5.6 Boiling point fractions of Crudes H and L detected by gas chromatography

The boiling point fractions generated from the integration of the chromatogram signal highlight the significant differences in composition of the two supplied crude oils. Lighter fractions heavy naphtha, kerosene and diesel oil make up the bulk (72%) of the analysed Crude L signal with overall 96% of the sample detected by the FID. For Crude H, being significantly heavier, only 51% of the sample was detected despite asphaltene removal prior to analysis. Of the signal analysed, diesel, gas oil and residue fractions constituted 25, 25 and 28% respectively. Only 21% of the analysed fractions were heavy naphtha and kerosene.

5.2.5 UV-fluorescence spectroscopy of crude oil fractions separated by solubility

Crude H and L and the solubility fractions of H were analysed via Synchronous UV fluorescent spectroscopy. The normalised spectra of Crudes H and L are given in Figure 5.7.

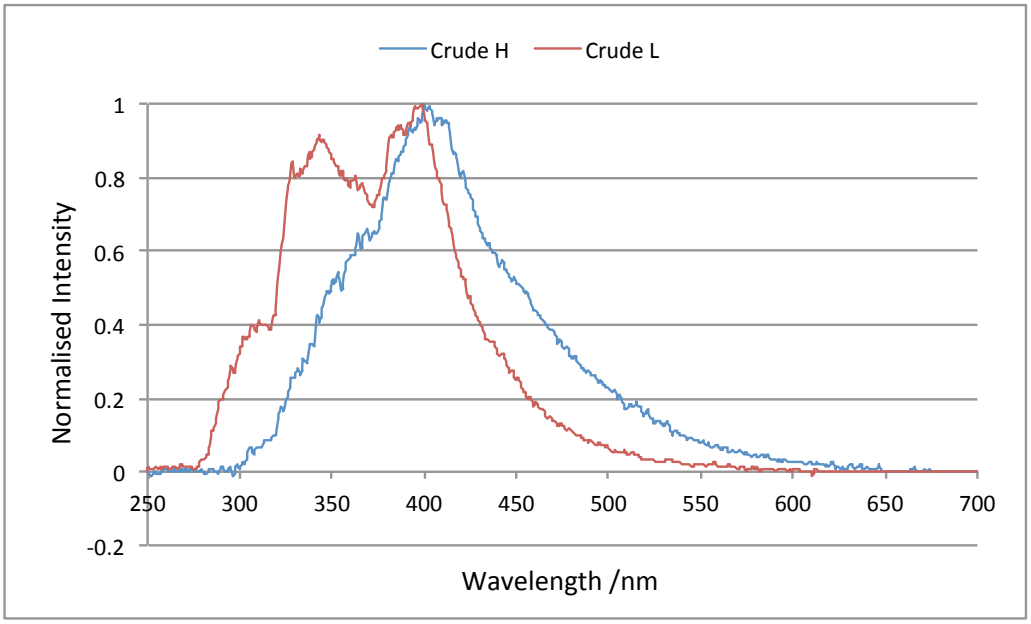


Figure 5.7 Synchronous UV-F spectra of whole Crude H and L dissolved in chloroform

The signal response for Crude H has a single maximum at 400 nm ranging between around 300 - 650 nm. Crude L has a bimodal distribution with a maximum at 399 nm, a second maxima at 343 nm with a signal range between 270 and 600 nm. The signal corresponds to the synchronous absorption and emission of light by the chromophores of large conjugated aromatic systems within the oil. The stronger signal response at longer wavelengths for Crude H indicates a greater proportion of larger aromatic systems, as expected with a significant asphaltene content. The signal from Crude L is much weaker above 410 nm, whereas the response is much stronger in Crude L below 370 nm, indicating an abundance of smaller aromatic systems, with a shoulder around 300 nm which is of very weak strength in the Crude H. Crude H was also compared against its maltenes and asphaltenes using the large-scale fractionation method described in section 4.2.3. Results are given in Figure 5.8.

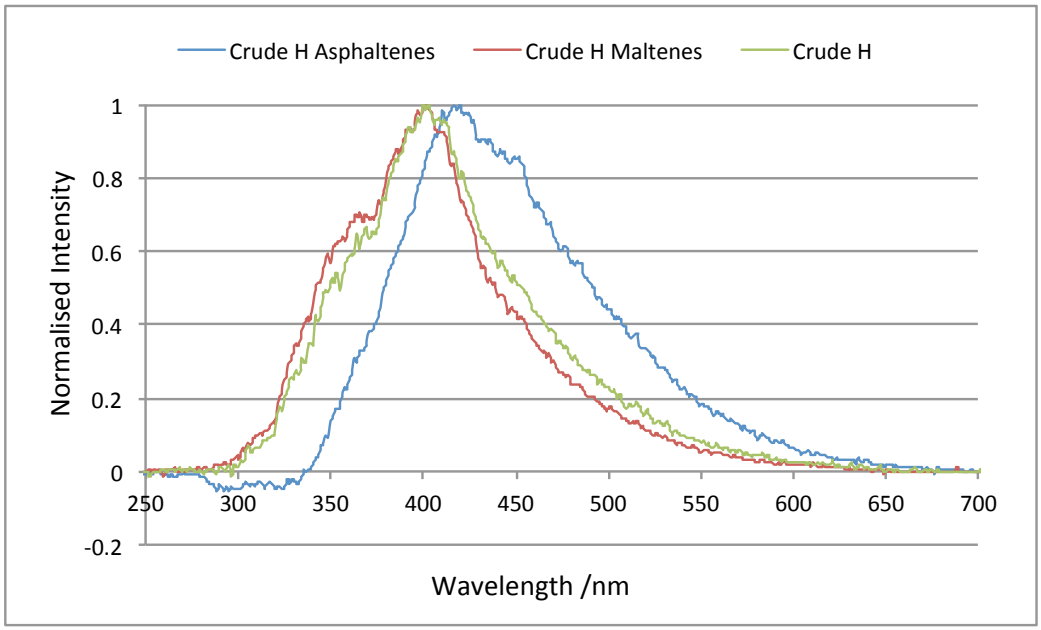


Figure 5.8 UV-fluorescence spectra of crude H and its solubility fractions

The signal responses from maltenes and the whole crude are similar as expected, although the maltene sample has a relatively higher response at shorter wavelengths, indicating a greater abundance of smaller aromatic systems, and a depressed signal at longer wavelengths characteristic of larger chromophores. The asphaltene signal response is markedly shifted towards larger aromatic systems, with a significantly greater signal at longer wavelengths and a maximum at 420 nm in contrast with ~ 400 nm for both the whole crude and its maltenes. A slight shoulder is also evident around 450 nm. The signal below 400 nm is significantly depressed in the asphaltene fraction indicating that only large aromatics are precipitated and this drops to zero at around 340 nm in contrast with the maltenes fraction at around 280 nm. This may be explained by the higher solubility of smaller aromatic molecules.

5.2.6 FTIR-ATR spectroscopy of crude oil and solubility-fractions

Crudes H and L were analysed using ATR-IR spectroscopy (Figure 5.9-5.12) as well as the asphaltene and maltene fractions derived from the large-scale fractionation with hot heptane and assigned from previous literature[170-171].

Crude L spectra is typical of a highly paraffinic oil. No peaks were detected in the 4000 - 3100 cm^{-1} range indicating a lack of OH and NH groups. The region 3100 - 3000 cm^{-1} where aromatic C-H may be found as a low intensity shoulder is also insignificant, indicating low concentration of aromatic groups. There is a very low intensity C=C bending mode at 1606 cm^{-1}, again indicating low aromatic content.

Strong peaks at 2951 cm^{-1} and 2852 cm^{-1} ($-CH_3$) and 2921 cm^{-1} ($-CH_2$) correspond to C-H stretching modes. 1457 and 1378 cm^{-1} correspond to C-H bending modes. Trace peaks at 810 cm^{-1} and 771 cm^{-1} correspond to aromatic C-H bending modes and that at 722 cm^{-1} is indicative of C-H rocking modes.

Crude H spectra are similar to crude L but with some noticeable differences. Again, no OH or NH peaks visible, aromatic C-H stretching shoulder between 3100-3000 cm^{-1} appear similar to crude L but the 1601 cm^{-1} aromatic C=C bending mode is stronger indicating greater aromatic content. C-H stretching modes at 2951, 2921 and 2852 as well as 1456 and 1376 alkyl C-H bending modes are also highly prominent. A small broad band centred at 1030 cm^{-1} is characteristic of C=S vibrational mode, confirming the presence of sulphur as observed in the elemental analysis. Peaks at 869 cm^{-1}, 810 cm^{-1} and 746 cm^{-1} correlate to the aromatic C-H bending mode and the peak at 722 cm^{-1} correlates to C-H rocking in straight chains with 4 or more carbons.

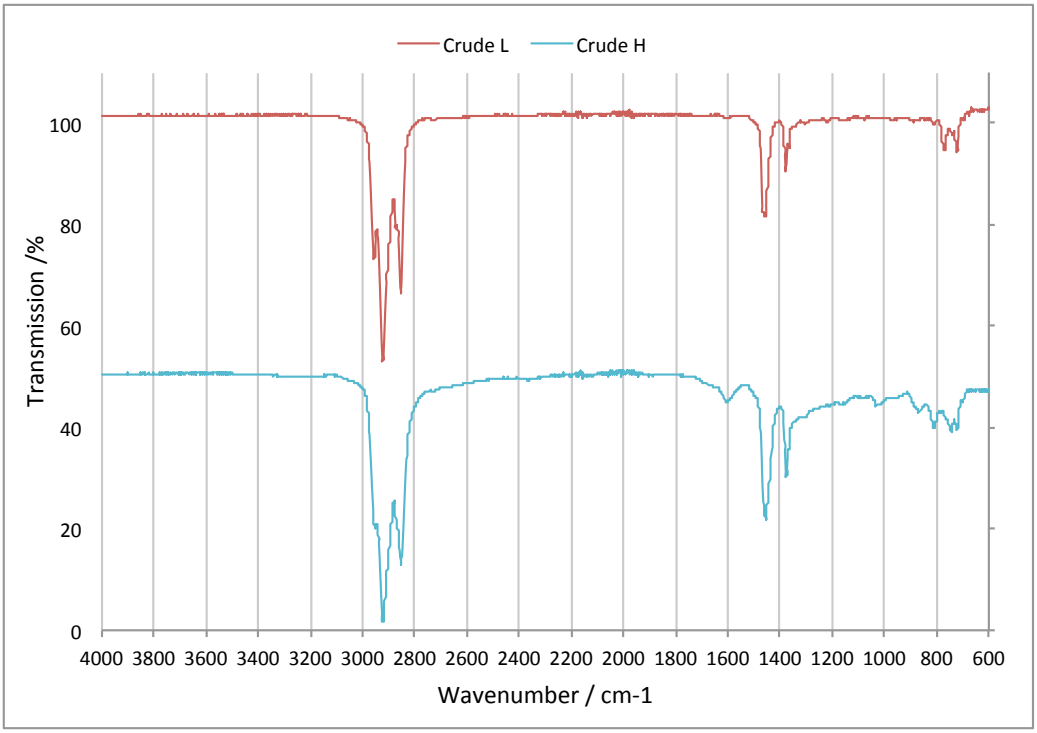


Figure 5.9 FTIR spectra for whole crude oils H and L

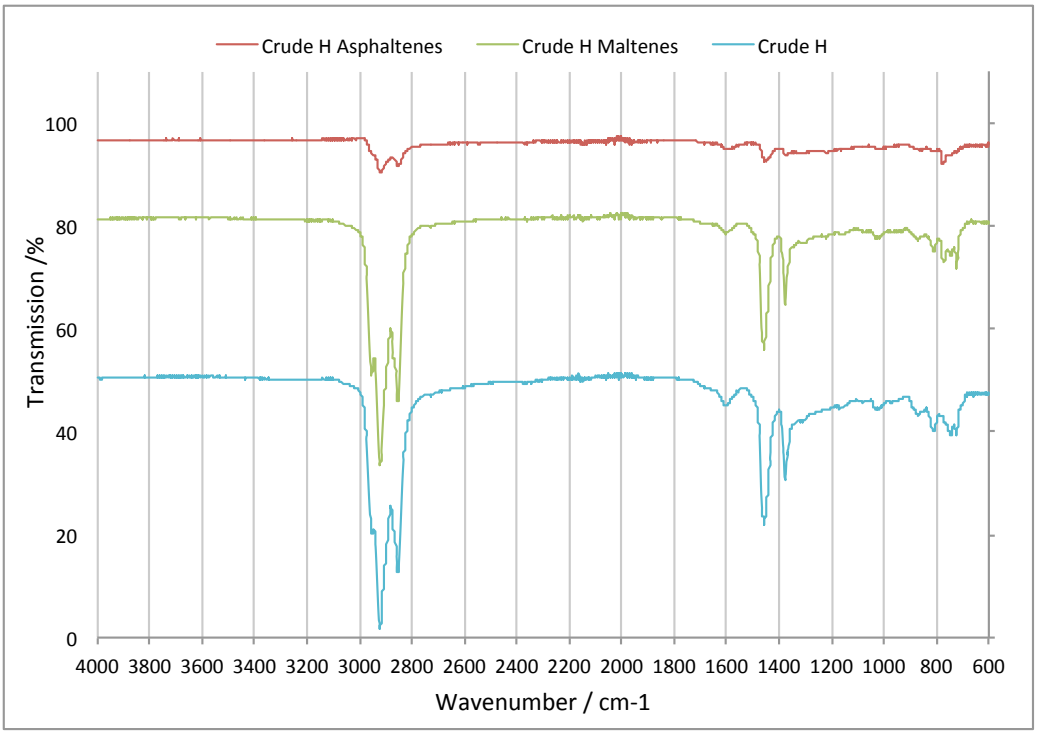


Figure 5.10 FTIR spectra for crude H, and the maltenes and asphaltenes fractions derived from it

The spectra of crude H and its maltene fraction are mostly indistinguishable from each other. Aliphatic C-H stretching, bending and rocking modes are equally strong, the aromatic C-H stretching shoulder between 3100 and 3000 cm^{-1} is equally strong in both samples and aromatic C-H bending modes are similar in the maltene fraction. C-H rocking modes remain largely similar to the whole oil as before. The 1606 cm^{-1} aromatic C=C vibrational peak is depressed in the maltene sample indicating less clustered aromatics as the asphaltenes have been removed. The peak at 1030 cm^{-1} indicating O=S is marginally weaker in maltene samples. A stronger peak at 722 cm^{-1} (C-H rocking mode with chains of 4 or more carbons) is indicative of residual heptane in the maltene fraction.

To compare the weaker absorbing asphaltenes and other crude oils or derivatives, the spectra should be normalised based on the most prominent C-H stretch absorption peak found at 2922 cm^{-1} [172]. Overlaid normalised spectra for Crude H and its asphaltenes are given in Figure 5.11.

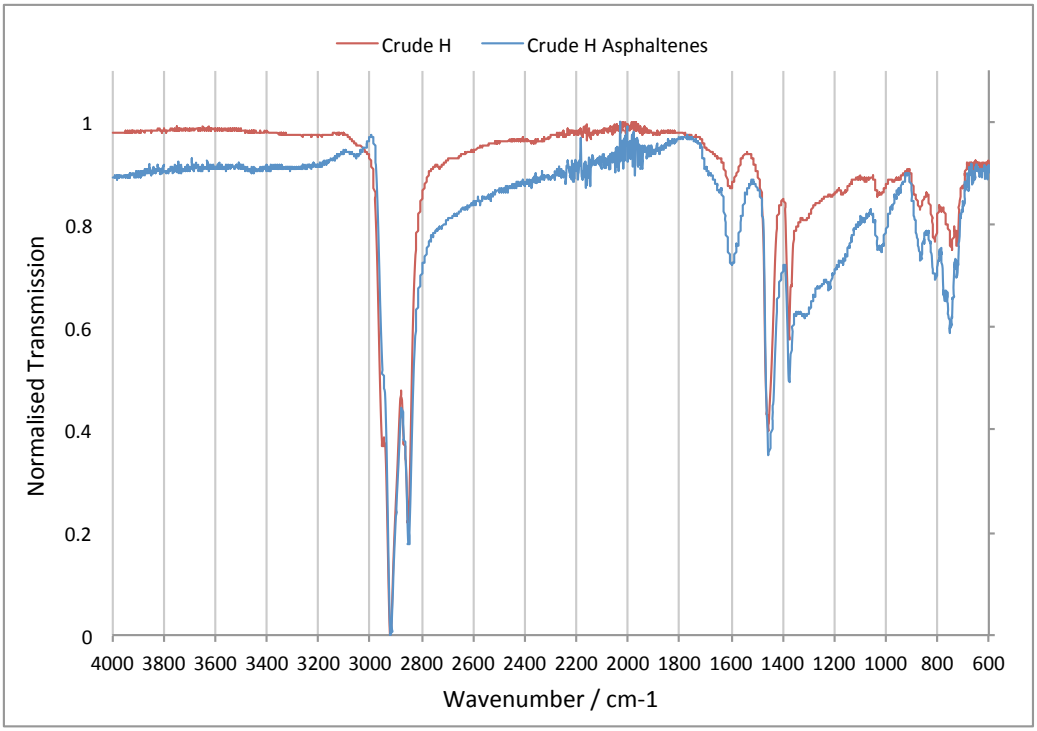


Figure 5.11 Normalised FTIR spectra of crude H and asphaltenes derived from it

Weak broad peaks around 3050 cm^{-1} are visible for both crude H and its asphaltene fraction. However, the crude H presents a shoulder on the adjacent C-H asymmetric stretch whereas the asphaltene fraction shows a more distinct weak broad peak. The C=C stretch at 1600 cm^{-1} is significantly more prominent, as expected from clustered aromatics typically found in the asphaltene fraction. S=O stretching peak at 1031 cm^{-1} is also more pronounced in the asphaltene fraction suggesting greater sulphur content.

5.2.7 Thermogravimetric analysis (TGA) of crude oil and its solubility fractions

Asphaltenes extracted from crude H were analysed using thermo-gravimetric proximate analysis according to the method described in Section 3.3.8. As well as obtaining proximate data for moisture, volatile matter, fixed carbon and ash, this method also reveals thermal pyrolysis behaviour during the heating phase of the program in inert gas. These were compared to the whole crude and its maltene fractions as shown earlier. Three repeats were made for crude oil and its fractions with good agreement. The weight-time data was repeated, normalised and averaged. TGA mass fractions are given in Table 5.2 TGA mass proximate analysis of crude H and its fractions

Table 5.2 TGA mass proximate analysis of crude H and its fractions

	Crude H Asphaltene	Crude H Maltene	Crude H	Crude L	3:2 H:L Blend
Light Volatiles	1.6%	42.3%	9.9%	53.7%	27.2%
Volatile Matter	67.3%	53.4%	82.0%	46.1%	68.0%
Fixed Carbon	31.0%	4.1%	7.7%	<0.5%	4.9%
Ash	<0.5%	<0.5%	<0.5%	<0.5%	<0.5%

The 'light volatiles' are the fraction of sample lost after heating to 105 °C and holding for 30 minutes. This is to remove any moisture and residual solvent in solid samples and in oil samples, the volatile organic molecules that are lost by evaporation. Mass loss in this fraction is higher than expected by boiling points due to the relatively high flow of nitrogen gas (100 mL min^{-1}) in the chamber. This is needed to purge the space around the sample pan and prevent air from entering the system and oxidising the sample, so vapour above the liquid is removed faster than if left to diffuse at equilibrium.

The 'volatile matter' fraction quantifies mass loss by evaporation of low volatility compounds and that from pyrolysis reactions. At temperatures above 400 °C, thermal cracking reactions occur, such as alkyl group cleavage, heteroatom loss and aromatisation of cyclic molecules, resulting in loss of hydrogen.[173] These volatile fragments are carried away with the flue gas.

The resultant mass remaining is fixed carbon, large polyaromatics of graphitic nature and amorphous and coke, along with metals and other non-volatile inorganics. The carrier gas is then switched to air to allow complete oxidation of all the carbonaceous material leaving only inorganic ash. It should be noted that oxidation of metals in the sample will lead to a rise in mass, meaning that for samples with high ash content, the calculation of fixed carbon will have errors.

TGA mass loss data for normalised weight and derivative weights is given in Figure 5.12 and Figure 5.13, respectively.

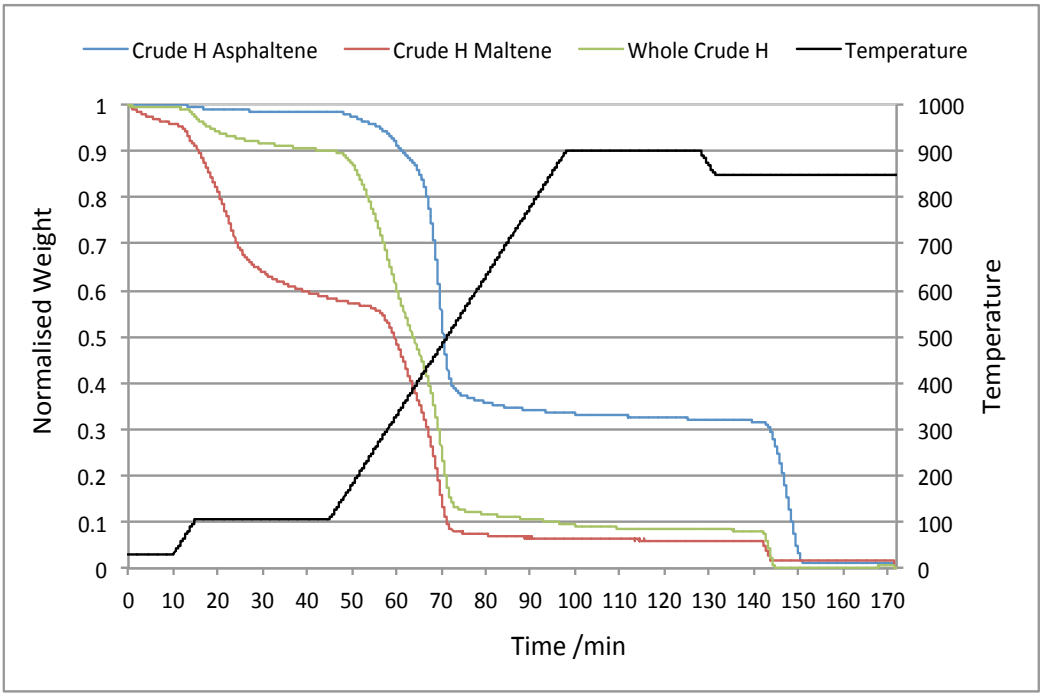


Figure 5.12 Normalised weight-time TGA Plot for crude H and its fractions, averaged over two repeats with temperature on second y-axis

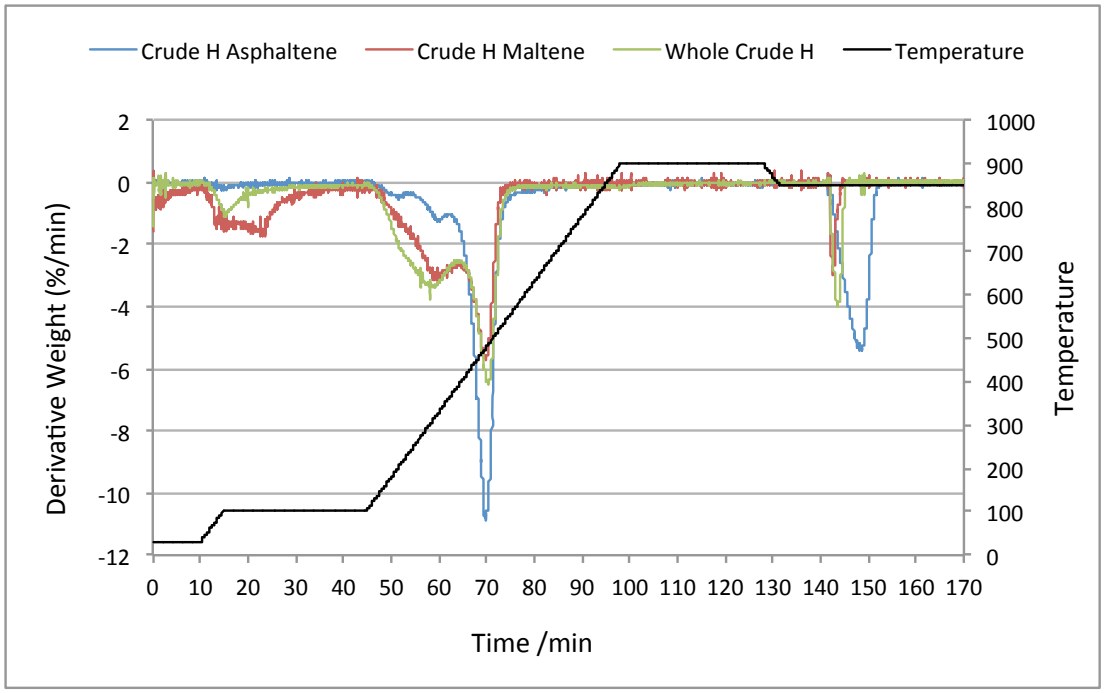


Figure 5.13 Derivative weight-time TGA Plot for Crude H and its fractions, averaged over two repeats with temperature on second y-axis

Observing Figure 5.12 and Figure 5.13, Crude H has a small fraction of light volatiles (9.9%). The majority of mass loss occurs in the volatile matter fraction as a result of volatilisation and pyrolysis,

which can be seen to overlap in Figure 5.13 at around 400 °C. The peak centre for pyrolysis occurs around 485 °C. Fixed carbon content is 7.7% and the ash content is below the 0.5% threshold for accurate reporting (as were all other crude oils and fractions analysed).

The maltene fraction has a significantly higher content of light volatiles (42.3%), which can be attributed in part to removal of asphaltenes but more significantly to a large content of residual heptane after rotary evaporation. Fixed carbon content as expected is much lower at 4.1%, likely as resins and large aromatics SARA fractions.

The asphaltene fraction, typically high molecular weight compounds, lost very little as light volatiles (1.6%), likely to be moisture or trace residual solvent from separation. Two small derivative weight loss peaks in Figure 5.13 indicate that some compounds were lost as volatiles before pyrolysis. The peak for pyrolysis mass loss occurred marginally earlier, at 475 °C. Fixed carbon content remaining is significantly greater, due to the large polyaromatic clusters found in asphaltene molecules.

For comparison, Crude L was also analysed by TGA, as well a 3:2 H:L crude blend used in the oil fouling experiments. Normalised weight and derivative weight loss results are given in Figure 5.14 and Figure 5.15.

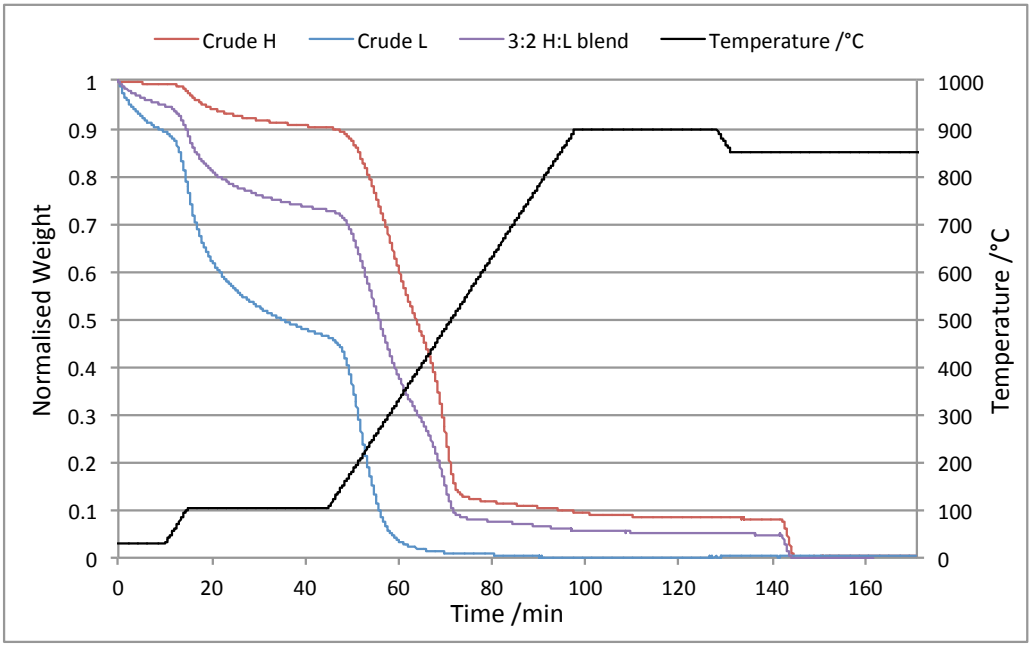


Figure 5.14 Normalised weight-time TGA plot for crude H, L and 3:2 H:L blend, averaged over two repeats with temperature on second y-axis

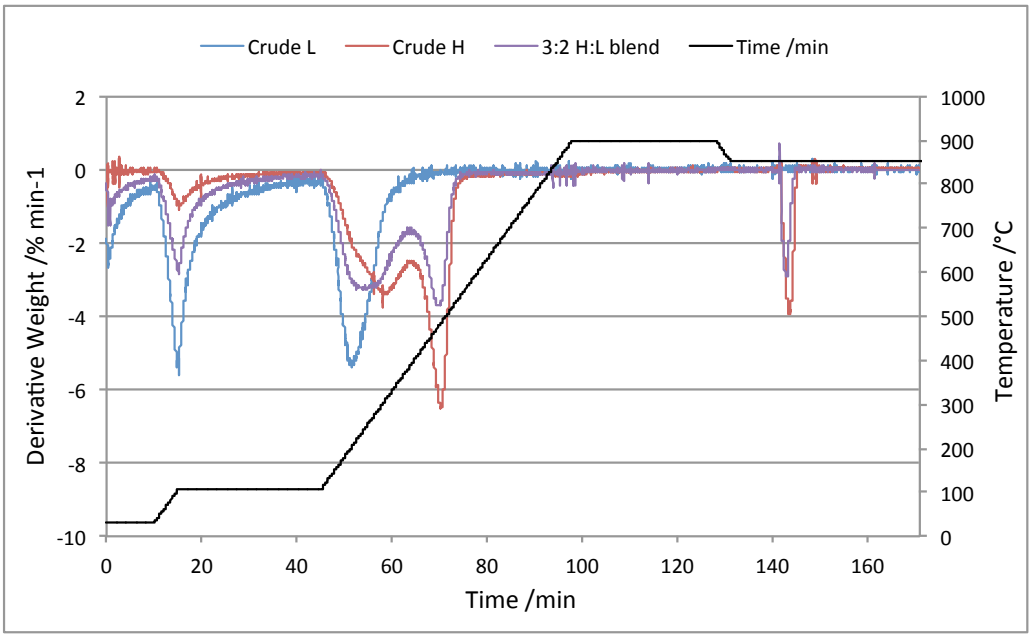


Figure 5.15 Derivative weight-time TGA plot for crude H, L and 3:2 blend and its fractions, averaged over two repeats with temperature on second y-axis

Figure 5.14 and Figure 5.15 show that, as expected, Crude L lost far greater mass in the light volatiles fraction (53.2%) when compared to crude H with considerable loss of volatiles during the initial 30 °C hold period from the carrier gas flow. The program was started as soon as the weight stabilised, minimising evaporation during this initial period. Figure 5.14 illustrates the scale of volitilisation, as by 400 °C, at the temperature of the onset of pyrolysis, very little mass (1.8%) remains and no discernible peak can be recognised above this temperature. Fixed carbon and ash content are below the limit for accurate reporting.

For crude oil fouling experiments, crudes H and L were blended in a ratio of 3:2 using the method described in Section 4.2.1. This ratio was chosen to allow a high content of asphaltene whilst being stable with respect to asphaltene precipitation and having an acceptable viscosity for loading and collection in the stirred batch-fouling reactor. The TGA plot for this blend follows an mass loss curve between crude H and L plots, tending slightly towards the heavy oil profile. Some volatilisation occurs at 30 °C under nitrogen flow, albeit to a lesser extent than for Crude L. A broader volatilisation peak occurs peaking around 250 °C with a similar but less prominent pyrolysis peak around 475 °C. 4.9 % fixed carbon is obtained with again no accurately measurable ash content.

5.2.8 Conclusions for the analysis of crude oils

The work presented describes the chemical and physical characteristics and differences between the heavy and light crude oils used for fouling experiments. Crude H has much higher density and contains a more varied structural and elemental composition compared with crude L.

Analysis via solvent fractionation (lost volatiles through drying), GC simulated distillation (boiling point fractions between 110 and 450 °C) and TGA (volatile loss) are in agreement with regards to the high volatility of crude L and low volatility of crude H. H/C atom ratio and FTIR, indicate greater aromaticity in crude H relative to crude L whilst red shifted UV-fluorescence spectrum indicate larger aromatic systems in crude H. FTIR S=O stretching peaks are supported by elemental microanalysis, although nitrogenous compounds are not obviously visible in the FTIR spectrum.

The solvent fractionation by heptane allowed for the separation of asphaltenes and maltenes for mass balance analysis and for use in experiments in Chapter 7 on fouling with fractionated crude oil mixtures. Analysis of asphaltene and maltene fractions highlights significant differences in chemical and physical characteristics, via UV-fluorescence, TGA and FTIR analysis.

Chapter 6 Commissioning of the Fouling Apparatus

6.1 Introduction

Before fouling experiments can be undertaken, the Taylor Couette batch-fouling reactor needed to be commissioned to optimise process control, calibrate rotation speed, evaluate liquid process flow behaviour and test confirm the production and repeatability of foulant production using fouling fluids. The batch-fouling reactor was subjected to a series of tests to determine performance characteristics and review and develop a standard operating procedure. The following work is split into three sections: hydrodynamics tests using a rheoscopic fluid, thermal/pressure characteristics using non-fouling fluids and fouling experiments using a crude oil blend supplied by BP.

6.2 Reactor hydrodynamic visualisation using rheoscopic fluids

Characterising the behaviour of the fluid in the reactor annulus is important for understanding the mass transfer properties of fouling precursors to the wall surface. The dynamic behaviour of the fluid in the reactor annulus may be better understood by visualisation techniques using a rhesocopic fluid. An identical body section was constructed from transparent poly(methyl methacrylate) (PMMA) for viewing the fluid under rotation (see Figure 6.1). The reactor was assembled with rubber gaskets for sealing due to the lower yield strength of the PMMA compared with steel.

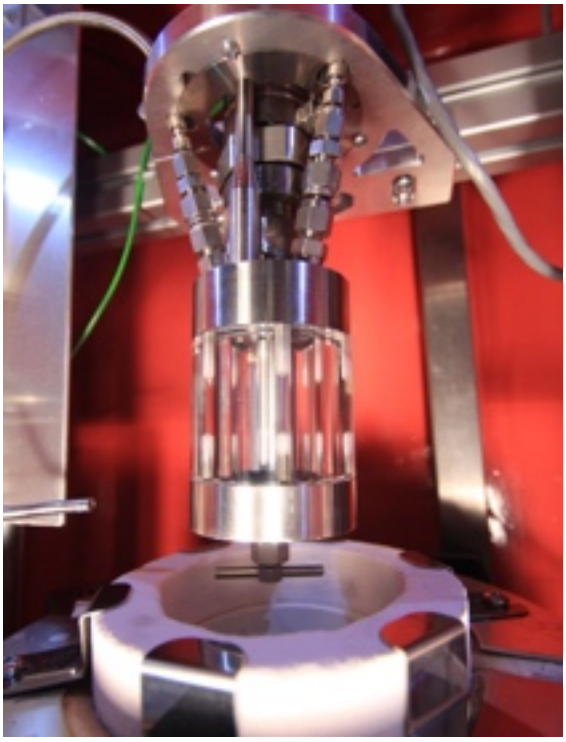


Figure 6.1 Batch fouling reactor with PMMA wall section installed

6.2.1 Reactor fluid loading test

The first commissioning test was to develop the protocol to ensure test fluid will be loaded into in a controlled manor without inclusion of bubbles resulting a one-phase system within the reactor. Deionised water used as the test fluid. The protocol for purging air from the system and loading liquid into the reactor is given below, and components are referenced to Figure 3.6:

1. If any traces of solvent remain in the system before use, dry the process line by keeping valve V3 closed and V2 and V4 to V8 open, open V1 to allow a steady flow of N_2 gas for 15 minutes.
2. Starting with the system at ambient pressure, ensure V2 is open, and valves V1, V3, V4, V5, V6, V7 and V8 are closed.
3. Remove plug on Tee 4 and fill sample vessel with 100 mL deionised water, replacing the plug afterwards.
4. Ensuring V1, V3, V4 and V8 are closed and V2, V5, V6, V7 are open, slowly open V1 until P1 and P2 display 145 psi, then close V1.
5. Slowly open V8 to release nitrogen gas from system, and close once the system is at ambient pressure
6. Repeat steps 4 and 5 two further times
7. Start the motor rotating slowly, at 5 volts.

8. Slowly open V2 until P1 reaches a pressure of 100 psi.
9. Open valve V4, and slowly open V6 allowing P1 begins decreasing in pressure at approximately 2 psi per second, monitoring the increase in P2 until the pressures in P1 and P2 are equal.
10. Slowly open and then close valve 7, allowing fluid to pressurise the tube section between V7 and V8
11. Open V8 to release the pressurised gas from the isolated tube section.
12. Repeat steps 10 and 11 until all the gas has been released from the system and sample liquid begins to flow from the exit stream. Close V7 and V8
13. Slowly open V1 to increase the system pressure to operational pressure.
14. Increase Motor voltage to operational speed

The sample liquid loads into the reactor by differential pressure between the sample vessel and the reactor/outlet line. Slow rotation of the motor during this step is thought to help mixing and encourage any bubbles to the surface of the liquid. When the liquid reaches the top of the reactor body, excess sample fluid fills into the outlet line until the pressure acting on the liquid in the sample vessel is equal to the pressure of the gas trapped in the outlet line. It is important in step 5 that the pressures in P1 and P2 equalise slowly as this will allow more viscous liquids to fill the annulus without the entrapment of gas bubbles. Careful discharge of a small, controlled volume of liquid in steps 6-8 prevents accidental release of a larger volume of sample fluid under pressure, which may be a health risk.

The commissioning tests with water and Paratherm NF confirmed that sample liquid from the inlet enters the reactor smoothly without slugs of gas and liquid fills the annulus including the recess for the outlet valve and the space under the rotor. Some experimental fluids with high viscosities may be harder to achieve filling without gas bubbles, but in these cases, the fluid will be loaded more slowly into the fouling apparatus, and if necessary, heated somewhat prior to injection to the loading vessel to reduce fluid viscosity. The liquid filled the annulus up to the head unit and into the outlet line without noticeable gas bubbles. After careful release of the trapped gas in the outlet line deionised water flowed from the outlet. Steps 7 and 8 were repeated a few more times to see if any further gas would be released from the outlet, which it did not. After this was complete, the system was slowly pressurised to 145 psi (10 bar) for further tests. No gas bubbles were observed after pressurisation to 10 bar.

6.2.2 Motor speed calibration

A high-speed video camera (Olympus i-SPEED 3) was used for used for motor rotational speed calibration and recording fluid behaviour at rotational frequencies ranging from 0-48.9 s^{-1} (0-2932 rpm).

The rotational velocity (in rpm) was calibrated against input voltage for the DC motor with deionised water in the reactor at 10 bar pressure and ambient temperature (see Figure 6.2). Time recorded for 30 revolutions was counted between 13 and 60 volts, with fewer rotations required for lower voltages see Appendix.

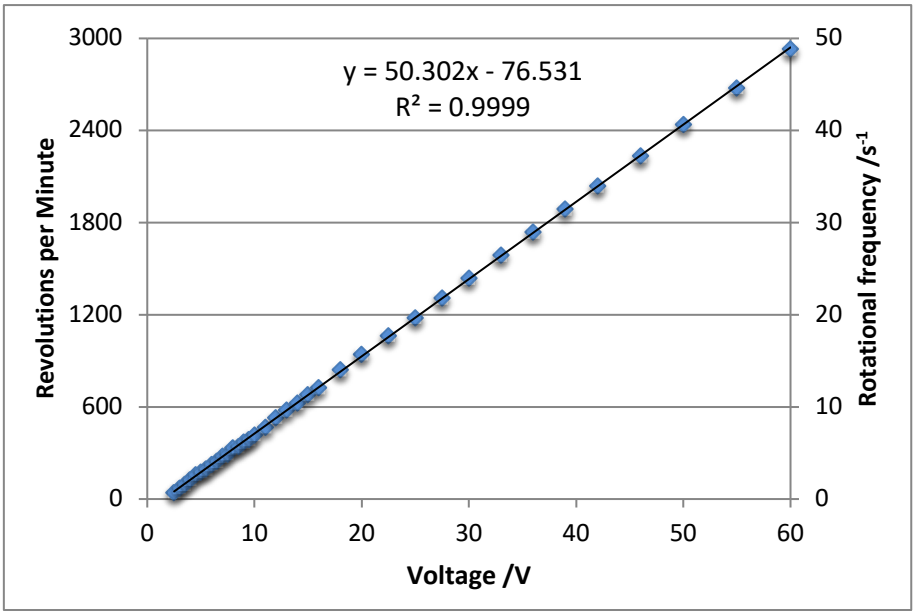


Figure 6.2 Calibration plot of motor input voltage against rotor rpm, measured using Olympus iSpeed-3 high-speed camera

The rotation speed showed highly consistent linearity for all voltages from 0 - 60 volts with a minimum starting voltage of 1.5 V and increasing by 50.3 rpm per volt. Rotational velocities above 2700 rpm (45 s^{-1}) were observed to suffer excess vibration. This test was repeated with Paratherm NF, a non-fouling fluid, to observe if rotational speed would be affected by fluid viscosity, but it was not, which is as expected for DC motor drives which provide good linear speed control by varying Voltage. Current draw was observed to be slightly higher for the more viscous fluid, which is also as expected, as electrical power is the voltage multiplied by the current, and more power is required to overcome the higher viscous forces.

6.2.3 Rheology visualisation

A rheoscopic fluid (suspension of powdered mica in deionised water) was used for visualisation experiments at ambient temperature. A low concentration of 0.2 g/L mica suspension was filled into the reactor using the fluid loading protocol described earlier, pressuring to 10 bar. The reactor was illuminated from the side to enable viewing of fluid particles flow patterns within the annulus section.

Stable Taylor Couette flow was observed in the reactor annulus from 100 to 600 rpm (1.67 - 10 s^{-1}) see Figure 6.3. Six axisymmetric toroidal vortices forming three counter-rotating pairs were observed within the wall section spaced equally apart with about 10 mm height and 8.4 mm width. Two nodes of low velocity stable flow occur where the toroid spiral back towards the rotor indicating lower shear stress, and equidistant to them is the region of highest velocity and unstable flow indicating higher shear stress.

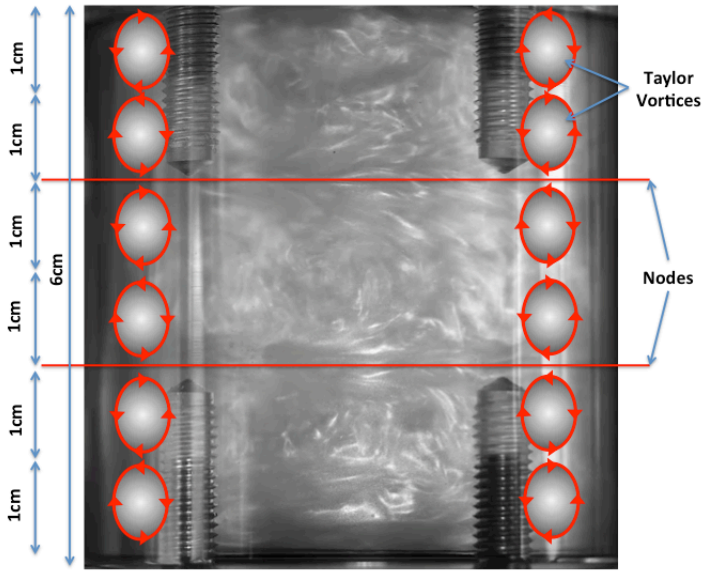


Figure 6.3 Taylor vortices present the reactor annulus at 100-600rpm. Rotor rotates from right to left as viewed from front. (Still shown here at 400 rpm)

Above 600 rpm, the vortices become wavy and unstable and indistinguishable turbulent flow appears to dominate above 1250 rpm (20.8 s^{-1}).

A higher concentration suspension of mica (1.0 g/L) was then loaded into the reactor and illuminated from the front, enabling the reflection of particles at the body wall surface where fouling is expected to occur. Rotational speeds from 100 - 2500 rpm (1.67 - 41.67s^{-1}) were recorded at up to 1500 frames per second. Still images of the reactor cell flow dynamics can be seen in Figure 6.4.

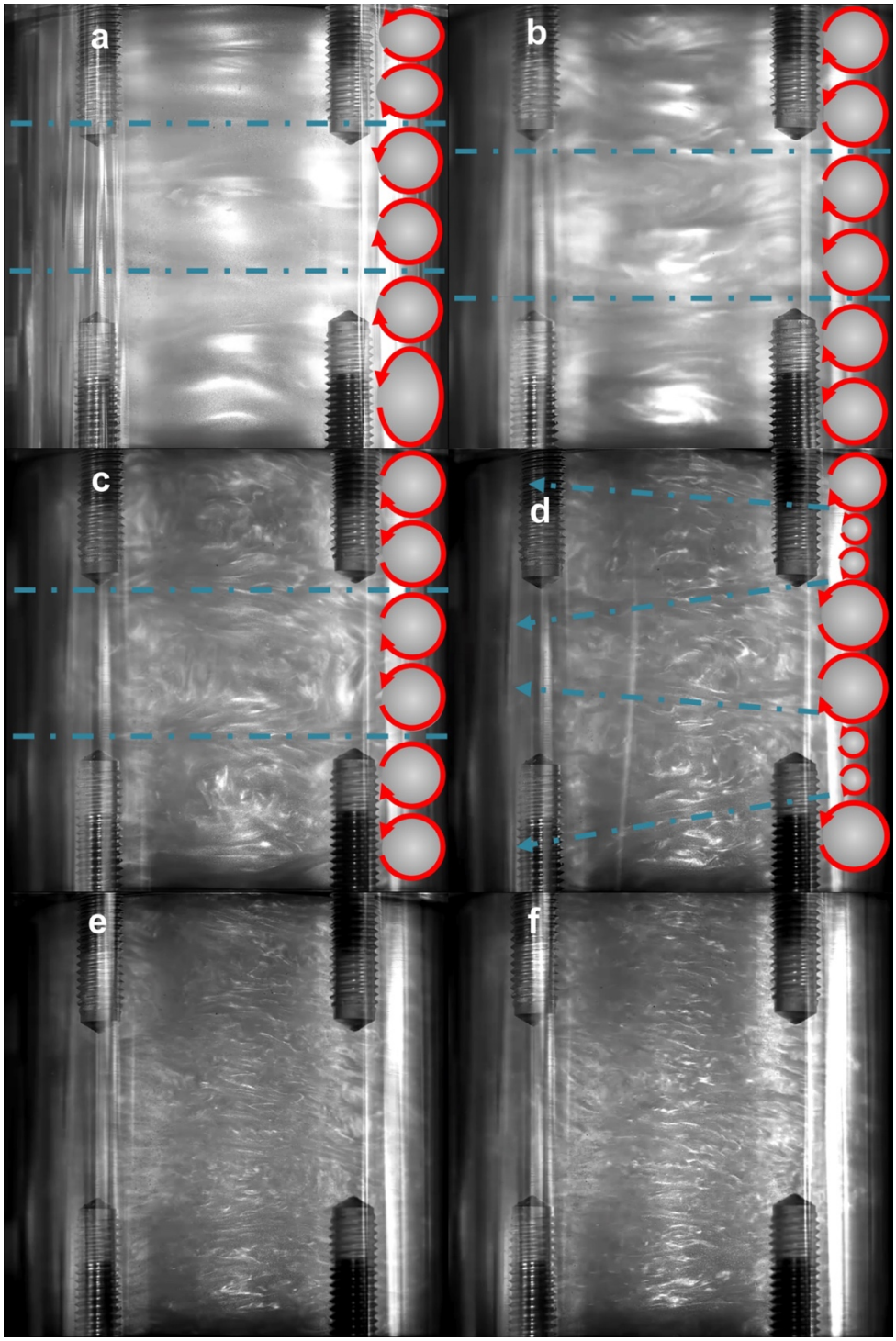


Figure 6.4 Still images of rheoscopic fluid under rotation inside the fouling rector with a PMMA body. a: 100rpm (1.67 s^{-1}), b: 200 rpm (3.33 s^{-1}), c: 400 rpm (6.67 s^{-1}), d: 750 rpm (12.5 s^{-1}), e, 1500 rpm (25.0 s^{-1}), f: 2500 rpm (41.7 s^{-1}). (Note: flange bolts in the wall -body are visible but not in the flow path)

The fluid flow characteristics at rotor speeds varying from 100rpm to 2500rpm are described in Table 6.1 as they were viewed using the high-speed camera footage.

Table 6.1 Observations from visual rheoscopic fluid dynamic investigations

Rotation Speed	Observations
100 rpm (1.67 s^{-1})	Three pairs of counter-rotating axisymmetric vortices are visible but not spaced equally, with an expanded vortex adjacent to the lower face and contracted vortex adjacent to the upper face.
200 rpm (3.33 s^{-1})	The three pairs of counter rotating vortices have become equally aligned, low shear nodes are spaced approximately 2 cm apart and from the upper and lower faces, vortices are 1 cm in the axial dimension.
400 rpm (6.67 s^{-1})	Three pairs of stable Taylor vortices remain although the high shear internodal region has visibly increased turbulence.
750 rpm (12.5 s^{-1})	Taylor vortices have become unstable and wavy, and the low shear nodes are mobile and no longer parallel.
1500 rpm (25.0 s^{-1})	Taylor vortices have broken down and largely undifferentiated turbulent flow dominates
2500rpm (41.7 s^{-1})	Flow is highly turbulent with no definable features; reflective rippling has become smaller.

The rheology visualisation experiment indicates that at speeds of 1500 and 2500 rpm (25.0 and 41.7 s^{-1}), relatively featureless turbulent flow is dominant at the surface of the reactor wall body. Reactor conditions in fouling experiments should operate under turbulent flow conditions, as the shear stress across the wall surface is approximately equal along its axis.

Tangential Reynolds numbers can be used to approximate flow conditions of dissimilar fluids at high temperature (as in the case of fouling experiments), by modelling viscosity of fluids at operational temperatures.

6.3 High temperature testing

Commissioning tests were split in two parts. First, experiments were made with a series of non-fouling fluids, to evaluate the thermal and pressure characteristics and to optimise reactor controls. Crude oils were then tested to develop the product recovery procedure, establish repeatability between experiments and if necessary, amend operation protocols for the main research experiments.

Before running experiments, due to the high cost and limited supply of sample fluids, it is important to determine the appropriate sample volume required for each experiment. Whilst the reactor itself

has an annular volume of 50.5 mL, fluid will also be in the lines of the inlet and outlet port during the experiment, and a minimum reserve volume should also be present in the sample vessel to limit the risk of gas bubbles being present in the system. The inlet and outlet lines were disconnected from rest of the system and filled completely with deionised water and the volume recovered was measured. The water recovered from the inlet line from valve V6 to the reactor port measured 5.4 cm^3. The water recovered from the outlet port to valve V8 measured 7.2 cm^3. 2 cm^3 was estimated to account for liquid in the reactor head and 10 cm^3 will be left excess in the sample vessel requiring a total volume of 75 cm^3 of liquid sample for each experiment.

6.3.1 Thermal behaviour with non-fouling fluid tests

Reactor thermal commissioning tests sought to understand reactor behaviour, and optimise operating parameters leading to a standard operating procedure for experimental research. The furnace operates a proportional integral derivative (PID) controller for maintaining furnace temperature to a set value. One operational drawback of the system is that the furnace PID controller runs off a temperature probe embedded in the furnace and it was not possible to exchange the probe connection to feedback from the reactor wall temperature probe directly without modifying the furnace equipment, which was against guidance from the manufacturer. As a result, the furnace must be monitored throughout the experiment and the furnace temperature manually controlled to maintain the wall thermocouple T_{wall} to the predetermined temperature. Despite this, when good thermal insulation is applied, once the reactor temperature stabilised after the initial heat-up phase, the temperature generally remained constant and was periodically monitored for changes.

The reactor was reassembled with the carbon steel body and copper gaskets. Heated commissioning experiments were initially conducted with Paratherm NF, followed by n-Dodecane and 1-MethylNaphthalene. The reactor loading protocol was maintained for loading Paratherm NF into the reactor, instead pressuring to 400 psi (27.7 bar) in steps 4 and 13. The motor was slowly accelerated to 31.4V (1500 rpm - 25 s^{-1}). The furnace temperature T_{furn} was set to 400, 500 and 600°C for the heating stage, and then after the reactor had reached approximately 85% of the final temperature, the furnace was set lower to determine the temperature required for maintaining 180, 220, 260, 300 and 320 °C wall temperature T_{wall}.

It was determined that during warm-up, setting T_{furn} to 500 °C for wall temperatures up to 260°C and 600 °C for higher wall temperatures produced an adequate heating rate without being difficult to control the system. In all cases, trials were run for 6 hours at operational temperature, defined as

within 1% of the temperature difference between ambient and target wall temperature, i.e. ± 3 °C for T_{wall} of 320 °C. The 6-hour reaction in this case begins when T_{wall} reaches 317 °C.

When switching the furnace set point from 600 °C to a lower value at a determined T_{wall}, the residual heat in the furnace continues to increase the reactor wall temperature to plateau at the target wall temperature. The guideline values are given in Table 6.2.

Table 6.2 Furnace heating programs for various target reactor wall temperatures

Target T_{wall} /°C	Initial $T_{furn\text{-}set}$ /°C	T_{wall} Switching Temp. /°C	Secondary $T_{furn\text{-}set}$ /°C
180	500	122	250
220	500	157	310
260	500	220	350
300	600	260	400
320	600	289	420

The ideal secondary $T_{furn\text{-}set}$ values were found to vary slightly depending on the fluid and the small fluctuations to the thermal insulation due to convective heat losses, so further fine adjustment is usually necessary.

An example of a typical 6-hour reaction profile with T_{wall} of 320 °C is shown in Figure 6.5 - Figure 6.8.

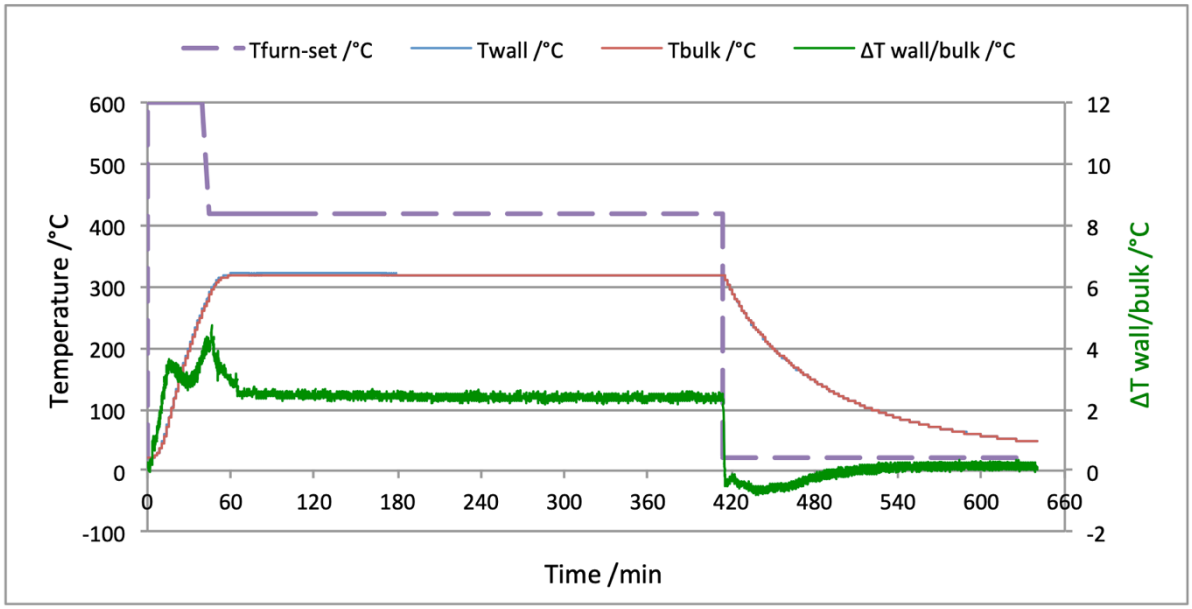


Figure 6.5 Temperature profile of a 6-hour commissioning experiment with n-dodecane as the test fluid. Wall Temperature is maintained at 320 °C. Wall temperature T_{wall}, Bulk fluid temperature T_{bulk},, Furnace set

temperature $T_{furn\text{-}set}$ are displayed on the left vertical axis while the temperature difference between the wall and the bulk fluid ΔT is given on the right axis.

The furnace is set to 600 °C for the heating up, reaching 599 °C within 20 minutes. When T_{wall} reaches 289 °C, the furnace $T_{furn\text{-}set}$ is switched to 420 °C, and the reactor wall temperature T_{wall} plateaus to 320 °C. Reaction time is begun at 54.3 min when T_{wall} passes 317 °C.

Figure 6.6 shows the Temperature profile to steady state for the heating phase of the reaction. The heating rate reaches a maximum of 9.5 °C/min at approximately 16 minutes, when the furnace PID controller reduces the power to the furnace, nearing the 600 °C set point and the temperature difference between the wall and bulk *ΔT wall/bulk* reaches a peak of 3.5 °C. At 44.2 minutes the wall temperature T_{wall} reaches the switching temperature of 289 °C, *ΔT wall/bulk* reaches second peak at 4.2 °C, which falls off to a steady state value as T_{wall} and T_{bulk} plateau.

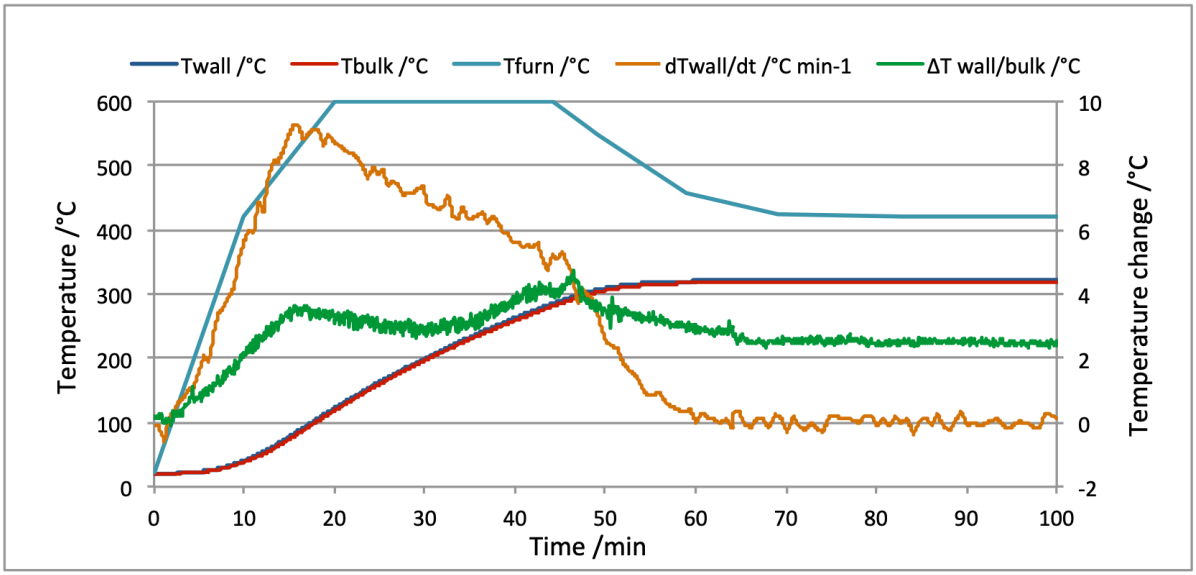


Figure 6.6 Temperature profile of the first 100 minutes of the earlier 6-hour experiment at 320 C. Wall temperature T_{wall}, Bulk fluid temperature T_{bulk},, Furnace probe temperature T_{furn} are displayed on the left vertical axis while the wall/bulk temperature difference ΔT and the wall heating rate dT_{wall}/dt are given on the right axis.

T_{wall} and T_{bulk} are held constant for 6 hours during which small adjustments are made to $T_{furn\text{-}set}$ at 94.2 minutes (419 °C) and at 138.5 minutes (417 °C) to maintain this temperature. The temperature difference between the bulk and the wall thermocouples is an average of 2.4 °C throughout the central 90 % of the reaction time with minimal deviation over the reaction time.

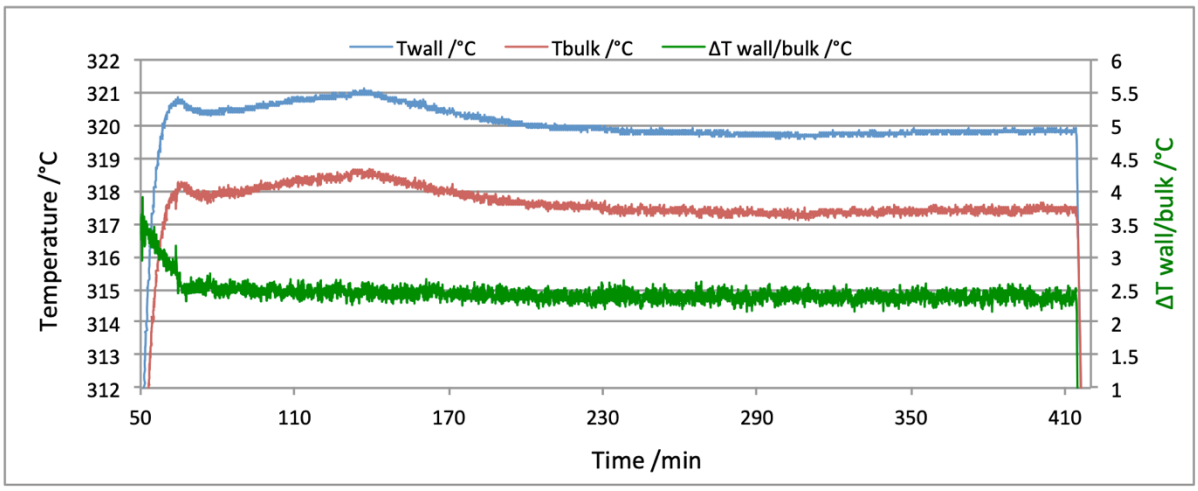


Figure 6.7 Close-up of the steady state temperature profile the earlier 6 hour commissioning experiment at 320 °C. Wall temperature T_{wall} and Bulk fluid temperature $T_{bulk,}$ are displayed on the left vertical axis while the temperature difference ΔT is given on the right axis.

After 360 minutes of reaction time elapses, the furnace is switched off, valve V6 is closed (to prevent fresh liquid entering the reactor during cooling/contraction) and reactor is raised out of the furnace by the motorised lifting mechanism. The reactor is allowed to cool passively in situ.

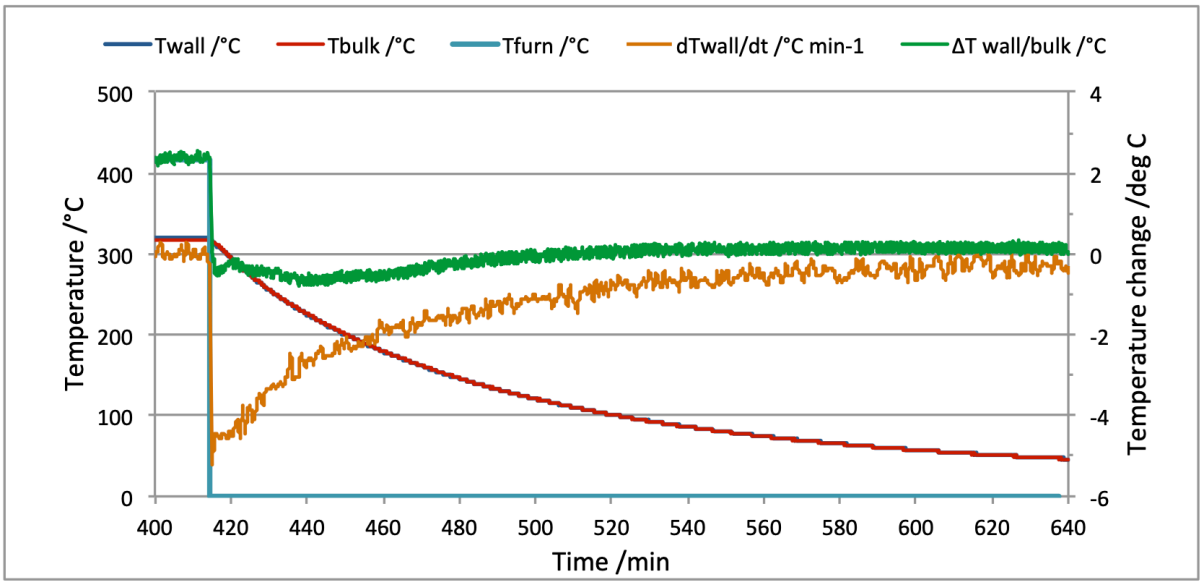


Figure 6.8 Temperature profile of the last 240 minutes of the earlier 6-hour experiment at 320 C. Wall temperature T_{wall}, Bulk fluid temperature $T_{bulk,}$, Furnace probe temperature T_{furn} are displayed on the left vertical axis while the wall/bulk temperature difference ΔT and the wall heating rate dT_{wall}/dt are given on the right axis.

Wall temperature decreases at an initial rate of 4.3 °C/min. T_{wall} falls to 200 °C after 36 minutes, and to 100 °C after 107 minutes. The reactor is left over night to cool to ambient (while still pressurised and under rotation) and the product contents are collected the following morning.

6.3.2 Thermal wall/bulk temperature gradient

Commissioning runs were made with n-dodecane and 1-Methylnaphthalene at 320°C to determine thermal similarity between experiments. Wall temperatures were controlled to within ± 3°C of the target wall temperature. Under steady experimental conditions, the *ΔT wall/bulk* temperature difference was averaged over the central 90 % of the reaction duration and results shown in Table 6.3.

Table 6.3 Mean reaction temperature difference between the wall surface and fluid bulk for reactions with dodecane and methylnaphthalene at 320 °C, 1500 rpm for 6 hours

Test	Test fluid	Mean *ΔT wall/bulk*
HT1	n-dodecane	2.4
HT2	n-dodecane	2.4
HT3	n-dodecane	2.6
HT4	1-Methylnaphthalene	1.8
HT5	1-Methylnaphthalene	2.5
HT6	1-Methylnaphthalene	1.5

For n-dodecane, mean *ΔT wall/bulk* are similar with an average of 2.5 °C, however for 1-Methylnaphthalene, HT5 is larger than HT4 and HT6. This could be due to a number of factors, for example, due to greater heat losses from the central rotor and head unit, either by incidental poor heat insulation of the cell (since the cell was manually insulated with glass wool during each experiment) or by the cooling air jet around the magnet zone of the motor with a stronger flow. Alternatively the anomaly could potentially be an operational issue such as improper positioning of the thermocouple during the run may have accounted for this discrepancy.

The temperature differences between n-dodecane and 1-methylnaphthalene are attributable to the physical properties of the two fluids. Thermal conductivity of liquid 1-Methylnaphthalene at 593K is predicted as 0.134 W/(m K) whereas for liquid n-dodecane at 593K it is 0.0758 W/(m K)[174]. Heat is therefore more effectively transferred from the wall surface to the fluid with 1-methylnaphthalene.

6.3.3 Pressure and thermal expansion

Pressure-time data was recorded for commissioning tests with 1-Methylnaphthalene and n-dodecane sample fluids. Both have similar boiling points but markedly different expansion coefficients. After loading the fluids into the reactor, dodecane was pressurised to 28.0 bar and 1-methylnaphthalene to 27.6 bar before heating. Results are shown in Figure 6.9:

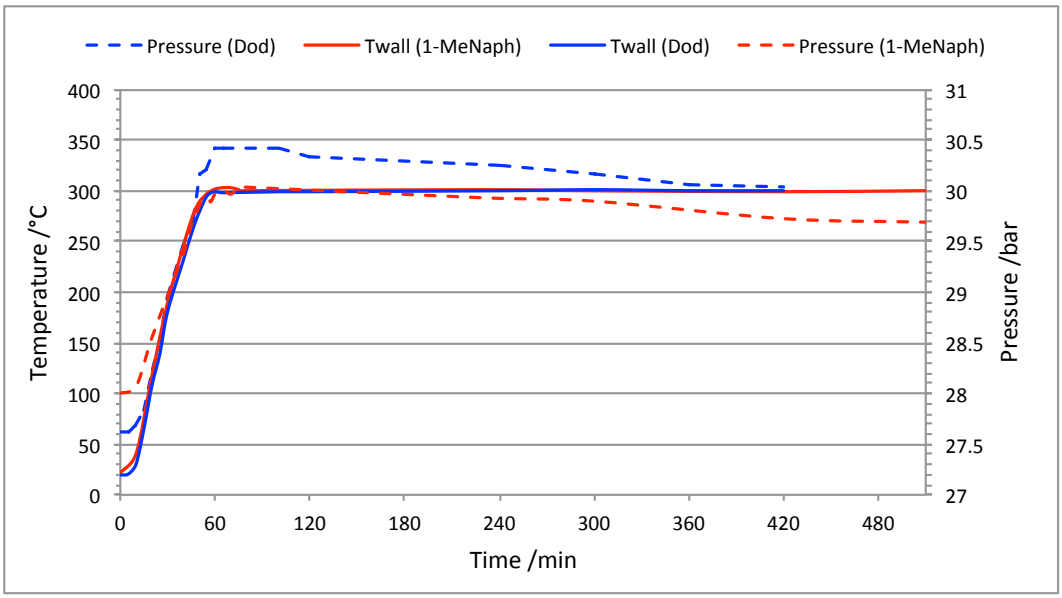


Figure 6.9 Pressure-time profile for typical experiments with dodecane and 1-methylnaphthalene at 300°C and 1500 rpm.

As expected, the pressure rise during heating was noticeably greater with n-dodecane than 1-methylnaphthalene. Dodecane recorded a maximum pressure rise of 2.79 bar compared with 2.03 bar for 1-Methylnaphthalene. Both pressure rises were anticipated such that at normal operating conditions, liquid pressures were intended to plateau at 30 bar. In both cases, the pressure did fall off slightly with time, indicating a very minor leak, losing 0.04 bar/hr (0.14 %/hr) pressure for the 1-methylnaphthalene trial and 0.06 bar/hr (0.21%/hr) for the dodecane trial. No evidence of leaked liquid was found; the leak was presumed to be small amounts of inert gas. This was believed to be acceptably low and not impact any experimental data, as the prime purpose for nitrogen pressurisation is to prevent boiling of the sample fluid.

6.3 Fouling fluid commissioning tests

6.3.1 Initial Tests

Two crude oils were supplied by the sponsor's research partners for high temperature fouling experiments. Chemical and physical analyses of the oils are provided in Chapter 5. Light and heavy crudes were initially blended in a weight ratio 1:1 with no further processing, and fouling experiments were conducted for 6 hours at temperatures of 180, 220 and 260 °C, and 30 bar pressure. Foulant mass adhered to outer wall surface was collected and weighed.

The reactor standard operating procedure and collection procedure is outlined in experimental methods section 4.3. A list of trial crude oil experiments is given in Table 6.4:

Table 6.4 Initial Trials with Crude oil blended 1:1 Heavy/Light by weight. Experiments conducted for 6-hours under 30 bar pressure

Experiment	Composition	T_{wall} /°C	σ /rpm	Wall solids /mg	Notes
CR-01	H:L - 1:1 unprocessed	180	1000	15.2	thin film
CR-02	H:L - 1:1 unprocessed	220	1000	17.3	thin film
CR-03	H:L - 1:1 unprocessed	260	1000	33.2	white salt and carbonaceous deposits
CR-04	H:L - 1:1 desalted	260	1500	46.7	carbonaceous deposit, visible striations
CR-05	H:L - 1:1 desalted	300	1500	36.6	yellow/brown deposit, no visible striations
CR-06	H:L - 1:1 desalted	300	1500	8.9	yellow/brown deposit, no visible striations

After the experiment is complete and the reactor was allowed to cool to ambient temperature, the liquid was drained from the system, rinsed with chloroform to remove the oil film and soluble compounds on the wall surface, and the insoluble foulant left adhered was removed by cleaning with chloroform and a nylon brush which removes the solids without damaging the wall surface. The suspension of chloroform and deposits were collected in a glass vial and the solvent removed by drying under a gentle N_2 gas jet at ambient temperature, then in an oven at 50 °C. Reactions at 180 °C and 220 °C produced small mass of brown/black deposits. At 260 °C, crystallisation fouling was observed on the cell wall surface as salts were visibly deposited on the wall surface (see Figure 6.10). The crude

oil received from BP was not desalted prior to arrival; normally in a refinery PHT, oil is heated to 110 - 150 °C and passed through the desalter unit before reaching heat exchangers at the high temperature end of the PHT. As such, the crude oils need to be desalted before use in the reactor, as is the case in normal refinery processes.

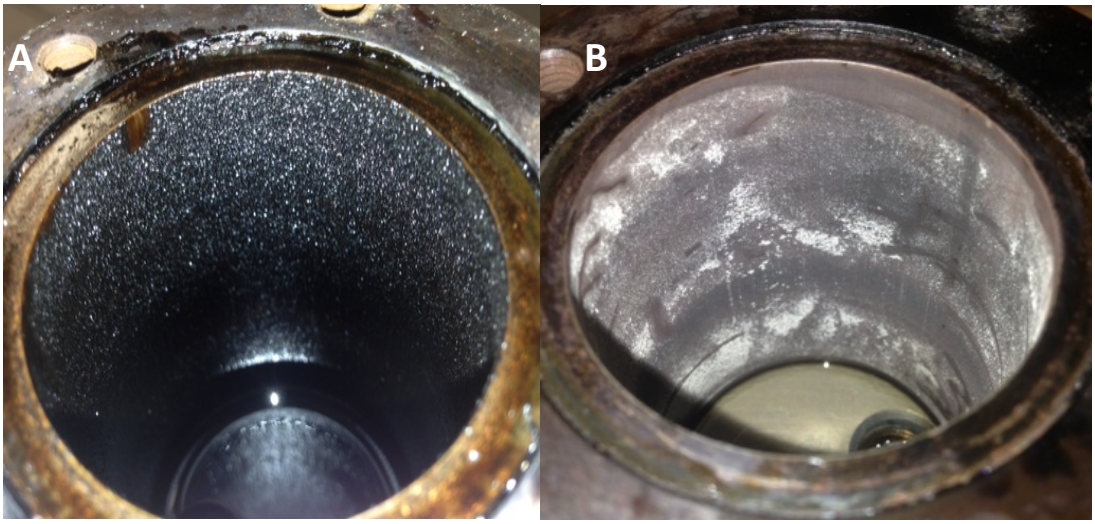


Figure 6.10 Photos of the reactor wall surface after draining and rinsing with chloroform leaving the insoluble foulant adhered to the wall surface. Image A: experiment CR-03 after draining oil from the reactor leaving behind the oil film and deposits Image B: - experiment CR-03 after rinsing with chloroform: salt deposits are clearly visible from the unprocessed crude oil.

6.3.2 Desalting Crude Oil Blends

The desalting method described in 4.2.2 was evaluated for a 5g sample of the 1:1 H:L blended crude oil. The electrical conductivity of the residual water was then measured. This process was repeated two further times measuring the conductivity for each residual water.

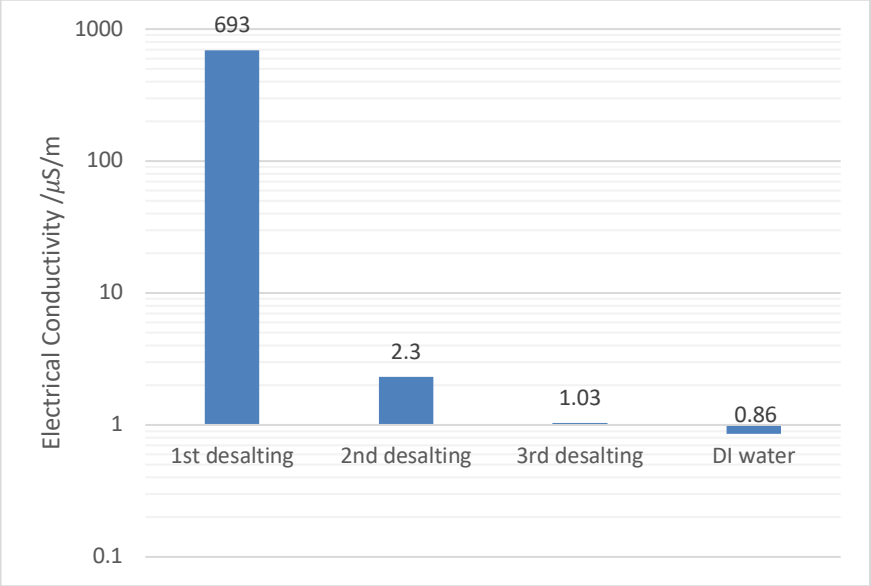


Figure 6.11 Electrical Conductivity of residual water on repeated desalting of H:L crude blend

Figure 6.11 results show the desalting process to be highly effective at removing suspended salts in the crude oils. The conductivity of residual water in the 2nd desalting process is only 0.33% of the first desalting process. One desalting process was believed to be sufficient for preparation of crude oils for fouling experiments.

Samples of heavy, light and 1:1 H:L blended crude oils were each desalted using the described method, and the residual water collected from the desalting process was filtered using 1 µm syringe filters and analysed using ICP-OES for determination of Na, Ca ion concentrations.

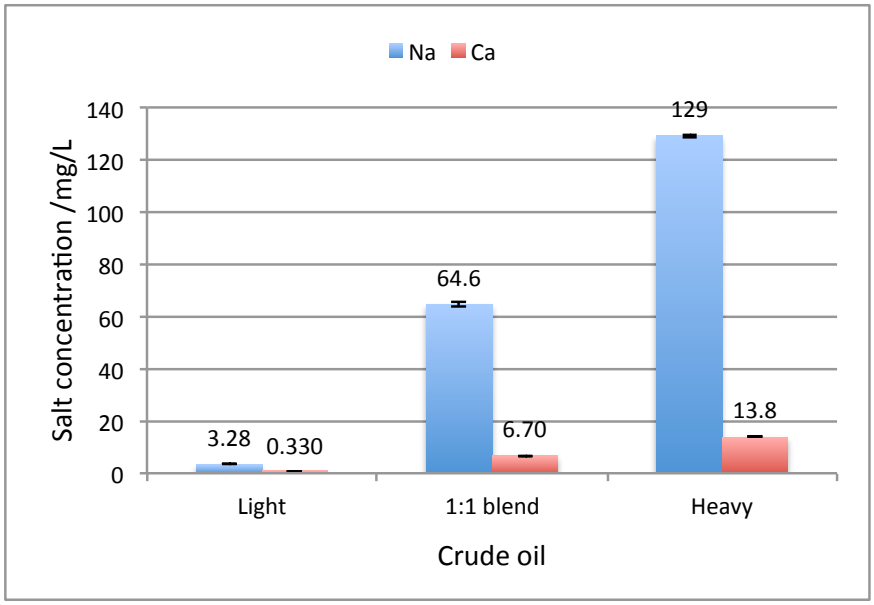


Figure 6.12 ICP-OES analysis of metal ions removed from crude oil in desalting water milligrams per litre of crude oil

As can be seen above, the presence of salt is far greater in the heavy crude oil sample than light, and sodium ions are the dominant species although calcium is also present in smaller concentration. The 1:1 blend, as is expected is approximately average the two concentrations.

6.3.3 Commissioning trials with desalted oils

After desalting the earlier crude oil blend, the fouling experiment was repeated. This time, carbonaceous fouling was present in the reactor, but with no white salt deposits were visible, however three bands of fouling deposit were present in the reactor, with lighter bands where no fouling had occurred (5.13A).

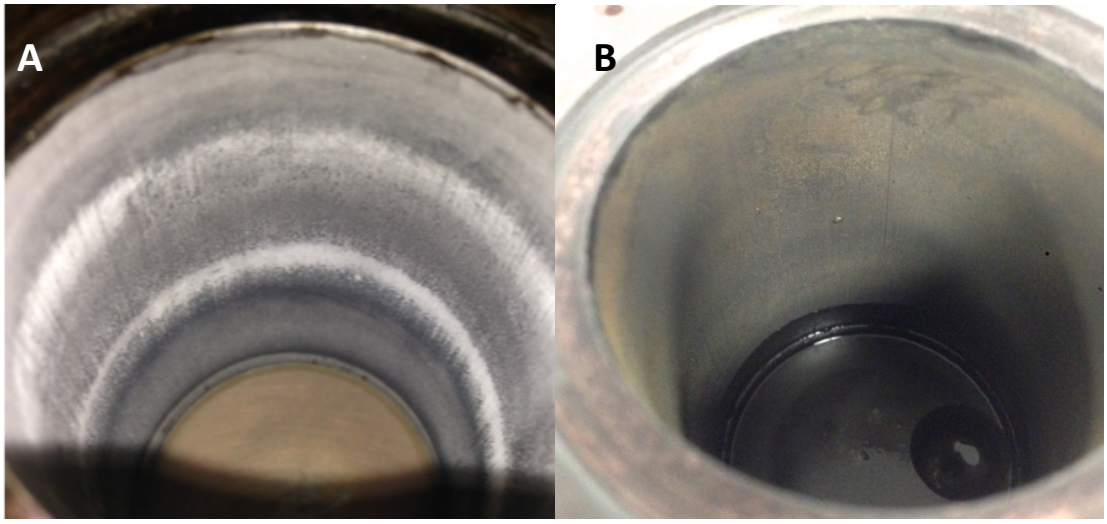


Figure 6.13 A: (experiment CR-04) Reactor wall after repeat of the experiment under the same conditions but using desalted oil. Deposits are carbonaceous and salts are no longer visible. B: (experiment CR-05) Reactor wall after draining and rinsing with remaining chloroform. As a result of higher temp. and rotation speed, deposit rings are no longer apparent

The structure of these bands corresponds exactly with the earlier rheological investigation when stable Taylor-vortex flow was apparent. The light bands where no fouling was observed occurs in the nodal region where flow directs radially towards the central rotor and hence where shear stress is lowest. In the deposited regions, flow directs radially towards the wall surface and shear stress is highest. This indicates that fouling deposition is a mass transfer limiting process, and that shear removal is not a dominant process under these conditions. Clearly the flow is not in the turbulent regime, so the following experiment was conducted at higher temperature (300 °C) and higher rotational speed (1500 rpm).

After draining the sample fluid and rinsing with chloroform (see product recovery method Section 4.3.2), the reactor deposit was distributed much more evenly around the reactor wall surface (Figure 6.13B), indicating that the stable vortex flow had been disrupted and deposit was observationally less dependent on axial height. Deposits appeared yellow/brown, in contrast to the black deposit observed in the previous experiment.

The experiment was repeated under the same conditions for CR-05 however the mass of insoluble deposits produced (8.9 mg) was considerably lower than previously. It is speculated that cleaning was not performed thoroughly in the earlier experiment. Fouling experiments were repeated, but adhered foulant masses were not consistent and most masses were around 10 mg. The temperature was increased to 320°C and the ratio of the ratio of heavy to light oil was increased to 60:40 by weight. It

was proposed that the heavy oil, containing more heteroaromatics and a higher proportion of asphaltenes might lead to greater fouling deposition.

6.3.4. Repeatability study

Early commissioning experiments with crude oil exhibited irregularities in the amounts of fouling deposits between experiments. A new series of fouling tests were undertaken at 320 °C for 6 hours at 1500 rpm and 30 bar pressure to assess the repeatability of fouling experiments under identical process conditions. Results are given in Table 6.5 and Figure 6.14 and named as RR-# (repeatability run number):

Table 6.5 Deposit masses produced in fouling experiments for repeatability study for desalted crude oil with heavy:light ratio 3:2 at 320 °C, 1500 rpm, 30 bar pressure (RR denotes repeatability run)

Experiment	Insolubles on Wall /mg	Insolubles in Film /mg	Total Insolubles /mg	Notes
RR-01	92.1	3.5	95.6	yellow/brown deposit
RR-02	61.0	2.9	63.9	yellow/brown deposit
RR-03	34.5	1.4	35.9	yellow/brown deposit
RR-04	28.0	5.8	33.8	yellow/brown deposit
RR-05	18.9	1.8	20.7	yellow/brown deposit
RR-07	10.2	5.8	16.0	yellow/brown deposit
RR-08	12.7	3.0	15.7	yellow/brown deposit
RR-09	14.5	2.6	17.1	yellow/brown deposit
RR-10	9.5	4.5	14.0	yellow/brown deposit
RR-11	8.8	3.9	12.7	yellow/brown deposit

Before the first experiment, the reactor had been inactive for some time and there was a very fine surface layer of oxidation on the carbon steel inner surface. The reactor was therefore cleaned with chloroform and the nylon brush thoroughly. In this series of experiments the liquid film layer was Buchner filtered as it was postulated that some foulant loosely adhered to the wall could also be washed off the wall surface. Masses were small in comparison to adhered masses but not insignificant.

Results for the chloroform insoluble deposit masses of RR-01 – RR-05 can be seen in Figure 6.14. Foulant mass was particularly high in the first run, decreasing with each subsequent run. The high activity of the wall surface was thought to be a result of surface heterogeneity as a result of surface

oxidation from earlier storage. This activity diminished on subsequent runs as the metal surface becomes passivated through exposure to oil and high temperature. As a result, the cleaning method was thus modified to produce a consistent interior wall surface for each experiment by wet sanding the inner surface of the wall body whilst rotating. The reactor body and base were sanded with 800 grit followed by 1200 grit alumina abrasive paper, then rinsed with DI water and oven dried before each experiment leaving a bright and smooth finish so that the surface exhibited no thermal history.

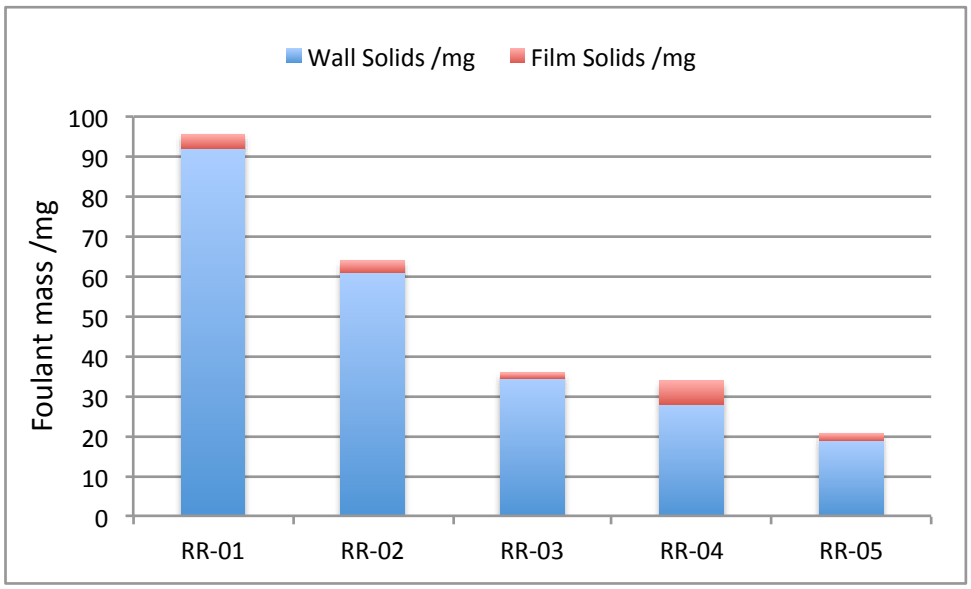


Figure 6.14 Masses of chloroform insoluble foulant on for a repeatability study of crude oil at 320°C for 6 hours, 1500 rpm and 30 bar pressure

The experiments were then repeated under the same conditions and found to exhibit significantly better repeatability than before changes were made to the cleaning method. The chloroform insoluble fouling deposit masses can be seen in Figure 6.15. The mean mass of chloroform insolubles was 15.1 mg with a standard deviation of 1.7 mg.

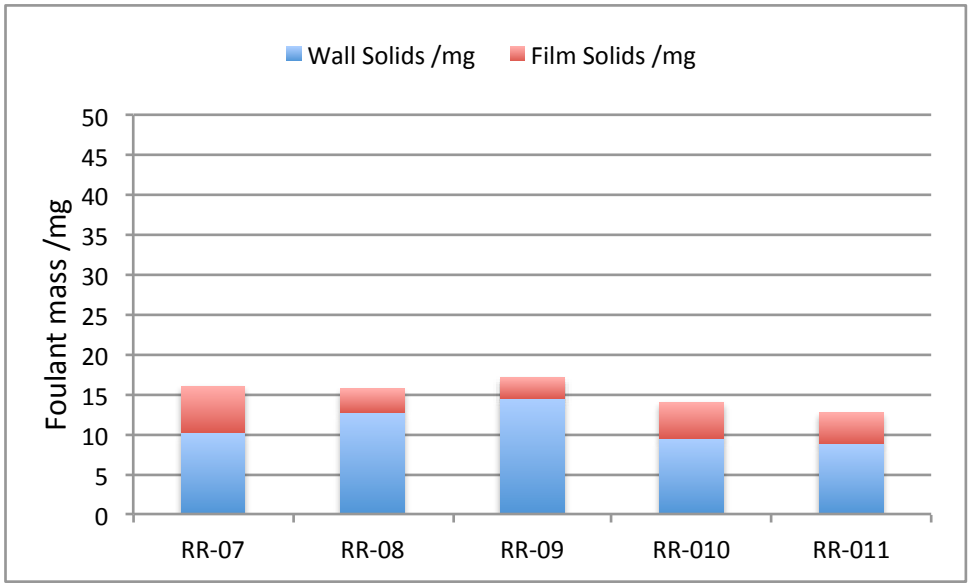


Figure 6.15 Masses of chloroform insoluble foulant on for the second repeatability study of crude oil at 320°C for 6 hours, 1500 rpm and 30 bar pressure, after changes to the cleaning method were applied

The surface roughness is known to influence mass and momentum transfer and shear stress is related to the surface roughness. Whilst surface roughness is not a focus for this work, its importance is recognised for maintaining consistency between experiments. This change to the cleaning method produced lower amounts of fouling compared with earlier experiments before fine sanding, however the much-improved repeatability compared to before was deemed imperative for procuring reliable data for the research work to follow.

6.3.4 Modifications following commissioning experiments

Draining spent liquid products from the reactor after an experiment into the product collection vessel is intended to be a safe and clean method to transfer liquids and safely relieve gas from the system by opening valve V9. Whilst the collection vessel achieves its intended function, some of the liquid volume resides in the tube and vessel walls as it passes through after collection into a liquid product vial, reducing the amount of liquid recovered and making cleaning between reactions more difficult. The loss is exacerbated for liquids that are highly viscous at ambient temperature as such significant mass of product is not recovered. As a result, for improved recovery, the liquid products were instead collected directly from the bleed valve into a glass vial so no liquid was lost in the process, making the fluid recovery vessel, V9 and associated process tubing redundant.

Reactions were in general conducted at the upper temperature limit of 320 °C to achieve higher fouling rates and to reduce the viscosity to maintain fluid in the turbulent regime, minimising striations arising from vortex flow in the reactor.

6.3.5 Later Modifications to the Taylor-Couette cell body to enable wall surface analysis

In later experiments (chapters 7 and 8), an alternative Taylor couette cell configuration was implemented for additional experiments in order to analyse the fouling deposit on the cell wall using SEM-EDX without removal from the wall surface which would disturb the deposit structure. A a second reactor wall body was fabricated with an slightly modified internal diameter to fit a steel sleeve which could be press fitted into the body with minimal force enough friction to remain static once in place. Sealing was achieved as before by compression of two annealed copper gaskets between the wall body and the flanges. The new body was manufactured from 304 Stainless Steel as corrosion resistance for improved corrosion resistance. The same head and base sections were used as normal. Seamless cold drawn steel tubing (38.1mm (1.5”) OD, 16g thickness) was ordered for the sleeve material; which is the same as often used in industrial tubes inside shell and tube heat exchangers.

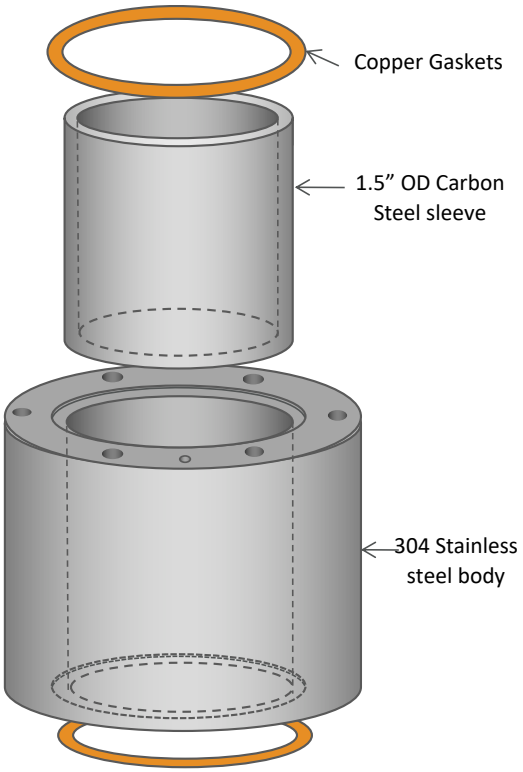


Figure 6.16 Modifications to reactor cell to enable inner wall surface analysis

The modified system has several advantages over the previous iteration. Firstly, as a new section of steel tubing could be inserted for each reaction, the inner surface would be consistent between experiments, second, preparation of the reactor could be slightly accelerated, as the reactor body required less cleaning and no sanding between experiments; the fouling solids attached to the

removed sleeve could also be processed once the new reaction is underway. Thirdly, the wall surface could be changed to test the effect of new materials and different surface preparations. However, this modification took place towards the end of the research timeline, and so for consistency, all quantitative experiments were conducted with the original body setup, and only repeat experiments performed with this new configuration to obtain for deposits for SEM.

6.4 Conclusions

The behavioural characteristics and performance of the Taylor Couette fouling reactor was investigated in terms of rheological properties, thermal and pressure control, heater reaction behaviour and repeatability study leading to the development of a standard operation procedure for further experimental studies.

The rheological studies presented here relate the flow conditions to that of a typical heat exchanger tube and enable the author to determine appropriate operating conditions for the reactor to simulate a realistic hypothetical flow condition in a refinery heat exchanger. Fouling experiments unless otherwise stated were therefore run at 320°C at 30 bar pressure and 1500 rpm. This also fits within the safe operating parameters of the equipment without causing excess wear.

One significant takeaway from the commissioning process is that the effectiveness of the cleaning procedure has a strong influence on the formation of insoluble inside the Taylor Couette cell, as residual deposits may act as nucleation sites for further precipitation, which may lead to inconsistent results. Equally, the preparation of a fresh metal surface with very fine 1200 grit alumina paper is required to keep the wall surface condition consistent between experiments. As a result, the time for preparation and sample recovery between experiments is much longer than previously anticipated. Also, due to the variability in deposit amounts between experiments, it is particularly beneficial to repeat experiments when changing the sample fluid composition, to reduce the potential of contamination and the uncertainty of fouling results. This is especially important when a new data set follows an experiment which recorded a high quantity of fouling solids, as it may be challenging to eliminate all insoluble particulates.

The impact of this is that experiments should be repeated to lower the chance of achieving poor data by inconsistencies in individual fouling experiment. A change of strategy was employed to obtain more reliable data. Two experiments were conducted for every composition or process condition, with the aim being to have two concordant results which were then averaged, and to rule out anomalous

fouling data which could not be repeated. It was therefore necessary to reduce the breadth of fouling experiments planned. A set of experiments which was originally planned to investigate the effect of adding heteroaromatic compounds (dibenzofuran, dibenzothiophene, indole and quinoline) to crude oil on fouling behaviour was therefore removed from this work, and forms part of the recommended future work from this thesis.

Chapter 7 Fouling experiments using blended Crude oils

7.1 Use of crudes H and L for fouling experiments in the Taylor Couette fouling rig

From the investigation above, the high asphaltene content, high heteroatom and metal content suggest that crude H may be a good candidate for fouling reactions, however, the viscosity is very high making it, unviable for PHT streams in its current form, and also less practical for laboratory research. For this reason, blending of crudes H and L was performed as preparation for fouling experiments to achieve a reduced viscosity but with significant asphaltene content and heteroatom content.

Crude oil was blended in a heavy:light 3:2 mass ratio according to the method in section 4.2.1 and desalted following the procedure described in section 4.2.2. Reaction protocol described in section 4.3 was followed for all experiments using 75 mL of test fluid for each fouling experiment. As per the commissioning experiments, impeller rotational speed was set to 1500 rpm and the test apparatus was heated to maintain a constant wall temperature of 320°C. This temperature, which is the highest operation temperature typically found in refinery systems, was chosen to increase the reaction rate, increase Reynolds numbers for higher turbulence and improve mixing, decrease viscosity and reduce the boundary layer for improved mass transfer to the wall surface. Higher temperatures were avoided as pyrolysis reactions begin to occur from approximately 350 °C and above which might produce greater quantities of 'coke like' fouling deposits not representative of refinery systems. All experiments were conducted under the following general conditions:

Table 7.1 General conditions applied to all fouling experiments in chapters 7, 8 and 9 where deposit masses have been measured

Reaction time at full temperature	12 hours
TC cell wall temperature	320 °C
Rotational velocity	1500 rpm (1.82 ms^{-1})
Pressure	30 bar
Desalted	yes
Wall surface	Carbon steel, no sleeve

7.1.1 Crude oil blend composition - mass analysis of fouling solids

In industry, crude oils are often blended before entering the preheat train in order to obtain acceptable overall physical properties for processing in terms of density, viscosity and solution stability. Blended oils need to have moderate physical properties and exhibit good phase stability before entering the refinery process. Improper blending of crude oils may negatively impact the solution stability. Fouling experiments were conducted for blends of the heavy and light oils with heavy-oil weight fractions between 0.5 and 1. This range was chosen due to the significantly greater presence of asphaltenes, metals and heteroatomic species being present in the heavy crude oil. Recovered insoluble deposit masses for the experiments can be seen in Table 7.2 and Figure 7.1:

Table 7.2 Average masses of fouling deposits: crude oil blend composition

Weight mass fraction Heavy oil	Insoluble Wall deposits /mg	St. Deviation	Insoluble Film Solids /mg	St. Deviation	Total Insoluble Wall and Film Deposits /mg	St. Deviation	Insoluble Bulk Solids /mg	St. Deviation
0.5	4.4	0.57	1.8	0.7	6.2	1.3	38.3	14.3
0.6	19.7	0.14	2.1	0.8	21.8	1.5	55.0	6.6
1	76.9	0.11	5.5	0.7	82.4	10.3	99.8	14.8

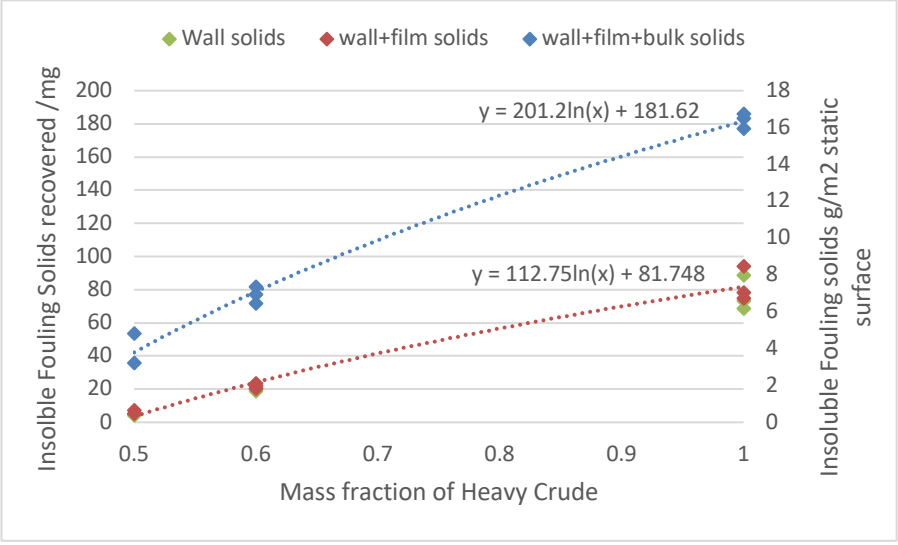


Figure 7.1 Deposit mass as a function of blend composition: crude oil blend composition, in both total mass (mg) and miligrams of fouling per square meter of wall surface mg m^{-2}

As seen above, there is a strong positive (logarithmic) correlation between the insoluble deposit masses recovered and the weight percent of heavy crude in the oil blend, similar trends exist for both deposits collected from the wall surface + film, and in the bulk fluid. The heavier oil blends

contain a higher concentration of asphaltenes, metals and heteroatomic functional groups, which are known to cause fouling. The nearly linear relationship indicates that the tested crude oils exhibit good overall phase stability within this range, as a major precipitation event would be visible as a significant departure from the trend. It should however be noted that heavier crude oil blends also have higher viscosity, shear stress in the Taylor-Couette cell and impacting mass transfer to and from the boundary layer. This may be an explanation for the non-linear relationship, as fewer fouling precursors are able to transfer to the wall surface for a given residence time.

Ideally more data points in the range would be desirable to confirm this however but in the interest of time and progress, the correlation was deemed to be sufficient. It should be noted that the trend cannot be extrapolated for lower weight fractions of heavy oil, as the crude may exhibit incompatibility regions, depending on its composition.

7.2 Time dependence on fouling with desalted 3:2 H:L crude oil

In industrial settings, the fouling of heated process tubes in refinery heat exchangers typically occurs over long periods and may have cleaning intervals on the order of months depending on performance. Laboratory experiment durations must be on the order of hours partly for safety reasons, mainly to obtain data within a reasonable time to allow for satisfactory progress such that a reasonable number of experiments may be made during the research duration. Building on the commissioning trials in Chapter 5, the first series of crude oil fouling experiments was to determine the on fouling of residence time within the test fouling apparatus. Averaged data obtained from the commissioning trials RR-07 to RR-11 formed the 6-hour residence time data set.

Crude oil Experiments were run at 6, 12 and 24 hours. The fouling experiments (RR-07 to RR-11) already described in the repeatability study in Section 6.3.4 with the updated cleaning and recovery method formed the 6-hour experiments as part of this study. Fouling experiments followed the general conditions outlined in Table 7.1 except for residence time which is the controlled variable.

Fouling products were recovered using the method described in section 4.3.2. Fouling experiments of 6 hour and 12-hour durations at operational temperature were conducted during single day run (Figure 7.2). Due to safety reasons, fouling experiments were not permitted to run overnight, so for 24-hour experiments, reactions were timed to run at full temperature for 12 hours, before the heater

was switched off overnight but with continued rotation. The heater was switched on again 8 hours later and run for the second 12-hour period at full temperature.

7.2.1 Mass analysis of fouling solids

The results can be seen in Table 7.3. and in Figure 7.2. Three runs were made for the 12 hour and two for the 24 hour set, and the results averaged. The mass of insoluble deposits recovered from the wall increases overall with time, correspondingly the mass of deposits recovered from the film decreased with time, this suggests that particles present in the boundary layer of the wall surface become bound to the surface as they reside for longer. However, after an initial fouling layer is deposited, the surface activity appears to be diminished as the total of the wall and film solids is barely changed between 12 and 24 hours, indicating little benefit from a longer run time. Overall wall deposit masses and yellow/light brown in colour, indicating inorganic deposits predominate for this oil under the process conditions. Recovered bulk deposits are relatively higher compared with the wall and film deposit masses, indicating that fouling precursors in the oil circulate in suspension. Although the average bulk deposit mass appears to dip after 24 hours, this is within the error bounds and not considered to be substantive.

Table 7.3 Deposit masses recovered from fouling experiments of 60:40 H:L crude oil blend at varying heated test time between 6 and 24 hours with associated errors. Wall Temperatures were maintained at 320 °C, rotation speed 1500 rpm.

Heated Time /hrs	Insoluble Wall deposits /mg	St. Dev	Insoluble Film Solids /mg	St. Dev	Total Insoluble Wall and Film Deposits /mg	St. Dev	Insoluble Bulk Solids /mg	St. Dev
6	11.1	2.39	4.0	1.27	15.1	1.74	61.4	14.68
12	19.7	0.14	1.9	0.84	21.6	1.51	55.0	1.51
24	22.4	0.35	1.1	1.20	22.7	1.56	47.2	1.56

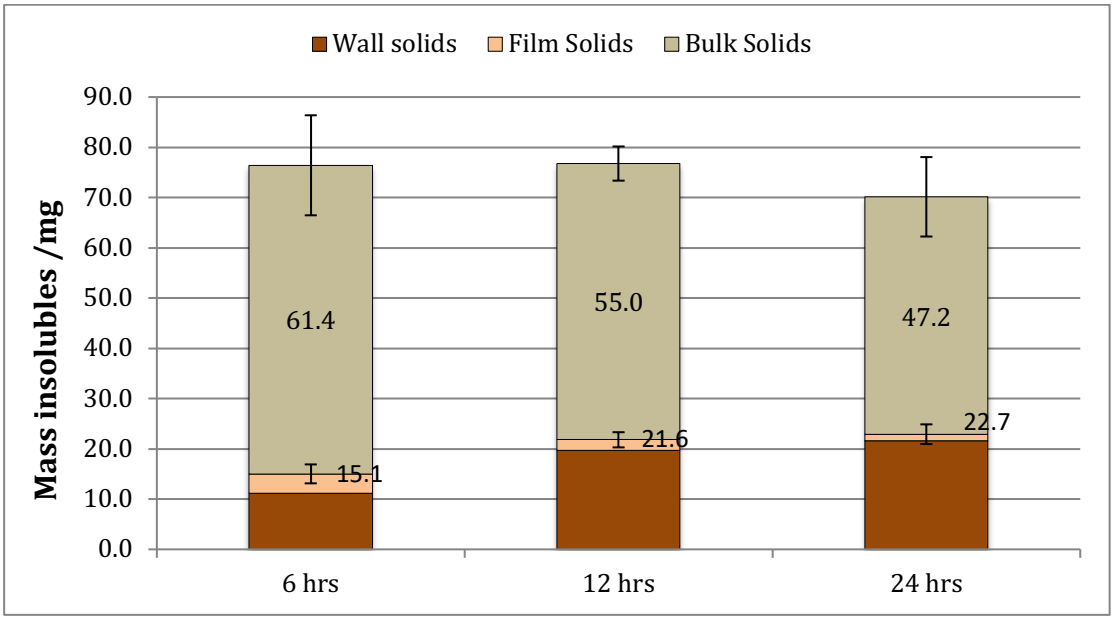


Figure 7.2 Insoluble deposit masses for crude oil fouling experiments at 6, 12 and 24-hours including error bars. Total insoluble solids in wall and film was 15.0mg for 6 hours, 21.6 mg for 12 hours and 22.7 mg for 24-hour residence times.

7.3 Conclusions of crude oil fouling experiments

The desalted crude oils supplied by BP were characterised using a number of chemical, physical and preparative techniques, providing insight into chemical makeup of both oils and their thermal cracking behaviour. Characterisation of the fractionated heavy-oil asphaltenes and maltenes was also compared to the 'natural' heavy oil, and provides the necessary insight for the following chapter exploring fouling behaviour of fractionated oil solutions.

Initial fouling experiments in Chapter 5 enabled the development of standard operating procedures for experiments in this section. Reactor temperatures, pressures and rotation speed were kept constant throughout all experiments. Fouling experiments in this chapter focused on blend ratio and residence time. Fouling deposits to the wall + film correlated positively with heavy oil mass fraction, between values of 0.5 and 1. Whilst deposits were very low for 1:1 blends, the mass of deposits was significant for experiments with 100% heavy oil, however its high viscosity makes it both impractical unblended, and unrealistic for use in refinery PHTs which typically are designed for medium oil characteristics once blended.

The aim of the crude oil fouling experimental series was to develop an understanding on how changes to the composition, and process conditions impact the prevalence of fouling. The experiments

provides an insight into the effect of changing process conditions, in this particular reaction setup, and forms a basis for comparing other fouling fluid compositions. Greater insight can also be gained from deposit characterisation further investigate the chemical nature of the deposits and how they might change by varying process conditions.

The limitation with the batch fouling reaction setup, is that the production of fouling data is a slow process. Each experiment requires a 30-minute sample preparation time, 1 hour start-up, 12-hour residence time at full temperature, 2-hour cool down, and 1 to 2-hour product collection and cleaning process and finally 1 to 2-hour product workup. Each set of experimental conditions must then be repeated once at minimum, to obtain a single data point on a composition or time series. Invariably fouling itself is a slow process in refinery conditions, necessitating long reaction times, however altering the phase behaviour can have a significant effect on the rate and amount of fouling production.

Chapter 8 Fouling experiments with fractionated crude-oil solutions

8.1 Introduction

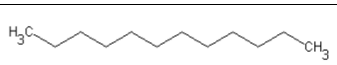
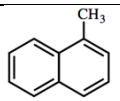
The work in this chapter focuses on the fouling behaviour of solvent fractionated maltenes and asphaltenes derived from the heavy oil – Crude H, either in isolation or in solution with model solvents, dodecane and 1-methylnaphthalene which represent the model saturates and aromatics fractions according to the SARA fractionation method. The aim of this work is to examine how both the physicochemical properties and solution stability affect the propensity and nature of the fouling behaviour. The test fluids are simplified relative to the crude oil from which they are derived, which forms the precursor to the fouling of fully synthetic crude oil model solutions in Chapter 9.

To enable a good comparison between test runs, the reaction times and process conditions, like Chapter 6 were fixed, and only the test fluid is varied in this chapter. In the first experimental series, the concentration of asphaltene is varied from 5 to 20% by weight in solutions of 1-Methylnaphthalene. In the second series, a 5% weight solution of asphaltene is tested in a model solvent solution of n-dodecane and 1-methylnaphthalene in varying proportions. The third series investigates the effect of the addition of n-dodecane to the heavy oil maltene fraction on fouling behaviour. Mixtures are prepared and tested containing varying weight fractions of n-dodecane.

8.1.1 Selection of model solvents and synthesis of model compounds

Two model solvents for use in semi-synthetic and fully synthetic oil fouling experiments were used extensively throughout this work, representing saturates and aromatics fractions within SARA fractionation model of crude oils. n-dodecane (dod) is an aliphatic hydrocarbon, representing the saturates fraction. 1-Methylnaphalene (MN) is a bicyclic aromatic hydrocarbon representing the aromatics fraction. Properties of these two molecules are given in Table 8.1.

Table 8.1 Properties of two key solvents used for fouling experiments

Name	n-Dodecane	1-Methylnaphthalene
Structure		
Molecular formula	$C_{12}H_{26}$	$C_{11}H_{10}$
C/H ratio	2.17	0.909
Molecular weight	170.34	142.20
Melting Point /°C	9.7 ± 0.3	-29 ± 9
Boiling Point /°C	216 ± 2	242 ± 7
Density @ 20 /kg m^{-3}	751.5	1021
Viscosity @ 20°C/mPa.s	1.55	3.31

8.1.2 Process conditions

As discussed in Chapter 4, conditions necessary to represent the late-stage refinery heat exchangers were suggested, and trials exhibited insoluble fouling deposits in the crude oil fouling experiments. As such, the reactor wall temperature was heated and maintained at a constant at 320 °C, pressure inside the reactor maintained with gas overpressure of 30 bar. Rotor velocity is maintained at 1500 rpm, and residence time of 12 hours at full temperature. This was the longest practical duration for heated experiments, without requiring over-night running.

8.2 Fouling experiments: Investigating the effect of asphaltene concentration on fouling in 1-methylnaphalene

C-7 Asphaltenes were separated using the method outlined in Section 4.2.3 and an analysis of the chemical properties of asphaltenes was described in sections 5.2. The asphaltenes obtained, being a solubility separated fraction, are immiscible in highly aliphatic solvents such as n-dodecane due to their polarity and aromaticity of the polyaromatics structures, but are fully miscible in the diaromatic solvent, 1-Methylnaphathalene, representing the aromatics fraction within the SARA classification system. These experiments followed the general reaction conditions as described in Table 7.1.

8.2.1 Sample preparation

Solutions of prepared asphaltenes, were first oven dried at 50 °C to drive off any moisture, then weighed asphaltenes were added to warm (50°C) 1-mehtylnaphthalene to a total 75g while stirring for 60 minutes, by which time the asphaltene was fully dissolved (no solids were found to remain in all cases). The solution was then added to the loading vessel and experiment run in the usual way. Insoluble deposit masses can be seen in Figure 8.1. Two congruent runs were made at each asphaltene concentration, and the deposit masses averaged in the data set.

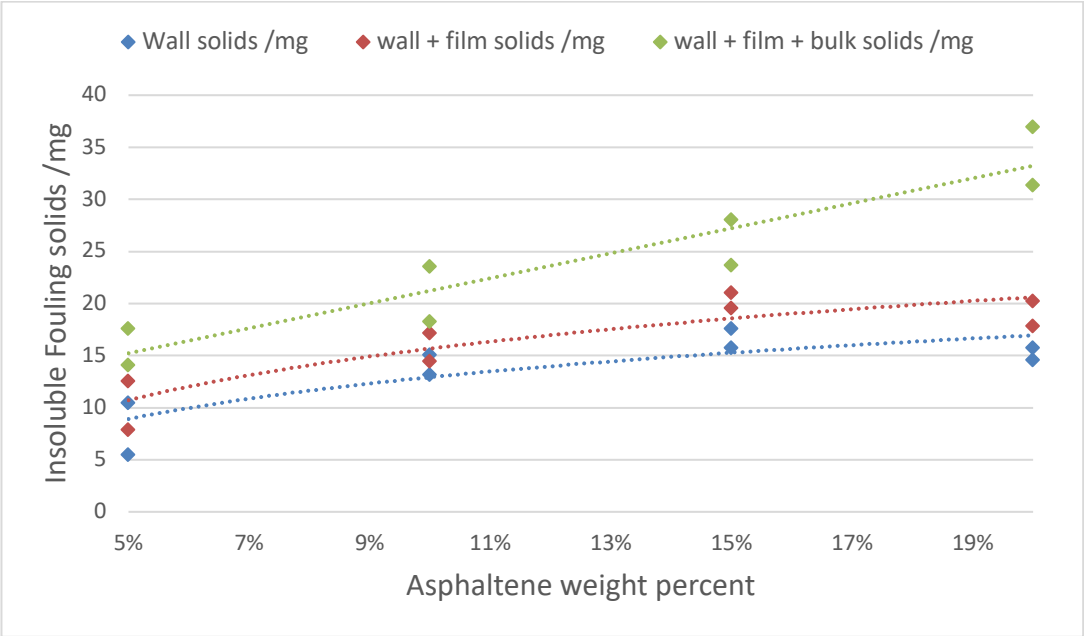


Figure 8.1 Insoluble fouling deposits recovered from reactor for experiments ranging from 5% to 20% asphaltenes by weight dissolved in 1-mehtylnaphthalene. Logarithmic trends are plotted for the wall and film deposits, while total deposits (including those extracted from the bulk) scale approximately linearly so is plotted with a linear trend line.

8.2.2 Discussion

The lower error bars represent the standard deviations of the sum of the wall and film solids, and the upper error bars are the standard deviations of the total deposit masses. Wall + film masses trend up from an average 10.3 mg in 5 % w/w asphaltene solutions in (MN) and 15.9 mg for 10 %, before flattening at around 20 mg insoluble wall + film deposits for 15% and 20 % solutions, however the total mass of foulant scale approximately linearly with asphaltene concentration. These numbers are overall still quite low, only leaving a fine film of yellow/brown (predominantly inorganic) deposit. This suggests that the asphaltene-MN solutions have a stable phase behaviour in high temperature fouling experiments, and that wall deposits are largely surface adhered inorganics deriving from the asphaltene. Deposit adheres at first to the active metal surface, until 15% where the mass of wall

solids flattens off, likely a result of high shear stress at the wall surface removing any particle that reach the wall surface and residing suspended in the bulk fluid.

8.3 Effect of solvent aromaticity on fouling behaviour using asphaltene solutions

In the previous set of experiments, very high weight percentages of asphaltenes dissolved in 1-mehtylnaphthalene exhibited relatively modest insoluble fouling masses, despite the positive correlation between asphaltene concentration and insoluble fouling mass. Since solutions appeared particularly stable, a following series experiments was set up to investigate the effect of decreasing the aromaticity of the solvent mixture by addition of n-dodecane, a model Saturate and poor solvent for asphaltenes, being very similar in chemistry to n-heptane, from which the asphaltenes were derived.

8.3.1 Preparation

5% w/w solutions of asphaltene in the binary solvent mixtures by first dissolving 3.75g dried crushed heavy oil asphaltenes in 71.25g warm 1-methylnaphaltne whilst stirring, followed by the addition of n-dodecane, and then loading to the sample vessel, after which the reactor standard operating procedure is followed as normal.

8.3.2 Experimental

Process conditions were maintained the same as the prior experimental set. Two fouling experiments were run at each sample composition, and the 0% dodecane data. Deposit masses were averaged over the two runs. Results are shown in Figure 8.2:

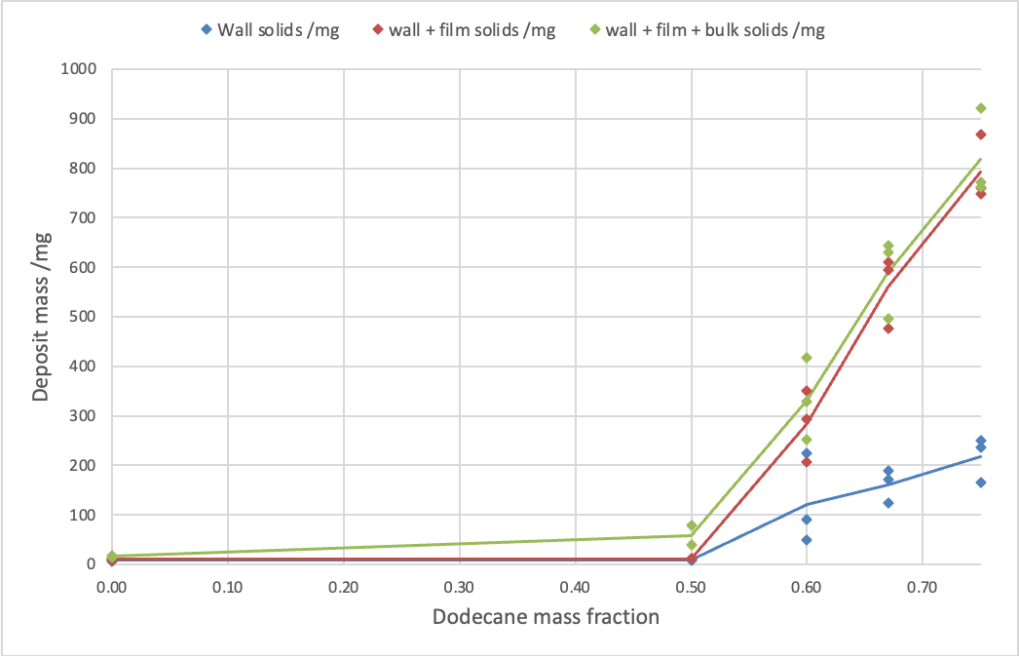


Figure 8.2 Scatter plot of insoluble fouling deposits for solutions of 5% asphaltene. The solvents were binary mixtures of n-dodecane and 1-methylnaphthalene in varying proportions. Mean deposit masses for each composition are plotted as lines of the same colour.

The results were remarkable. Total fouling deposit masses collected were low in solutions of 0% and 50% dodecane by weight, but deposits increased significantly in solutions exceeding 0.5 w/w dodecane, increasing linearly with concentration greatest insoluble deposit masses recorded for solutions of 0.75 dodecane. Solutions with dodecane mass fractions above 0.5 maintained a fairly uniform ratio of deposit adhered to the wall on average (approximately one quarter) and just under three quarters collected from the film, however very little of the deposits was collected from the bulk fluid, likely due to agglomeration and phase separation of the asphaltenes from the liquid before further reaction to form insoluble deposits. Much of the insoluble film solids were visibly larger (on the order of 1-5 mm diameter) than in previous experiments with predominantly inorganic deposits and thus did not flow out of the bleed valve during collection. Whilst phase separation with high concentrations of saturated solvents was expected to occur at higher dodecane concentrations, the extent of thermal polymerization to form insoluble deposit was a far greater surprise. Had the precipitated fouling remained as asphaltene deposits, these would have been fully solvated during the chloroform rinsing stage, and would not have been classed as insoluble deposits.

The rinsed wall-adhered fouling deposits (wall solids) can be observed in Figure 8.3. Adhered deposits are visible as a fine (likely inorganic) white/yellow precipitate the photograph a) which tests an asphaltene and 1-methylnaphthalene solution without addition of n-dodecane. Fouling is likely

sulphur, inorganics and metals deposited from the asphaltene. In photograph b (w_{dod}= 0.5), the yellow deposit layer is more pronounced and darker shade of yellow/brown, likely sulphur and inorganics with some organic deposits in areas and on the lower flange. In photograph c (w_{dod}= 0.6), a significant quantity of organic deposits can be seen around the wall surface, and on the lower flange. Also of note: occasionally some larger carbonaceous fragments could be easily dislodged in the rinsing process (was always performed with as little force as possible to prevent this) and were too large to be pipetted into the film fraction. These are accounted in the "wall solids" fraction, whereas fine particles which are dislodged after rinsing would be collected into the "film solids" fraction. In photographs d, e and f, the quantities of wall adhered solids were substantial, and large deposit structures can be seen to form bands around the center of the reactor circumference. In photographs e/f, a clumped masses of organic deposit adhered to the the lower flange in the void between the rotor and the flange. Fluid velocity and this wall shear stress is expected to be low in this region and as such, organic particulates settled and polymerized, adhering to the surface as a large amorphous clump.

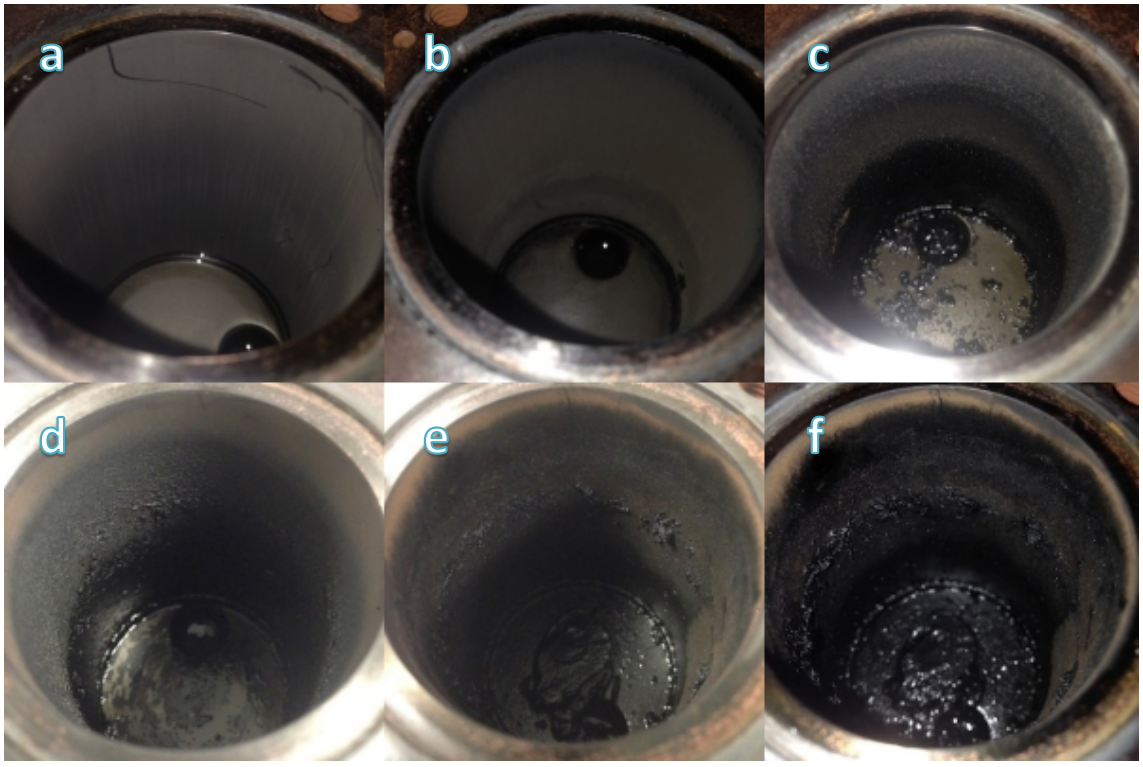


Figure 8.3 Photographs of reactor interior walls after rinsing film with chloroform. Dodecane mass fractions (w_{dod}): a=0, b=0.5, c=0.6, d=0.67, e (no flash) & f (flash) =0.75.

Significant fouling deposits were also visible on the rotor surface (see Figure 8.4), which was unexpected due to the higher Reynolds numbers expected at the inner surface.

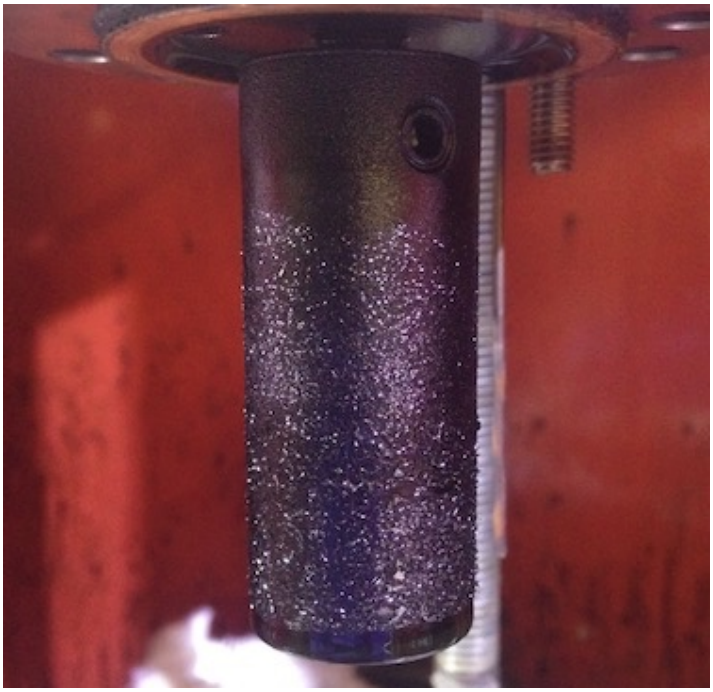


Figure 8.4 Visible carbonaceous fouling adhered to rotor 5% asphaltene, w_{dod} = 0.75

8.3.2 Fouling experiments using solutions of maltenes in dodecane

Experiments so far in this chapter have focused on fouling of asphaltene containing crude oils and solutions of asphaltenes. The deasphaltenated maltene fraction conations the aromatics, saturates and resins as classified by the SARA fractionation method. Resins present in maltenes have similar properties to asphaltenes but differ by their solubility class[182], and within any defined solubility class exists a range of compounds including marginally soluble resins which retained in the maltene fraction. These can have similar properties to the "almost" soluble asphaltenes which were precipitated in hot heptane. Asphaltenes of differing physicochemical properties may also be fractionated off using different n-alkane solvents, shifting the threshold between asphaltene and resin[183].

This series of experiments is aimed at investigating the propensity of the separated maltene fraction to cause fouling in the Taylor Couette cell, and varying the maltene solution properties by the addition of dodecane. During the large-scale fractionation described in Section 4.2.3, the prepared maltene sample contains a significant quantity of residual heptane from the separation process (22.2 mg/ml) even after atmospheric rotary evaporation at 125°C for 4 hours. It was decided that it was preferable not to lose the volatile constituents naturally present in Crude H in the process of removing as much of heptane as possible.

Neat dodecane was tested for fouling (none found), followed by a series of binary mixtures of maltene and dodecane, mixed at room temperature for 10 minutes and loaded directly into the reactor. No deposition was observed during the mixing process.

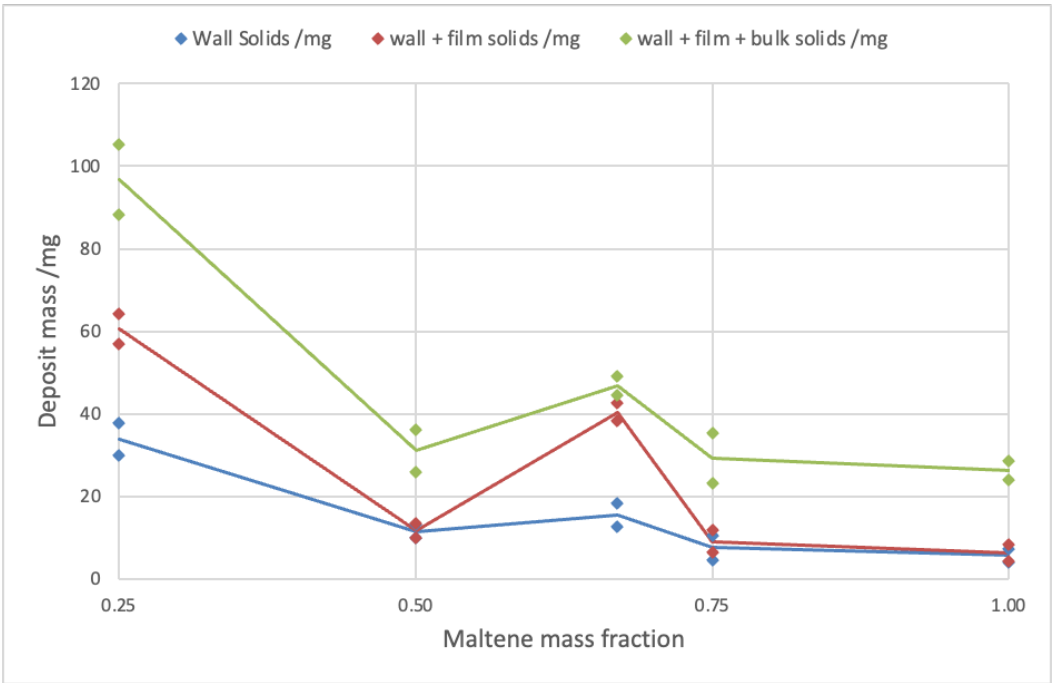


Figure 8.5 Scatter plot of fouling deposit mass for dodecane/maltene mixtures. Mean deposit masses for each composition are plotted as lines of the same colour.

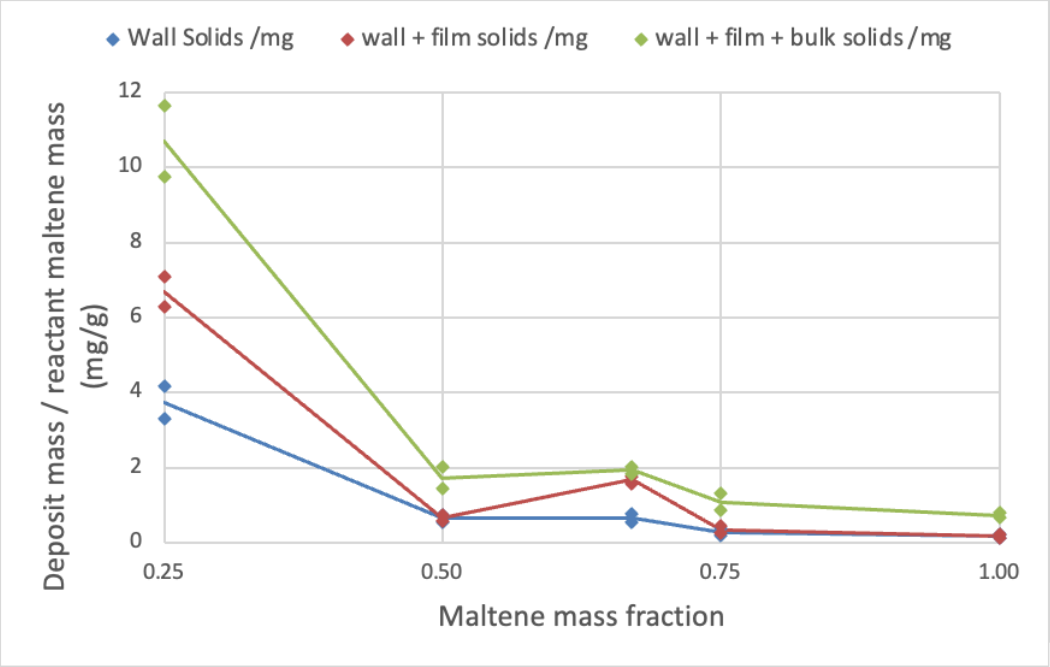


Figure 8.6 Scatter plot of deposits mass (mg) divided by mass of maltene starting material (g). Mean deposit masses for each composition are plotted as lines of the same colour.

Deposits masses were low for experiments with maltene mass fractions 0.5 or higher. Whilst there was a slight break in the pattern at 0.66 maltene mass fraction, this was put down to error as a result of the large number of manual operations, and not a feature of the phase behaviour. Fouling was observed to be far greater in the solution with a maltene mole fraction of 0.25. This is especially visible in Figure 8.6 which divides the mass of deposits in mg by the mass of maltene present in the TC cell reactor in g during the reaction. Mass of maltene present was calculated by:

$$\mathrm{m}_{\mathrm{malt}} = \rho V_{TC} \qquad 7.1$$

Where ρ = density of the mixture and $V_{reactor}$ = fluid volume of the TC cell. This measurement conversion is considered important since deposits derive solely from the maltenes and not the dodecane which is effectively inert. This amplifies the result, indicating that the solution with a mass fraction of 0.25 is highly unstable at elevated temperatures, leading to significant fouling. The deposits were also carbonaceous in nature. A repeat of this was performed using the modified fouling as described in the section below.

8.3.6 Fouling reactor modifications to enable wall surface analysis by SEM-EDX

At this stage in the project, a decision was made to fabricate a second Taylor Couette body with the ability to insert replaceable steel sleeves for removal and subsequent visualisation and chemical characterisation by SEM-EDX analysis. A description of this configuration is provided in section 6.3.5. These experiments also followed the general reaction conditions as described in Table 7.1 with the exception of the wall surface (with cold drawn carbon steel sleeve).SEM micrographs of the removable sleeve and carbonaceous fouling can be seen in Figure 8.7. A repeat of the 3:1 w/w dodecane:maltene fouling experiment was made using the new setup and the wall body. Deposits were visible in micrographs b and c below.

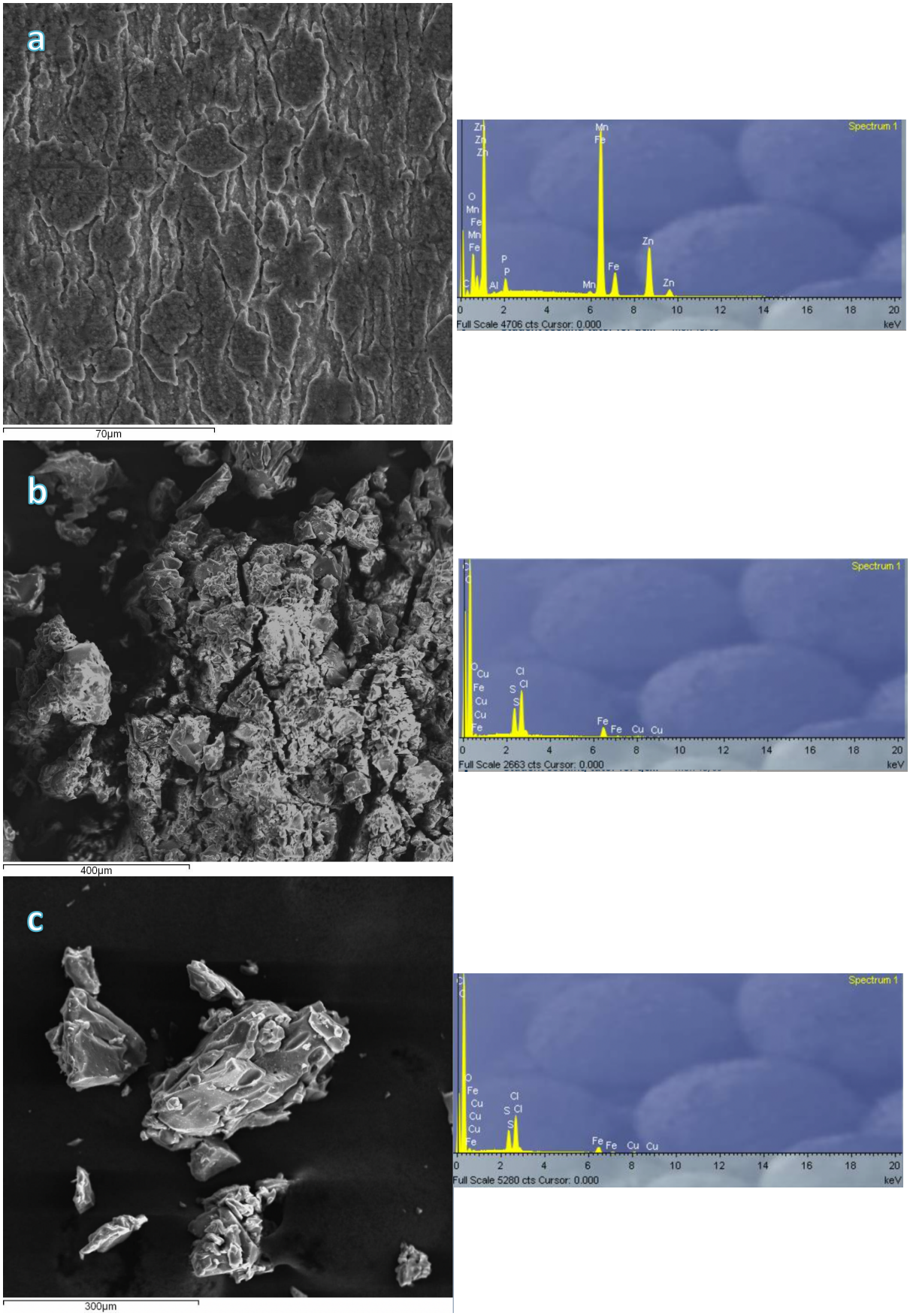


Figure 8.7 SEM micrographs of a) the inner wall surface of an unused carbon steel sleeve, b & c) carbanaceous deposits from 3:1 Dod/malt mixture in different locations

Micrograph shows the surface topology of a new cold drawn steel tubes sleeve used for fouling experiments with the removable sleeve. The EDX spectra shows the presence of zinc (galvanisation) coating on the surface. Images b and c are of carbonaceous deposits derived from the unstable test fluid at elevated temperatures. The material is globular with particles on the order of 200μm diameter. The EDX spectra also reveals the presence of Sulphur on the sleeve surface. (Chlorine peaks are likely residual from the washing process and not derived from the reaction).

8.4 Conclusions

The experiments presented in this chapter have explored fouling characteristics of crude oil maltene and asphaltene fractions blended with high boiling point solvents characteristic representing saturates and aromatics. The research focused on varying solution compositions whilst maintain operational run conditions constant for all sets of experiments, based on the parameters optimised from Chapter 6. Fouling propensity was shown to be highly dependent on the test fluid composition, and samples with poor solution stability at the operating conditions (generally, asphaltene containing solutions with highly saturated solvent mixtures) lead to significant levels of fouling. This trend is also seen in work by Rogel et al.[122], where fouling rates were measured against compatibility parameters. Solutions of asphaltenes in 1-methylnaphthalene increased in total fouling mass with time, however, a greater proportion of fouling solids were recovered from filtration of the bulk fluid whilst the wall adhered solids plateaued at approximately 15% w/w solutions. This suggests that fouling precursors either polymerised in the bulk fluid phase or were removed from the wall surface after polymerisation by shear forces of the fluid in turbulent flow.

Similarities can be found between the fractionated oil solutions and crude oils in that both exhibited higher fouling in solutions with greater asphaltenes, however in most cases, the asphaltenes were stable in solution, and deposit masses were very small. Furthermore, much of the deposit for stable solutions is yellow and is inorganic in nature verified by Sulphur EDX signature from on SEM images. Heavy organic fouling only occurred during experiments where the test fluid was unstable at high temperatures, resulting in agglomeration and polymerisation over the 12 hour residence time which was recovered as chloroform insoluble.

Further crude oil fouling research that has been undertaken since the end of experimental work on project has been conducted almost entirely using the new wall section and removable steel sleeve setup because of the advantages highlighted earlier. It has been observed that the reduction in manual

preparative steps in the cleaning process improves the repeatability of fouling experiments and their data.

Chapter 9 Synthesis, Characterisation and Fouling Experiments of Model Asphaltenes

9.1 Introduction

This chapter discusses the potential use of synthetic asphaltene solutions as simplified models of crude oil for the purpose of researching thermal fouling behaviour. As discussed in detail in Chapter 2, there are many possible routes to fouling in refinery heat exchangers, which can be broadly categorised as inorganic or organic fouling. This work is focused on organic fouling behaviour, although it should be noted that inorganic fouling can play a significant part in this phenomenon.

Asphaltenes are a continuum of organic compounds with broadly varying molecular size, functionalities and physical characteristics, all falling within a solubility classification. In crude oils, according to the Yen-Mullins model[184], asphaltenes exist in solution in as nanoaggregates associated via pi-bonding moieties and clustered in solution. The classical colloidal asphaltene/oil model suggests a system where colloids of asphaltenes are stabilised by resins in a solution of aromatics and saturates according to the SARA oil classification method. The major limitation of any research involving natural crude oils or fractions thereof, is the variable nature and proportions of each solubility class within the crude oil. As presented in the thesis aims, the desire is to produce a number of potential model asphaltenes and test their potential as asphaltene models for fouling research. Large PAHs with alkyl derivaties would be prohibitively expensive on gram scale quantities required for fouling experiments such as this work, as such, chemical synthesis was necessary in preparation for this section of fouling research.

9.2 Synthesis of alkylpyrene asphaltene models

9.2.1 Synthesis and characterisation

Alkylpyrenes were chosen as target asphaltene simulants, as the molecules contain both aromatic and aliphatic properties, and are synthesized with good yield from pyrene in a 2-step process according to literature[185]. Two alkylpyrene targets were chosen, with butyl and decyl substitutions. (Figure 9.1)

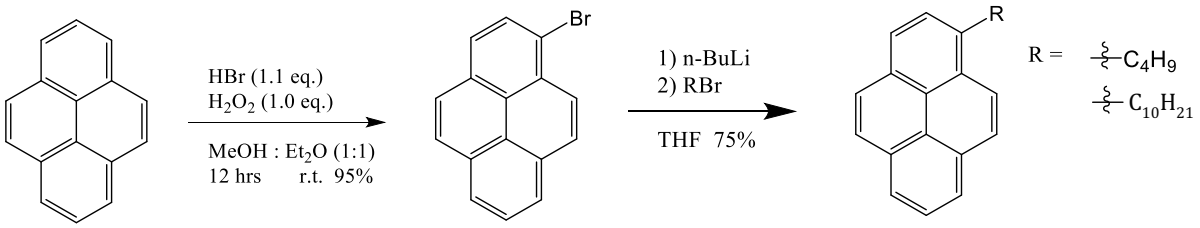


Figure 9.1 Synthesis of 1-bromopyrene and 1-alkylpyrenes via 1-bromopyrene`

The first step of the alkylation process is an oxyhalogenation, employing a positive bromine species to enable electrophillic substitution at the 1-position of the pyrene. The reaction is efficient and avoids the need for the hazardous elemental bromine[186]. In the second reaction, a lithium halogen exchange reaction takes place between n-butyl-lithium and 1-bromopyrene to form the Li-pyrene intermediate which is kinetically controlled, followed by substitution with the appropriate alkyl halide, with the lithium halide salt formed as a by-product as shown in Figure 9.2.

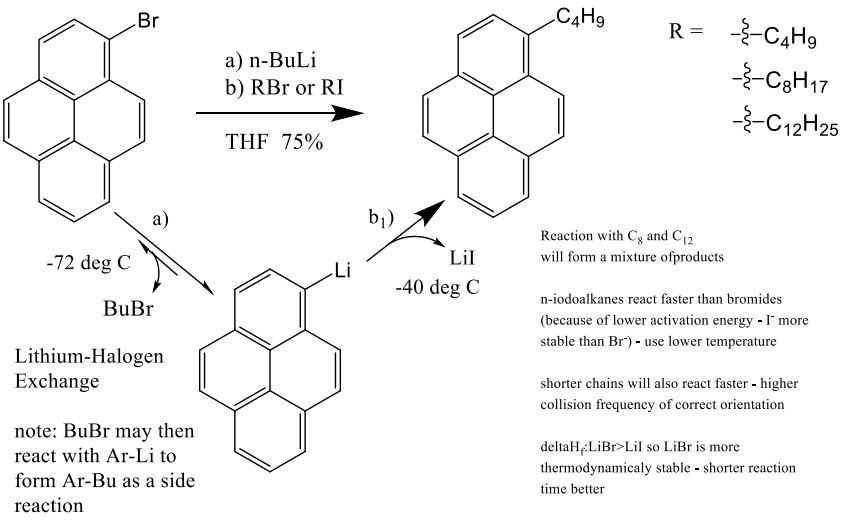


Figure 9.2 Reaction mechanism for the alkylation of 1-bromopyrene via lithium halogen exchange

9.2.2 Experimental section – Synthesis of pyrene models

All reagents and solvents used during the synthesis of compounds in this chapter were sourced from Sigma-Aldrich.

Synthesis of 1-bromopyrene

To a stirred solution of pyrene (35.77 g; 177 mmol) and hydrobromic acid (22.02 mL of a 48% aq. solution; 195 mmol) in methyl alcohol (~250 mL) was slowly added hydrogen peroxide (10.21 g; 20.75 mL of a 30% aq. solution; 177 mmol) over a period of 20 min at 10–15°C in a water bath. The reaction was left at room temperature for 12 hrs whilst monitoring its progress by thin layer chromatography. After bromination, the solvent was removed under reduced pressure and the crude product was taken in ethyl acetate and washed with water, brine and dried over anhydrous magnesium sulphate. The pure product was isolated by careful column chromatography on silica gel (100–200 mesh) using a mixture of ethyl acetate and hexane (1:10) to give pure 1-bromopyrene as a light brown solid and confirmed by GC-FID. This was recrystallized in toluene to obtain the target product, as determined by GC-MS with mass 258m/z. A trace amount of pyrene remained in the product and minor products of the di-brominated pyrene form.

Synthesis of 1-butylpyrene and 1-decylpyrene

To a solution of 1-bromopyrene (28.12 g; 100 mmol) in anhydrous tetrahydrofuran (THF) (~250 mL) was added a 2.5 M solution of n-butyllithium in hexane (60 ml - 150 mmol) dropwise under an N_2 atmosphere at −78 °C and stirred for 30 min, and then 1-bromobutane (20.55g – 150 mmol) or 1-iododecane (40.23g – 150 mmol) was added dropwise to the solution. The mixture was allowed to warm to room temperature and then stirred for 3 hrs. After carefully quenching the reaction with water in an ice bath, the organic layer was extracted with diethyl ether and dried over $MgSO_4$. The solvent was removed in vacuo, and the residue was purified by short-plug column chromatography on silica gel with hexane as the mobile phase, followed by recrystallization in ethanol to give the target compounds.

1-butylpyrene and 1-decylpyrene were afforded with good yield (1-butylpyrene – 21.59g, 83.6mmol - 83.6% and 1-decylpyrene – 24.2g, 70.7 mmol – 70.6%). The resultant products were further purified with a second ethanolic recrystallisation following GC analysis yielding the target compounds.

Table 9.1 Solubility tests of Perylene based compounds

	Solvent	1-butylpyrene	1-decylpyrene
non-polar aliphatic	Dodecane	good solubility	good solubility
Aromatic non-polar	1-Methylnaphthalene	good solubility	good solubility

9.3 Asphaltene models using perylenetetracarboxylic diimide

Perylene is a five ring PAH which has been found present in crude oils.[187]

Perylenetetracarboxylic diimides are commercially available compounds used in dyes are well researched for applications in optoelectronics and conductive molecular wires. They display high thermal stability characteristics and a molecular architecture comparable to that of Island model asphaltenes. Synthesis is a one-step reaction from the parent perylene-3,4,9,10-tetracarboxylic dianhydride (PDA) using a zinc acetate catalyst and evolving water as a by-product (Figure 9.3).

9.3.1 Synthesis of symmetrical perylenetetracarboxylic diimides

Synthesis of diimides with differing properties can be made by simply varying the amine to be reacted with PDA. This enables the testing of each for suitability as asphaltene models. Perylene diimides were synthesized from propylamine, dodecylamine and 2,4-dimethlaniline to form N,N'-Bis(3,5-dimethylphenyl)-3,4,9,10-perylenetetracarboxylicdiimide.

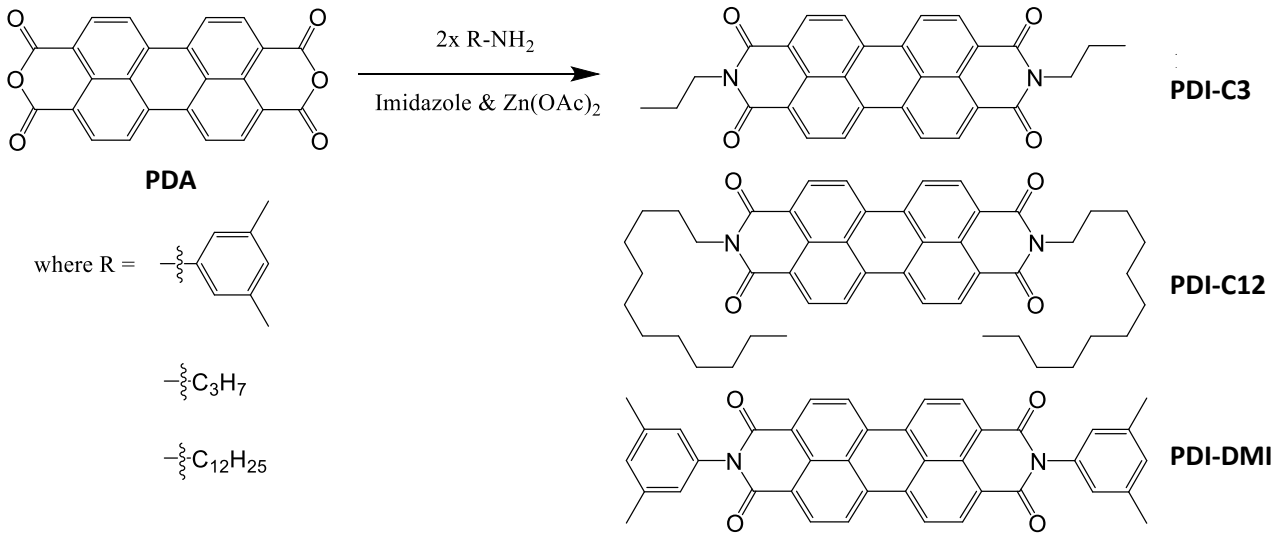


Figure 9.3 Synthesis of Perylene diimides (N,N'-Bis(3,5-dimethylphenyl)-3,4,9,10-perylenetetracarboxylicdiimide - PDI-DMI, PDI-C3 – N,N'-bispropyl-3,4,9,10-perylenetetracarboxylic diimide, N,N'-bisdodecyl-3,4,9,10-perylenetetracarboxylic diimide – PDI-C12) from perylene tetracarboxylic dianhydride (PDA)

Perylene-3,4,9,10-tetracarboxylic dianhydride (PCA) (24.72 g, 63 mmol) and the relevant amine or ammonium salt (propylamine hydrochloride (C_3), dodecylamine (C_{12}), 3,5-Dimethylaniline (DMI)) (148 mmol) were dissolved in a round bottomed flask with a reflux condenser containing molten imidazole (50 g, 734 mmol) and zinc acetate (5.19 g, 76.3 mmol) at 160 °C for 4 hours. After cooling to room temperature, the mixture was dissolved in minimum amount of THF and precipitated in 500 mL 2N HCl/MeOH 2:1 *v/v*. The precipitate was collected by filtration, washed with H_2O followed by MeOH and dried at 80 °C in vacuum. The crude product was then extracted into $CHCl_3$ using Soxhlet extraction and dried under vacuum.

The three products were synthesized with good yield (PDI-C_3: 78%, PDI-C_{12}: 83.5%, PCI-DMI: 87.5%) (FTIR spectra in Appendix 11.8) and tested for solubility with solvents representing SARA fractions in crude-oil. All compounds exhibited very low solubility in volatile solvents (see appendix 11.8.3). PDI-DMI was virtually insoluble in all solvents so was abandoned as a potential asphaltenes model. 1-methylnaphthalene was found to be the best solvent and represented an aromatic model solvent for oil. PDI-C_3 was very sparingly soluble, and PDI-C_{12} had slight solubility at room temperature. (Solubility tests with a range of solvents are given in Figure 9.4).

	Solvent	PDI-DMI	PDI-C3	PDI-C12	PDA
non-polar aliphatic	Pentane	-	-	-	-
	Hexane	-	-	-	-
	Heptane	-	-	-	-
	Dodecane	-	-	-	-
	Squalane	-	-	-	-
Halogenated aprotic	dichloromethane	v. sparingly soluble	v. sparingly soluble	v. sparingly soluble	-
	Chloroform	v. sparingly soluble	sparingly soluble	sparingly soluble	-
Naphthenic non-polar	Cyclohexane	-	-	-	-
	Decalin	-	-	-	-
Aromatic non-polar	Toluene	-	-	-	-
	1-Methylnaphthalene	v. sparingly soluble	-	partially soluble	v. sparingly soluble
	Diphenyl methane	v. sparingly soluble	-	sparingly soluble	-
Aromatic polar	Diphenyl ether	-	-	sparingly soluble	-
	Tetrahydrofuran	-	v. sparingly soluble	sparingly soluble	-
	n-methylpyrrolidone	-	-	v. sparingly soluble	-
Polar Aprotic	Benzaldehyde	v. sparingly soluble	-	-	-
	Acetone	-	-	-	-
Polar Protic	Methanol	-	-	-	v. sparingly soluble
	Ethanol	-	-	-	-
	isopropanol	-	-	-	-
	n-Butanol	-	-	-	-
	H_2O	-	-	-	v. sparingly soluble
	imidadole/H_2O	-	-	-	partially soluble

Figure 9.4 Solubility tests of perylene based compounds in various solvents

9.3.2 Solubility vs temperature

Temperature dependence on solubility was investigated to determine the feasibility for PDI use as asphaltenes models in solution for fouling experiments. The concentration was measured by UV/Vis absorption spectroscopy against a calibration curve (Appendix 11.8.4). A known mass of purified perylene diimide was dissolved in 1-methylnaphthalene followed by serial dilution to between 2 and 14 µg/g solution. Solutions were measured using a Perkin Elmer Lambda 40 UV/VIS Spectrometer between 350 and 800 nm. Spectra revealed three absorption peaks at 471, 502 and 540 nm, the latter being the strongest absorbing and used for calibration of the solution concentration.

The solubility of PDI-C3 and C_{12} solutions were found to be highly temperature dependant (additional data in Appendix 11.8). PDI-C3 had very low solubility (3.56 µg/g at room temperature). Even at 100 °C, solution concentrations saturated at less than 50 mg per 100 mL. This was deemed to be too low for fouling reaction experiments and thus PDI-C_3 was disregarded for this use.

PDI-C_{12} exhibited better solubility than the other two PDI compounds (although still relatively low at ambient temperatures), forming deep red solutions in 1-methylnaphthalene. A 20% w/w suspension was prepared and kept at controlled temperatures between 20 and 100 °C in an oil bath while stirring. After 15 minutes held at this temperature, the stirrer was stopped and the solid allowed to settle. One drop of supernatant was pipetted into a new vial, its mass recorded and diluted with further 1-methylnaphthalene to reach a concentration within the range of the calibration plot (Figure 9.5).

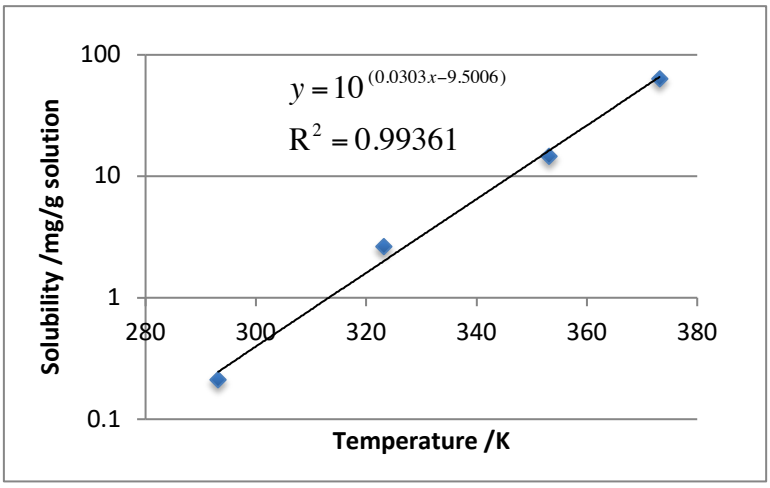


Figure 9.5 Temperature dependence of PDI-C12 solubility in 1-methylnaphthalene

To enable the use of PDI-C_{12} model asphaltene solutions for practical use in fouling reactions, it was concluded that solutions of up to 1% w/w in 1-Methylnaphthalene could be kept stable as long as the

system temperature was maintained comfortably above the precipitation temperature of the solution. Whilst not ideal, this approach was preferable to running fouling experiments with PDI-C_{12} model concentrations only stable at ambient temperatures.

9.4 Fouling experiments with alkylpyrene model asphaltenes

9.4.1 Use of 1-butylpyrene and 1-decylpyrene solutions for fouling experiments

Dodecane and 1-Methylnaphthalene solvents used in the chapter 8 fouling experiments were again considered for fouling tests using the synthesised asphaltene models described earlier. n-Dodecane was chosen due to its low reactivity at elevated temperatures and acceptable solubility in the pyrene models. 10% w/w solutions of the asphaltene models were made up and fouling tests run at the same conditions as for dissolving Asphaltenes in 1-methylnaphthalene. General reactor conditions were applied during all model asphaltene solution as provided in Table 7.1.

9.4.2 Results and discussion

Even using 10% model asphaltene by weight both 1-ButylPyrene and 1-DecylPyrene @ 10% w/w solutions in n-dodecane produced no discernible fouling deposits on the reactor wall or in the bulk. Total recovered mass in both cases was <1mg.

This result was likely a result of the product structure having no reactive functionality except for the aromatic cluster. Solutions were stable even slightly warm temperatures >40 °C, although precipitation was observed days following the product collection, and at elevated temperatures, the precipitated compounds would re-dissolve again. Alkyl pyrenes were not tested for fouling in 1-methlynaphthalene, as this solvent was expected to be a better solvent than n-dodecane as pi association of the naphthalene aromatic centre to the pyrene aromatic cluster.

9.4 Fouling of PDI-C_{12} solutions in 1-methylnaphthalene

9.4.1 Preparation

Solutions of 0.5% and 1% w/w PDI-C_{12} were required for use fouling reaction experiments. Using the best-fit curve of solubility vs temperature, 1% w/w solutions in 1-methylnaphthalene precipitate at temperatures below 34 6K (73°C). For this reason, experiments using PDI-C_{12}/1-methylnaphthalene

were prepared at 110 °C and injected into the pre-heated system before the start of the fouling experiments. An electrical heating tape was wrapped around the sample vessel and preheated to 110°C prior to reaction. The reactor cell was also preheated in the furnace to a wall temperature of 110°C prior to loading into the Taylor Couette cell to prevent PDI-C_{12} precipitation before the reaction began. Three fouling experiments were conducted and the fouling masses are given in the table below:

Table 9.2 Deposit masses for PDI-C12 solutions in 1-methylnaphthalene

Fouling Reaction	Wall Solids /mg	Film solids /mg
SO-01 (0.5% w/w)	12.4	1.3
SO-02 (1%)	142.1	12.7
SO-03 (1%)	168	10.4

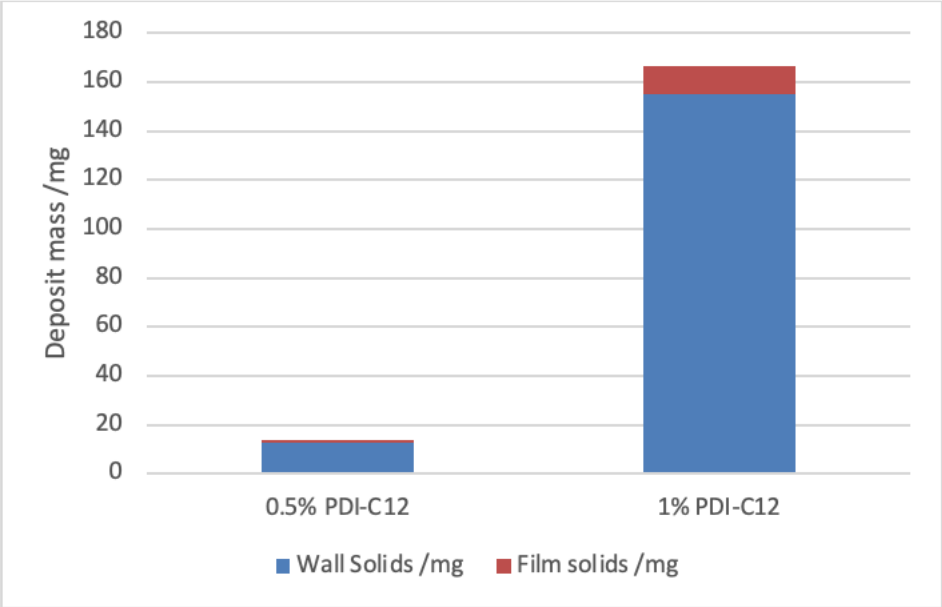


Figure 9.6 Total deposit fouling masses in for PDI-C12 solutions

Fouling deposits were small but measurable for the 0.5% w/w solution in 1-methylnahthalene: a cream-coloured precipitate was visible on the inner surface of the reactor walls. The next fouling experiment was conducted at 1% w/w in 1-methylnahthalene. The result was noteworthy. Significant fouling was visible around all the reactor surfaces, leaving thick white layer and a rough surface. The most significant of the two fouling deposits is shown in the photographs in Figure 9.7

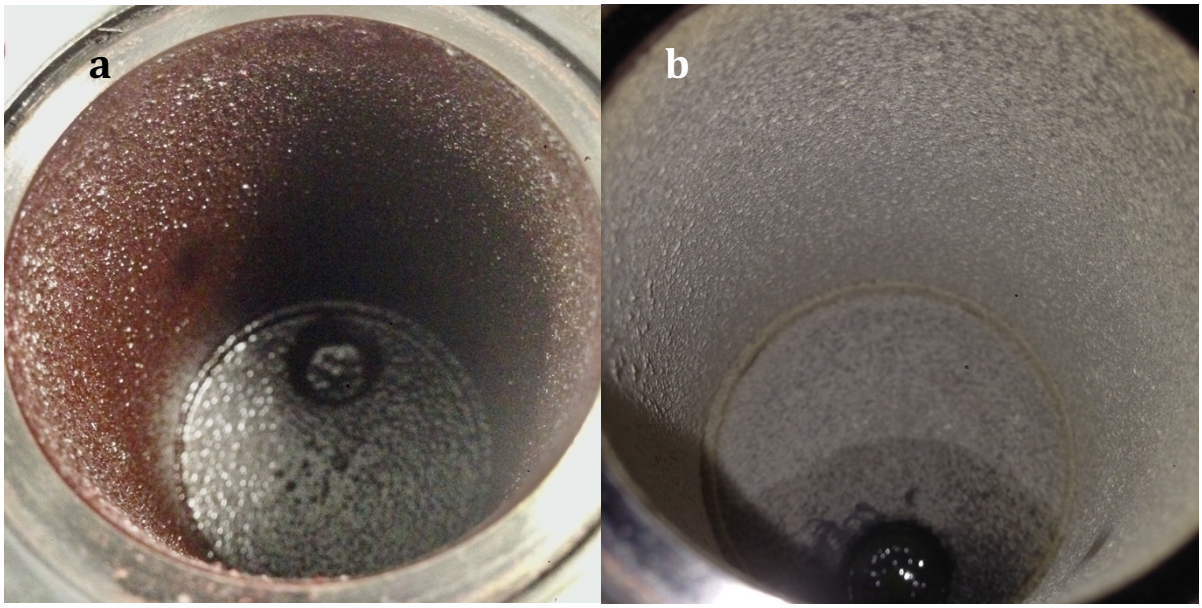


Figure 9.7 Fouling deposits visible on the reactor wall a) after draining from the cell and b) rinsing with chloroform leaving a cream residue. Fouling deposits are uniformly adhered to all outer surfaces resulting in elevated surface roughness

9.4.2 FTIR data – PDI-C_{12} vs fouling products

Fouling deposits from experiments SO-01 to SO-03 and the PDI-C_{12} model were analysed by FTIR as shown in Figure 9.8:

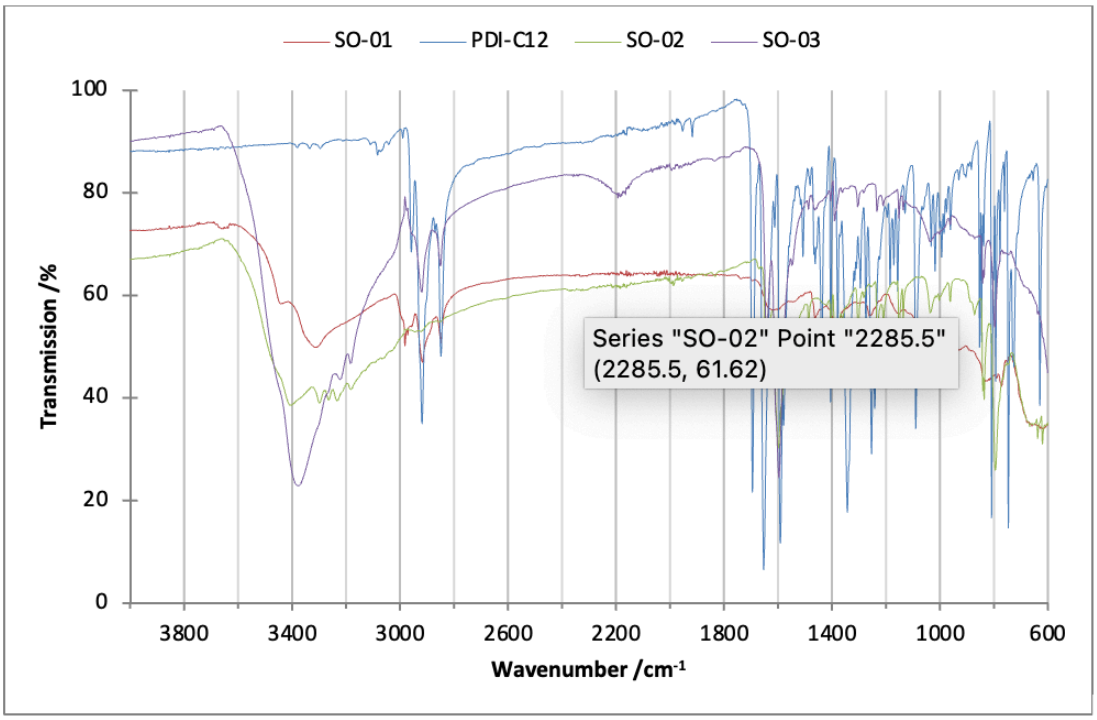


Figure 9.8 FTIR ATR Sectra for PDI-C12 and its fouling deposits

Deposit material from reactions SO-01, SO-02 and SO-03 notably all lack the absorption peak at 1695 cm^{-1} which corresponds to the amide C=O stretch of the parent perylene compound. The aromatic amide C-N stretching peak of the parent model asphaltene at 1340 is also absent in the fouling deposits, indicating destruction of the carboxamide groups.

The strong alkane C-H stretching frequencies of the parent PDI-C12 at 2936, 2918 and 2848 are reduced in the deposit spectra although still present. SO-03 spectra strong absorption in the 3500-3100 cm^{-1} range indicates the presence of water. Minor broad peak at centred at 2200cm^{-1} is believed to be a combination band also related to the water presence. SO-01 spectrum is relatively poorly defined and likely contains significant inorganics.

9.5 SEM images of PDI-C_{12} deposits

A replicate fouling experiment with 1 % w/w PDI-C12 in 1-methylnaphthalene was performed using the removable steel sleeve to observe fouling deposit physical characteristics under scanning electron microscope imaging using a Jeol JSM-6400 with EDX. On completion of the reaction, the removed steel sleeve was rinsed thoroughly with heptane, which is miscible with the 1-methylnaphthalene solvent but fully immiscible with the PDI-C12 model asphaltene, leaving a tan/brown fouled surface with red speckling on the inner wall surface. The sleeve was then cut longitudinally in two, and one half was rinsed thoroughly with chloroform until the red surface residue was no longer visible (left in Figure 9.9). The right half was not rinsed in chloroform. Both were dried at 50°C in the drying oven for 2 hours. Two 8mm x 8mm square sections of the sleeve were cut out and taken for surface analysis, one at the top of sleeve with visible read particles, and the other in the centre of the sleeve which appeared to have a thick layer of tan/brown deposit. The sleeve samples were coated with gold film by electrospray and viewed under SEM as shown in Figure 9.10.

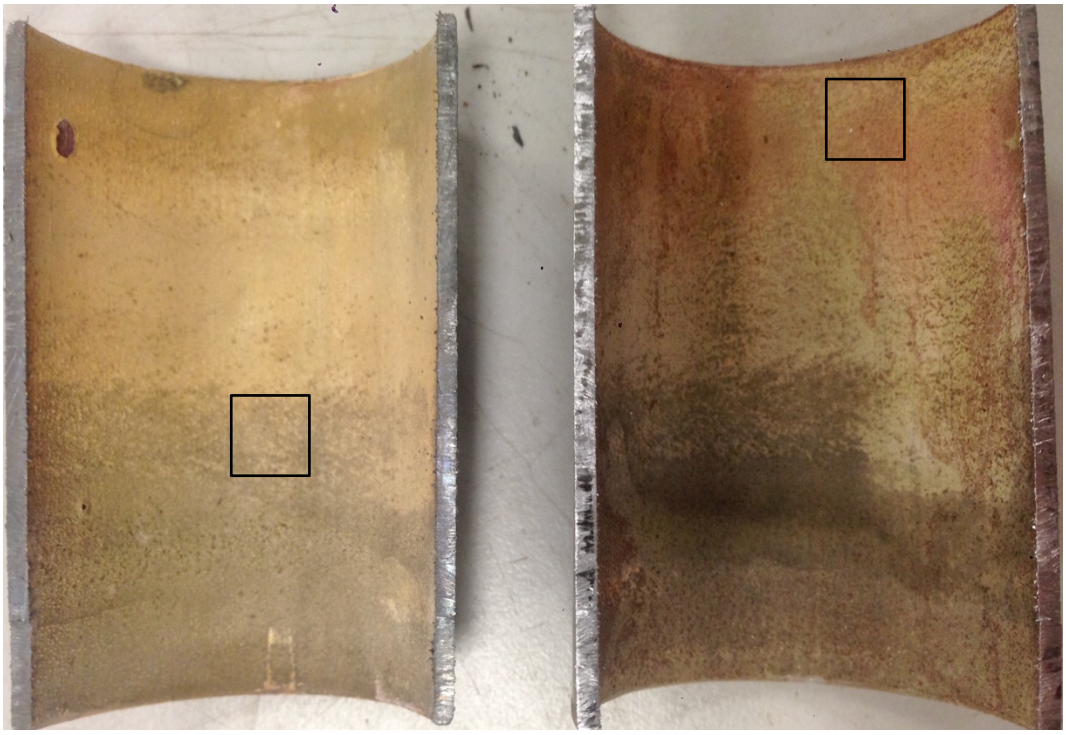


Figure 9.9 Fouled inner sleeve following heated fouling reaction with PDI-C12 in 1-methylnaphthalene for 12 hours at 320 °C. The left half has been fully washed with $CHCl_3$ until no red PDI-C12 starting material is visible. The right half was washed with heptane. The squares represent areas of the wall section which were cut out for SEM imaging

Micrographs a) and b) show two distinct structures defining the surface topology. The subsurface is a layer of sharp irregular deposited material with dimensions in the range of 10μm, above which residually adhered planar sheets of PDI-C12 rest on the fouled surface with dimensions on the order of 50-100μm.

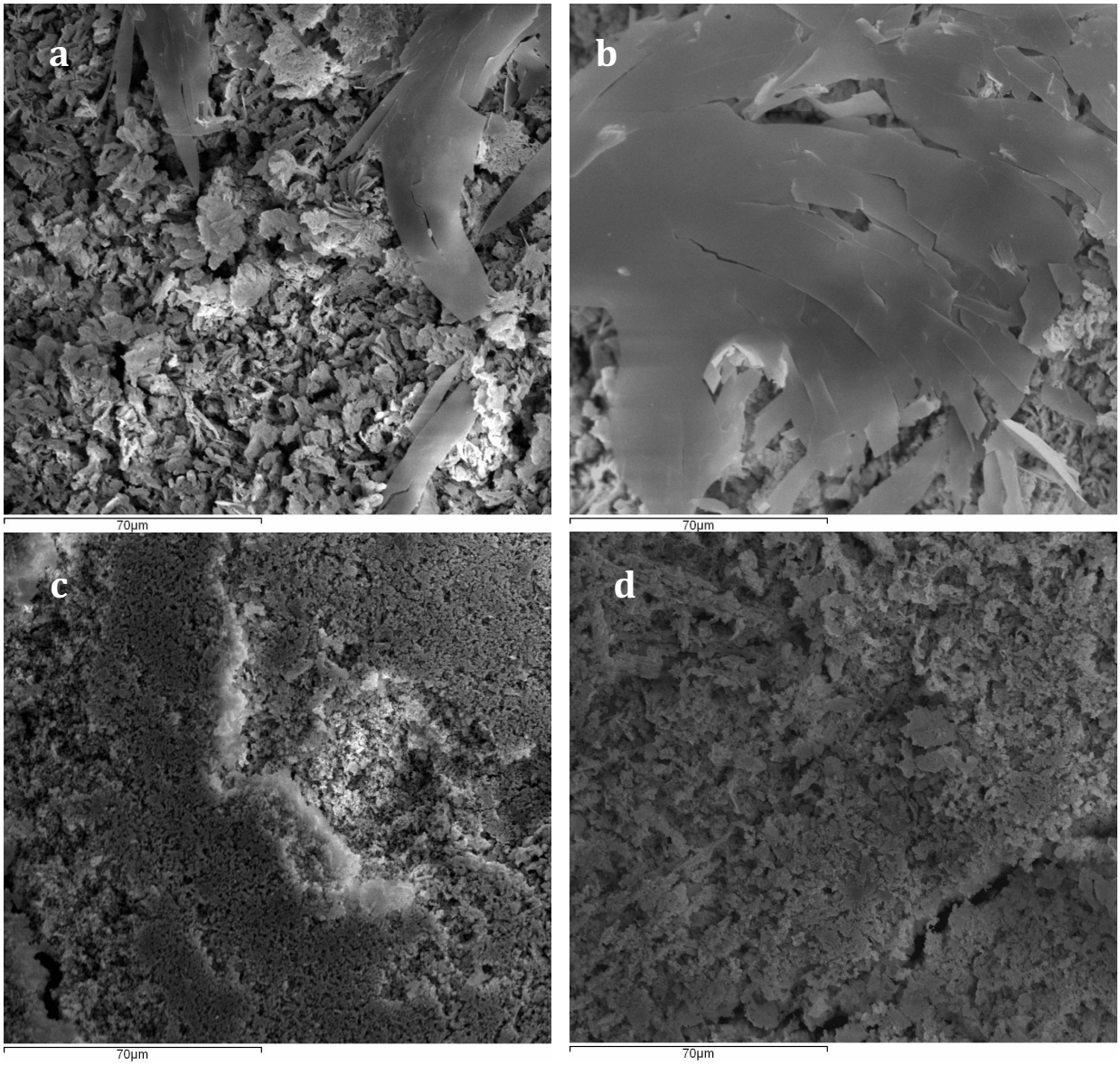


Figure 9.10 a-d Scanning Electron Micrograph of the PDI-C_{12} fouled surface. a) and b) show partially washed sleeve wall surface near the top of the reactor and c) and d) show the fully rinsed wall surface in the central section of the reactor sleeve

Micrographs c) and d) are found in the middle of the wall section after complete washing with chloroform leaving no starting material behind, as visualised by the lack of planar sheets. The deposits have similar irregular fouling structures in the however the characteristic grain structure is smaller (on the order of 5µm) owing to the anisotropic conditions between the two areas, such as higher fluid velocity in the central section of the wall than the top of the cylinder.

9.6 Conclusions

Alkylpyrenes and perylene dicarboximides were synthesised as possible asphaltene models and tested as model asphaltene solutions in fouling experiments using the Taylor Couette cell reactor experimental conditions similar to those found in refinery heat exchangers.

Alkyl-Pyrenes exhibited good solubility in both 1-methylnaphthalene and n-dodecane, the latter of which was selected for fouling experiments. Perylene dicarboximide compounds exhibited poor solubility properties, due to the large aromatic PAH core making them insoluble in n-dodecane but PDI-C_{12} exhibited partial solubility in 1-methylnaphthalene, which was found to increase exponentially with temperature. PDI-DMI and PDI-C_3 were thus disregarded as potential asphaltenes due to being too insoluble. For future consideration of perylene dicarboximides, research should focus on compounds with greater solubility for greater practicality.

It was found that solutions of 1-butylpyrene and 1-decylpyrene did not produce any fouling deposits, due to the lack of reactive functional groups on the molecule. Increasing the solute concentration further, or using a different solvent may be possible but would increase the cost of test fluid to an impractical level. Significant fouling was observed for 1% w/w solutions of PDI-C_{12} in 1-methylnaphthalene in the Taylor Couette reactor. Deposit characterisation highlighted amorphous deposits of a somewhat comparable nature to crude oil fouling deposits. The deposits exhibited both organic and corrosion fouling due to destruction of the heteroatomic functional groups. FTIR spectra on the fouling deposits revealed the carboxamide functional groups to have degraded during the reaction, and TGA revealed not only organic matter but also a significant quantity of inorganic ash due to corrosion of the carbon steel wall surface.

The perylene compound PDI-C_{12} represents the most promising example of a synthetic asphaltene model which shows strong propensity to fouling under refinery heat exchanger conditions and the amorphous deposits are somewhat comparable in structure asphaltene deposits. The solutions do not however capture the complex phase behaviour present in crude oil. It is believed that the broad chemical and structural diversity of real asphaltenes may contribute to their solubility in aromatic solvents despite the large molecular weights and extended PAH structures, relative to a single perylene compound which may more easily associate and lead to precipitation. The poor solubility of the tested solutions limits its use as the model compound precipitates readily at ambient temperatures which poses a significant challenge to cleaning. More research is required to achieve the stated research goal, however, significant and reliable deposit fouling was achieved by the perylene compound.

Chapter 10 Conclusions

10.1 Evaluating the research objectives

In the production of this thesis, it was necessary to employ a range of research and practical work in chemical synthesis, analytical methods, reactor development and perform numerous practical experiments to develop a deeper understanding of the properties and behaviour of crude oils undergoing crude oil fouling and how operators may mitigate its effects in process equipment.

The conclusions are summarised below:

- A purpose-built laboratory fouling apparatus was designed, constructed commissioned and used to undertake crude oil fouling research, building upon the knowledge and experience of previous group members and improving on previous designs, incorporating flow and compared to refinery heat exchanger conditions

- Crude oil fouling experiments were conducted using a blend of crude oils at a range of compositions and process conditions, providing a standard operating procedure and a basis for comparison against further experiments.

- Solutions of asphaltenes and maltenes, fractionated from a heavy crude were investigated for fouling behaviour. Fouling was found to be highly dependent on solution stability, with principally inorganic deposits being obtained in stable asphaltene solutions of 1-MeNaphthalene

- Model asphaltenes based on alkylpyrene and perylene diimides were synthesised and solutions thereof were tested as synthetic oil models for novel fouling research. PDI-C_{12} was demonstrated to be a promising candidate. Solutions and resultant deposits shared numerous characteristics with marginally stable oil mixtures, however, modification to the molecular structure may result in more appropriate solubilities at ambient temperature

1. Design, Construct and Commission a new fouling apparatus for studying crude oil fouling.

The Taylor Couette fouling apparatus presented here improves upon prior work in the research group[128], by incorporating a turbulent flow Taylor Couette reactor, with greater functionality and flexibility than in prior systems. The apparatus was designed to subject test fluids to similar

temperatures, pressures, and flow velocities to those found in heat exchangers operating in refineries. It also incorporated a control system to maintain good control of those conditions for durations of 12 hours or longer. The hydrodynamics were modelled to ensure turbulent flow inside the annulus; confirmed by high-speed videography using a transparent polymer cell body. A standard operating procedure was developed, including comprehensive cleaning and surface preparation steps to improve repeatability. Since the completion of this work, the system has been since been modified to automate the temperature control of the reactor wall by means of a PID controller (during experiments related thesis reactor wall temperature was manually controlled, while furnace temperature was maintained by PID control).

2. Characterise the supplied crude oils and fractions thereof and provide a method for preparations of oils for use in fouling experiments

The crude oils were supplied in their non-desalted state, and were desalted prior to fractionation, analysis and fouling experiments. Heavy oil was fractionated into maltenes and asphaltenes by a modification of the D6560 ASTM method necessary to process larger quantities of oil. The crude oils and fractions were characterized using pycnometry, SARA fractionation, FTIR, GC-FID, Elemental analysis, TGA, UV-Vis spectroscopy. A 3:2 weight/weight heavy:light crude blend used extensively in fouling experiments was also analysed. The two crudes showed extremely dissimilar physical and chemical properties. The light oil contained only trace asphaltenes and low quantities of heteroatoms, while the heavy oil contained significant asphaltene and heteroatom content and also significantly more viscous with a high API gravity.

***3. Test the fouling characteristics of crude oils in a range of process conditions*.**

Initial fouling commissioning trials on crude oil blends produced significant salt deposits on the heated wall surface. After commissioning, all crude oils were run with desalted oils. Crude oil fouling experiments formed the benchmarks against which the results of fractionated oil solutions and synthetic crude oil solutions were compared. Fouling deposit masses increased with mass fraction of heavy oil, and increasing residence time up to 12 hours with no noticeable difference between 12 and 24 hours. Since significant work has been done in this area, the focus was on studying the fouling characteristics of synthetic crude complexes. Repeatable fouling data was heavily dependent on a meticulous cleaning regime and maintaining tight process control. Inserting a sleeve into the modified reactor body is the most suitable means to achieve this.

4. Prepare solutions of asphaltenes and maltenes in high boiling temperature solvents and investigate fouling behaviour of these solutions

High boiling-temperature solvents were selected with chemical and physical characteristics representative of the crude oils from which they came, also considering the conventional SARA oil solubility fractions, reactivity and rheological properties. Fouling experiments were conducted to investigate the effect of composition on fouling behaviour. Specific studies were conducted to study the effect of enriching the 60:40 crude oil mixture with 5% w/w asphaltenes on the fouling deposit mass over a range of residence times and the effect of asphaltene concentration on fouling behaviour of solutions of asphaltenes in 1-methylnaphthalene (5-20% w/w). The effect of phase stability on fouling behaviour of asphaltenes in mixtures of 1-methylnaphthalene and n-dodecane and the fouling behaviour of maltenes diluted in varying concentrations of n-dodecane was also investigated.

5. Synthesis of model asphaltene compounds, solution properties and fouling experiments using model asphaltene solutions

Asphaltene models based on pyrene and perylene were synthesised, purified, and dissolved in either 1-methylnaphthalene or n-dodecane and tested for fouling under the same process conditions as earlier experiments. Alkylpyrene based asphaltene model compounds exhibited good solubility in dodecane and 1-methylnaphthalene whereas Perylene Diimide models compounds only exhibited partial solubility in 1-methylnaphthalene. Of the three perylene diimides, only N,N'-bisdodecyl-3,4,9,10-perylenetetracarboxylic diimide (PDI-C_{12}) exhibited sufficient solubility for initiating fouling experiments.

Monosubstituted alkylpyrene solutions were unreactive at the process conditions tested, due to their lack of heteroatom functionality and phase stability in n-dodecane. Perylene diimide PDI-C_{12} solutions in 1-methylnaphthalene exhibited strong fouling behaviour because of thermal degradation of the heteroatom moieties. Insoluble deposits were recovered from the wall surfaces exhibiting both carbonaceous fouling and inorganic corrosion fouling, and SEM images highlighted an amorphous foulant layer under a sheet of deposited PDI-C_{12} precipitated in layers, likely because of the pi-orbital association between the polyaromatic clusters. The experiments with model asphaltene solutions indicate that the complex composition of hydrocarbons which make up crude oils define its behaviour; variable fluids and simplified model solutions exhibit different properties. However, the fouling propensities of crude oils and synthetic mixtures only depend on the phase stability and reactivity in solution. Thus, the composition and chemistry of model asphaltene solutions should accurately mimic

these chemical characteristics. Asphaltene structure should also reflect both; structural properties and functional groups present in real asphaltenes.

6. Use the output of the experimental fouling work to describe the practical learning outcomes from the presented research

The experiments in this work focused on fouling behaviour across a range of samples of varying chemistries. Simplified oil solutions, both using fractionated oils and model asphaltenes in high boiling-temperature solvents, are useful to study controlled aspects of fouling behaviour from both a chemical stability and reactivity perspective, but it should be understood that such significant simplification of test fluid composition will invariably change the type of fouling processes, phase behaviour at operational conditions, and the nature of the deposits produced on heated test surfaces. This may be provide useful representatives of crude oil and allow for focused investigation of specific chemistries but these will cannot capture the immense complexity found in natural crude oils. not necessarily predictive without full understanding of the crude oil's natural chemistry, which is itself highly variable.

Adjustments to the physical conditions and compositional were found to change both the nature and amount of fouling deposits produced in these fouling experiments, however the most striking practical lesson was that the phase stability of the test fluid at process conditions was by far the most important variable with respect to the production of carbonaceous fouling deposits. In section 8.3, deposit mass was asphaltene concentration dependant, however even 20% w/w asphaltene solutions in 1-methylnaphthalene produced low overall deposit masses compared to a 5% asphaltene solution destabilised with a saturated solvent such as n-dodecane. Furthermore, phase separated asphaltenes which adhered to the wall surface readily polymerised into amorphous carbonaceous deposits which could not be washed away by either fluid shear inside the cell, nor solvation with chloroform during the cleaning process. This process was thus irreversible and would be expected to rapidly cause operational problems within an operating PHT. Being aware of this dependency, it is easy to see how in a practical application this could happen in a refinery setting:

Crude oils destined for refining undergo routine characterisation of their chemical and physical properties to provide data for blending ratios to achieve average physical and chemical properties which are suitable oils for processing through the PHT and are expected to be within stability regions according to CII, CSI or a similar stability model, the reality may deviate substantially from the model prediction. Crude oil chemistry/composition can vary significantly not just between oil fields, but

within the same oilfield over its life, or by sedimentation and stratification of oil layers during the transport and storage stages. The properties and phase stability of blended oil entering the PHT will also deviate from expectation either momentarily (when new oils are introduced to the blend) or for extended periods as the bulk oil properties change and could easily fall regions where fouling quickly becomes a problem.

Such practical issues are part of what makes the phenomena of crude oil fouling such a difficult and persistent problem to deal with. Regular online sample testing can help to alleviate some of these unknowns, however since the crude oils have such complex chemistries, it may be expensive and impractical to collect detail analysis and a cost benefit analysis will have to be made by operators to arrive at an optimal solution.

10.2 Future work

The work in the preceding sections used a novel experimental apparatus and methodology to study the fouling of crude oils, their fractions, and chemically synthesised model asphaltene solutions. The below sections discuss possible work which may be carried out in the future to gain a deeper insight into crude oil fouling phenomena and strategies for their mitigation.

Further characterisation of existing deposits

Additional analysis of the deposits would provide greater detail into their nature, particularly where significant inorganics were deposited. This could also be possible with ICP-OES. TGA with MS would reveal significant structural information about deposit functionality and thermal lability and mass spectrometry would provide insight on the fragments lost during the thermolysis process.

Fouling experiments on fractionated oil solutions

Crude oils may be further split into subfractions (resins aromatics and saturates) and the fouling behaviour of each subfraction investigated either individually or in solution could provide information on how the fractions change over time, and which fractions contribute towards fouling.

Upgrades and modifications to the Taylor Coutte fouling reactor

Upgrades to the fouling apparatus could include:

- Adjustments to the TC cell geometry, for example, increasing the size of the inner rotor, would allow for increased shear stress for a given rotational frequency

- Automation and remote monitoring for longer reaction durations (in excess of 12 hours).
- an additional port for either for sampling during an experiment for kinetics investigation, or addition of an antisolvent or fouling initiator during reactions.
- The Taylor-Couette reactor could be converted into a CSTR with the modification of the lower flange to allow for continuous outflow of fluid. This could be used in single pass or recirculated flow depending on need.
- A cooling loop for the bulk fluid to enable a greater temperature differential between the heated wall surface and the bulk fluid – this would also help to more faithfully mimic heat exchanger process conditions.
- Further use of sleeves with variable controlled surface conditions would further allow the investigation of effect of the wall surface characteristics on fouling deposition

Further research on synthetic asphaltene model solutions

Further work is necessary to improving existing model asphaltene solutions, and future possible models. Fouling has been demonstrated to be strongest in solutions which are marginally stable in ambient conditions but destabilised when subjected to conditions present in the PHT.

Alyklpyrenes: may be possible to obtain significant fouling behaviour if the alkylpyrenes are made up in solutions where they exhibit marginal stability. This might be achieved through more concentrated solutions, or by selection of a different solvent(s). Alternatively, Alkyl pyrenes could be synthesised with heteroatomic moieties such as alkyl sulphides which likely exhibit higher reactivity.

Perylene diimides: Perylene diimides were found to exhibit low solubilities in most solvents, due to their large polyaromatic core. Perylene diimide derivatives with branched aliphatic substituents have been reported to exhibit significantly higher solubilities allowing the class of compounds to be more usable as models for further studies in thermal fouling studies[188]. The addition of resin like cosolvents could help to stabilise the existing Perylene diimides and form the basis for further experiments

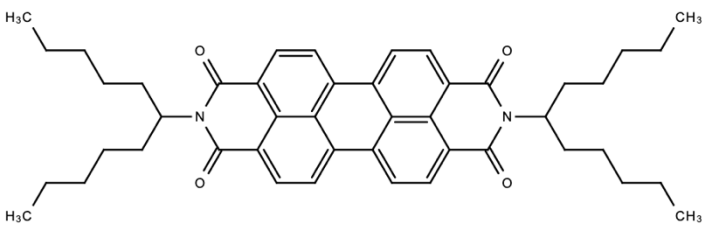


Figure 8.10.1 Branched alkyl substituted perylene diimide with good reported solubility

Another polyaromatic diimide based on naphthene could be a promising model asphaltene target using similar simple synthetic routes to those based on perylene demonstrated in this work in chapter 9. Such molecules would be expected to be more soluble due to the smaller polyaromatic core somewhat reducing aggregation through π-bonding. A broad range of synthetic routes are presented in a review Langford et al[189]. Another interesting structure derived from the diimide is an alkyl-substituted tetrahydro-2,7-diazapyrene synthesized by removal of the four carbonyl groups through a simple reduction with lithium aluminium hydride under a Lewis acid (see Figure 10.2):

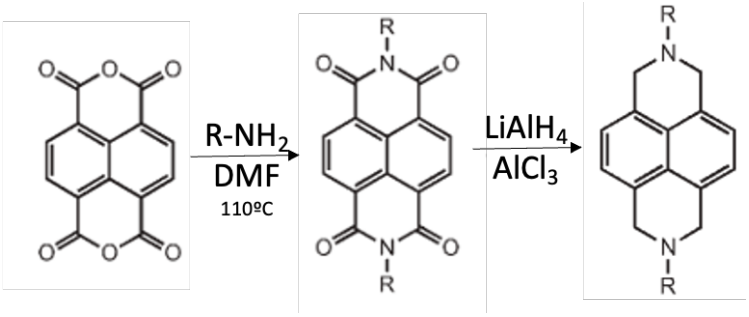


Figure 10.2 Naphthene diimide and tetrahydro-2,7-diazapyrene synthetic route from 1,4,5,8-naphthalene-tetracarboxylic dianhydride (molecular structures from Langford et al.189**)**

Carbonyl groups are uncommon in most crude oils except for those suffering from oxidation degradation usually due to poor storage, so the target amine molecule would better represent the chemical functionality of asphaltenes whilst still incorporating a heterocyclic functionality.

References

[1] BP Energy Outlook 2020.

[2] E. Billing, A. Ferro, T. Fitzgibbon, Global downstream outlook to 2035, 2021 McKinsey & Company.

[3] US oil price below zero for first time in history, https://www.ft.com/content/a5292644-958d-4065-92e8-ace55d766654, accessed on 28/09/2021.

[4] IEA Oil Market Report, April 2022.

[5] H. Muller-Steinagen, Fouling of heat exchangers surfaces, *Chemistry & Industry*, 1995, Issue 5, pp. 171-175.

[6] H. Muller-Steinhagen, M. R. Malayeri, A. P. Watkinson, Heat Exchanger Fouling: Environmental Impacts, *Heat Transfer Engineering*, 2009, **30**, p773-776.

[7] H. Muller-Steinhagen, M. R. Malayeiri, A. P. Watkinson, Heat exchanger fouling: environmental impacts, *Heat Transfer Engineering*, 2009, **20**, p773-776.

[8] ESDU, Heat exchanger fouling in the preheat train of a crude oil distillation unit. 2001, ESDU International plc: London.

[9] C. B. Panchal, E. P. Huangfu, Effects of mitigating fouling on the energy efficiency of crude-oil distillation. *Heat Transfer Engineering*, 2000. 21, **3**, p3-9.

[10] R. A. Ismaili, M. W. Lee, D. I. Wilson, V. S. Vassiliadis, Heat exchanger network cleaning scheduling: From optimal control to mixed-Integer decision making, *Computers & Chemical Engineering*, 2018, **111**, p1-15.

[11] C. S. Hsu, C. L. Hendrickson, R. P. Rodgers, A. M. McKenna, A. G. Marshall, Petroleomics: advanced molecular probe for petroleum heavy ends. *Journal of Mass Spectrometry*, 2011, **46**, p337–343.

[12] A. G. Marshall, R. P. Rodgers, Petroleomics: chemistry of the underworld, *Proceedings of the National Academy of Sciences of the United States of America*, 2008, **105**, p18090–95.

[13] ASTM D2007-93: "Standard Test Method for Characteristic Groups in Rubber Extender and Processing Oils by the Clay-Gel Adsorption Chromatographic Method," ASTM, 1993.

[14] T. Fan, J. S. Buckley, Rapid and Accurate SARA Analysis of Medium Gravity Crude Oils, *Energy & Fuels*, Vol. 16, No. 6, 2002, p1571-1575.

[15] T. Fan, J. Wang, J. Buckley, Evaluating Crude Oils by SARA Analysis, *Society of Petroleum Engineers*, 2002, 75228.

[16] ASTM D6560, Standard Test Method for Determination of Asphaltenes (Heptane Insolubles) in Crude Petroleum and Petroleum Products, 2005, ASTM International

[17] O. C. Mullins, The Asphaltenes, *Annual Review of Analytical Chemistry*, 2011, **4**, 393–418.

[18] O. C. Mullins, B. Martinez-Haya, A. G. Marshall, Contrasting perspective on asphaltene molecular weight, *Energy Fuels*, 2008, **22**, p1765–73.

[19] O. C. Mullins, The modified Yen model, *Energy Fuels*, 2010, **24**, p2179–207.

[20] O. C. Mullins, E. Y. Sheu, A. Hammami, A. G. Marshall, Asphaltenes, Heavy Oils and Petroleomics, Springer: New York, 2007; Chapters 7 and 23.

[21] M. A. Anisimov, I. K. Yudin, V. Nikitin, G. Nikolaenko, A. Chernoutsan, H. Toulhoat, D. Frot, Y. Briolant, Asphaltene Aggregation in Hydrocarbon Solutions Studied by Photon Correlation Spectroscopy, Journal of Physical Chemistry, 1995, **99**, p9576.

[22] V. I. Lesina, Y. A. Koksharovc, G.B. Khomutovc, Viscosity of liquid suspensions with fractal aggregates: Magnetic nanoparticles in petroleum colloidal structures, Colloids and Surfaces A: Physicochem. Eng. Aspects 392 (2011) 88– 94.

[23] Sirota, E. B, Physical Structure of Asphaltenes. Energy Fuels, 2005, 19, 1290.

[24] P. Luo, Y. Gu, Effects of asphaltene content on the heavy oil viscosity at different temperatures, Fuel 86 (2007) 1069–1078.

[25] O. A. Adeyanju, L. O. Oyekunle, A new Unified Model for Predicting Non-Newtonian Viscosity of Waxy Crudes, Petroleum Science and Technology, 2012, 30, 904-914.

[26] N. Rocha, C. Gonzales, A preliminary study on the magnetic treatment of fluids, Petrol. Sci. Technol. 18 (2000) 33.

[27] A. Hinklea, E. Shinb, M. W. Liberatore, A. M. Herring, M. Batzle, Correlating the chemical and physical properties of a set of heavy oils from around the world, Fuel, 2008, 87, 3065–3070.

[28] S. Hashmi, K. Zhong, A. Firoozabadi, Acid–base chemistry enables reversible colloid-to-solution transition of asphaltenes in non-polar system, Soft Matter, 2012, **8**, p8778.

[29] T. Maqbool, P. Srikiratiwong, H. S. Fogler, Effect of Temperature on the Precipitation Kinetics of Asphaltenes, Energy Fuels, 2011, 25, 694–700.

[30] Lambourn, G.A., Fouling in crude oil preheat trains, in Heat Exchangers Theory and Practice, H.a.A. Taborek, Editor. 1983, Hemisphere: NY. p841-852.

[31] S. Ashoori, M. Sharifi, M. Masoumi, M. Salehi, The relationship between SARA fractions and crude oil stability, *Egyptian Journal of Petroleum*, 2017, **26**, 209-213.

[32] S. Asomaning, A.P. Watkinson, Petroleum stability and heteroatom species effects in fouling of heat exchangers by asphaltenes, *Heat Transfer Eng.*, 2000, **21**, p10-16.

[33] A. Saboor, N. Yousaf, J. Haneef, S. I. Ali, S. M. Lalji, Performance of asphaltene stability predicting models in field environment and development of new stability predicting model (ANJIS), *Journal of Petroleum Exploration and Production Technology*, 2022, **12**, p1423–1436.

[34] L. Raminez, I. Moncayo-Riascos, F> B. Cortes, C. A. Franco, R. Ribadeneira, Molecular Dynamics Study of the Aggregation Behavior of Polycyclic Aromatic Hydrocarbon Molecules in n-Heptane–Toluene Mixtures: Assessing the Heteroatom Content Effect, *Energy Fuels*, 2021, **35**, (4), p3119-3129.

[35] European Commision, Cleaner Air in 2020: 0.5% sulphur cap for ships enters into force worldwide, https://ec.europa.eu/commission/presscorner/detail/en/IP_19_6837, website accessed on 29/09/2021.

[36] Shivanthan, M. C., Perera H., et al, Hydrogen sulphide inhalational toxicity at a petroleum refinery in Sri Lanka: a case series of seven survivors following an industrial accident and a brief review of medical literature, *Journal of Occupational Medicine and Toxicology*, 2013; **8**, 9.

[37] S. K. Rhee, J. H. Chang, Y. K. Chang, H. N. Chang, Desulfurization of Dibenzothiophene and Diesel Oils by a Newly Isolated Gordona Strain, CYKS1, Appl. Environ. Microbiol., 1998, 64, 2327-2331.

[38] J. H. Hale, M. C. Simmons, F. P. Whisenhunt, Catalytic Desulfurization of Crude Oil, *Industrial & Engineering Chemistry*, 1949, **41** (12), 2702-2708.

[39]Y. P. Asmara, The Roles of H2S Gas in Behaviour of Carbon Steel Corrosion in Oil and Gas Environment, *Journal Teknik Mesin*, 7, **1**, p37-43.

[40] C. N. Satterfield S. Giiltekln, Effect of Hydrogen Sulfide on the Catalytic Hydrodenitrogenation of Quinoline, *Industrial Engineering Chemical Process Design and Development*, 1981, **20**, p62-68.

[41] E. Strelnikov, L. Stakhina, O. Serebrennikova, Separation of ketones and acids from crude oils, *Petroleum & Coal*, 2005, **47**, p16-20.

[42] A. M. Danilov, Problems of oxidative stability of secondary medium-distillate fuels, Petroleum chemistry, 1992, **32,** p340-348.

[43] E. G. Jones, W. J. Balster, Phenomenological Study of the Formation of Insolubles in a Jet-A Fuel. *Energy Fuels*, 1993, **7**, p968-977.

[44] W. Rudzinski, L. Oehlers, Yi. Zhang, B. Nejera, Acid-selective mass spectrometric analysis of petroleum fractions, *Energy & Fuels*, 2002**, 16**, p1178-1185.

[45] ASTM D664 - Standard Test Method for Acid Number of Petroleum Products by Potentiometric Titration

[46]G. H. C. Prado, Y. Rao, A. Klerk, Nitrogen Removal from Oil: A Review, *Energy Fuels*, 2017, 31, p14−36.

[47] F. G. A. van den Berg, E. H. Munsterman, Feedstock Effects in Fouling of Crude Oil Heat Exchangers, Proc. 4th International Conference on Petroleum Phase Behavior and Fouling. Trondheim, Norway. Paper 62.

[48] M. F. Ali, S. Abbas, A review of methods for the demetallization of residual fuel oils, *Fuel Processing Technology* 2006, **87**, p573–584.

[49] G. Murphy, J. Campbell, Fouling in Refinery Heat Exchangers: Causes, Effects, Measurement and Control. In Fouling Mechanisms, M. Bohnet et al., Eds, pp. 249 261, GREThSeminar, Grenoble, 1992.

[50] J. G. Speight, Handbook of Petroleum Product Analysis, John Willey & Sons, New Jersey, 2002, p42–43.

[51] B. Gui, Q. Y. Yang, H. J. Wu, X. Zhang, Y. Lu, Study of the Effects of Low-Temperature Oxidation on the Chemical Composition of a Light Crude Oil, *Energy Fuels*, 2010, **24**, p1139–1145.

[52] J.R. Becker, Crude oil waxes, emulsions, and asphaltenes, Ch. 11, 1997, Published by Pennwell Books, Tulsa, Oklahoma.

[53]M. F. Ali, S. Abbas, A review of methods for the demetallization of residual fuel oils, Fuel Processing Technology 2006, **87**, p573–584.

[54]I. A. Wiehe, P. Rahimi, Y. D. Oh, R. McNamara, T. Alem , Flocculation Test for Oils without Asphaltenes, *Energy & Fuels*, 2008, **22**, p753–756.

[55] H. K. Bisoyi, S. Kumar, Discotic Nematic Liquid Crystals: Science and Technology. *Chemical Society Reviews*, 2010, **39**, (1), p264–285.

[56] K.A. Gould, I. A. Wiehe., Natural hydrogen donors in petroleum resids. *Energy Fuels*, 2007, **21**, p1199–204.

[57] A. H. Alshareef, A. Scherer, X. Tan, K. Azyat, J. M. Stryker, R. R. Tykwinski, M. R. Gray, Effect of Chemical Structure on the Cracking and Coking of Archipelago Model Compounds Representative of Asphaltenes, *Energy Fuels*, 2012, **26**, p1828−1843.

[58] S. Reza Bagheri, Murray, R. Gray, William, C. McCaffrey, Influence of Depressurization and Cooling on the Formation and Development of Mesophase, *Energy & Fuels*, 2011, **25**, (12), p5541-5548.

[59] Z. Fan, A Watkinson, Kinetic and Structural Evolution during Aging of Coker Vapour Deposits, Proceedings of International Conference on Heat Exchanger Fouling and Cleaning VIII, 2009, Schladming, Austria.

[60] N. F. Carnahan, Properties of Resins Extracted from Boscan Crude Oil and Their Effect on the Stability of Asphaltenes in Boscan and Hamaca Crude Oils, *Energy & Fuels*, 1999, **13**, p309-314.

[61] D. Langevin, J. F. Argillier, Interfacial Behaviour of asphaltenes, *Advances in Colloid and Interface Science*, 2016, **233**, p83–93.

[62] .Coletti, B.D.Crittenden, S.Macchietto, Chapter 2 - Basic Science of the Fouling Process, Crude Oil Fouling, *Gulf Professional Publishing*, , 2015. P23-50.

[63] J. Czarnocka, A. Matuszewska, M. Odziemkowska, Autoxidation of Fuels During Storage, Storage Stability of Fuels, Ch 6, p157-188.

[64] T. R. Bott and J. S. Gudmundsson, "Deposition of paraffin wax from kerosene in cooled heat exchanger tubes," Can. J. Chem. Eng., 1977, **55**, (4), p381–385.

[65] J. Berce, M. Zupančič, M. Može, I. Golobič, A Review of Crystallization Fouling in Heat Exchangers, *Processes*, 2021, **9**, (8), 1356.

[66] M. V. Kök, M. A. Varfolomeev, D. K. Nurgaliev, Wax appearance temperature (WAT) determinations of different origin crude oils by differential scanning calorimetry, Journal of Petroleum Science and Engineering, 2018, **168**, p542-545.

[67] E. Diaz-Bejarano, E. Behranvand, F. Coletti, Mohammad, R. Mozdianfard, S. Macchietto, Organic and Inorganic Fouling in Heat Exchangers – Industrial Case Study: Analysis of Fouling Rate, *Ind. Eng. Chem. Res,* 2019, **58**, (1), p228–246.

[68] A. P. Watkinson, Chemical reaction fouling: A review. Experimental Thermal and Fluid Science, 1997. **14** (4), p361-374.

[69] S. Aminanea, M. Sicarda Y. Mellitia F. Sera, L. Sicard, Experimental study of the kinetics of degradation of n-dodecane under thermo-oxidative stress at low temperature and mechanism inferred, *Fuel*, 2022, **307**, 121669.

[70] B. D. Crittenden, S. A. Hout, and N. J. Alderman, Model experiments of chemical reaction fouling, *TransIChemE* Part A, 1987, **65**, 165-170.

[71] B. D. Crittenden, S. T. Kolaczkowski, T. Takemoto and D. Z. Phillips, Crude Oil Fouling In A Pilot-Scale Parallel Tube Apparatus, Heat Exchanger Fouling and Cleaning VII, 2007, Vol. RP5, Article 5.

[72] G. Dickakian, Asphaltene precipitation primary crude exchanger fouling mechanism. *Oil and Gas Journal*, 1988. **86**, p47-50.

[73] S. Chiaberge, G. Guglielmetti, L. Montanari, M. Salvalaggio, L. Santolini, S. Spera, Pietro Cesti, Investigation of Asphaltene Chemical Structural Modification Induced by Thermal Treatments, *Energy & Fuels*, 2009, **23,** p4486–4495.

[74] M. Yang, A. Young, A. Niyetkaliyev, B. Crittenden, Modelling fouling induction periods, *International Journal of Thermal Sciences*, 2012, **51**, p175-183.

[75] J. Yang, Computational fluid dynamics studies on the induction period of crude oil fouling in a heat exchanger tube, *International Journal of Heat and Mass Transfer*, 2020, **159**, 120129.

[76] B. D. Crittenden, S. T. Kolaczkowski, T. Takemoto and D. Z. Phillips, Crude Oil Fouling in a Pilot-Scale Parallel Tube Apparatus, *Heat Exchanger Fouling and Cleaning VII*, 2007, Vol RP5, Article 5.

[77] E. Diaz-Bejarano, F. Coletti, S. Macchietto, Thermo-hydraulic analysis of refinery heat exchangers undergoing fouling, *AIChE Journal*, 2017, **63**, 3, p984-1001.

[78] A. Nakao, A. Valdman, A. L. Costa, M. J. Bagajewicz, E. M. Queiroz, Incorporating fouling modeling into shell-and-tube heat exchanger design*, Industrial & Engineering Chemistry Research*, 2017, **56**, p4377-4385.

[79] M. Ghorbani, R. Maddahian, Investigation of asphaltene particles size and distribution on fouling rate in the crude oil preheat train, *Journal of Petroleum Science and Engineering*, 2021, **196**, 107665.

[80] E. Rammerstorfer, T. Karner, M. Siebenhofer, The kinetics and mechanisms of fouling in crude oil heat transfer, *Heat Transfer Engineering*, 2020, **41**, (8), p, 691-707.

[81] Coletti F, Macchietto S, Polley GT. Effects of fouling on perfor-mance of retrofitted heat exchanger networks: a thermo-hydraulicbased analysis, *Computers and Chemical Engineering*, 2011, **35**, (5), p907–917.

[82] H. Muller-Steinhagen, Heat Exchanger Fouling: Mitigation and Cleaning Strategies, *Heat transfer engineering*, 2011, **32**, p189-196.

[83] E. A. Blekkan, A. Holmen, Coke Formation on Metal Foils From Heavy Oils, *Carbon*, 1987, **25** (6), p827-835.

[84] Speight J. G., Oil and Gas corrosion Prevention – From Surface facilities to Refineries, Elsevier, 2014, e8.

[85] https://www.silcotek.com/silcotek-coating-applications/oil-gas-coating-applications, website accessed on 28/09/2021.

[86] D. Smith, Solving Surface Fouling with New Non-Stick CVD Coatings, Technical presentation, obtained from www.silotec.com/semi-coating-blog/how-to-stop-heat-exchanger-fouling-and-tube-fouling-, accessed on 28/09/2021.

[87] G. Barone, D. Smith H. Higgins, Characterizing the Performance of Surface Modifications that Enhance Sensitivity, Reliability, Reproducibility and Accuracy of Analytical Instruments, Technical insight paper – www. siloteck.com, accessed on 28/09/2021.

[88] K. Kraiwattanawong, H. S. Fogler, S. G. Gharfeh, P. Singh, W. H. Thomason, S. Chavade, Effect of asphaltene dispersants on aggregate size distribution and growth, *Energy Fuels*, 2009, **23**, (3), pp. 1575-1582.

[89] L. C. Rocha Junior, M. S. Ferreira, A. C. da Silva Ramos, Inhibition of asphaltene precipitation in Brazilian crude oils using new oil soluble amphiphiles, *Journal of Petroleum Science and Engineering*, 2006, **51**, (1–2), 2006, p26-36.

[90] M. M. Abdullah, H. A. Al-Lohedan, Synthesis and characterization of tannic acid esters and their performances as asphaltenes dispersants, *Journal of Petroleum Science and Engineering*, 2021, **201**, 108389.

[91] F. Trejo, J. Ancheyta, T. J. Morgan, A. A. Herod, R Kandiyoti, Characterization of Asphaltenes from Hydrotreated Products by SEC, LDMS, MALDI, NMR, and XRD, *Energy Fuels* 2007, **21** (4), p2121– 2128.

[92] H. Groenzin, O. C. Mullins, Molecular sizes of asphaltenes from different origin, *Energy Fuels*, 2000, **14**, p677–684.

[93] H. Groenzin, O. C. Mullins, S Eser, J. Mathews, M. G. Yang, D. Jones, 2003, Molecular size of asphaltene solubility fractions. *Energy Fuels*, 2003, **17**, p498–503.

[94] A. B. Andrews, R. Guerra, O. C. Mullins, P. N. Sen PN, Diffusivity of asphaltenemolecules by fluorescence correlation spectroscopy. *Journal of Physical Chemistry A*, 2006, **110**, p8095–8097.

[95] N. V. Lisitza, D. E. Freed; P. N. Sen, Y. Q. Song, Self-assembly of Asphaltene: Enthalpy, Entropy of Depletion and Dynamics at Crossover, *Magnetic Resonance Imaging*, 2007, **25**, p544-591.

[96] L. Socrates, L. Gutierrez, N. Gabriel, J. Pereira, M. Bernardo, F. Delolme, G. Dessalces, D. Broseta, Molecular Weight of Petroleum Asphaltenes: A Comparison between Mass Spectrometry and Vapor Pressure Osmometry, *Energy Fuels*, 2005, **19**, (4), 1548 – 1560.

[97] Y. Ruiz-Morales, O. C. Mullins, Polycyclic aromatic hydrocarbons of asphaltenes analyzed by molecular orbital calculations with optical spectroscopy. *Energy Fuels*, 2007, **21**, p256–65.

[98] Y. Ruiz-Morales, X. Wu, O. C. Mullins, Electronic Absorption Edge of Crude Oils and Asphaltenes Analyzed by Molecular Orbital Calculations with Optical Spectroscopy, *Energy Fuels,* 2007, **21**, (2), p944–952.

[99] E. Buenrostro-Gonzalez, H. Groenzin, C. Lira-Galeana, O.C. Mullins, The Overriding Chemical Principles that Define Asphaltenes, *Energy Fuels*, 2001, **15**, p972-978.

[100] S. Akmaz, O. Iscan, M. A. Gurkaynak, M Yasar, The Structural Characterization of Saturate, Aromatic, Resin, and Asphaltene Fractions of Batiraman Crude Oil, *Petroleum Science and Technology*, 2011, **29**, p160–171.

[101] V. Calemma, P. Iwanski, M. Nali, R. Scotti, L. Montanari, Structural characterization of asphaltenes of different origins, *Energy and fuels*, 1995, **9**, p225-230.

[102] A. M. McKenna, J. M. Purcell, R. P. Rodgers, A. G. Marshall, Atmospheric pressure photoionization Fourier transform ion cyclotron resonance mass spectrometry for detailed compositional analysis of petroleum. Presented at 10th International Conference Petroleum Phase Behaviour Fouling, 10th, Rio de Janeiro, Brazil.

[103] P. E. Savage, M. T. Klein, Asphaltene reaction pathways. 2. Pyrolysis of n-penta-decylbenzene, *Industrial & Engineering Chemical Research,* 1987, **26**, p488–494.

[104] C. M. Smith, P. E. Savage, Reactions of Polycyclic Alkylaromatics. 2. Pyrolysis of 1,3-Diarylpropanes, *Energy & Fuels*, 1991, **5**, (1), p146-155.

[105] A. H. Alshareef, A. Scherer, J. M. Stryker, R. R. Tykwinski, M. Grey, Thermal Cracking of Substituted Cholestane–Benzoquinoline Asphaltene Model Compounds, *Energy & Fuels*, 2012, 26, 6, p3592-3602.

[106] K. Akbarzadeh, D.C. Bressler, J. Wang, K.L. Gawrys, M.R. Gray, P.K. Kilpatrick, H.W. Yarranton, Association behavior of pyrene compounds as models for asphaltene, *Energy and Fuels*, 2005, **19**, p1268-1271.

[107] P. E. Savage, M. T. Klein, Asphaltene reaction pathways. 5. Chemical and mathematical modelling, *Chemical Engineering Science*, 1989, **44**, p393–404.

[108] C. M. Smith, P. E. Savage, Polycyclic Alkylaromatics. 1. Pathways, Kinetics, and Mechanisms for 1-Dodecylpyrene Pyrolysis, *Industrial & Engineering Chemical Research*, 1991, **30**, p331–339.

[109] A. H. Alshareef, X. Tan, C. Diner, J. Zhao, A. Scherer, K. Azyat, J. M. Stryker, R. R. Tykwinski, M. Gray, Binary Interactions in Coke Formation from Model Compounds and Asphaltenes, *Energy Fuels*, 2014, **28**, (3), p1692–1700.

[110] E. L. Nordgård, J. Sjoblom, Model Compounds for Asphaltenes and C80 Isoprenoid Tetraacids. Part I: Synthesis and Interfacial Activities, *Journal of Dispersion Science and Technology*, 2008, **29**, (8), p1114-1122.

[111] A. Sharma, H. Groenzin, A. Tomita, O. C. Mullins, Probing Order in Asphaltenes and Aromatic Ring Systems by HRTEM, *Energy & Fuels*, 2002, **16**, p490-496.

[112] Venditti S., 2010, Characterization of petroleum fouling with respect to operational parameters, Phd Thesis, Imperial College London.

[113] Rostani K., 2013, Effect of Crude Oil Vanadyl Porphyrin Content and Blending on Heat Exchanger Fouling, PhD Thesis, Imperial College London.

[114] S. F. Zhang, B. Xu, S. A. Moore, A. A. Herod, R. Kandiyoti, Comparison of hydrocracking reactivities of coal extracts from a flowing-solvent reactor, a mini-bomb and a pilot plant, *Fuel*, 1996, **75** (5), p597–605.

[115] Ebert, W.A. and C.B. Panchal, Analysis of Exxon Crude Oil Slip-Stream Coking Data, in Fouling Mitigation of Industrial Exchange Equipment. 1995, Begell House, New York, p. 451-460.

[116] Yiantsios, S.G., Fouling of tube surfaces: modeling of removal kinetics. *AIChE Journal*, 1994, **40**, (11), p1804-1813.

[117] M. Yang, Z. Wood, B. Rickard, B. Crittenden, M. Gough, P. Droegemueller, T. Higley, Mitigation of crude oil fouling by turbulence enhancement in a batch stirred cell, *Applied Thermal Engineering*, **54**, (2), 2013, p516-520.

[118] A. Young, S. Venditti, C. Berrueco, M. Yang, A. Waters, H. Davies, S. Hill, M. Millan, B. Crittendedn, Characterisation of crude oils and their fouling deposits using a stirred batch cell system, *Heat Transfer Engineering,* 2011, **32**, (3-4), p216-227.

[119] P. Singh, S. Krishnaswamy, P. Krishnaswamy, A. Verma, J. Rawat, Crude Oil Foulant Deposition Studies on a Heated Surface Using a Novel Batch Stirred Coupon Test Rig, *International Journal of Chemical Engineering*, 2022, 5443317.

[120] Commercial brochure available on website: https://www.expotechusa.com/catalogs/alcor/manuals/hlps.pdf accessed on 18/02/23.

[121] Z. Fan, P. Rahimi, R. McGee, Q. Wen, T. Alem, Investigation of Fouling Mechanisms of a Light Crude Oil Using an Alcor Hot Liquid Process Simulator, Energy Fuels 2010, **24**, (11), p6110–6118.

[122] E. Rogel, K. Hench, F. Cibotti, E. Forbes, L. Jackowski, Investigation on Crude Oil Fouling Behavior, *Energy Fuels*, 2022, **36**, (2), p818–825.

[123] T. Xing, M. Ali, T. Alem, R. Gieleciak, J Chen, Fouling tendency of bitumen visbreaking products, *Fuel*, 2021, **289**, 119735.

[124] J. Pental, Design and Commissioning of a Crude Oil Fouling Facility, PhD Thesis, 2011, Imperial College London.

[125] Z. B. Tajudin, Experiments, Modelling and Validation of Crude Oil Fouling on Large Scale Rig, PhD Thesis, 2016, Imperial College London.

[126] C. A. Bennet; S. Appleyard, M. Gough, R. P. Omán, H. M. Joshi, D. C. King, T. Y. Lam, T. M. Rudy, S. E. Stomierowski, Industry-Recommended Procedures for Experimental Crude Oil Preheat Fouling Research, *Heat Transfer Engineering*, 2006, **27**, (9), p28-35.

[133] website: http://wtt-pro.nist.gov/ accessed on 1st March 2017.

[134] Stratton S. W., Bearce H. W., Peffer E. L., Density and Thermal Expansion of American Petroleum Oils, Technologic Papers of the Bureau of Standards, 1916, p13-16.

[135] Mukherjee R., Effectively Design Shell-and-Tube Heat Exchangers, *Chemical Engineering Progress*, 1998, **94**, (2), p21-37.

[136] M. Fénot, Y. Bertin, E. Dorignac, G. Lalizel, A Review of Heat Transfer between Concentric Rotating Cylinders with or without Axial Flow, *International Journal of Thermal Sciences*, 2011, **50**, p1138-1155.

[137] Chaudhry, M. H., Applied Hydraulic Transients, 2013, (3rd ed.), Springer. p45.

[138] Mory M., Fluid Mechanics for Chemical Engineering, 2013, J. Wiley & Sons, Ch.4.2.

[139] Moody M., Friction Factors for Pipe Flow, 1944, *Transactions of the A.S.M.E.*, **66**, (8) p671-684.

[140] Gabor Takacs, 2015, Sucker-Rod Pumping Handbook, Elsevier, Hungary, 2015 Ch 2.

[141] H. Magande, A. G. McDonald, Introduction to Thermo-Fluids Systems Design, *John Wiley & Sons*, 2012, A.1.

[142] P. K. Vijayan, A. K. Nayak, N. Kumar, Single-Phase, Two-Phase and Supercritical Natural Circulation Systems, Woodhead Publishing, 2019, Ch3.

[143]G. P. Smith, A. A. Townsend, Turbulent Couette flow between concentric cylinders at large Taylor numbers, *Journal of Fluid Mechanics*, 1982, **123**, pp.187-217.

[145] S. G. Huisman, D. P. M. van Gils, S. Grossmann, C. Sun, D. Lohse, *Physical Review Letters*, 2012, **108**, 024501.

[146] Roberts, P. H., The solution of the characteristic value problems, 1965, Proceedings of the Royal Society of London., **A, 283**, p550-556.

[147] Koschmieder E. L., Turbulent Taylor Vortex Flow, *Journal of Fluid Mechanics*, 1979, **93**, 515 – 527.

[148] Akbarzadeh K.; Zougari M., Introduction to a Novel Approach for Modeling Wax Deposition in Fluid Flows, 1, 2008, Taylor-Couette System, Industrial & Engineering Chemistry Research, **47**, (3), p953-963.

[149] Webpage: https://thermalprops.paratherm.com/NFFrange.asp; accessed on 25/02/2023.

[150] ASTM D3279-12, Standard Test Method for n-Heptane Insolubles, ASTM Inernational, West Conshohocken, PA, 2012.

[151] Arcellus Arrillaga, P; Heavy Oil Upgrading through Oxidative Cracking in Near-critical and Supercritical Water, PhD Thesis, 2016, Imperial College London.

[152] L. Hoejslet, C. Agerbo, A. Agerbo, Determination of sulfur and heavy metals in crude oil and petroleum products by energy-dispersive x-ray fluorescence spectrometry and fundamental parameter approach, *Analytical Chemistry*, 1981, **53**, (12), p1788–1792.

[153] ASTM D4294, Standard Test Method for Sulfur in Petroleum and Petroleum Products by Energy Dispersive X-ray Fluorescence Spectrometry.

[154] E. Diaz-Bejarano, E. Behranvand, F. Coletti, M. R. Mozdianfard, S. Macchietto, Organic and Inorganic Fouling in Heat Exchangers – Industrial Case Study: Analysis of Fouling State, *Applied Energy*, 2017, **206**, p1250-1266.

[155] A. A. Herod, K. D. Bartle, T. J. Morgan, R. Kandiyoti, Analytical Methods for Characterizing High-Mass Complex Polydisperse Hydrocarbon Mixtures: An Overview, Chem. Rev. 2012, 112, p3892−3923.

[156] T. J. Morgan, M. Millan, M. Behrouzi, A. A. Herod, R. Kandiyoti, On the Limitations of UV-Fluorescence Spectroscopy in the Detection of High-Mass Hydrocarbon Molecules, *Energy & Fuels* 2005**, 19***,* p164-169.

[157] ASTM D-5291, Standard Test Methods for Instrumental Determination of Carbon, Hydrogen, and Nitrogen in Petroleum Products and Lubricants.

[158] A. Y. Leon, A. Guzman, D. Laverde, R. V. Chaudhari, B. Subramaniam, J. J. Bravo-Suarez, Thermal Cracking and Catalytic Hydrocracking of a Colombian Vacuum Residue and Its Maltenes and Asphaltenes Fractions in Toluene, *Energy Fuels*, 2017, **31**, (4), 3868–3877.

[159] T. Cantlay, D. J. Bain, J. Curet, R. F. Jack, B. C. Dickson,P. Basu, J. Stoltz, Determining conventional and unconventional oil and gas well brines in natural sample II: Cation analyses with ICP-MS and ICP-OES, *Journal of Environmental Science and Health, Part A*, 2019, p11-23.

[160] Y. Ma, S. Y. Li, The pyrolysis, extraction and kinetics of Buton oil sand bitumen. Fuel Processing Technology, 2012, 100, p11−15.

[161] P. F. Liu, M. M. Zhu, Z. Z. Zhang, W. C. Wan, S. Yani, D. K. Zhang, Thermogravimetric Studies of Characteristics and Kinetics of Pyrolysis of Buton Oil Sand., *Energy Procedia*, 2014, **61**, p2741−2744.

[162] R. C. Schucker, Thermogravimetric determination of the coking kinetics of Arab heavy vacuum residuum, *Industrial & Engineering Chemistry Process Design and Development*, 1983, **22**, (4), p615−619.

[163] ASTM D7528-15, Standard Test Methods for Proximate Analysis of Coal and Coke by Macro Thermogravimetric Analysis, ASTM International, West Conshohocken, PA, 2015.

[164] A. A. Herod, K. D. Bartle, R. Kandiyoti, Characterisation of Heavy Hydrocarbons by Chromatographic and Mass Spectrometric Methods An Overview, *Energy Fuels*, 2007, **21**, 2176-2203.

[165] ASTM D2887-16a - Standard Test Method for Boiling Range Distribution of Petroleum Fractions by Gas Chromatography, ASTM, International, West Conshohocken, PA, 2016.

[167] R. J. Hwang, A. S. Ahmed, J. M. Moldowan, Oil composition variation and reservoir continuity: Unity field, Sudan, *Organic Geochemistry*, **21**, (2), 1994, p171-188.

[168] ASTM D1480, Standard Test Method for Density and Relative Density (Specific Gravity) of Viscous Materials by Bingham Pycnometer, ASTM International.

[169] H. Puron, Novel Mesoporous Catalysts for Vacuum Residue Hydrocracking, Imperial College London, 2013.

[170] Asphaltenes: Chemical Transformation during Hydroprocessing, by J. Ancheyta et al, 2010, p29.

[171] M. Asemani, A. R. Rabbani, Oil-oil correlation by FTIR spectroscopy of asphaltene samples, *Geosciences Journal*, 2016, **20**, (2), p273-283.

[172] P. Doumenq, M. Guiliano, M. K. Kister, Approche méthodologique directe et continue du processus d'oxydation des bitumes par spectroscopie infrarouge à transformée de Fourier, Analytica Chimica Acta, 1991, **242**, p137–141.

[173] E. Alvarez, G. Marroquín, F. Trejo, G. Centeno, J. Ancheyta, J. A. I. Díaz., Pyrolysis kinetics of atmospheric residue and its SARA fractions, *Fuel,* 2011*,* **90**, p3602–3607.

[174] Property predictions from: http://wtt-pro.nist.gov/; accessed on 1 March 2017.

[182] S. Akmaz, O. Iscan, M. A. Gurkaynak, M. Yasar The Structural Characterization of Saturate, Aromatic, Resin, and Asphaltene Fractions of Batiraman Crude Oil, *Petroleum Science and Technology*, 2011, **29**, (2), p160-171.

[183] M. L. Chacón-Patiñoa, J. Nelson, E. Rogel, K. Hench, L. Poirier, F Lopez-Linares, C. Ovalles, Vanadium and Nickel distributions in Pentane, In-between C5-C7 Asphaltenes, and heptane asphaltenes of heavy crude oils, *Fuel*, 2021, **292**, , p120-259.

[184] Mullins, O. C. The Modified Yen Model, *Energy Fuels*, 2010, **24**, p2179−2207.

[185] Y. Niko, S. Kawauchi, S. Otsu, K. Tokumaru, G. Konishi, Fluorescence Enhancement of Pyrene Chromophores Induced by Alkyl Groups through σ–π Conjugation: Systematic Synthesis of Primary, Secondary, and Tertiary Alkylated Pyrenes at the 1, 3, 6, and 8 Positions and Their Photophysical Properties, *Journal of Organic Chemistry*, 2013, **78**, (7), p3196-3207.

[186] P. Vyas, A. Bhatt, G. Ramachandraiah, A. Bedekar, Environmentally benign chlorination and bromination of aromatic amines, hydrocarbons and naphthols, *Tetrahedron Letters*, 2003, **44**, p4085-4088.

[187] P. Juyal, A. M. McKenna, A. Yen, R. P. Rodgers, C. M. Reddy, R. K. Nelson, A. B. Andrews, E. Atolia, S. J. Allenson, O. C. Mullins, A. G. Marshall, Analysis and identification of biomarkers and origin of blue color in an unusually blue crude oil, *Energy Fuels*, 2011, **25**, p172−182.

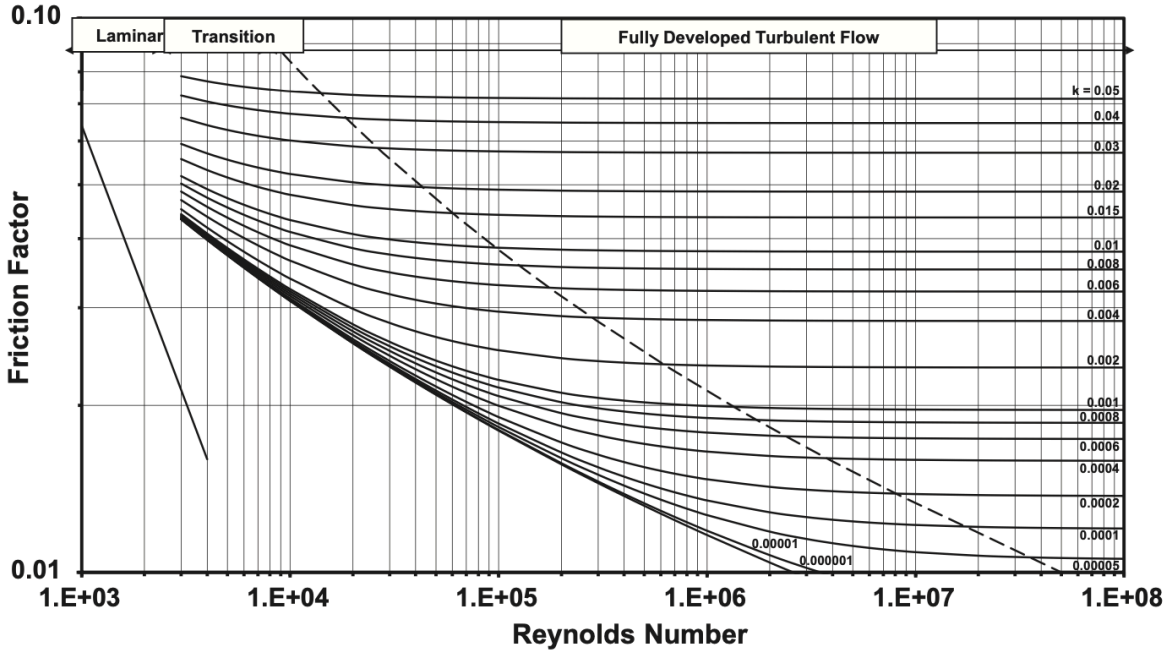
[188] G. Turkmen, S. Erten-Ela, S. Icli, Highly soluble perylene dyes: Synthesis, photophysical and electrochemical characterizations, *Dyes and Pigments*, 2009, **83**, p297–303.

[188] S. V. Bhosale, C. H. Jani, S. J. Langford, Chemistry of naphthalene diimides, Chemical Society Reviews, 2007, **37**, p331-342

11. Appendix

11.3 Design and development of fouling apparatus

11.3.1 Moody Diagram – Friction Factors vs Reynolds numbers for pipe flow (from Sucker-Rod Pumping Handbook[140])



11.3.2 Modelling flow data for Taylor Couette Cell Reactor (relates to Figs 3.14, 3.16, 3.17)

Flow in Taylor Couette Reactor

Temperature (°C)	kinematic viscosity	Dynamic Viscosity	density /kg/m^3	rotor surface velocity /m/s	r.p.m.	Angular velocity	Reynolds number	Dimensionless Torque (G	Wall Shear Stress (τ_w)	Taylor number *Ta*
60	9.81	0.008476	864	1	823	86.2	1713	2.07E+05	6.9	1.56E+06
70	7.5	0.006443	859	1	823	86.2	2240	3.10E+05	6.0	2.67E+06
80	5.85	0.004996	854	1	823	86.2	2872	4.50E+05	5.2	4.38E+06
90	4.66	0.003956	849	1	823	86.2	3605	6.33E+05	4.6	6.91E+06
100	3.78	0.003187	843	1	823	86.2	4444	8.66E+05	4.2	1.05E+07
110	3.11	0.002603	837	1	823	86.2	5402	1.16E+06	3.7	1.55E+07
120	2.61	0.002169	831	1	823	86.2	6437	1.51E+06	3.4	2.20E+07
130	2.21	0.001823	825	1	823	86.2	7602	1.94E+06	3.1	3.07E+07
140	1.9	0.001556	819	1	823	86.2	8842	2.43E+06	2.9	4.16E+07
150	1.65	0.001341	813	1	823	86.2	10182	3.02E+06	2.7	5.51E+07
160	1.45	0.001170	807	1	823	86.2	11586	3.76E+06	2.5	7.14E+07
170	1.28	0.001024	800	1	823	86.2	13125	4.64E+06	2.4	9.16E+07
180	1.15	0.000912	793	1	823	86.2	14609	5.57E+06	2.3	1.13E+08
190	1.04	0.000817	786	1	823	86.2	16154	6.61E+06	2.2	1.39E+08
200	0.94	0.000732	779	1	823	86.2	17872	7.85E+06	2.2	1.70E+08
210	0.86	0.000664	772	1	823	86.2	19535	9.13E+06	2.1	2.03E+08
220	0.8	0.000611	764	1	823	86.2	21000	1.03E+07	2.0	2.34E+08
230	0.74	0.000560	757	1	823	86.2	22703	1.18E+07	1.9	2.74E+08
240	0.69	0.000517	749	1	823	86.2	24348	1.33E+07	1.9	3.15E+08
250	0.65	0.000482	741	1	823	86.2	25846	1.47E+07	1.8	3.55E+08
260	0.61	0.000447	733	1	823	86.2	27541	1.64E+07	1.8	4.03E+08
270	0.58	0.000421	725	1	823	86.2	28966	1.78E+07	1.7	4.46E+08
280	0.55	0.000394	716	1	823	86.2	30545	1.95E+07	1.7	4.96E+08
290	0.527	0.000373	708	1	823	86.2	31879	2.10E+07	1.6	5.40E+08
300	0.505	0.000353	699	1	823	86.2	33267	2.26E+07	1.6	5.88E+08
310	0.486	0.000335	690	1	823	86.2	34568	2.41E+07	1.6	6.35E+08
320	0.467	0.000318	681	1	823	86.2	35974	2.58E+07	1.5	6.88E+08

Temperature (°C)	kinematic viscosity	Dynamic Viscosity	density /kg/m^3	rotor surface velocity /m/s	r.p.m.	Angular velocity	Reynolds number	Dimensionless Torque (G	Wall Shear Stress (τ_w)	Taylor number *Ta*
60	9.81	0.008476	864	2	1646	172.4	3425	5.86E+05	19.4	6.24E+06
70	7.5	0.006443	859	2	1646	172.4	4480	8.76E+05	16.9	1.07E+07
80	5.85	0.004996	854	2	1646	172.4	5744	1.27E+06	14.8	1.75E+07
90	4.66	0.003956	849	2	1646	172.4	7210	1.79E+06	13.1	2.76E+07
100	3.78	0.003187	843	2	1646	172.4	8889	2.45E+06	11.7	4.20E+07
110	3.11	0.002603	837	2	1646	172.4	10804	3.34E+06	10.7	6.21E+07
120	2.61	0.002169	831	2	1646	172.4	12874	4.49E+06	10.1	8.81E+07
130	2.21	0.001823	825	2	1646	172.4	15204	5.96E+06	9.6	1.23E+08
140	1.9	0.001556	819	2	1646	172.4	17684	7.71E+06	9.1	1.66E+08
150	1.65	0.001341	813	2	1646	172.4	20364	9.80E+06	8.6	2.20E+08
160	1.45	0.001170	807	2	1646	172.4	23172	1.22E+07	8.2	2.85E+08
170	1.28	0.001024	800	2	1646	172.4	26250	1.51E+07	7.9	3.66E+08
180	1.15	0.000912	793	2	1646	172.4	29217	1.81E+07	7.6	4.54E+08
190	1.04	0.000817	786	2	1646	172.4	32308	2.15E+07	7.3	5.55E+08
200	0.94	0.000732	779	2	1646	172.4	35745	2.55E+07	7.0	6.79E+08
210	0.86	0.000664	772	2	1646	172.4	39070	2.97E+07	6.7	8.12E+08
220	0.8	0.000611	764	2	1646	172.4	42000	3.36E+07	6.5	9.38E+08
230	0.74	0.000560	757	2	1646	172.4	45405	3.83E+07	6.3	1.10E+09
240	0.69	0.000517	749	2	1646	172.4	48696	4.31E+07	6.1	1.26E+09
250	0.65	0.000482	741	2	1646	172.4	51692	4.78E+07	5.9	1.42E+09
260	0.61	0.000447	733	2	1646	172.4	55082	5.32E+07	5.8	1.61E+09
270	0.58	0.000421	725	2	1646	172.4	57931	5.80E+07	5.6	1.78E+09
280	0.55	0.000394	716	2	1646	172.4	61091	6.34E+07	5.5	1.98E+09
290	0.527	0.000373	708	2	1646	172.4	63757	6.82E+07	5.3	2.16E+09
300	0.505	0.000353	699	2	1646	172.4	66535	7.33E+07	5.2	2.35E+09
310	0.486	0.000335	690	2	1646	172.4	69136	7.83E+07	5.1	2.54E+09
320	0.467	0.000318	681	2	1646	172.4	71949	8.38E+07	5.0	2.75E+09

Temperature (°C)	kinematic viscosity	Dynamic Viscosity	density /kg/m^3	rotor surface velocity /m/s	r.p.m.	Angular velocity	Reynolds number	Dimensionless Torque (G	Wall Shear Stress (τ_w)	Taylor number *Ta*
60	9.81	0.008476	864	3	2470	258.6	5138	1.08E+06	35.6	1.40E+07
70	7.5	0.006443	859	3	2470	258.6	6720	1.61E+06	31.0	2.40E+07
80	5.85	0.004996	854	3	2470	258.6	8615	2.34E+06	27.2	3.95E+07
90	4.66	0.003956	849	3	2470	258.6	10815	3.34E+06	24.5	6.22E+07
100	3.78	0.003187	843	3	2470	258.6	13333	4.77E+06	22.9	9.45E+07
110	3.11	0.002603	837	3	2470	258.6	16206	6.65E+06	21.4	1.40E+08
120	2.61	0.002169	831	3	2470	258.6	19310	8.95E+06	20.2	1.98E+08
130	2.21	0.001823	825	3	2470	258.6	22805	1.19E+07	19.0	2.77E+08
140	1.9	0.001556	819	3	2470	258.6	26526	1.54E+07	18.1	3.74E+08
150	1.65	0.001341	813	3	2470	258.6	30545	1.95E+07	17.2	4.96E+08
160	1.45	0.001170	807	3	2470	258.6	34759	2.43E+07	16.4	6.42E+08
170	1.28	0.001024	800	3	2470	258.6	39375	3.01E+07	15.7	8.24E+08
180	1.15	0.000912	793	3	2470	258.6	43826	3.61E+07	15.1	1.02E+09
190	1.04	0.000817	786	3	2470	258.6	48462	4.28E+07	14.5	1.25E+09
200	0.94	0.000732	779	3	2470	258.6	53617	5.08E+07	13.9	1.53E+09
210	0.86	0.000664	772	3	2470	258.6	58605	5.91E+07	13.4	1.83E+09
220	0.8	0.000611	764	3	2470	258.6	63000	6.68E+07	13.0	2.11E+09
230	0.74	0.000560	757	3	2470	258.6	68108	7.63E+07	12.6	2.47E+09
240	0.69	0.000517	749	3	2470	258.6	73043	8.60E+07	12.2	2.84E+09
250	0.65	0.000482	741	3	2470	258.6	77538	9.51E+07	11.9	3.20E+09
260	0.61	0.000447	733	3	2470	258.6	82623	1.06E+08	11.5	3.63E+09
270	0.58	0.000421	725	3	2470	258.6	86897	1.15E+08	11.2	4.01E+09
280	0.55	0.000394	716	3	2470	258.6	91636	1.26E+08	10.9	4.46E+09
290	0.527	0.000375	708	3	2470	258.6	95636	1.36E+08	10.7	4.86E+09
300	0.505	0.000356	699	3	2470	258.6	99802	1.46E+08	10.5	5.30E+09
310	0.486	0.000338	690	3	2470	258.6	103704	1.56E+08	10.3	5.72E+09
320	0.467	0.000318	681	3	2470	258.6	107923	1.67E+08	9.9	6.19E+09

11.3.2 Modelling flow data for Paratherm fluid in a pipe (relates to Figs 3.16, 3.17)

Temperature (°C)	kinematic viscosity	density /kg/m^3	Pipe ID /m	velocity /m/s	Reynolds number	Correlated Darcy friction factor (f_D)	Wall Shear Stress (τ_w) /Pa
60	9.81	864	0.02118	1	2159	0.0464	5.01
70	7.5	859	0.02118	1	2824	0.0434	4.66
80	5.85	854	0.02118	1	3621	0.0408	4.35
90	4.66	849	0.02118	1	4545	0.0385	4.09
100	3.78	843	0.02118	1	5603	0.0366	3.85
110	3.11	837	0.02118	1	6810	0.0348	3.64
120	2.61	831	0.02118	1	8115	0.0333	3.46
130	2.21	825	0.02118	1	9584	0.0320	3.30
140	1.9	819	0.02118	1	11147	0.0308	3.15
150	1.65	813	0.02118	1	12836	0.0297	3.02
160	1.45	807	0.02118	1	14607	0.0288	2.90
170	1.28	800	0.02118	1	16547	0.0279	2.79
180	1.15	793	0.02118	1	18417	0.0271	2.69
190	1.04	786	0.02118	1	20365	0.0253	2.49
200	0.94	779	0.02118	1	22532	0.0248	2.41
210	0.86	772	0.02118	1	24628	0.0244	2.35
220	0.8	764	0.02118	1	26475	0.0240	2.29
230	0.74	757	0.02118	1	28622	0.0236	2.24
240	0.69	749	0.02118	1	30696	0.0233	2.18
250	0.65	741	0.02118	1	32585	0.0230	2.13
260	0.61	733	0.02118	1	34721	0.0227	2.08
270	0.58	725	0.02118	1	36517	0.0225	2.04
280	0.55	716	0.02118	1	38509	0.0223	1.99
290	0.53	708	0.02118	1	39962	0.0221	1.96
300	0.51	699	0.02118	1	41529	0.0219	1.92
310	0.49	690	0.02118	1	43224	0.0218	1.88
320	0.47	681	0.02118	1	45064	0.0216	1.84

Temperature (°C)	kinematic viscosity	density /kg/m^3	Pipe ID /m	velocity /m/s	Reynolds number	Correlated Darcy friction factor (f_D)	Wall Shear Stress (τ_w) /Pa
60	9.81	864	0.02118	2	4318	0.0390	16.85
70	7.5	859	0.02118	2	5648	0.0365	15.67
80	5.85	854	0.02118	2	7241	0.0343	14.64
90	4.66	849	0.02118	2	9090	0.0324	13.75
100	3.78	843	0.02118	2	11206	0.0307	12.95
110	3.11	837	0.02118	2	13621	0.0293	12.25
120	2.61	831	0.02118	2	16230	0.0280	11.64
130	2.21	825	0.02118	2	19167	0.0269	11.09
140	1.9	819	0.02118	2	22295	0.0258	10.58
150	1.65	813	0.02118	2	25673	0.0247	10.02
160	1.45	807	0.02118	2	29214	0.0240	9.70
170	1.28	800	0.02118	2	33094	0.0230	9.18
180	1.15	793	0.02118	2	36835	0.0225	8.91
190	1.04	786	0.02118	2	40731	0.0220	8.65
200	0.94	779	0.02118	2	45064	0.0216	8.41
210	0.86	772	0.02118	2	49256	0.0212	8.18
220	0.8	764	0.02118	2	52950	0.0209	7.98
230	0.74	757	0.02118	2	57243	0.0206	7.79
240	0.69	749	0.02118	2	61391	0.0203	7.60
250	0.65	741	0.02118	2	65169	0.0200	7.43
260	0.61	733	0.02118	2	69443	0.0198	7.25
270	0.58	725	0.02118	2	73034	0.0196	7.10
280	0.55	716	0.02118	2	77018	0.0194	6.94
290	0.53	708	0.02118	2	79925	0.0192	6.81
300	0.51	699	0.02118	2	83059	0.0191	6.67
310	0.49	690	0.02118	2	86449	0.0189	6.54
320	0.47	681	0.02118	2	90128	0.0188	6.40

Temperature (°C)	kinematic viscosity	density /kg/m^3	Pipe ID /m	velocity /m/s	Reynolds number	Correlated Darcy friction factor (f_D)	Wall Shear Stress (τ_w) /Pa
60	9.81	864	0.02118	3	6477	0.0352	34.26
70	7.5	859	0.02118	3	8472	0.0330	31.85
80	5.85	854	0.02118	3	10862	0.0310	29.76
90	4.66	849	0.02118	3	13635	0.0293	27.95
100	3.78	843	0.02118	3	16810	0.0273	25.86
110	3.11	837	0.02118	3	20431	0.0258	24.27
120	2.61	831	0.02118	3	24345	0.0244	22.82
130	2.21	825	0.02118	3	28751	0.0236	21.91
140	1.9	819	0.02118	3	33442	0.0229	21.11
150	1.65	813	0.02118	3	38509	0.0223	20.37
160	1.45	807	0.02118	3	43821	0.0217	19.70
170	1.28	800	0.02118	3	49641	0.0212	19.05
180	1.15	793	0.02118	3	55252	0.0207	18.48
190	1.04	786	0.02118	3	61096	0.0203	17.96
200	0.94	779	0.02118	3	67596	0.0199	17.44
210	0.86	772	0.02118	3	73884	0.0195	16.98
220	0.8	764	0.02118	3	79425	0.0193	16.56
230	0.74	757	0.02118	3	85865	0.0190	16.15
240	0.69	749	0.02118	3	92087	0.0187	15.76
250	0.65	741	0.02118	3	97754	0.0185	15.41
260	0.61	733	0.02118	3	104164	0.0183	15.05
270	0.58	725	0.02118	3	109552	0.0181	14.74
280	0.55	716	0.02118	3	115527	0.0179	14.40
290	0.53	708	0.02118	3	119887	0.0177	14.13
300	0.51	699	0.02118	3	124588	0.0176	13.85
310	0.49	690	0.02118	3	129673	0.0175	13.56
320	0.47	681	0.02118	3	135191	0.0173	13.27

11.4 Experimental methods

11.4.1 Methods used for Gas Chromatography analysis

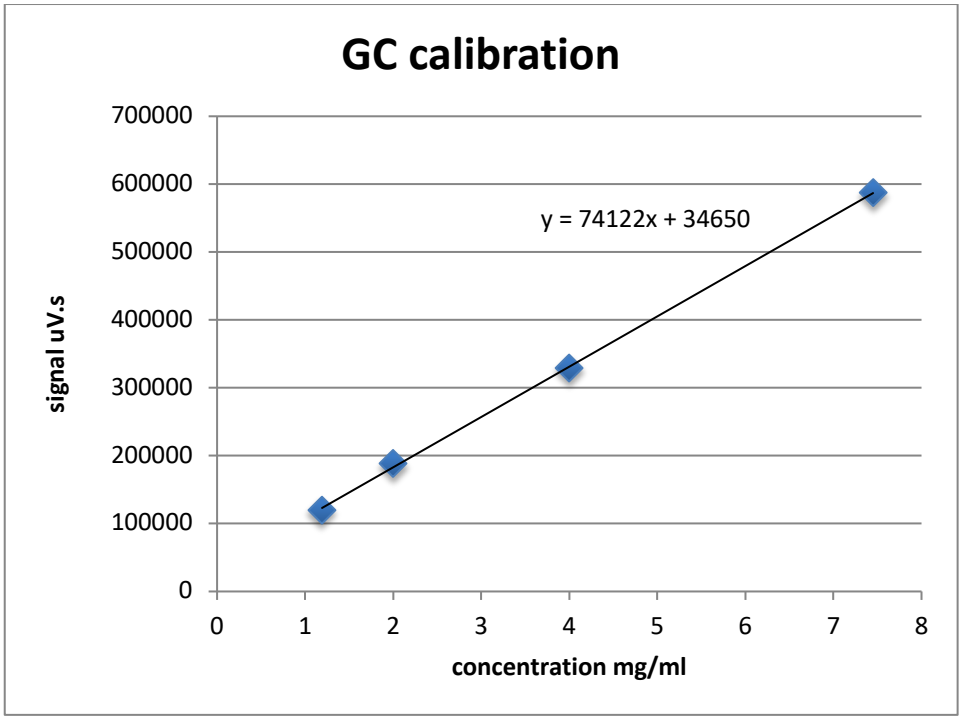
D2887 Method for Crude oil Analysis

Total Run Time	**34.87 minutes**
Step	**Details**
Initial Hold	40 °C – Hold for 1 min
Ramp 1	15 °C/min to 350°C
Hold	350 °C – Hold for 2 mins
Ramp 2	25 °C/min to 380°C
Hold	380 °C for 10 mins

Aquathermal Method Program – Used for the analysis of model compounds and solutions thereof for synthesis and reactions

Total Run time	43 minutes
Step	**Details**
Initial Hold	50°C - Hold for 0 mins
Ramp 1	5 °C/min to 100 °C
Hold	100 °C Hold for 1 min
Ramp 2	10 °C/min to 320°C
Hold	320 °C – Hold for 10 mins

11.4.2 GC-FID calibration for residual heptane concentration in maltene fraction after Large Scale fractionation.



11.6 Density modelling at reactor wall temperature

Density at temperature *t* is given by the form:

$$D_t = D_T + \alpha(t - T) + \beta(t - T)^2$$

where:

D_t = density at temperature *t*

D_T = density at standard temperature (25 °C)

α & *β* = constant coefficients

and substituting for $D_t = \frac{m}{V_t}$, this becomes:

$$V_t = \frac{D_T V_T}{D_T + \alpha(t - T) + \beta(t - T)^2}$$

where:

V_t = volume at temperature t

V_T = volume at temperature T (25 °C)

Thermal expansion has been studied for a range of American crude oils from 0.83-0.94 g/ml at 25°C[188]. For the lowest density crude oil (0.8067 g/ml), α = -0.00074, β = 0 so coefficient of expansion is 7.4 x 10^{-4} K^{-1}

At 320°C:

$$D_t = 0.8067 - 0.00074(295) = 0.5884 g/ml$$

$$V_t = \frac{0.8067 * 60}{0.8067 + 0.00074(295)} = 82.26\ ml = +37\%\ \text{volume}$$

For the highest density crude oil (0.9183 g/ml), α = -0.00068, β = 0 so with a lower coefficient of expansion is 6.8 x 10^{-4} K^{-1}

At 320°C:

$$D_t = 0.9183 - 0.00068(295) = 0.7177 g/ml$$

$$V_t = \frac{0.9183 * 60}{0.9183 + 0.00068(295)} = 76.77\ ml$$ = +28% volume

11.7 Fouling Experiments with blended crude oils

11.7.1 Experiments investigating the effect of Crude blend on fouling deposit mass

Repeat	Reaction Time /hrs	Component (S1)	M_{S1}	Component (S1)	M_{S2}	Wall Solids /mg	wall + Film solids /mg	Wall + film + bulk solids /mg
1	12	Crude H	0.5	Crude L	0.4	4.0	5.3	35.6
2	12	Crude H	0.5	Crude L	0.4	4.8	7.1	53.3
1	12	Crude H	0.6	Crude L	0.4	20.3	22	77.1
2	12	Crude H	0.6	Crude L	0.4	20.1	23.2	81.5
3	12	Crude H	0.6	Crude L	0.4	18.6	20.2	71.7
1	12	Crude H	1.0			68.5	74.8	185.9
2	12	Crude H	1.0			73.3	78.2	183.4
3	12	Crude H	1.0			88.8	94.1	177.2

11.7.2 Experiments investigating the effect of residence time on fouling deposit mass

Repeat	Reaction Time /hrs	Component (S1)	M_{S1}	Component (S1)	M_{S2}	Wall Solids /mg	wall + Film solids /mg	Wall + film + bulk solids /mg
1	6	Crude H	0.6	Crude L	0.4	10.2	16	51.8
2	6	Crude H	0.6	Crude L	0.4	12.7	15.7	64.6
3	6	Crude H	0.6	Crude L	0.4	14.5	17.1	60.1
4	6	Crude H	0.6	Crude L	0.4	9.5	14	76.7
5	6	Crude H	0.6	Crude L	0.4	8.8	12.7	53.8
1	12	Crude H	0.6	Crude L	0.4	20.3	22	77.1
2	12	Crude H	0.6	Crude L	0.4	20.1	23.2	81.5
3	12	Crude H	0.6	Crude L	0.4	18.6	20.2	71.7
1	24	Crude H	0.6	Crude L	0.4	21.9	24.4	69.5
2	24	Crude H	0.6	Crude L	0.4	21.4	24.4	64.6
3	24	Crude H	1.6	Crude L	1.4	23.8	25.4	74.8

11.8 Fouling Experiments with solvent fractionated crude oils

11.8.1 Experiments investigating the effect of asphaltene concentration in 1-Methylnaphthalene on fouling

Repeat	Component M1	M_1	Component (S1)	M_{S1}	Wall Solids /mg	wall + Film solids /mg	Wall + film + bulk solids /mg
1	Asphaltene	0.05	1-MeNaphthalene	0.95	10.5	12.6	17.6
2	Asphaltene	0.05	1-MeNaphthalene	0.95	5.5	7.9	14.1
1	Asphaltene	0.10	1-MeNaphthalene	0.90	13.2	14.5	18.3
2	Asphaltene	0.10	1-MeNaphthalene	0.90	15.1	17.2	23.6
1	Asphaltene	0.15	1-MeNaphthalene	0.85	17.6	21.1	23.7
2	Asphaltene	0.15	1-MeNaphthalene	0.85	15.8	19.6	28.1
1	Asphaltene	0.20	1-MeNaphthalene	0.80	14.6	17.9	37.0
2	Asphaltene	0.20	1-MeNaphthalene	0.80	15.8	20.3	31.4

11.8.2 Experiments investigating the effect of solvent aromaticity on fouling behaviour using asphaltene solutions

Repeat	Component M1	M_1	Component (S1)	M_{S1}	Component (S2)	M_{S2}	Solvent Ratio S1:S2	Fraction S2	Wall Solids /mg	wall + Film solids /mg	Wall + film + bulk solids /mg
1	Asphaltene	0.05	1-MeNaphthalene	0.950					10.5	12.6	17.6
2	Asphaltene	0.05	1-MeNaphthalene	0.950					5.5	7.9	14.1
1	Asphaltene	0.05	1-MeNaphthalene	0.475	Dodecane	0.475	1:1	0.5	10.3	11.1	38.7
2	Asphaltene	0.05	1-MeNaphthalene	0.475	Dodecane	0.475	1:1	0.5	8.7	11.4	78.1
1	Asphaltene	0.05	1-MeNaphthalene	0.570	Dodecane	0.38	3:2	0.6	49.3	207.4	251.1
2	Asphaltene	0.05	1-MeNaphthalene	0.570	Dodecane	0.38	3:2	0.6	90.4	293.0	328.6
3	Asphaltene	0.05	1-MeNaphthalene	0.570	Dodecane	0.38	3:2	0.6	225	351.4	418.2
1	Asphaltene	0.05	1-MeNaphthalene	0.633	Dodecane	0.317	2:1	0.67	188.1	476.8	496.6
2	Asphaltene	0.05	1-MeNaphthalene	0.633	Dodecane	0.317	2:1	0.67	170.5	594.6	629.1
3	Asphaltene	0.05	1-MeNaphthalene	0.633	Dodecane	0.317	2:1	0.67	124.5	611.0	643.8
1	Asphaltene	0.05	1-MeNaphthalene	0.713	Dodecane	0.238	3:1	0.75	249.7	867.3	921.0
2	Asphaltene	0.05	1-MeNaphthalene	0.713	Dodecane	0.238	3:1	0.75	164.7	747.9	762.4
3	Asphaltene	0.05	1-MeNaphthalene	0.713	Dodecane	0.238	3:1	0.75	237.1	759.3	770.9

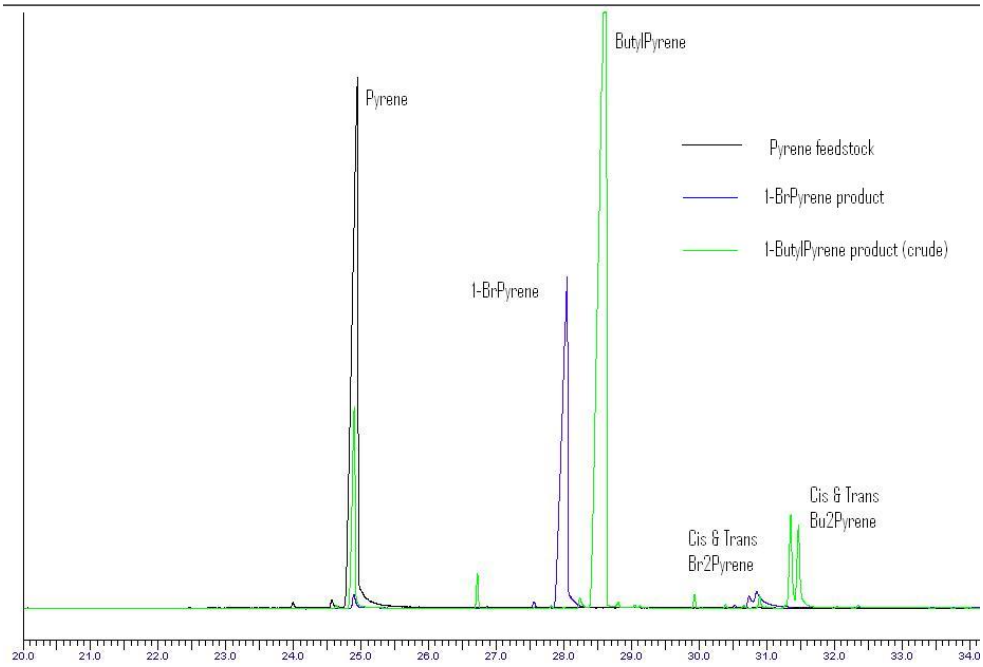
11.8.3 Experiments investigating the effect of Maltene:Dodecane mass ratios on fouling behaviour

									Deposits (mg) divided by reactant maltene mass (g)		
Repeat	Component (S1)	M_{S1}	Component (S2)	M_{S2}	Fluid Ratio S1:S2	Wall Solids /mg	wall + Film solids /mg	Wall + film + bulk solids /mg	Wall Solids /mg/g	wall + Film solids /mg/g	Wall + film + bulk solids /mg/g
1	Maltenes	0.250	Dodecane	0.750	1:1	37.8	56.9	105.3	4.18	6.29	11.63
2	Maltenes	0.250	Dodecane	0.750	1:1	30.0	64.2	88.2	3.31	7.09	9.74
1	Maltenes	0.500	Dodecane	0.500	3:2	10.0	10.1	36.3	0.55	0.56	2.00
2	Maltenes	0.500	Dodecane	0.500	3:2	13.2	13.4	26.0	0.73	0.74	1.44
1	Maltenes	0.667	Dodecane	0.333	2:1	12.7	42.6	49.0	0.52	1.76	2.02
2	Maltenes	0.667	Dodecane	0.333	2:1	18.3	38.3	44.4	0.75	1.58	1.83
1	Maltenes	0.750	Dodecane	0.250	3:1	10.5	11.9	35.3	0.39	0.44	1.30
2	Maltenes	0.750	Dodecane	0.250	3:1	4.7	6.4	23.3	0.17	0.24	0.86
1	Maltenes	1.000				7.3	8.4	28.6	0.20	0.23	0.79
2	Maltenes	1.000				4.1	4.3	24.1	0.11	0.12	0.67

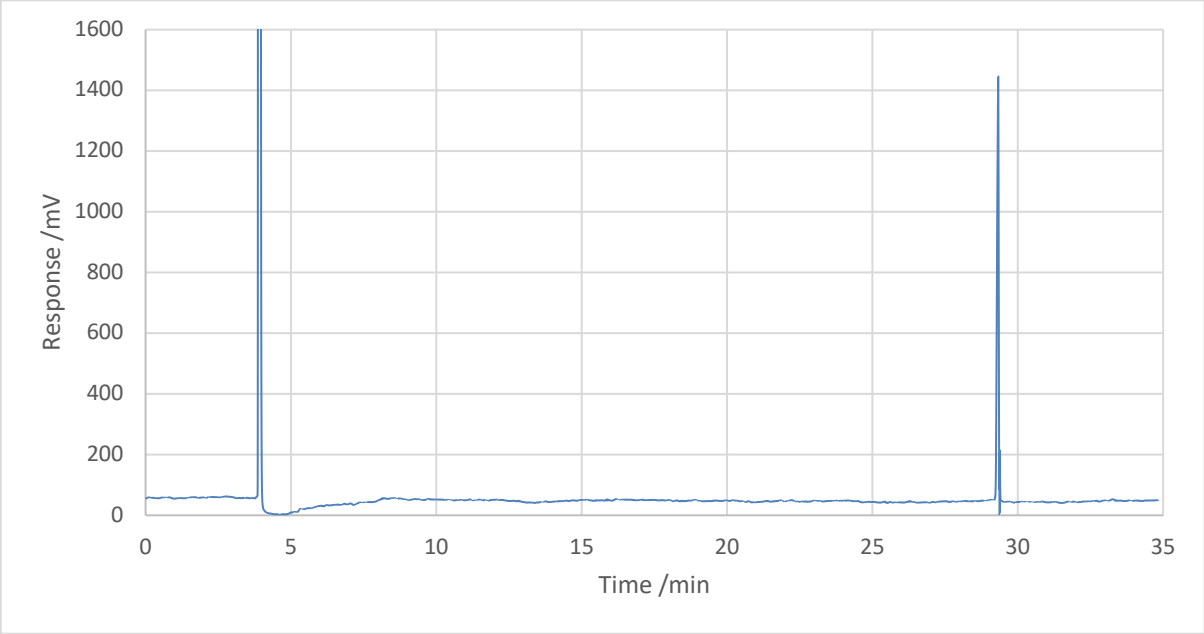
11.9 Synthetic model asphaltenes

Analytical data for synthesised alkyl-pyrene models

GC-FID peak data for synthesis of 1-butylpyrene



GC-FID Chromatogram for recrystallised 1-Decylpyrene product



Analytical Data for Synthesised Perylene compounds

11.8.2 Solubility tests of pyrene based compounds

	Solvent	1-butylpyrene	1-decylpyrene
non-polar aliphatic	Dodecane	good solubility	good solubility
Aromatic non-polar	1-Methylnaphthalene	good solubility	good solubility

Figure 11.8.4 Absorption spectra for PDI-C3 and PDI-C12 (no absorption above 600 nm)

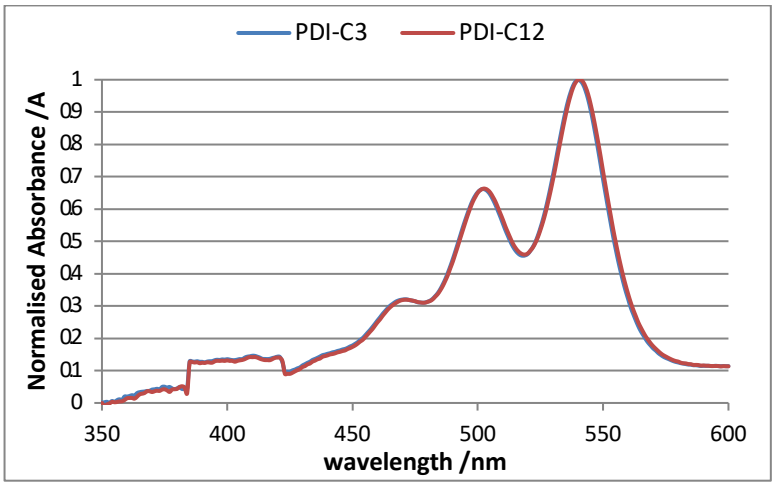
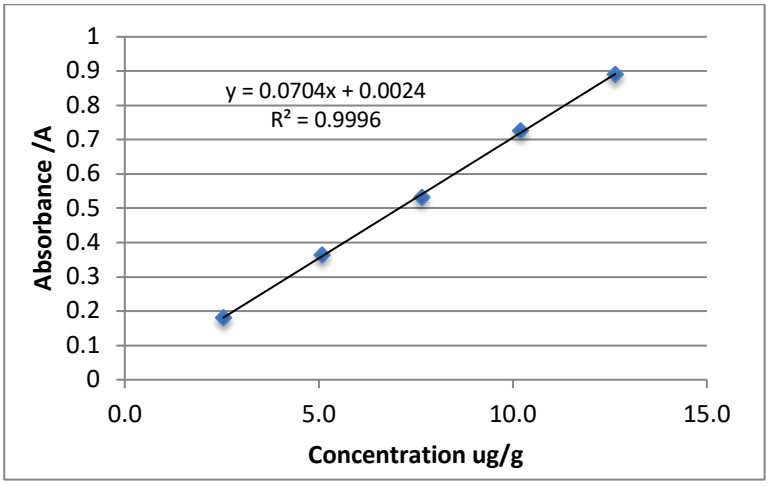
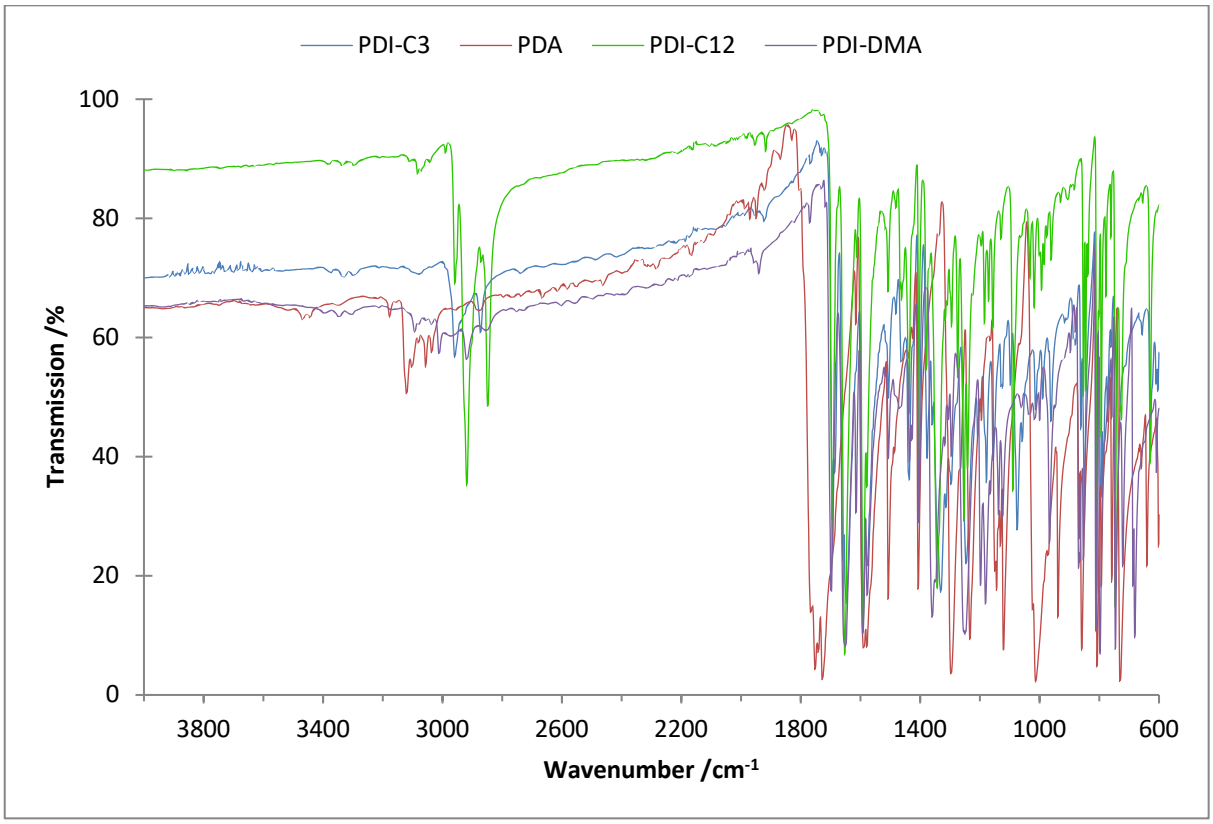


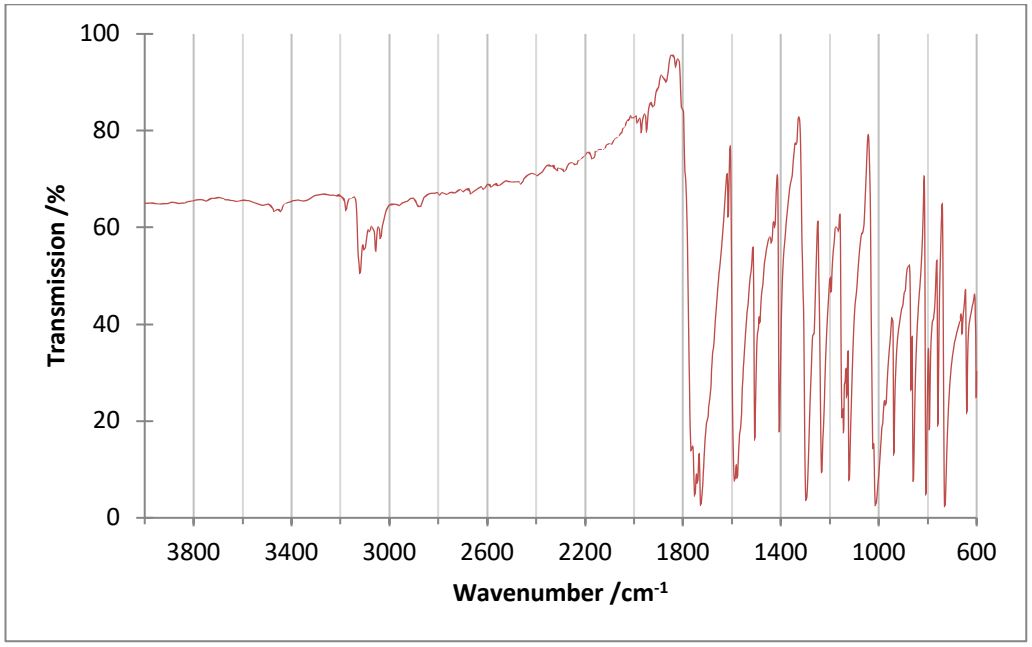
Figure 11.8.5 Calibration plot for PDI-C12 in 1-methylnaphthalene



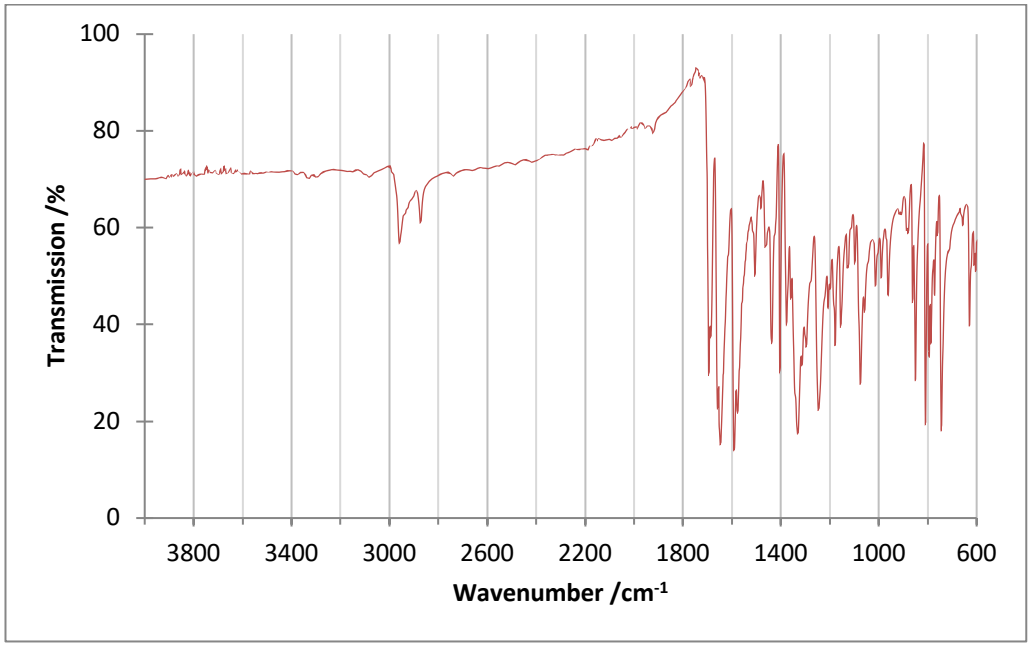
11.8.4 FTIR-ATR spectra for all perylene compounds



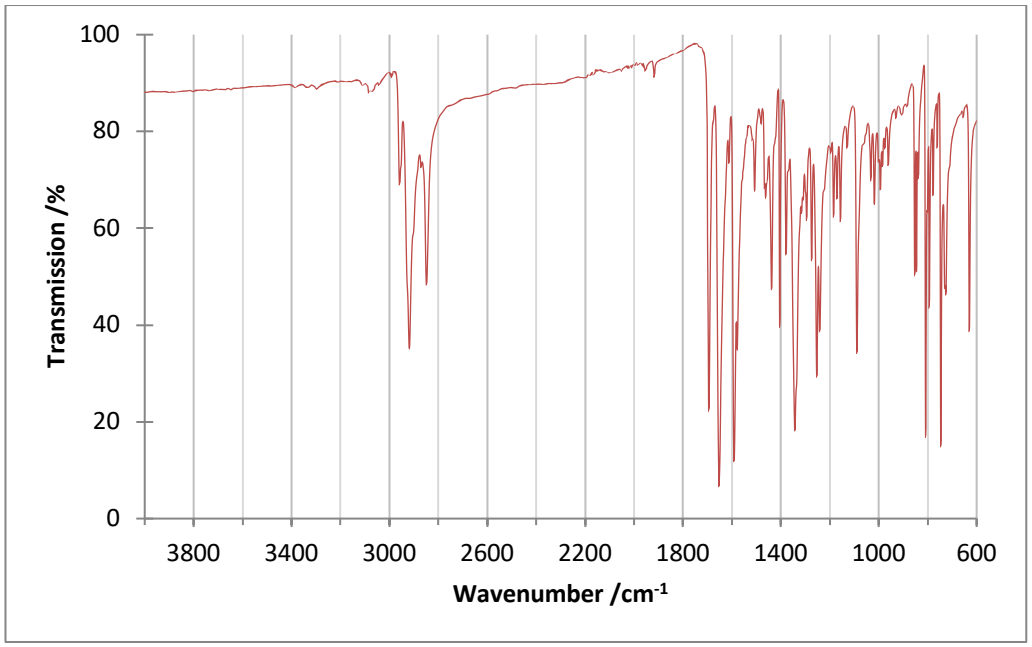
11.8.4 FTIR-ATR Spectra for perylene tetracarboxylic dianhydride (PDA)



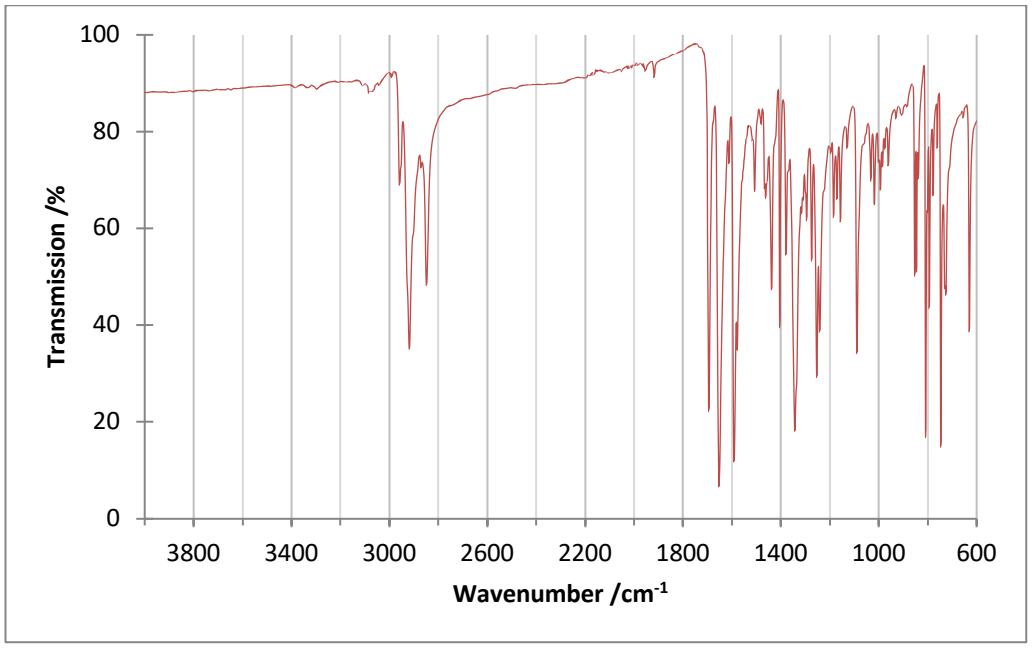
11.8.5 FTIR-ATR spectra for perylene propyl-diimide PDI-C3



11.8.6 FTIR transmission spectra for perylene dodecyl-diimide PDI-C12



11.8.7 FTIR transmission spectra for perylene dimethylaniline diimide PDI-DMA



11.8.8 PDI-C12 in 1-methyl naphthalene - stock solution

compound mass /mg	solution mass /g	solution Concentration µg/g
10.3	10.22	1007

11.8.9 PDI-C12 in 1-methyl naphthalene – calibration curve

Calibration point	Pipetted stock sol. Mass/g	Total Solution mass /g	solution conc. /µg/g	Dilution Factor	Absorbance /A
1	0.01262	5.005	2.54	396.6	0.181
2	0.02532	5.005	5.09	197.7	0.363
3	0.038005	5.005	7.65	131.7	0.532
4	0.051072	5.005	10.27	98.0	0.726
5	0.0628343	5.005	12.64	79.7	0.890

* Serial dilution required for appropriate solution concentrations

11.8.10 PDI-C12 in 1-methyl naphthalene - solution vs solubility

Temperature /° C	Temperature /K	Pipetted Mass/g	Total Solution Mass /g	Absorbance /A	Dilution Factor	Solubility /mg/g
20	293.16	0.08920	7.1130	0.189	79.7	0.2114
50	323.16	0.02417*	10.0017	0.455	414	2.6602
80	353.16	0.004263*	9.9628	0.446	2337	14.725
100	373.16	0.0007034*	11.7856	0.27	16756	63.690

* Serial dilution required for appropriate solution concentrations

According to the best-fit curve, stable temperature T_{stable} for PDI-C12 solution:

$$T_{stable} > \frac{\log[solution]}{0.0303} = 346.6\text{K} = 73.4°\text{C}$$